Mechanism of the Pinacol Rearrangement of Thiele Cage Diols Over a C(sp^3)-C(sp^3) Bond

by

Austin Luke Burman
Bachelor of Science (Honours), University of Calgary, 2018

A Thesis Submitted in Partial Fulfillment
of the Requirements for the Degree of

MASTER OF SCIENCE

in the Department of Chemistry

We acknowledge and respect the lək̓ʷəŋən peoples on whose traditional territory the university stands and the Songhees, Esquimalt and W̱SÁNEĆ peoples whose historical relationships with the land continue to this day.

Supervisory Committee

Mechanism of the Semi-pinacol Rearrangement of Thiele Cage Diols Over a C(sp^3)-C(sp^3) Bond

By

Austin Luke Burman
Bachelor of Science (Honours), University of Calgary, 2018

Supervisory Committee

Dr. Jeremy E. Wulff, Department of Chemistry
Supervisor

Dr. Lisa Rosenberg, Department of Chemistry
Departmental Member

Dr. David C. Leitch, Department of Chemistry
Departmental Member

Abstract

Supervisory Committee

Dr. Jeremy E. Wulff, Department of Chemistry
Supervisor
Dr. Lisa Rosenberg, Department of Chemistry
Departmental Member
Dr. David C. Leitch, Department of Chemistry
Departmental Member

In our previous publication of Thiele cage diols, we describe the first pinacol rearrangement to occur over a $C(sp^3)$–$C(sp^3)$. Two mechanisms were initially proposed: a concerted mechanism and a stepwise mechanism, proceeding through a carbocation intermediate. Interestingly, the rearrangement provides only a single diastereomer. The aim of this thesis is to investigate the nature of the reaction by measuring the relative rates of reaction with varying substituents that either stabilize or impede the formation of carbocations. From the relative rates, we can narrow in on whether the mechanism is stepwise or concerted, based on substituent effects, and determine how the reaction may provide a single diastereomer.

In Chapter 1, the pinacol rearrangement is introduced, and each analogue that followed after, including stereoselective pinacol rearrangements and a series of different semipinacol rearrangements that provide useful synthetic pathways for chemists with desirable stereochemical outcomes.

In Chapter 2, we describe the isolation and characterization of two analogues of a key side product. The structure of each analogue was determined through a series of spectroscopic techniques including ^{1}H-^{1}H COSY, HSQC, HMBC, and 1D-selective gradient NOE NMR. From the solved structures, we proposed a possible mechanism to describe their formation during the main rearrangement reaction – one that shares a carbocation intermediate with the stepwise mechanism already proposed.

In Chapter 3, we prepared five Thiele cage diol analogues with aryl substituents with different electronic properties: two substituents that stabilize carbocation intermediates (*p*-OCH_3 and *p*-CH_3), two that destabilize (*p*-F and 3,5-diOCH_3), and the base tetraphenyl Thiele cage diol. We measured the rates of reaction of each diol with *p*-toluenesulfonic acid at 25°C, 35°C, 45°C, and 52°C via variable temperature quantitative ^{1}H-NMR over time. From the rates of reaction, we found that diols with carbocation-stabilizing aryl substituents reacted faster than the destabilizing analogues, providing evidence that the rearrangement proceeds through a carbocation intermediate. We also found that the diols with electron-deficient aryl substituents showed an increase in the entropy of activation with increasing electron-deficiency in the aryl groups, suggesting an associative pathway for the electron-deficient substituents toward the rearrangement product. Considering the pathway proposed for the side product, we propose an updated stepwise mechanism. Based on computational studies and a previously-isolated X-ray crystal structure, we determined that the diastereoselectivity of the reaction was facilitated by favourable π-π stacking interactions between two aryl substituents. The interaction of the aryl groups twists the geometry of the molecules, placing the migrating aryl substituent in the ideal position for the rearrangement to occur stereoselectively.

Table of Contents

List of Tables

List of Figures

List of Schemes

List of Abbreviations

^{13}C NMR	carbon nuclear magnetic resonance
^{13}C{^{1}H}	proton-decoupled carbon nuclear magnetic resonance
2,2-DMP	2,2-dimethoxypropane
1D NOE	1D-selective gradient nuclear Overhauser spectroscopy
^{19}F NMR	fluorine nuclear magnetic resonance
^{19}F{^{1}H}	proton-decoupled fluorine nuclear magnetic resonance
^{1}H NMR	proton nuclear magnetic resonance
Å	Angstrom
app.	apparent
AQ	acquisition time
Ar	aryl
$BF_3{\cdot}Et_2O$	boron trifluoride diethyl etherate
BINOL	1,1'-bi-2-naphthol
Bn	benzyl
Boc	*t*-butoxycarbonyl
br	broad
Bu	butyl
CDI	1,1'-carbonyldiimidazole
cm^{-1}	wavenumber
COSY	^{1}H–^{1}H correlation spectroscopy
CPA	chiral phosphoric acid
D1	relaxation delay
D10	spectra acquisition delay
d	doublet
dd	doublet of doublets
DMP	Dess-Martin periodinane
DNB	1,4-dinitrobenzene
d.r.	diastereomeric ratio
ee	enantiomeric excess
ESI	electron spray ionization
Et	ethyl
Et_2O	diethyl ether
EtOAc	ethyl acetate
FDA	Food and Drug Administration
FTIR	Fourier transform infrared spectroscopy
HFIP	hexafluoroisopropanol
HMBC	heteronuclear multiple bond coherence spectroscopy
HRMS	high resolution mass spectrometry
HSQC	heteronuclear single-quantum coherence spectroscopy
Hz	hertz, s^{-1}
i	iso
IR	infrared spectroscopy
J	coupling constant
J_{HF}	coupling constant – proton to proton
J_{HH}	coupling constant – proton to fluorine
k	rate constant

M	molar
m	multiplet
$[M + Na]^+$	exact mass of the molecule plus mass of a sodium ion
$[M - H]^-$	exact mass of the molecule minus the mass of a proton
mCPBA	meta-chloroperoxybenzoic acid
MHz	megahertz
mM	millimolar
mmol	millimoles
mol	moles
mp	melting point
M.S.	molecular sieves
MS	mass spectrometry
Ms	mesylate or methanesulfonate
MTBE	methyl *t*-butyl ether
NBS	*n*-bromosuccinimide
NMR	nuclear magnetic resonance
NOE	nuclear Overhauser effect
NOESY	nuclear Overhauser effect spectroscopy
O1P	spectral center
p	para
Ph	phenyl
ppm	parts per million
Pr	propyl
PTSA	*p*-toluenesulfonic acid
q	quartet
R.T.	room temperature
s	singlet
S_N1	unimolecular nucleophilic substitution
S_N2	bimolecular nucleophilic substitution
SW	sweep width/spectral width
%T	transmittance
T	temperature
t	triplet
tdd	triplet of doublet of doublets
t or *tert*	tertiary
TBAF	tetrabutylammonium fluoride
TBS	*t*-butyldimethylsilyl ether
Tf	triflate or trifluoromethanesulfonate
TFA	trifluoroacetic acid
THF	tetrahydrofuran
TLC	thin layer chromatography
TMS	trimethylsilyl ether
tol	toluene
TS	transition state
UV	ultraviolet
δ	chemical shift

Acknowledgements

I would like to thank my supervisor, Dr. Jeremy Wulff, for the opportunity to work with him and his wonderful group. Secondly, I would like to thank Dr. Stefania Musolino for all her help in and out of the lab, her incredible guidance and advice, and for being a great friend. My thanks to Dr. Mathieu Lepage, Dr. Chakri Simhadri, Dr. Liam MacFarlane, Dr. Rashid Nazir for their guidance and friendship during my graduate career, and for the many beers, laughs, and games we shared. I would also like to thank the wonderful Wulff group: Liting Bi, Jon Sader, Derek Blevins, Ben Godwin, and Dr. Tong Li. My accomplishments (and caffeine addiction) are in part thanks to their support and the joy they bring with them, in and out of the lab. Thank you to the excellent undergrads that I have had the opportunity to work alongside: Julia Levy and Bryce Mulder.

I would like to thank both of my committee members for their support throughout my degree: Dr. Lisa Rosenberg and Dr. David Leitch. A thousand thanks and many more to the UVic staff who helped me throughout my degree, especially Chris Barr and Dr. Tyler Trefz, as well as the Senior Lab Instructors I have had the great pleasure of working alongside.

Thank you to the wonderful friends I made during my time in Victoria: Nyko Coffey, Sean Hunter, Selkirk Watmough, Martin Henderson, Connor Leies, and Kyle Joly. Thank you to the friends I made virtually during the pandemic: Chris, Jeremy, Bob, Jake, James, Evan, and Wes. Thank you to my family for their support throughout my life and for doing the very best to understand my long-winded rambling about chemistry.

And lastly, thank you to my great friend, Curtis Thompson. Curt has been my closest friend since early in high school and has supported me ever since, always cheering me on and making fun of me in the way that friends do. He taught me to hit as hard as possible, in rugby and in life, and how to laugh even when things get a bit tough. I'll never forget the times that I needed a friend most and you were there, right outside my house, ready to go for a drive in Big Red to grab a burger and just chat. Thank you for everything, Brother.

Dedication

Dedicated to the memory of my grandfather, Kenneth C. Karlenzig (1941-2003).

I don't want to trickle out. I want to pour till the pail is empty, the last bit going out in a gush, not drops.

Emily Carr

Chapter One

Introduction

1.1.0 – Defining Pinacol Rearrangements

In 1860, the first pinacol rearrangement was described by Fittig.[1] By acidifying pinacol **1** with sulfuric acid, a ketone, pinacolone **2**, was produced through a 1,2-methyl shift (**Scheme 1**). Though the identity of the product was not described until 1873 by Butlerov,[2] the pinacol rearrangement would become one of the earliest examples of a molecular rearrangement to be described in the chemical literature.[3] Today, pinacol rearrangements are defined as the dehydration of a vicinal diol by a strong Brønsted acid or a Lewis acid to produce a ketone or aldehyde.[3,4] As shown in **Scheme 2**, the addition of an acid generates a carbocation through dehydration at either carbinol center, which is then primed for a 1,2-migration of a hydride, alkyl, or aryl substituent. The regiochemistry of a given pinacol rearrangement is largely dictated by the stabilization of the carbocation intermediate, with strong electron donating substituents forming carbocations faster and preferentially over electron withdrawing substituents.[5] However, if the carbinol carbons are similarly activated by their substituents (stabilizing the carbocations generated), a mixture of 2 regioisomers would be produced. Moreover, if the four substituents on the diol are all different, each one can in principle undergo 1,2-migration, and (in the absence of some chiral influence) each product will be formed as a mixture of enantiomers. As a result, up to 8 products are possible, as illustrated in **Scheme 2**. Migratory aptitude can also affect the regiochemistry of a given pinacolic rearrangement, with some substituents being more likely to migrate than other substituents. The relative geometry of the migrating substituent and the leaving hydroxyl group affects both regio- and stereochemistry. Antiperiplanar geometry is preferred and proceeds at a higher rate of reaction than synperiplanar geometry, though rearrangement can occur at a slower rate with a differing geometry. Despite these challenges, the scope of pinacol rearrangements is wide with virtually any vicinal diol having the ability to undergo a 1,2-migration under acidic (or even basic) conditions. Diols themselves are readily prepared, especially with stereoselective methods such as asymmetric dihydroxylations or epoxidations with ring-opening to reveal the diol. With a large scope and stereochemical and regiochemical issues to consider, the use of pinacol rearrangements in organic synthesis poses a unique challenge (but also an attractive opportunity) to synthetic chemists.

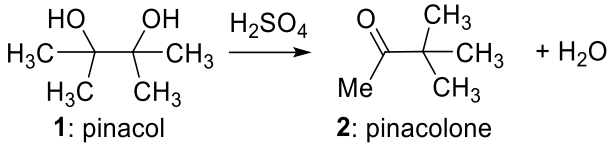

Scheme 1 The rearrangement of pinacol to pinacolone with sulfuric acid, discovered by Fittig, and the identity of the product discovered by Butlerov.

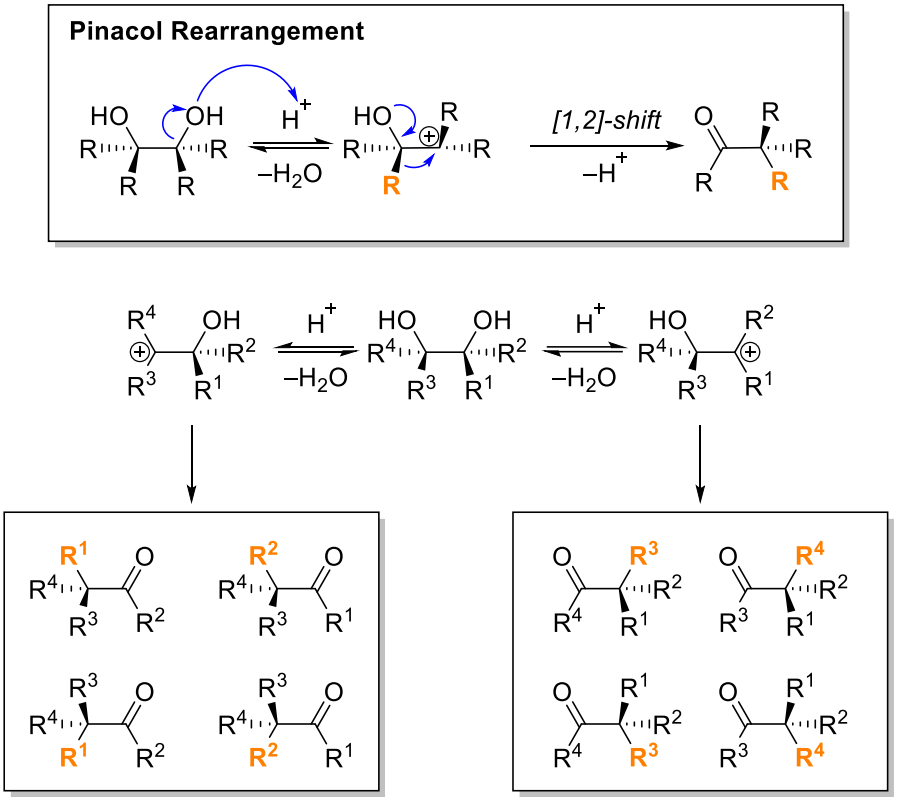

Scheme 2 A general reaction scheme for a pinacol rearrangement producing four racemic mixtures of regioisomers.

1.2.0 Pinacol Rearrangements in Natural Product Synthesis

As part of a structure activity relationship study of combretastatin A derivatives, Pettit and coworkers targeted hydroxyphenstatin for synthesis (**5**, **Scheme 3**) due to its strong anticancer and antimitotic activity.[6] While preparing other combretastatin A-series molecules, the reaction of (*R*,*R*)-diol **3** with boron trifluoride etherate produced a racemic mixture of aldehyde **4**. Though **3** was used as a single enantiomer, the product isolated from the pinacol rearrangement was a racemic mixture with the loss of chiral information likely originating from the carbocation intermediate generated in a stepwise manner. Fortunately, in the case of hydroxyphenstatin the target compound is achiral and a loss of chirality is not detrimental to the overall synthesis. With desilylation and decarbonylation of **4** with tetrabutylammonium fluoride, **5** is isolated in 49% yield. While the removal of the *t*-butyldimethylsilyl groups was expected, the decarbonylation with TBAF was not. Thus, Pettit and coworkers proposed that the decarbonylation occurred through a base-catalyzed autoxidative radical process in the presence of air.[6] While the racemic mixture isolated was not of concern for the synthesis of **5**, other methods should be used if a stereochemically pure target is desired. In the case of the rearrangement of cyclic diols, relative stereochemistry of adjacent substituents can help in predicting the stereochemical outcome of a given rearrangement.

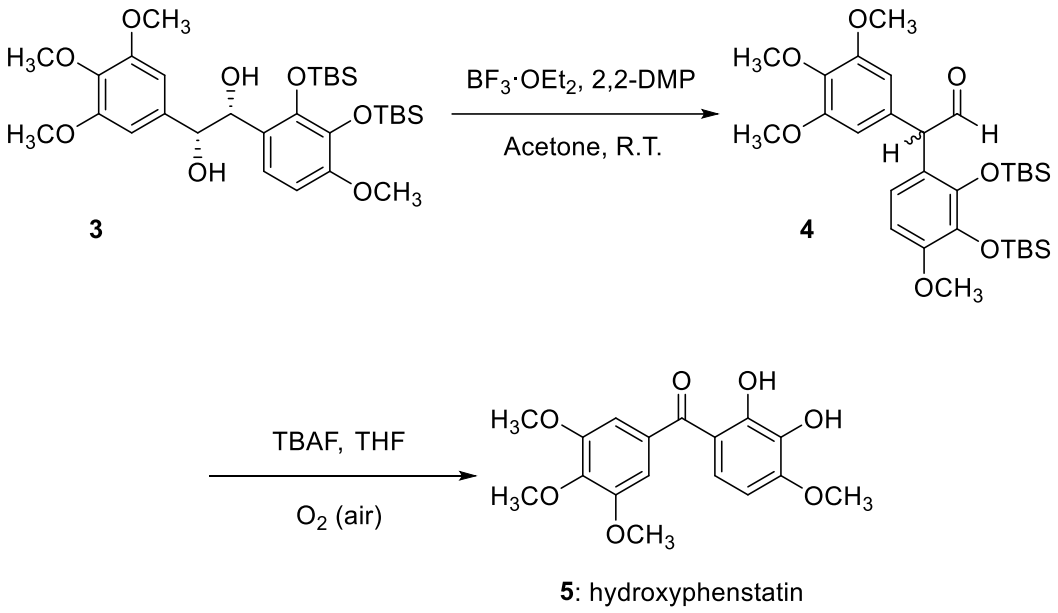

Scheme 3 Synthesis of hydroxyphenstatin through a pinacol rearrangement of diol **3** and desilylation of **4**.

Bode and coworkers developed a method for a stereoretentive pinacol rearrangement in their synthetic study toward the synthesis of polyketide natural products.[7] By using an isoxazole core (**Scheme 4**), the regiochemistry of the pinacol rearrangement is predetermined by stabilization of the generated carbocation toward the isoxazole moiety. Starting with enantioenriched ketol **6**, syn-diol **7a** is prepared by careful addition of **6** to vinyllithium resulting in a 99% yield. Diol **7a** was then rearranged with boron trifluoride etherate to produce ketone **8** with 98% enantiomeric excess in 96% yield. Though formation of the carbocation at the benzylic position would be facilitated by the presence of the vinyl substituent, delocalization of the carbocation to the isoxazole moiety forms preferentially and provides the desired product. Chiral information is retained in the rearrangement of **7a** to **8** likely through a combination of conformational constraints of the tricyclic core, rigidifying of the core through delocalization of the carbenium to the isoxazole moiety, and a preferential antiperiplanar relative geometry of the migratory vinyl and the leaving hydroxyl group.[7] Bode and coworkers also note the high aptitude of the vinyl substituent as a migratory group. Also, worth noting is that the antiperiplanar geometry contributes to the kinetics of the rearrangement but is not essential for the stereochemical outcome of the reaction. Diastereomer **7b**, which has synperiplanar geometry with respect to the leaving hydroxyl and migratory substituent, proceeds with similar enantiomeric excess and yield, albeit with a longer reaction time.

Despite the reaction's shortcomings, pinacol rearrangements can be utilized in synthesis by taking advantage of conformational constraints of cyclic systems or through the use chiral catalysts. While acyclic systems typically rearrange with a loss of chiral information from the starting diol, cyclic systems can retain this information. As a result, migration can be predicted by considering the appropriate orbital alignments with respect to the migrating substituent. A substituent is likely to migrate faster if the leaving hydroxyl group is antiperiplanar with respect to the substituent.

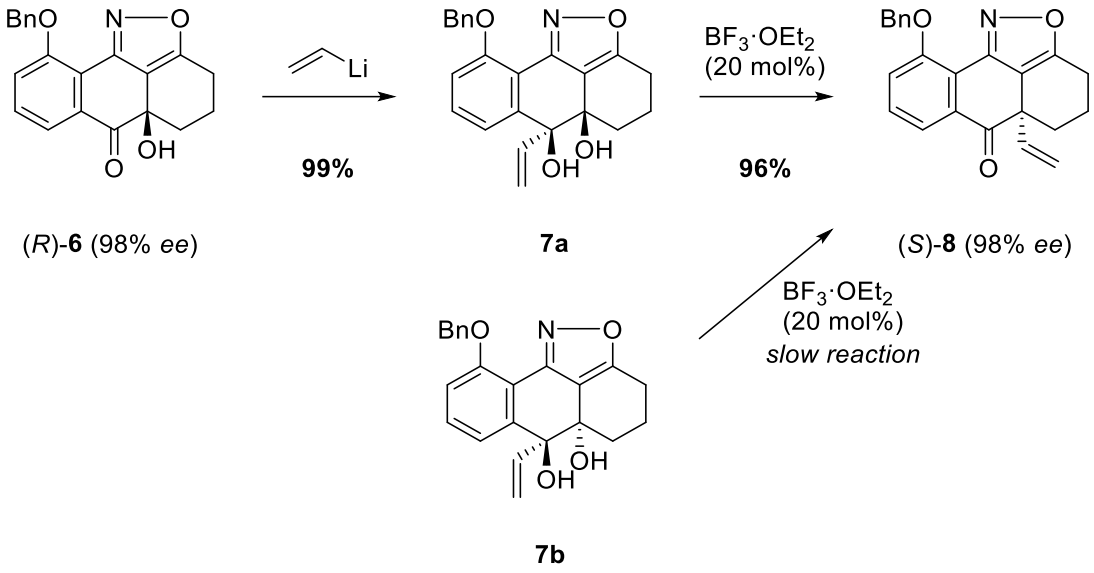

Scheme 4 A stereoretentive pinacol rearrangement of an isoxazole-based diol **7**.

Following the isolation and determination of its anticancer activity, (–)-diazonamide A (**9**, **Scheme 5**) was the subject of many synthetic studies. Harran and coworkers performed the synthesis of **9** starting with chiral pool molecules that led them to the isolation of olefin **10**.[8] Following alkylation of the phenolic moiety, **10** was dihydroxylated using a chiral complexed osmium (VIII) tetroxide (OsO_4) reagent to produce diol **11** as the desired diastereomer with a diastereomeric ratio (d.r.) of 93 to 7. The 12-member macrolactam core of **9** (highlighted in orange, **Scheme 4**) was formed through a pinacol ring-contraction resulting from treatment of **11** with *p*-toluenesulfonic acid (PTSA). Interestingly, macrolactam **13** was isolated as a single C10 diastereomer from **11** with the high stereochemical retention likely due to the phenonium ion transition state **12**. As Harran and coworkers noted, the only deliberate stereochemical manipulations made are from **10** to the formation of **13**. Further transformations took advantage of cyclic constraints to produce (−)-diazonamide A and other derivatives with the desired stereochemistry.

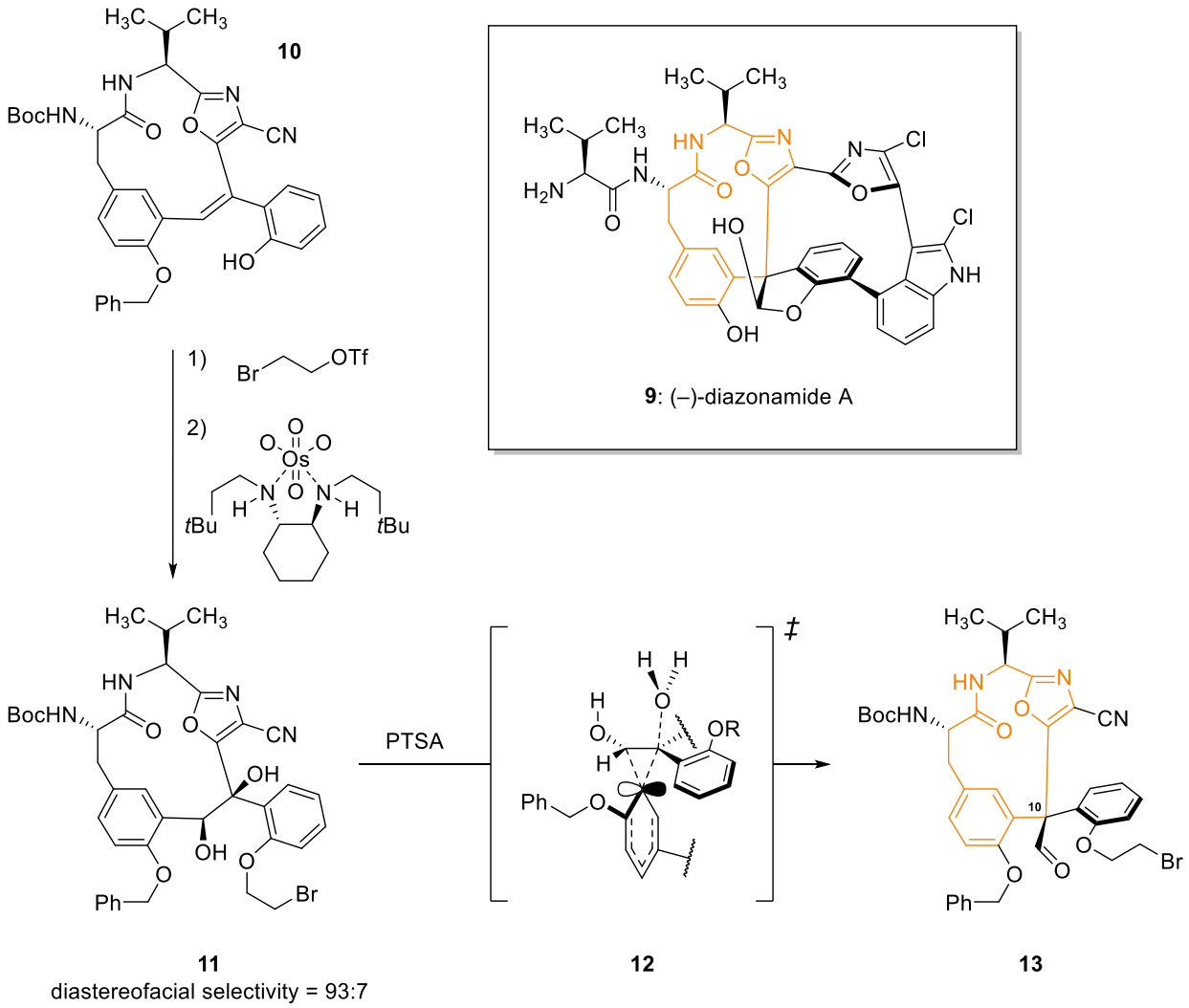

Scheme 5 Synthesis of the 12-membered lactam core (in orange) towards the isolation of (–)-diazonamide A.

1.3.0 Stereoselective Pinacol Rearrangements with Chiral Phosphoric Acid Derivatives

To solve the problem of stereoselective control in acyclic pinacol rearrangements, Antilla and coworkers employed the use of BINOL-derived chiral phosphoric acids (CPA) with indoyl diols (**Scheme 6**, **14**).[9] Indoyl diols were selected specifically for the stabilization of the carbenium intermediate (stabilized through formation of an iminium **18** as seen in **Scheme 7**), dictating the regiochemistry. After optimizing reaction conditions and determining that the 2-naphthyl derived CPA, (*R*)-**16**, provided the highest enantioselectivity, the substrate scope was expanded to demonstrate a wide variety of substituents on the migrating aryl groups. The scope ranged from moderately electron deficient (4-Cl) to electron rich (4-OCH_3) and included bulkier aryl groups such 2-naphthyl substituents, though longer reaction times were required (14 hours instead of the usual 6 hours). To understand the transfer of chiral information from **16** to the substrate, Antilla and coworkers proposed the mechanism shown in **Scheme 7**.

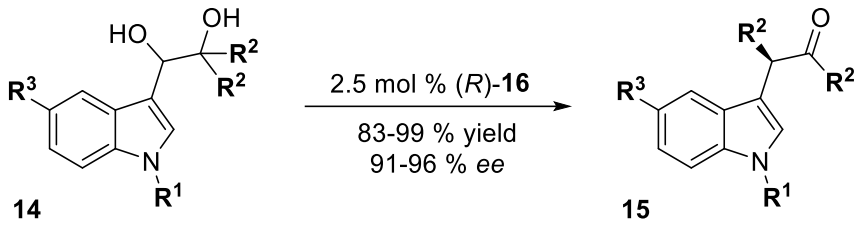

R[1]= Me, Bn, Allyl **R**[2]= Ph, 4-FC_6H_4, 4-ClC_6H_4, 4-$MeOC_6H_4$, 3,5-$Me_2C_6H_3$, 2-naphthyl **R**[3]= H, F, Cl, Br, Me, MeO

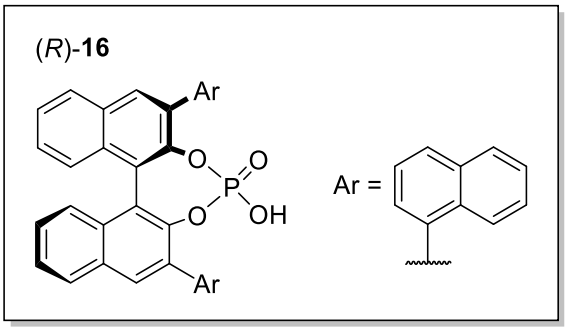

Scheme 6 Enantioselective pinacol rearrangement of indoyl diols.

Following the proposed mechanism (**Scheme 7**) and a concurrent computational study of the mechanism by Falcone et al.,[10] enantioselectivity is a result of the anionic interaction of the chiral phosphate to the iminium intermediate generated, called chiral ion-pair contact catalysis.[11] Following the dehydration of iminium of **18** from **17**, the phosphate interacts through hydrogen bonding to the remaining alcohol of **18** and H1 of the iminium moiety, pre-arranging the migrating aryl substituent (shown in orange, **Scheme 7**) to be facing inward toward the core of the phosphate. Were the migration occurring along the back face of the carbenium moiety, the rotation required to attain the necessary transition state geometry would result in greater steric interaction between the non-migrating aryl substituent and the BINOL moiety of the phosphate. As such, the change in the Gibbs free energy of the transition state ($\Delta\Delta G^{\ddagger}$) leading to the product is lower than the enantiomer by 1.6 kcal·mol^{-1}.[10] With a variety of substituents on the migratory groups, the enantioselective pinacol rearrangement of indoyl diols under catalytic conditions affords a single enantiomer of α-substituted ketone with good to excellent yield and excellent enantioselectivity.

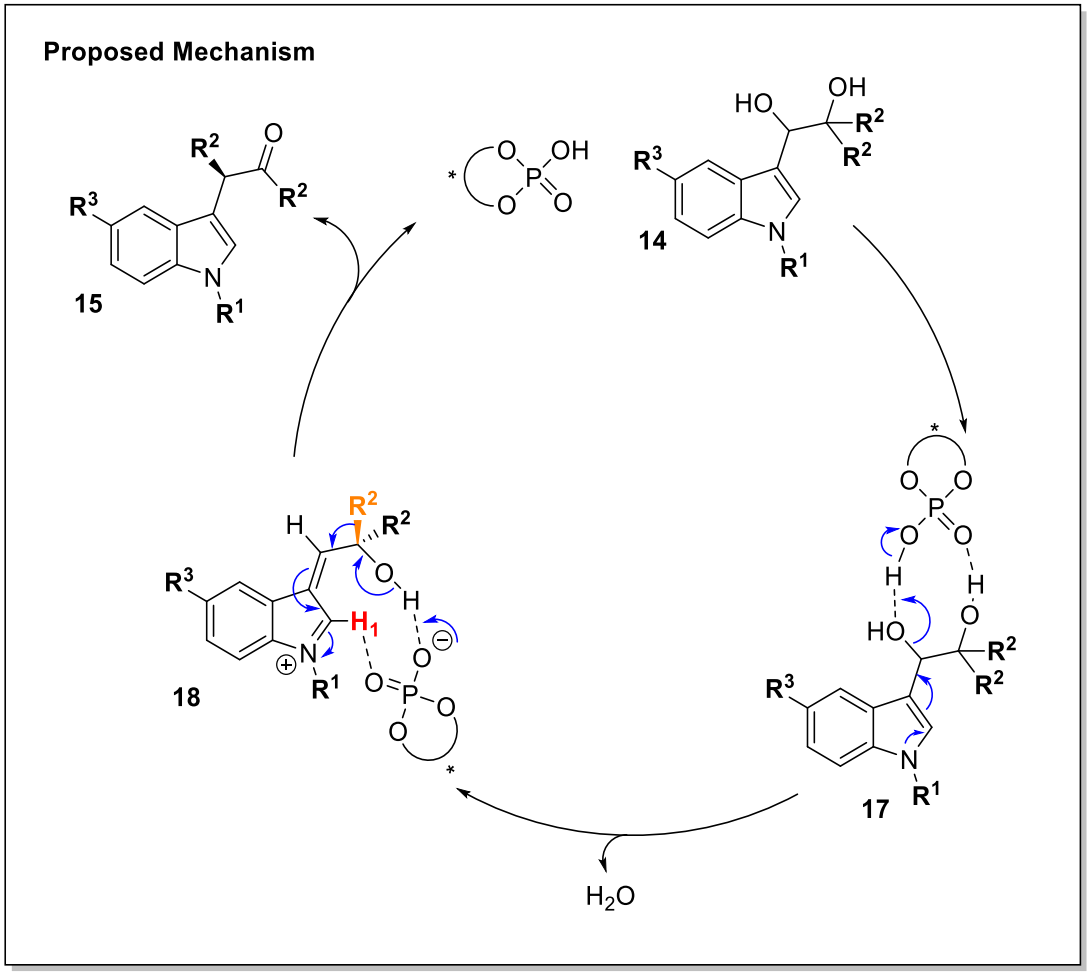

Scheme 7 The proposed mechanism of chiral information transfer from a CPA catalyst to the indoyl substrate during the pinacol rearrangement of diol **14**.

Using a similar approach to that of Antilla and coworkers, Zhu and coworkers presented an organocatalytic pinacol rearrangement for the generation of quaternary center-containing cyclohexanones through chiral phosphoramides (**Scheme 8**).[12] With substituents ranging from electron-rich to electron-poor, varying electronic effects on the alkyne migrating group do not negatively affect the rearrangement and allow a wide variety of scaffolds. The activating substituent in the case of these syntheses is typically an electron-rich aryl substituent that can better stabilize the carbocation generated than the cyclopentane at the other side of the diol. Despite the limitation on permissible activating groups, each diol **19** rearranges to its respective cyclohexanone **20** when reacted with chiral phosphoramide (*S*)-**21** with good to excellent yield (ranging from 75 to 99%) and excellent enantiomeric excess (*ee* of 81 to 94%). Notably, the cyclohexanones **20** bear an enantioenriched quaternary-center, a critical motif in natural product synthesis.

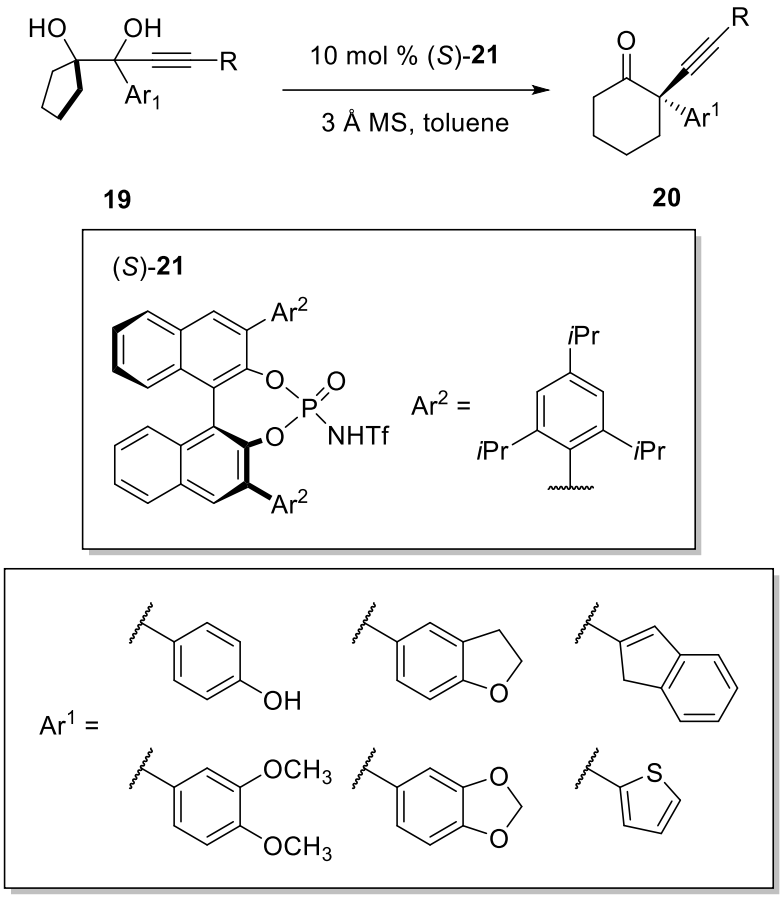

Scheme 8 Enantioselective synthesis of quaternary center-containing cyclohexanones through a pinacol ring expansion with use of chiral phosphoramides.

As a showcase of the chemistry developed for the rearrangement of alkyne-containing diols to enantioenriched cyclohexanones, the synthesis of (+)-mesembrane (**Scheme 9**, **26**) was undertaken.[12] Friedel–Crafts acylation of 1,2-dimethoxybenzene (**22**) with cyclopentanecarbonyl chloride (**23**) generated a ketone intermediate that was then brominated at the α-position to the carbonyl group. Nucleophilic attack (trimethylsilyl)acetylide at the ketone resulted in Darzens-type closure of an unstable epoxide, which was then hydrolyzed to afford the desired functionalized diol **24**. With **24** in hand, the quaternary center-containing cyclohexanone was produced with 90% enantiomeric excess using the chiral phosphoramide **21** in toluene, with desilylation using potassium carbonate to produce **25**. A Ru-catalyzed hydration of **25** provided an aldehyde, which leads to **26** following reductive amination with methylamine.

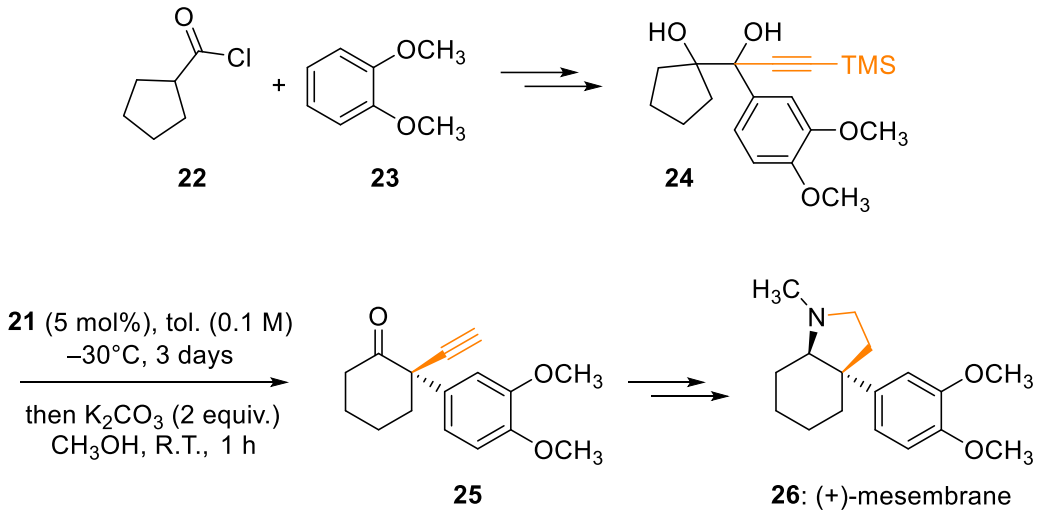

Scheme 9 Total synthesis of (+)-mesembrane with the 2 carbons from the alkyne group in diol **24** highlighted in orange to show the final position of each respective carbon in the target, **26**.

In 2012, Snyder and coworkers synthesized hopeanol (**Scheme 10**, **30**) that included the first pinacol rearrangement with a chiral Brønsted acid in a natural product synthesis.[13] Diol **27** was prepared through Grignard addition to a precursor aldehyde as a mixture of diastereomers. The rearrangement of **27** to aldehyde **28** was observed to rearrange under strong acidic conditions with achiral Brønsted acids such *p*-toluenesulfonic acid and phosphoric acid, however, diastereoselectivity (~3:1 d.r.) and yields were modest (38-60%). The diastereomer of **27** with the hydroxyl groups anti to each other required higher temperatures and longer reaction times to undergo the rearrangement to the same desired product as the syn-diastereomer. There were, unfortunately, more side products—the most notable of which was the epoxide, which failed to rearrange to the desired product under the conditions employed for the reaction. Using chiral phosphoric acid **29** with **27** (as a mixture of diastereomers) in chloroform at 100°C for 1 hour provided the desired diol **28** with a d.r. of 18.4:1 in 56% yield. Interestingly, the (*S*)-enantiomer of **29** provided similar results when using similar conditions with a d.r. of 18.9:1 in 56% yield, while a racemate of **29** provided a d.r. of 13.6:1 in 59% yield. At the time of writing, they were no speculations made by Snyder and coworkers to describe the diastereoselectivity of the reaction with chiral acids. The desired product **30** was isolated in 6 steps from aldehyde **28** for a total of 15 steps and an overall yield of 2.8%.

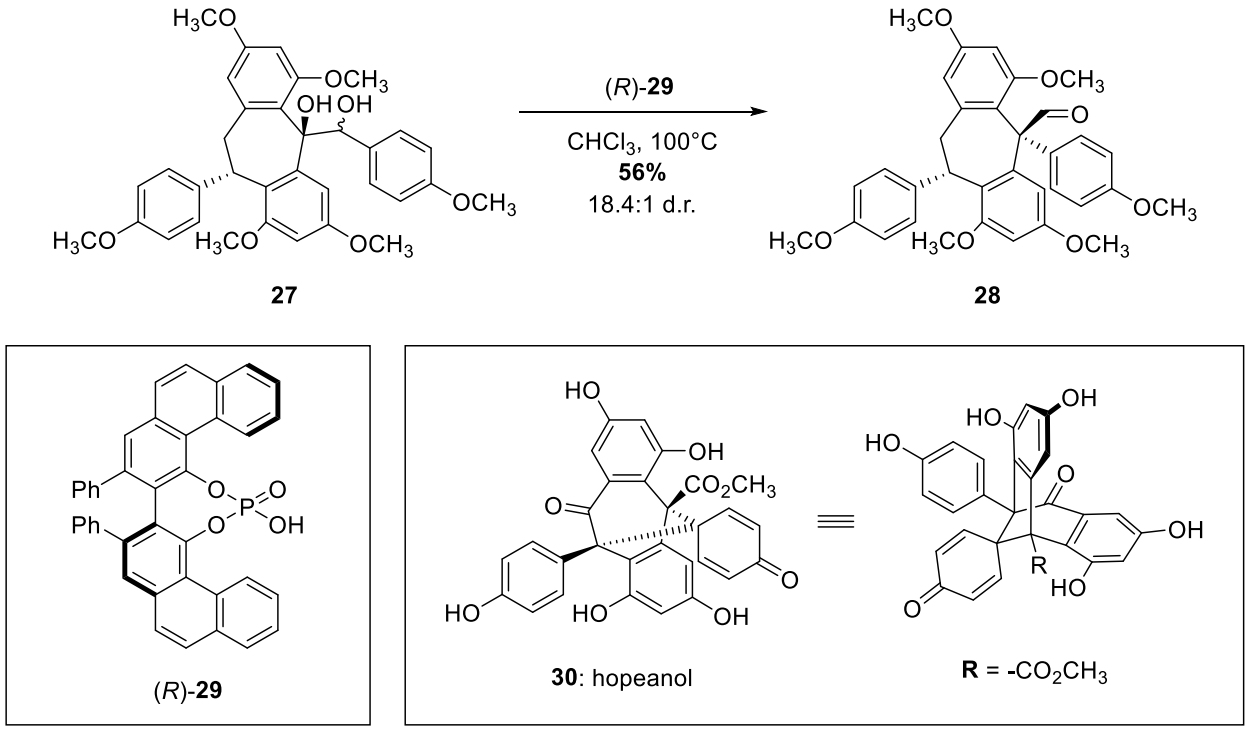

Scheme 10 Pinacol rearrangement with a chiral phosphoric acid, **29**, toward the synthesis of hopeanol.

1.4.0 - Semipinacol rearrangements

During retrosynthetic analysis, a chemist may envision using a pinacol rearrangement to achieve a desired structure or functional group, such as a ring contraction or expansion product. However, as previously discussed, an intended pinacol rearrangement may have a lack of regioselective control, especially if the adjacent functional groups are relatively inert or non-activating/stabilizing for the formation of a carbenium ion. Another possibility is that the diol required to carry out the expected rearrangement may be unstable and thus not isolable. Another hurdle to overcome is poor control of stereoselectivity due to the planarity of the carbocation intermediates generated. To overcome these challenges, a semipinacol rearrangement is often a better synthetic choice in practice. Semi-pinacol rearrangements are modified forms of the traditional pinacol rearrangement, utilizing diol-derived functionalities with a similar desired outcome to a pinacol rearrangement, but with high regio- and stereoselective control. Certain functionalities could be utilized to dictate regiochemistry, such as selective triflation of a 1,2-diol, while others, such as epoxides, would dictate the stereoselectivity of a rearrangement through predetermined geometry due to ring strain or other, similar, structural constraints.[3] Herein are presented illustrative examples of semipinacol rearrangements used in chemical studies and natural product synthesis from a variety of rearranging substrates including: vinylogous 1,4-diols, 2-heterosubstituted alcohols, allylic alcohols (realized through the Prins-pinacol rearrangement), epoxides, and α-hydroxy ketones.

1.4.1 – Rearrangement of Vinylogous Diols

An example of a semipinacol rearrangement of vinylogous 1,4-diols in natural product synthesis is the rearrangement of **31** to **32** (**Scheme 11**) by Baran and coworkers, which was employed as part of a

synthesis of ingenol (**34**).[14] A key derivative of **34** is the 2-methyl-2-butenoate ingenol Picato® (**33**), an FDA-approved pharmaceutical for the treatment of the precancerous skin condition actinic keratosis. Production of **33**, however, is limited to semisynthesis from **34** and isolation from natural sources with low isolation yields. While higher amounts of ingenol **34** can be found in natural sources, the quantities extracted are still too low for commercial demands. At the time of publication, synthetic efforts toward ingenol were elegant but lengthy. Requiring anywhere from 37 to 45 steps, production of **34** on a large scale was limited. Baran and coworkers set out to rectify this deficiency and developed a method to produce **34** in 14 steps, utilizing a vinylogous semipinacol rearrangement to generate the core [4.4.1]-bicycloundecane core of the molecule. The stereochemistry of **31** was set through 7 steps carefully constructing 5 stereocenters and 7 carbon-carbon bonds to the precursor olefin that was dihydroxylated with OsO_4 and protected with carbonyldiimidazol (CDI) as carbonate **31**. Initial conditions used were ineffective for performing the vinylogous rearrangement of **31** to ingenane **32**, but addition of boron trifluoride etherate ($BF_3{\cdot}Et_2O$) provided the desired product in 80% yield with the desired stereochemistry of the bicyclic core.

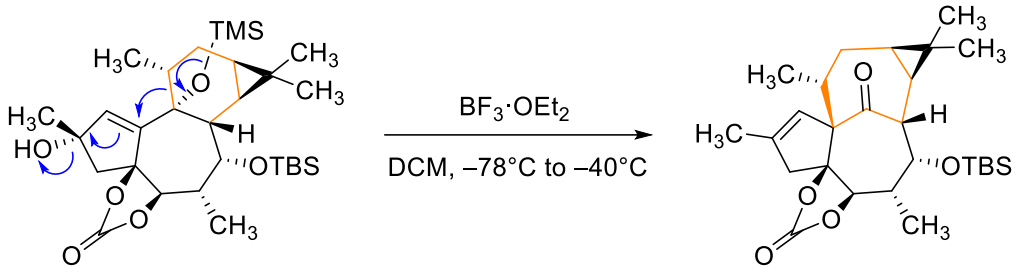

Scheme 11 Vinylogous pinacol rearrangement of **31** to **32**, forming the final 7-membered ring of ingenol **34**.

1.4.2 – Rearrangement of 2-Heterosubstituted Alcohols

A common example of 2-heterosubstituted alcohols that can undergo semipinacol rearrangement are 2-hydroxy sulfonates, as they are primed for 'dehydration' due to the stability of the sulfonate anion generated. Other 2-heterosubstituted alcohols include halogens, sulfides, selenides and diazonium salts.[3] In the divergent synthesis of four cembrane-type diterpenoids, Ding and coworkers[15] performed a pinacol rearrangement of a 2-hetereosubstituted, such as a mesylate, alcohol to acquire the [6,5,7]-tricyclic core of (–)-pavidolide B (**Scheme 12**, **38**) from diol precursor **35**. Initial attempts to isolate the desired ketone **37** rearrangement product through the mesylate with Lewis acids resulted in decomposition and an

intramolecular aldol cyclization of the sulfonate.[7] However, when the authors generated the triflate at the tertiary alcohol of **35** (highlighted in red, **Scheme 12**) and treated the molecule with potassium *t*-butoxide in *t*-butanol, they were able to fashion the desired core structure with 69% yield. From this precursor, **38** was provided following a lactonization and an epimerization of C11 from **37**.

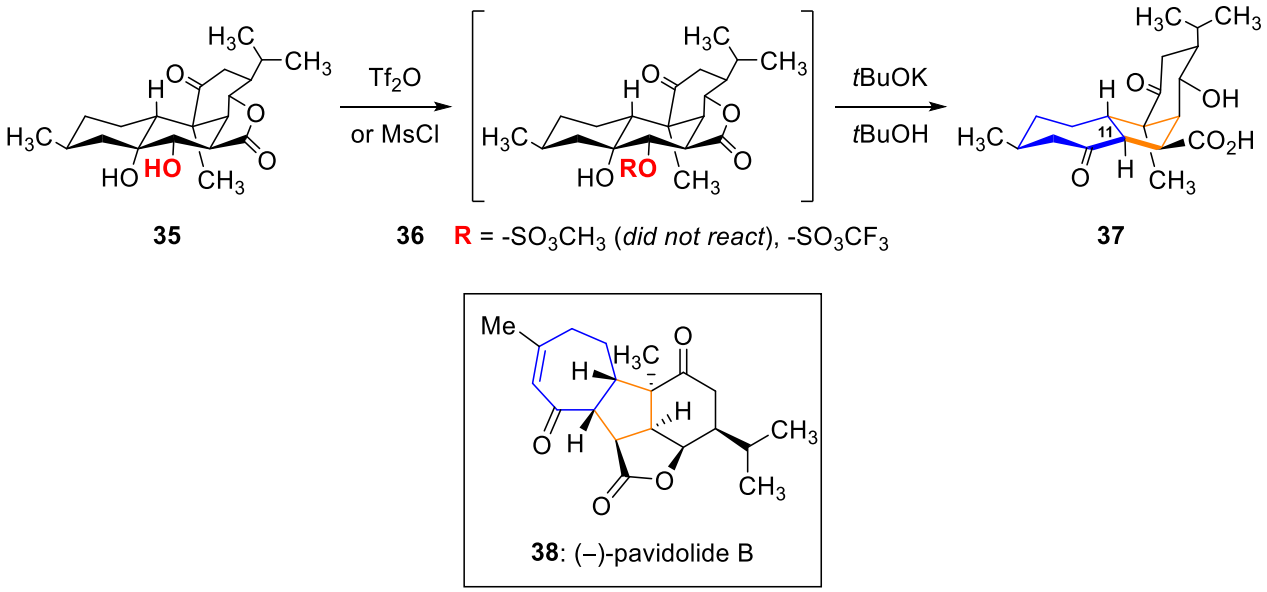

Scheme 12 2-Heterosubstituted ring-contraction/ring-expansion semipinacol rearrangement toward the synthesis of (−)-pavidolide B, fashioning two core cycles of the tetracyclic product.

1.4.3 – Chiral Phosphoric Acid Derivatives for Stereoselective Seminpinacol Rearrangements

In the case of Baran and coworkers' synthesis of ingenol (**34**), cyclic conformational constraints likely assisted in the generation of stereochemically preferred product. However, for acyclic vinylogous semipinacol rearrangements, stereo- and regiochemical outcomes can be ambiguous. Inspired by Antilla and coworkers' use of CPAs in the stereoselective rearrangements of indoyl diols, Zhu and coworkers set to develop a method of performing acyclic vinylogous semipinacol rearrangements through use of chiral Brønsted acids.[16] Using stereochemically pure diol **39** (**Scheme 13**) as a test substrate (largely due to the regiochemical influence imparted by both *p*-OCH_3-substituted phenyl groups), initial trials with chiral phosphoric acids in toluene provided β,γ-unsaturated ketone **40** in moderate yields (35 to 52%) and low enantiomeric excess (22-28% *ee*). When the authors changed the acid source to chiral phosphoramides (which are stronger Brønsted acids), they observed an increase in yields (72 to 99%) with optimization leading to the use of chiral phosphoramide **21** as the acid source. They posit that following protonation of the leaving hydroxyl group, the phosphoramide anion generated coordinates with the allylic cation that is generated, with the BINOL backbone of the chiral counterion dictating the stereochemistry of the migratory phenyl group. The rearrangement showed a wide tolerance for migrating substituents with varying aryl substitutions, including electron deficient *p*-trifluoromethylphenyl (68%, 90% *ee*) and electron rich *p*-methoxyphenyl (97% yield, 75% *ee*) substitution. Notably, while the *ee* was reduced (41% *ee*), benzyl migratory substituents were isolable in 72% yield. Directing substituents were limited to electron rich aryl substituents such as *p*-OCH_3 (as seen in the model substrate), 2- or 3-thiophenyl, or 3,4-dimethyoxyphenyl substituents. To demonstrate the use of the vinylogous rearrangement, Zhu and coworkers used ketone **39** to synthesize **41** and **42** (**Scheme 14**). Tetrahydrofuran **41** was isolated with

>20:1 diastereoselectivity through CBS reduction of the ketone with (*S*)-**43** and subsequent electrophilic-induced cyclization with NBS. Compound **42** was produced through reduction of the carbon-carbon double bond, reduction of the ketone with $NaBH_4$, and electrophilic aromatic substitution of the adjacent *p*-anisole substituent with generation of a carbocation through catalytic dehydration of the alcohol with trifluoroacetic acid.

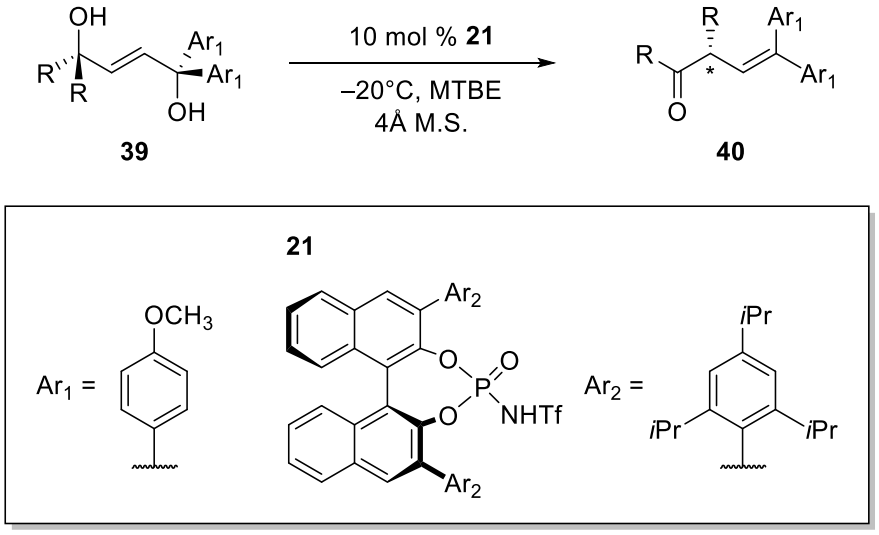

Scheme 13 Stereoselective acyclic rearrangement of vinylogous 1,4-diols.

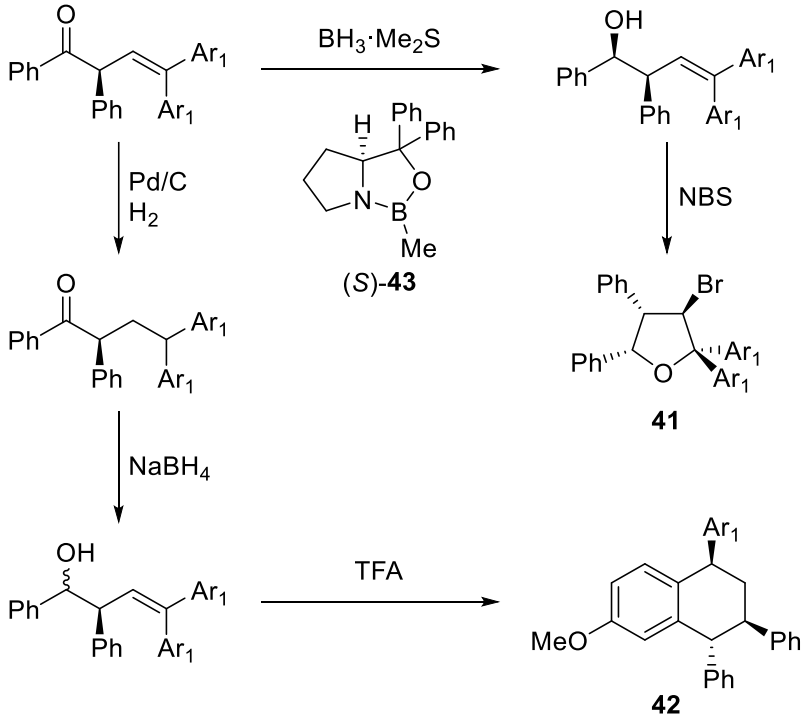

Scheme 14 Synthesis of synthetically interesting enantioenriched compounds **41** and **42**.

1.4.4 Prins-Pinacol Cyclizations

Another example of a semipinacol is the rearrangement of an allylic alcohol following the addition of an electrophile. Some electrophiles that can initiate these rearrangements include halonium ions, selenium cations, and Brønsted acids.[3] An excellent example of a widely-used allyl alcohol pinacol rearrangement is the Prins-pinacol rearrangement. The reaction is initiated through the addition of a carbenium to the carbon-carbon double bond of the allylic alcohol, priming the alcohol for 1,2-migration to form a furanyl molecule or carbocyclic aldehyde or ketone.[17] One of the earliest examples of one of these rearrangements is from 1969 when Mousset and coworkers discovered the pinacol terminated Prins reaction while trying to synthesize the acetonide of diol **44** (**Scheme 15**).[4,17,18] Instead, the condensation product **45** was generated and underwent a Prins cyclization to produce a carbocation at C3 of the dihydropyran core to set the stage for the pinacol rearrangement to produce tetrahydrofuran **47**. Gratifyingly, the Prins-pinacol cascade proceeds with high stereoselectivity, likely due to the chair-like geometry of intermediate oxonium **45**. Following the discovery of the Prins-pinacol rearrangement, Overman and coworkers have since worked extensively to expand the chemical space accessible through oxacyclic and carbocyclic annulations with the rearrangement.[17]

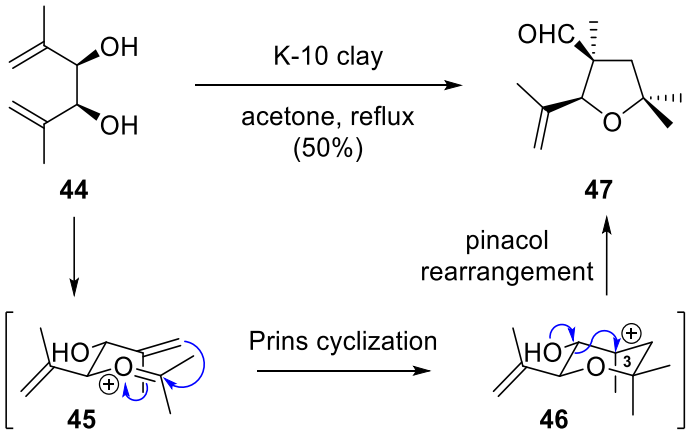

Scheme 15 Prins-pinacol rearrangement with following the condensation of acetone to diol **44**.

Much of our current understanding on pinacol and semipinacol rearrangements is due to the extensive work of the Overman group on these transformations.[18,19] In an early showcase of the chemistry they had developed, Overman and coworkers set out to synthesize sesquiterpene *trans*-kumausyne **48** (**Scheme 16**), an isolate from a family of red algae (genus *Laurencia*) located off the coast of Hokkaido, Japan.[20] Their synthesis started with what would later be referred to as the Prins-pinacol rearrangement, generating the tetrahydrofuran core of **48**. Diol **49** was then reacted with 2-(phenylmethoxy)acetaldehyde ($BnOCH_2CHO$) and PTSA to produce bicyclic tetrahydrofuran **52**. As with the rearrangement presented by Mousset, the cascade begins with condensation of the aldehyde to generate oxocarbenium intermediate **50,** which is primed for a Prins cyclization to generate carbocationic **51** with the carbocation at C4. Pinacol rearrangement of **51** yields the cis-fused, bicyclic **52**.

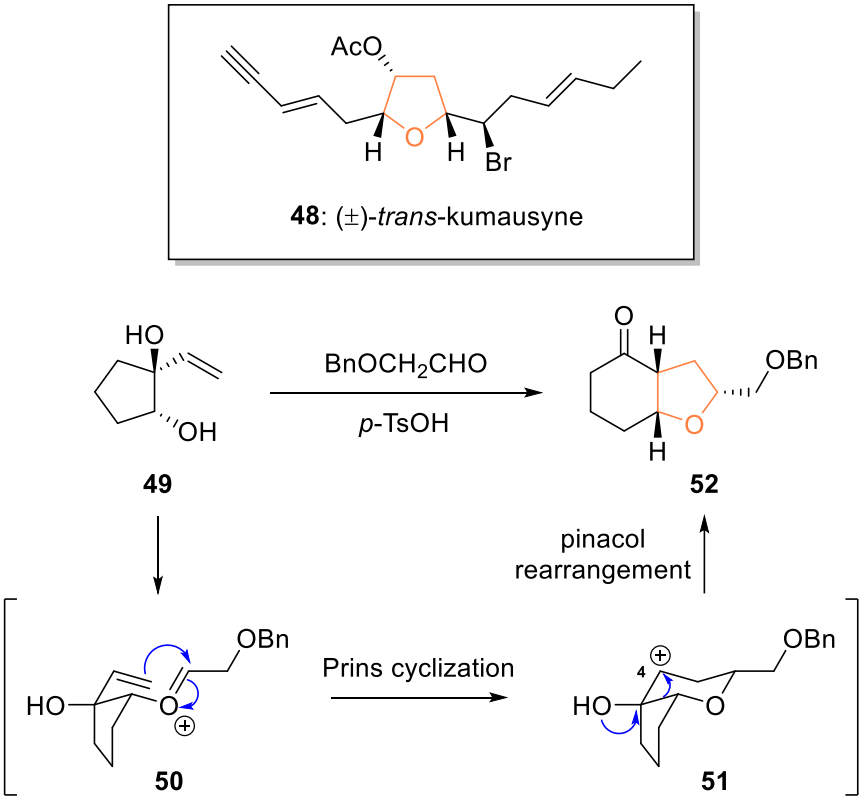

Scheme 16 Prins-pinacol rearrangement of **49** toward the synthesis of (±)-*trans*-kumausyne.

1.4.5 – Rearrangement of Hydroxy Epoxides

In a recent publication, Schindler and coworkers synthesized both (+)- and (−)-lingzhiol (**(+)-58**, **Scheme 18**).[21] In their retrosynthetic analysis, they envisioned a one-pot cascade semipinacol-reduction-lactonization from a hydroxy epoxide with treatment of triethyl aluminium to fashion the rotary-door product **54**. As shown in **Scheme 17**, the one-pot cascade was performed on a test substrate starting with semipinacol rearrangement of epoxide **53**, followed by a hydride transfer for the complexed triethyl aluminium to the aldehyde moiety, setting the stage for the anionic oxygen to react with the neighbouring ester to generate the desired rotary door motif for **58**. An important note is that the complexation of the diethyl aluminium conformationally restricts the remaining bicyclic structure to form the lactone on the bottom face of the molecule exclusively.

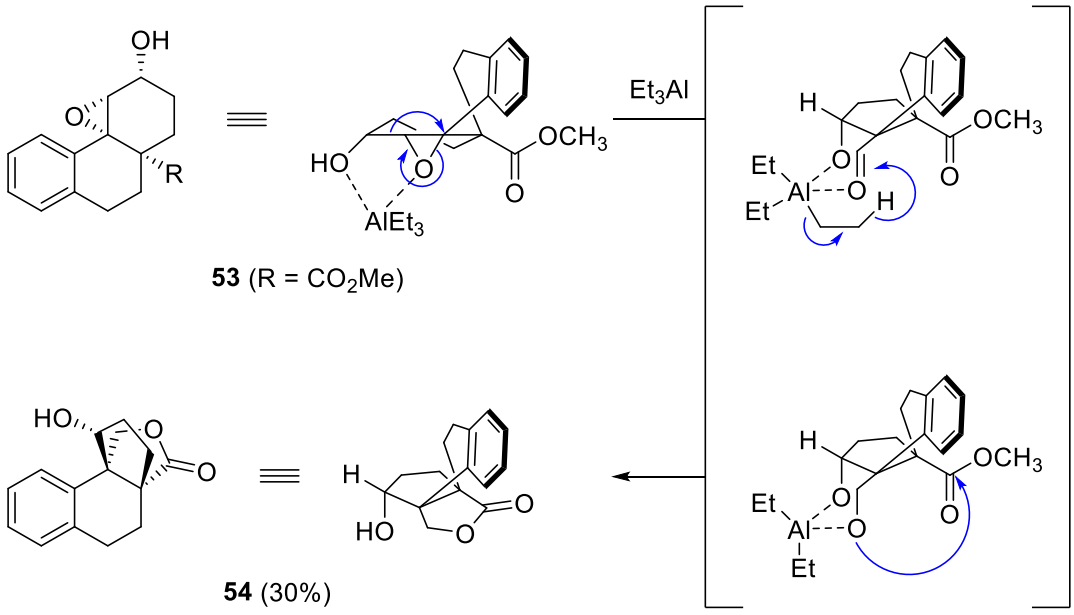

53 (R = CO_2Me)

54 (30%)

Scheme 17 One-pot cascade synthesis of model substrate **54**.

With the model substrate demonstrating the feasibility of the one-pot cascade reactions, Schindler and coworkers set out to utilize the conditions to synthesize **54** in the synthesis of **58** (**Scheme 18**). However, upon epoxidation of allyl alcohol **55** with *m*-chloroperoxybenzoic acid (*m*CPBA), the desired epoxide **56** was not isolated. The prematurely-rearranged aldehyde **57** was instead isolated in 70% yield as the epoxide **56** underwent semipinacol rearrangement upon epoxidation (possibly due to acidification with *m*CPBA). Aldehyde **57** was instead subject to the necessary reduction (with $NaBH_4$) and the lactonization upon workup with hydrochloric acid. An allylic oxidation fashioned the benzylic ketone and subsequent demethylation with *t*-butylthiol and aluminium chloride provided **58**.

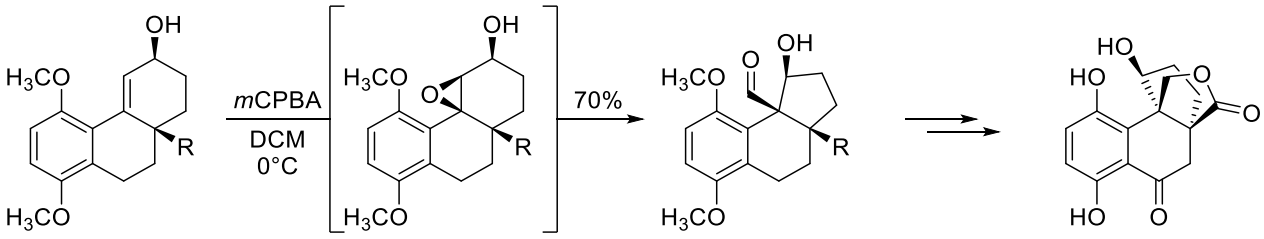

55 (R = CO_2CH_3) **56** (R = CO_2CH_3) **57** (R = CO_2CH_3) **58**: (+)-lingzhiol

Scheme 18 Pinacol rearrangement of a hydroxy epoxide toward the synthesis of (+)-linghzhiol.

An example of an α-hydroxy ketone semipinacol rearrangement can be found in the transannular generation of bicyclic tetrahydrofuran **62** by Oltra and coworkers.[22] From diol **59**, oxidation of the tertiary alcohol with Dess-Martin periodinane (DMP) provides α-hydroxy ketone **60**. In these reactions, epoxide ring-opening facilitates the transannular ring closure and thus ketone **60** was reacted with *m*-chloroperoxybenzoic acid (*m*CPBA) to produce epoxide **60**. Treatment of **60** with trimethylsilyl chloride (Me_3SiCl) and sodium iodide resulted in transannular cyclization and ring contraction leading to the formation of tetrahydrofuran **62**. The mechanism of the tandem reactions is initiated with coordination of the Lewis acid to the outward facing epoxide (as shown in **61**, **Scheme 19**).[3] With pushing of electrons

of the hydroxyl group to the generate a ketone, the adjacent carbon bond migrates to the carbonyl center (ring-contraction), priming the carbonyl for the transannulation that opens the epoxide ring to generate **62**.

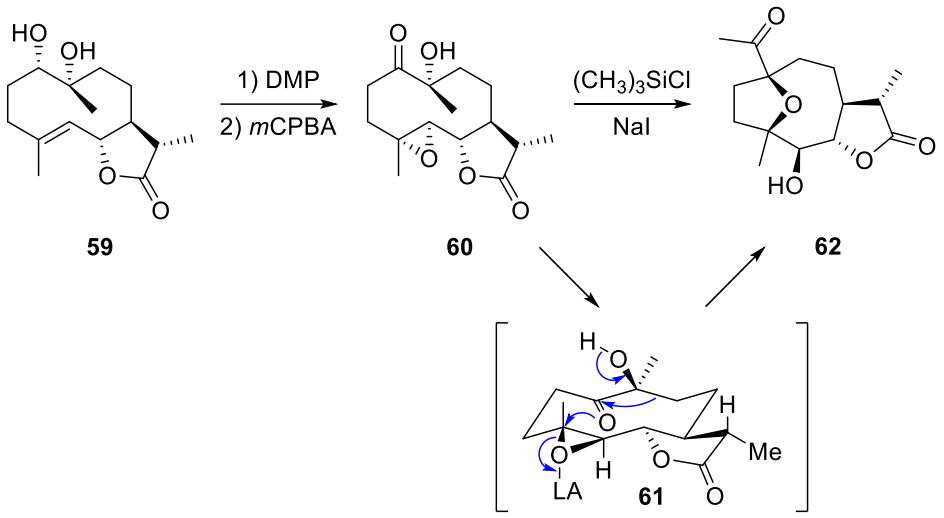

Scheme 19 Tandem transannulation and semipinacol rearrangement of **60**.

1.5.0 A C(sp^3)-C(sp^3) Extended Pinacol Rearrangement

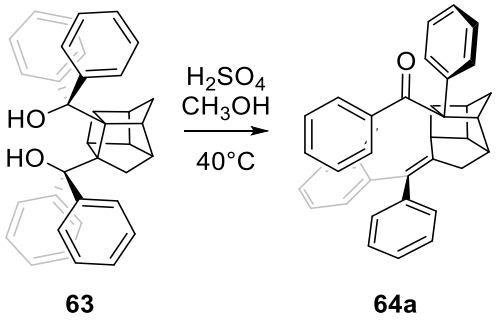

Scheme 20 1,4-extended pinacol rearrangement of the tetraphenyl Thiele cage diol.

In 2019, our group described a rearrangement over a sp^3-hybridized carbon – carbon bond within a bishomocubane derived from Thiele's ester (referred to as Thiele cage).[23] The result of treating a tetra-aryl substituted Thiele cage diol with a strong acid, such as sulfuric acid, afforded the formation of ketone **64a** as the major product, along with a minor side product (see Chapter 2). Surprisingly, diastereomers **64c-d** were not isolated, leading to the question: under which mechanism would a single diastereomer be provided? Pinacol rearrangements, and some semipinacol rearrangements, proceed through a carbocation intermediate followed by a 1,2-migration of a hydride, alkyl or aryl substituent. Following this mechanism, we propose the stepwise mechanism in **Scheme 21**. The elimination of either hydroxyl group through acidification with strong acid generates a carbocation at the benzylic position. Generation of the carbocation is then followed by a breakage of the C(sp^3)–C(sp^3) bond of the cyclobutane moiety that is attached to each of the quaternary alcohols. The bond breakage is facilitated by the formation of a C–C double bond and a release of strain within the bishomocubane core. An additional pathway is feasible at this point in the mechanism: given the close proximity of the remaining alcohol to the carbocation center

(perhaps through prearrangement of the substituents from hydrogen bonding interactions between the two hydroxyl groups), the oxygen could add to the carbocation through nucleophilic attack to produce a tetrahydrofuranyl Thiele cage structure **65**. Indeed **65** is isolable and observed during kinetic analysis through ^{1}H-NMR (see Chapter 3). The breaking of the C–C bond is followed by the migration of one of the aryl substituents from the remaining quaternary alcohol carbons to the adjacent tertiary carbocationic center, generating the ketone. According to the proposed mechanism, depending on the rotation of the quaternary alcohol, one of four possible diastereomers **64a-d** is produced.

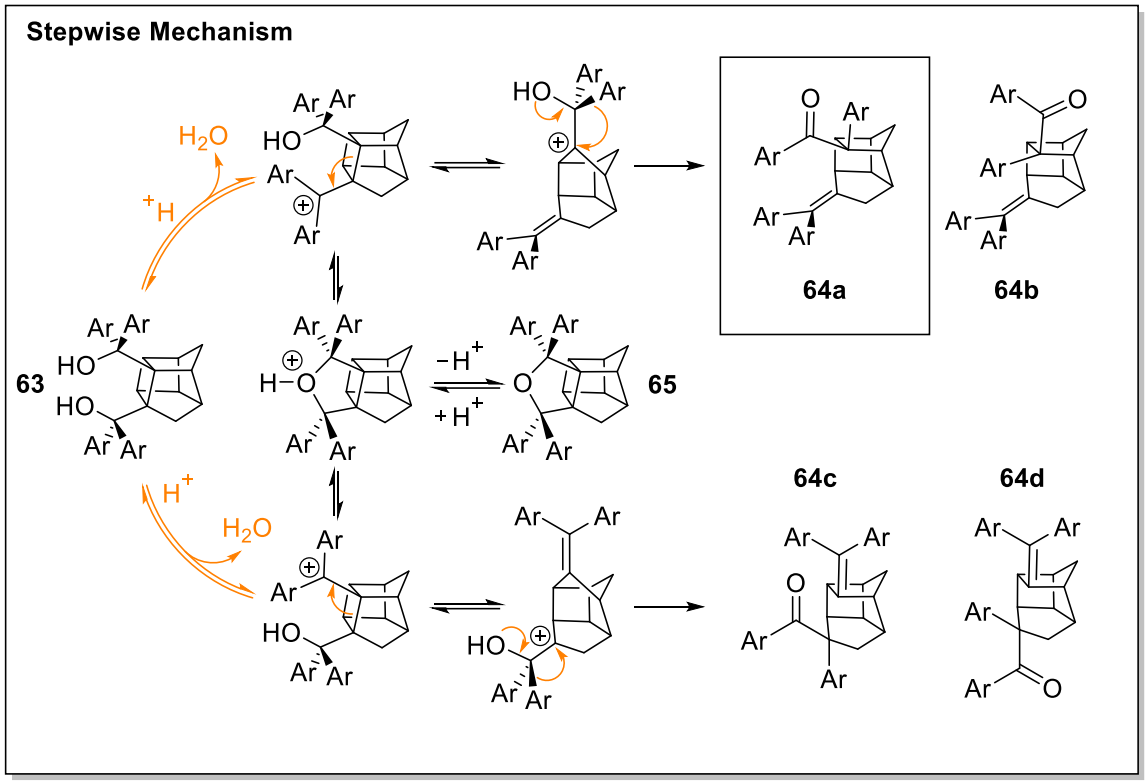

Scheme 21 Proposed stepwise mechanism for the observed 1,4-extended pinacol rearrangement of Thiele cage diols.

Despite the stepwise mechanism proposed suggesting a mixture of products, only **64a** of the 4 proposed diastereomers is isolated. To try to justify the regioselectivity of the rearrangement, a concerted mechanism was also proposed (**Scheme 22**). Following protonation of either one of the hydroxyl groups, the proton coordinates between both OH groups. The rotation of the quaternary alcohol centers are locked into position by the coordination to the proton, pre-arranging the migrating aryl group (**Aryl A**) to be antiperiplanar to the breaking C(sp^3)-C(sp^3) bond. Electrons would then move from the oxygen of the top-faced hydroxyl group to the C–O bond, with concurrent 1,2-migration of **Aryl A** to the adjacent carbon, breaking the C–C bond, pushing towards the other quaternary center generating a carbon double bond while water is released as a leaving group.

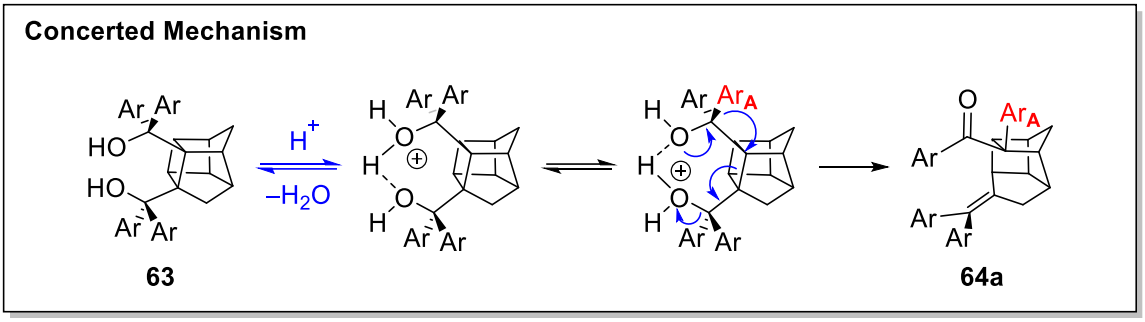

Scheme 22 Proposed concerted mechanism for the observed 1,4-extended pinacol rearrangement of Thiele cage diols.

In this thesis, the identification of a minor product of the aliphatic extended pinacol rearrangement will be described along with discussion of the product's implication on the proposed mechanism. The synthesis and analysis of a Hammett series of substrates via ^{1}H-NMR kinetics will be used to better understand the mechanism and to propose a final mechanism based on the kinetic analysis. Should the rearrangement occur through a carbocation intermediate, we would expect to see higher rates of reaction with electron-rich substituents since they would stabilize the carbocation intermediate indicating a more stepwise-like rearrangement. With a better understanding of the rearrangement and its mechanism, we can look toward the development of more general extended pinacol rearrangements for use towards synthetically interesting targets.

1.6.0 - References

1. Fittig, R. *Liebigs Ann. Chem.* **1860**, *114*, 54-63.
2. Butlerov, A. *Liebigs Ann. Chem.* **1873**, *170*, 151-162.
3. Song, Z.-L.; Fan, C.-A.; Tu, Y.-Q. *Chem. Rev.* **2011**, *111*, 7523-7556.
4. Gao, A.X.; Thomas, S.B.; Snyder, S.A. Pinacol and Semipinacol Rearrangements in Total Synthesis. In *Molecular Rearrangements in Organic Synthesis*, First Edition, Rojas, C.M., ed.; Wiley, **2016**; pp 3-33.
5. Gualandi, A.; Cozzi, P.G. *Synlett.* **2013**, *24*, 281-296.
6. Pettit, G.R.; Lippert, J.W., 3rd; Herald, D.L. *J. Org. Chem.* **2000**, *65*, 7438-7444.
7. Suzuki, K.; Takikawa, H.; Hachisu, Y.; Bode, J.W. *Angew. Chem. Int. Ed.* **2007**, *46*, 3253-3254.
8. Li, J.; Jeong, S.; Esser, L.; Harran, P.G. *Angew. Chem. Int. Ed.* **2001**, *40*, 4765-4769.
9. Liang, T.; Zhang, Z.; Antilla, J.C. *Angew. Chem. Int. Ed.* **2010**, *49*, 9734-9736.
10. Falcone, B.N.; Grayson, M.N.; Rodriguez, J.B. *J. Org. Chem.* **2018**, *83*, 14683-14687.
11. Rueping, M.; Uria, U.; Lin, M.-Y.; Atodiresei, I. *J. Am. Chem. Soc.* **2011**, *133*, 3732-3735.
12. Wu, H.; Wang, Q.; Zhu, J. *J. Am. Chem. Soc.* **2019**, *141*, 11372-11377.
13. Snyder, S.A.; Thomas, S.B.; Mayer, A.C.; Breazzano, S.P. *Angew. Chem. Int. Ed.* **2012**, *51*, 4080-4084.
14. Jørgensen, L.; McKerrall, S.J.; Kuttruff, C.A.; Ungeheuer, F.; Felding, J.; Baran, P.S. *Science*, *341*, 878-882.
15. He, C.; Xuan, J.; Rao, P.; Xie, P.-P.; Hong, X.; Lin, X.; Ding, H. *Angew. Chem. Int. Ed.* **2019**, *58*, 5100-5104.
16. Wu, H.; Wang, Q.; Zhu, J. *Angew. Chem. Int. Ed.* **2016**, *55*, 15411-15414.
17. Overman, L.E.; Pennington, L.D. *J. Org. Chem.* **2003**, *68*, 7143-7157.
18. Martinet, P.; Mousset, G. Michel, M. *C. R. Acad. Sci. Paris, Ser. C* **1969**, *268*, 1303-1306.
19. Overman, L.E. *Tetrahedon* **2009**, *65*, 6432-6446.
20. Brown, M.J.; Harrison, T.; Overman, L.E. *J. Am. Chem. Soc.* **1991**, *113*, 5378-5384.

21. Riehl, P.S.; Richardson, A.D.; Sakamoto, T.; Schindler, C.S. *Org. Lett.* **2020**, *22*, 290-294.
22. Rosales, A.; Estevez, R.E.; Cuerva, J.M.; Oltra, J.E. *Angew. Chem. Int. Ed.* **2005**, *44*, 319-322.
23. Dao, N.; Sader, J.K.; Oliver, A.G.; Wulff, J.E. *Chem. Commun.* **2019**, *55*, 1600-1603.

Chapter Two
Characterization of a Side Product and its Mechanistic Implications

2.0.0 – Contributions

Compound **68** was isolated and characterized by Austin Burman.

Compound **69** was isolated by Jonathan Sader and characterized by Austin Burman.

2.1.0 – Isolation of an Unidentified Side Product

For a typical pinacol rearrangement, diastereoselectivity is often difficult to control. Preferential formation of a diastereomer is formed either through extenuating circumstances, such as ring strain, or through the use of chiral catalysts such as chiral phosphoric acids as shown in **Scheme 23a**.[1] It is curious, then, that the Thiele cage diols, previously isolated by our group and observed to undergo a diastereoselective extended pinacol rearrangement, would form a single diastereomer under acidic conditions. By analyzing the structure and proposing a mechanism, we would expect that a mechanism that proceeds through a carbocation intermediate would result in a mixture of the four diastereomers. A concerted mechanism could produce a single diastereomer but would seem unlikely given the propensity of the oxonium generated through protonation of an alcohol to leave and form a carbocation. This discrepancy led to our studies on how varying aryl substituents, from electron-rich to electron-poor, would affect the rate of reaction based on the stabilization effects of said substituents on a carbocation. While analyzing two of the species, diols **63** (**Scheme 23b**) and **66** (**Scheme 24**), we noted that there appeared to be an unaccounted-for side product.

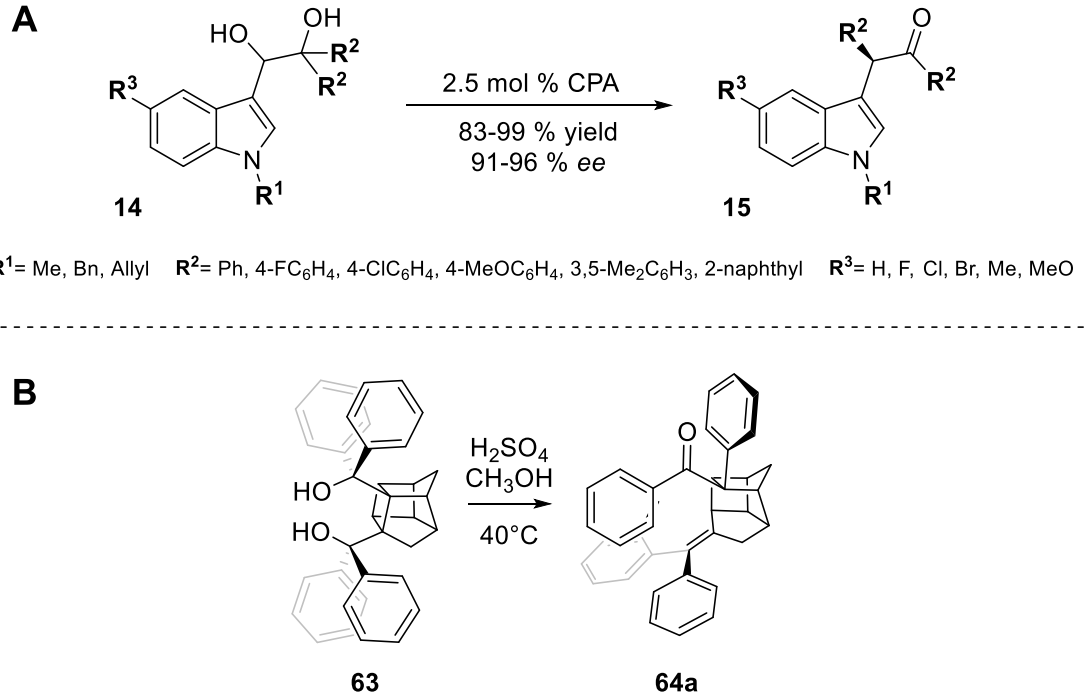

Scheme 23 Reaction **A** shows the use of a chiral phosphoric acid (CPA) for an enantioselective pinacol rearrangement. Reaction **B** shows the rearrangement of **63** to a single diastereomer, **64a**.

In the initial analysis of the rearrangement *in situ*, we noted that there was an unexpected loss of material. While there is some degradation of material at elevated temperatures over extended periods of time, as noted in the isolation yields of the rearrangement products, the loss of material seen in the early stages of the rearrangement process accounted for about 5 to 10% of the starting material at the beginning of the reaction.[1]

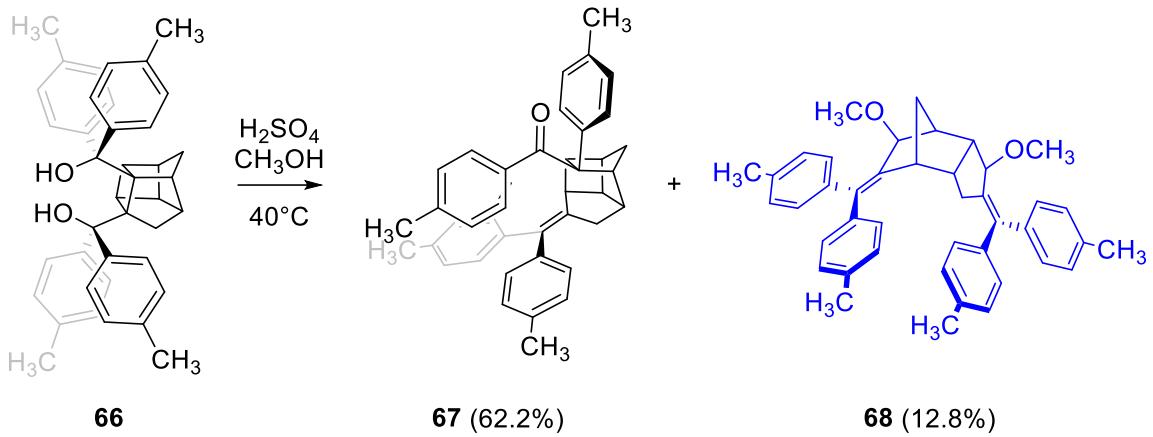

66 **67** (62.2%) **68** (12.8%)

Scheme 24 Rearrangement of diol **66** to major product **67** and the side product **68** in blue.

During the preparation of the rearrangement product from the tetraphenyl Thiele cage diol,[1] an unidentified side product was isolated. While the resonances in the alkyl region (0 to 3 ppm) of the side product's ^{1}H-NMR spectra were well resolved, resonance crowding was observed in the aromatic region (6 to 8 ppm) as shown in **Figure 1**. Ambiguity from overlapping aryl resonances made initial attempts to identify the structure difficult. Included as a part of the Hammett series for kinetic studies (described in Chapter 3), the *p*-tolyl Thiele cage diol **66** was reacted similarly with sulfuric acid in methanol at 40°C (**Scheme 24**) to isolate the previously unidentified side product with the expectation that the para-substitution would resolve certain regions in the spectra. Along with the major product **67** (in 62% yield), side product **68** was isolated in 13% yield and characterized. As expected, the inclusion of a methyl group helped to resolve the aromatic region of the ^{1}H-NMR spectra, but the resonances corresponding to the 4 methyl groups occupied part of the alkyl region (2.25 to 2.38 ppm) resulting in crowding around the resonances corresponding to protons in the core of the molecule (**Figure 2**). In addition to resonance crowding, the other alkyl peaks were not as resolved as they were in the phenyl derivative **69** (**Figure 1**). To solve the structure of this side product, ^{1}H–^{1}H correlation spectroscopy (COSY), ^{1}H–^{13}C heteronuclear single quantum coherence (HSQC), ^{1}H–^{13}C heteronuclear multi bond correlation (HMBC), and ^{1}H–^{1}H 1D–selective gradient nuclear Overhauser effect (1D-NOE) spectra from both isolated side products were used alongside mechanistic considerations. Using the collective data, the assignments of each of the resonances to their corresponding H and C shown in **Table 1** were made to identify product **68** and **69** in **Table 2**.[2-5] Product **68** was confirmed by high resolution mass spectrometry using electron spray ionization (ESI-HRMS – calculated for $[M+Na]^{+}$: 603.3234, found: 603.3233) with a notable fragmentation peak of M^{+}=549.3152, indicating the loss of an OCH_3 group during the ionization process.

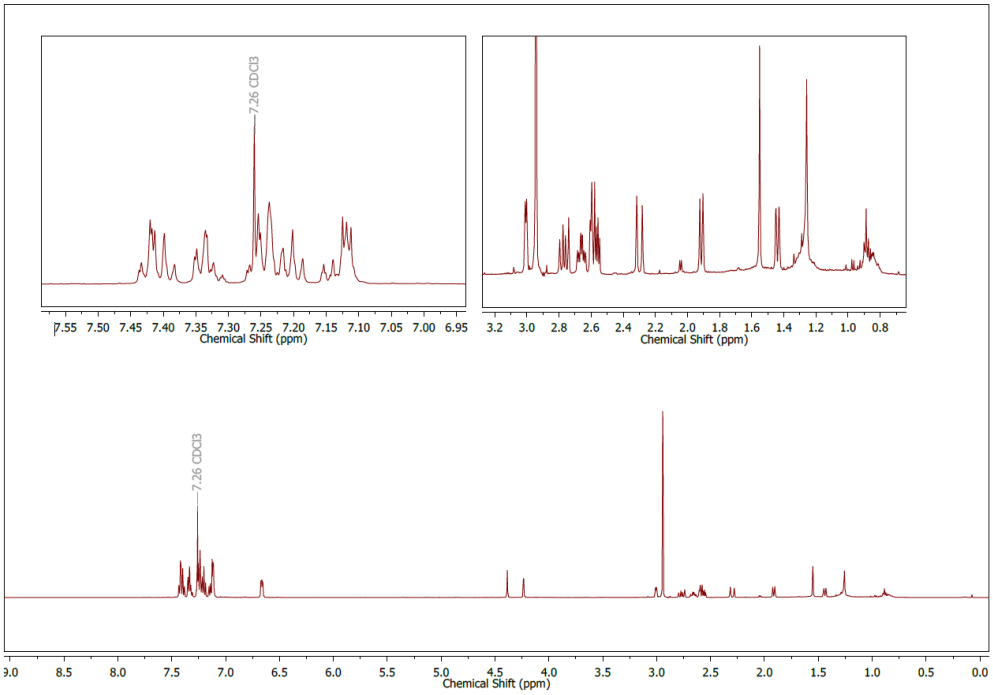

Figure 1 The ^{1}H-NMR spectra of compound **69**. Note the resonance crowding around the chloroform solvent peak, in the aromatic region. The resonances are difficult to distinguish due to overlapping multiplets from the phenyl substituents.

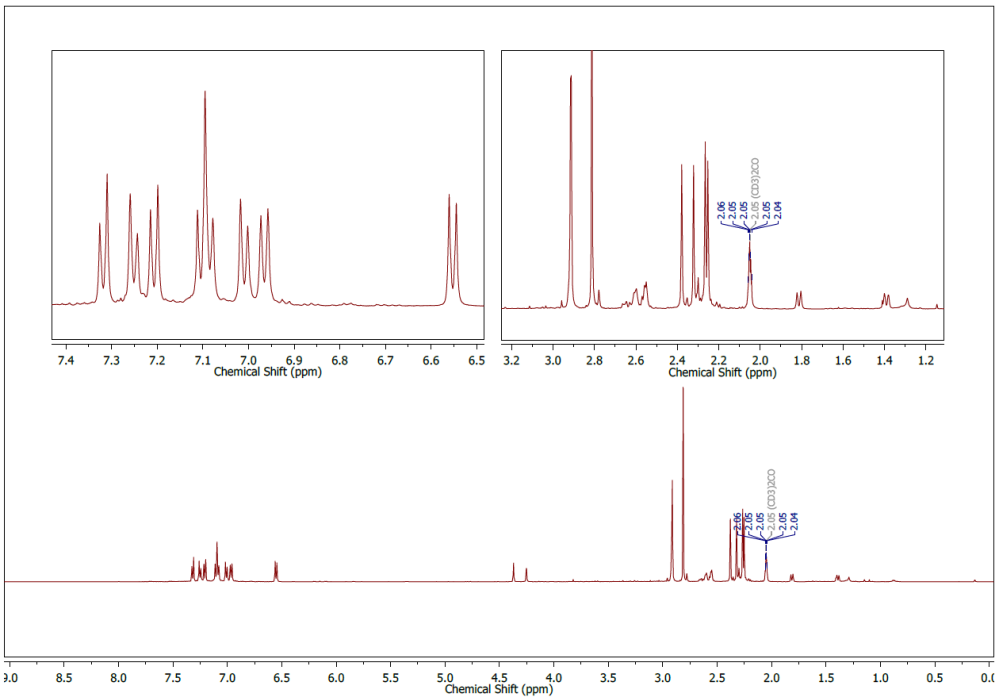

Figure 2 The ^{1}H-NMR spectra of compound **68**. Note the resonance crowding around the acetone peak ($(CHD_2)_2CO$ = 2.05 ppm), in the alkyl region. The resonances for the methyl groups from 2.20 to 2.40 ppm are overlapping with resonances corresponding to the core of the side product. Additionally, the resonance for one of the methoxy (OCH_3) substituents overlaps with a key resonance that is resolved in **69** at 3.01 ppm.

2.2.0 – ^{1}H and ^{13}C NMR Assignments for Compound 68 and 69

Compound 68

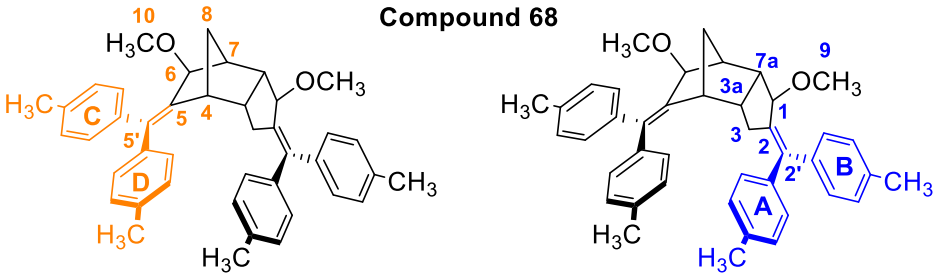

#	^{1}H	^{13}C
4	2.94	46.09
5	-	141.51
5'	-	138.40
6	4.25	79.28
7	2.59	43.99
8	1.39/1.81	37.50
10	2.92	56.63

#	^{1}H	^{13}C
1	4.37	82.25
2	-	143.09
2'	-	137.20
3	2.65	33.08
3a	2.62	43.80
7a	2.55	49.42
9	2.91	54.74

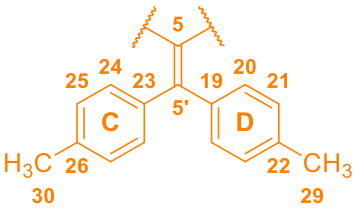

#	^{1}H	^{13}C
19	-	135.52
20	6.55	129.19
21	6.97	128.66
22	-	140.37
23	-	135.35
24	7.10	128.54
25	7.01	127.73
26	-	140.10
29	2.25	20.21
30	2.27	20.23

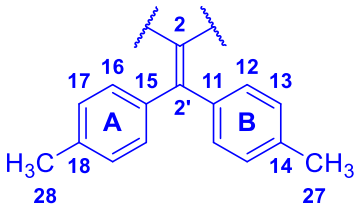

#	^{1}H	^{13}C
11	-	136.13
12	7.32	129.57
13	7.25	128.72
14	-	140.21
15	-	136.30
16	7.21	129.95
17	7.09	128.03
18	-	139.67
27	2.38	20.27
28	2.27	20.23

Table 1 ^{1}H and ^{13}C assignments for the *p*-tolyl side product **68** – Assignments are based on observed HMBC and HSQC correlations. The chemical shifts for the ^{1}H and ^{13}C nuclei are in parts-per-million (ppm).

Compound 69

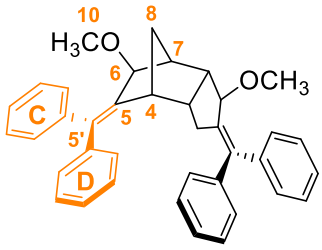

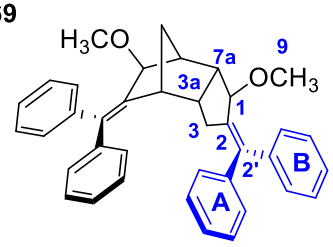

#	^{1}H	^{13}C
4	3.01	46.01
5	-	142.06
5'	-	139.39
6	4.23	79.76
7	2.57	44.32
8	1.44/1.91	38.21
10	2.94	57.74

#	^{1}H	^{13}C
1	4.39	82.88
2	-	142.10
2'	-	137.94
3	2.77	33.44
3a	2.66	44.06
7a	2.30	49.63
9	2.94	56.07

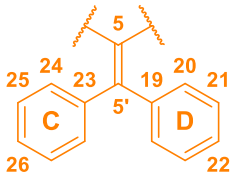

#	^{1}H	^{13}C
19	-	142.77
20	6.65-6.67	129.42
21	7.11-7.12	128.15
22	7.11-7.12	126.35
23	-	142.74
24	7.24-7.25	127.74
25	7.19-7.20	127.58
26	7.14-7.15	126.42

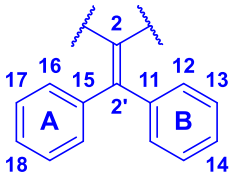

#	^{1}H	^{13}C
11	-	142.99
12	7.42-7.43	129.84
13	7.38-7.40	130.21
14	7.32-7.35	126.92
15	-	143.86
16	7.32-7.35	127.03
17	7.38-7.40	128.03
18	7.24-7.25	128.79

Table 2 ^{1}H and ^{13}C assignments for the phenyl side product **69** – Assignments are based on observed HMBC and HSQC correlations. The chemical shifts for the ^{1}H and ^{13}C nuclei are in parts-per-million (ppm).

2.3.0 – Determination of the Side Product Through 2D NMR Techniques

Some of the key correlations for establishing the structure of the dicyclopentane core of the side product were determined by observing correlations from the four tolyl substituents to the vinyl carbon centers. The most notable correlations are of the *ortho* proton resonances of the aryl substituents to resonances for **C2'** and **C5'** as shown in **Figure 3**. In the HMBC spectra for **68**, protons **H16** and **H12** both correlate to **C2'**, identified as a vinyl carbon due to the absence of its resonance in the DEPT-135 spectra, lack of HMBC correlations from the tolyl CH_3 groups resonance, and its chemical shift of 137.20 ppm.[6] Protons **H20** and **H24** similarly correlate to vinyl **C5'**. We have labelled the aryl group with **H16** as **Aryl A**, the group with **H12** as **Aryl B**, the group with **H24** as **Aryl C**, and the group with **H20** as **Aryl D.** For each of these protons, their resonances correlate to the respective meta proton resonance for their aryl group in the COSY spectra, further confirmed by a correlation of the CH_3 proton resonances to the meta carbon resonances. From a mechanist perspective, these connections imply elimination of both hydroxyl groups instead of a 1,2-migration of an aryl substitution.

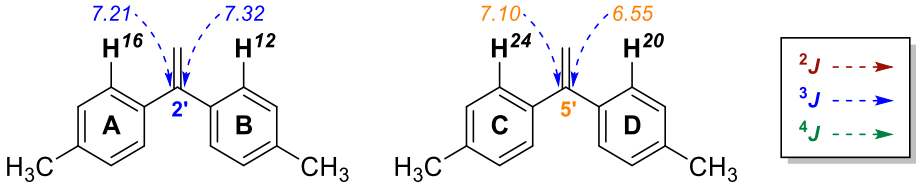

Figure 3 HMBC correlations of **H12**, **H16**, **H20**, and **H24**.

Many key assignments were made based on HMBC correlations stemming from the interactions of carbinol protons **H1** (a singlet) and **H6** (a doublet) with nearby carbons (**Figure 4**). The resonance of proton **H1** correlates to the resonance of **C9**, the methoxy substituent attached to **C1**. Correlation to methylene **C3** and bridgehead **C3a** of the cyclopentane indicates that **H1** is on the *endo* cyclopentyl moiety of the dicyclopentane core. Correlation to **C2'** situates aryl groups **A** and **B** at the *endo*-cyclopentane adjacent to **C1**. Selective pulsing at the frequency of **H1** (4.47 ppm) through 1D-NOE shows spin polarization transfer to **H12**, the ortho proton of **Aryl B**, placing **Aryl B** cis relative to **H1**.[5] In the 1D-NOE spectra, there is also an observable interaction of **H1** to bridgehead **H7**, indicating **H1** is facing inward toward the core, setting the stereochemistry of the carbinol center as *exo*.

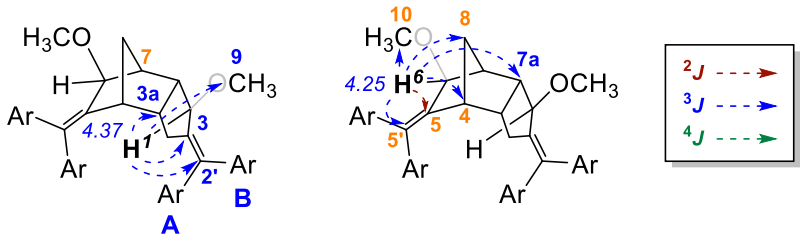

Figure 4 HMBC correlations from **H1** and **H6**.

For **H6**, the correlation of its resonance to bridging the methylene **C8** resonance situates the carbinol center **C6** on the left side of the molecule, allylic to **C5**. Correlations to resonances **C5** and **C5'** place aryl substituents **C** and **D** adjacent to **C6**, though selective pulsing of **H6** in a 1D-NOE experiment does not reveal the relative geometry of the alkene. While ^2J correlations are uncommon in HMBC, the cross-peak of resonances **H6** to **C5** may arise from a spin transfer from the interaction of **H1** to **C4**, another

observed correlation in the HMBC data.[4] Correlation to the resonance of **C7a** places it adjacent to **C3a** as a bridgehead to the *endo*-cyclopentane, though assignments of **C3a** and **C7a** are made clearer when looking at correlations to the resonances of the bridging methylene's protons, **H8** and **H8'**.

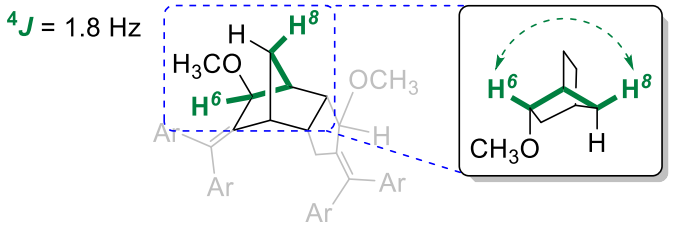

Figure 5 COSY correlation of **H6** and **H8**, consistent with ^4J coupling with a frequency of 1.8 Hz. The W-shape of the dicyclopentane core between **H6** and **H8** is highlighted in green.

The initial assignment of **H8** and **H8'** was made based on their coupling to each other (^2J = 9.3 Hz) and a lack of coupling to bridgehead protons, **H4** and **H7**, due to their relative dihedral angles.[8] The ^{1}H-^{1}H correlated spectroscopy (COSY) correlation of the resonance of **H6** to the resonance of **H8** also informs the stereochemistry of the carbinol center **C6** since it has the appropriate geometry for the ^4J coupling (W-coupling) with a frequency of 1.8Hz (**Figure 5**).[8,9] The correlation of **H6** to **H8** is shown in both COSY spectra of **68** and **69**, but due to peak broadening, **H6** appears as a broad singlet in the ^{1}H-NMR spectra of **68**. In the ^{1}H-NMR spectra of **69** the peak appears as a narrow doublet. Considering the COSY correlation of **H6** to **H8**, **H8** is positioned pointing toward the *endo*-cyclopentane moiety. As shown in **Figure 6**, Proton **H8** shows correlations to **C5** and **C6**, while **H8'** correlates to **C3a** and **C7a**. Correlation of the **H8** resonance to the **C5** resonance confirms its connectivity with **C6** and **C5'** on the Western half of the molecule.

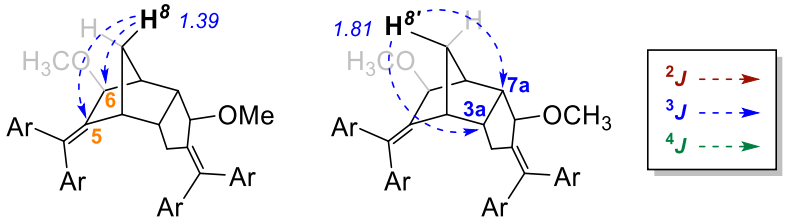

Figure 6 HMBC correlations of **H8** and **H8'**.

For **H3a**, there was a strong observed cross-peak to the **C2** resonance, with weaker ^3J correlations to resonances of **C1** and **C5**, perhaps from poor spin transfer interactions due to the bond angles of the bridgehead C–H bonds.[7] There are also observable ^2J correlations of the resonance of **H3a** to the resonances of **C3**, **C4**, and **C7a**. Proton **H3a** appears as a triplet of doublet of doublets, borne from coupling to protons **H3**/**H3'**, **H4,** and **H7a**. The ^{1}H–^{1}H coupling likely results in an enhanced ^2J correlation signal in the HMBC spectra for the respective carbons to **H3a** through spin polarization transfer.[4] The HMBC correlations of **H7a** are largely ^3J, with correlation to resonances of **C2**, **C3**, **C4**, and **C6**, and a ^2J correlation to the resonance of **C1**. The correlations of **H3a** and **H7a** to the carbons of the Eastern half of the molecule comfortably place the two protons at the bridgehead positions adjacent to **C4** and **C7** respectively.

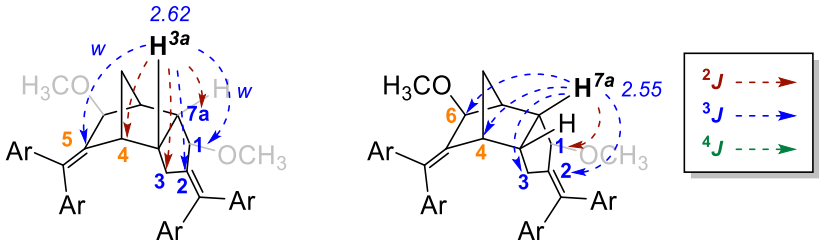

Figure 7 HMBC correlations of **H3a** and **H7a**. Note: the angle of **H3a** in the figure is not representative of the actual angle of the C–H bond of **H3a** to **C3a**.

The methylene protons of the *endo*-cyclopentane ring, *endo*-**H3** and *exo*-**H3'** (**Figure 8**), bear key correlations in the HMBC spectra that position **C4** between carbons **C3a** and **C5**. Correlations of resonances of **H3** to **C1, C2', C4**, and **C7a** help to solidify the assignments already made on the Eastern half of the molecule. Correlations of **H3'** to **C2** and **C3a** resonances are observed, alongside ^{2}J correlation to the resonances **C3a** and **C2**. The ^{2}J correlations are likewise observed for **H3**. From the 1D-NOE spectra of **H3**, through-space correlation of **H3** to **H4** positions both protons to be within proximity of each other (hence the *endo* assignment of **H3**). Small correlations to carbinol protons **H1** and **H6** are observed, collating the assignment of the *exo*,*exo*-diastereomer **68/69**. There is of course correlation to **H3'** and a slight correlation to **H3a**, likely resulting from spin transfer from the interaction of **H3a** to **H3'** and **H3'** to **H3**.[4] There is also a notable, observable 1D-NOE correlation of **H3** to **H16** (*ortho*-proton of **Aryl A**) and **H20** (*ortho*-proton of **Aryl D**) which informed the placement of **Aryl A** and **Aryl D** relative to the dicyclopentadienyl core of the molecule (**Table 1**).

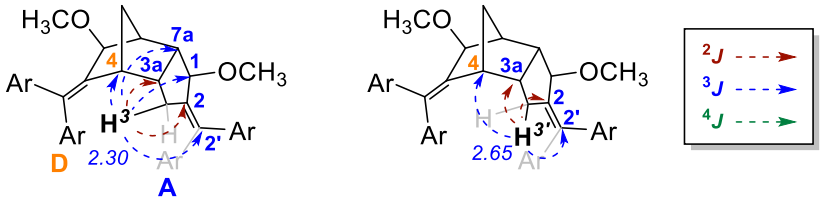

Figure 8 HMBC correlation of **H3** and **H3'**.

Finally, the HMBC correlations of **H4** and **H7** are shown in **Figure 9**. The correlations of the resonance of **H4** to the resonances of **C5'**, **C6**, and **C7a** comfortably situate **H4** three bonds away from each carbon at the norbornene bridgehead **C4**. Correlation of the resonance of **H7** to the resonance of **C1** place it opposite to **H4**. Both of the resonances of **H4** and **H7** also show a ^{3}J correlation to the carbon resonance bearing the other proton (**H4** to **C7** and vice-versa), further confirming their positions at the bridgehead carbon centers.

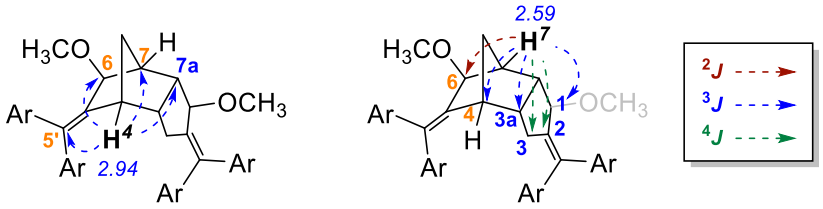

Figure 9 HMBC correlations of **H4** and **H7**.

2.4.0 – Mechanistic Implications of the Side Product on the Extended Pinacol Rearrangement

The proposed mechanism for the formation of the side product is shown in **Scheme 24** to justify the formation of the alkene moieties at both ends of the dicyclopentane core. From diol **63**, the mechanism follows the same initial step as the proposed mechanism for the extended pinacol rearrangement: protonation of either OH group results in the generation of a benzylic carbocation **I**. Facilitated by the release of ring strain and formation of the alkene on one face of the core, the bishomocubane opens to produce the second benzylic carbocation **II**, with the charge vicinal to the remaining OH. Though methanol could react with the carbocation to generate a quaternary ether, steric congestion at the core of the molecule due to the cupped-hand-like nature of the cage structure would impede the attack. From the ring-opened carbocation **II**, release of the cyclobutene ring-strain would drive the reaction forward to generate the resonance stabilized allylic cation **III**. Nucleophilic attack of methanol at the β-position of the allylic carbocation quenches the positive charge, providing the first carbinol center at **C1** in molecule **IV**. The remaining OH group is then protonated to the corresponding oxonium and leaves as water, affording the second allylic cation on **V**. As with the previous carbinol center, **C6** is generated with addition of methanol at the β-position of the allylic carbocation, resulting in side product **70**. It is likely that formation of the *endo*-**C6** diastereomer would be prevented through steric clashing with the Eastern half of the molecule on the opposite side of the molecule and so **68** and **69** were isolated as the *exo*-**C6** diastereomers. For many of the HMBC correlations, assignments were made using the spectra from **69** due to better baseline separation of the dicyclopentane core peaks with confirmation from the HMBC correlations for **68**. 1D-NOE correlations from **69** were also used to justify assignments of aryl substituent placement on the exocyclic C=C double bonds.

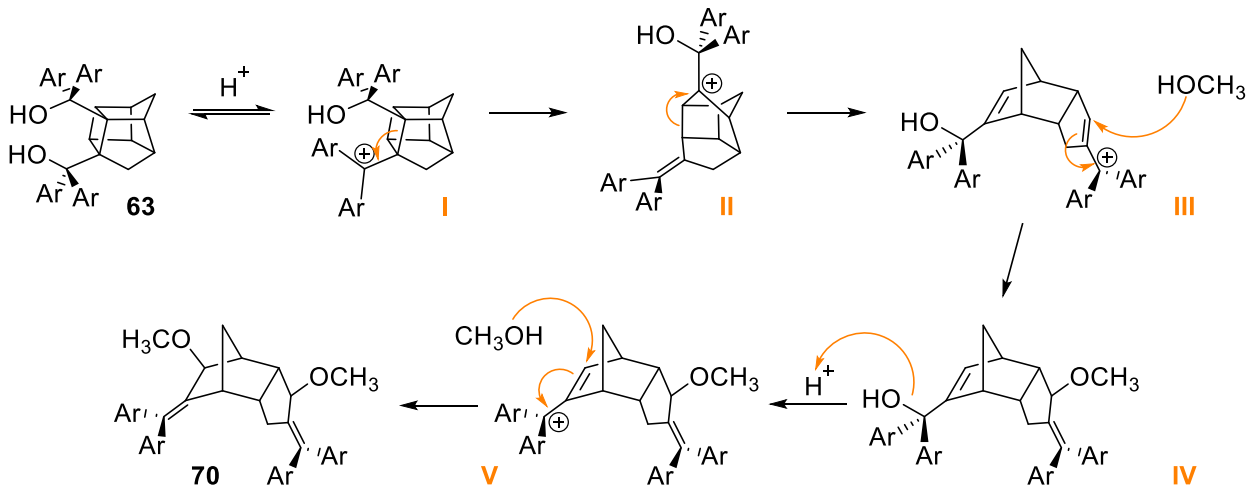

Scheme 25 Proposed mechanism for the generation of side product **70** from diols **65**.

Considering the proposed stepwise mechanism and the structure of the side product, we believe that it is likely that the rearrangement does pass through a carbocation intermediate. Thus, the process should be stabilized by electron-donating substituents and deactivated by electron withdrawing species. Following the identification of the two side products, we then looked into determining the mechanism of the extended pinacol rearrangement of Thiele Cage Diols through single-scan ^{1}H-NMR kinetics.

2.5.0 – References

1. Dao, N.; Sader, J.K.; Oliver, A.G.; Wulff, J.E. *Chem. Commun.* **2019**, *55*, 1600-1603.
2. Hurd, R.E. *J. Magn. Reson.* **1990**, *87*, 422-428.
3. Bodenhausen, G.; Ruben, D.J. *Chem. Phys. Lett.* **1980**, *69*, 185-189.
4. a. Bax, A.; Summers, M.F. *J. Am. Chem. Soc.* **1986**, *108*, 2093-2094.
   b. Willker, W.; Leibfritz, D.; Kerssebaum, R.; Bermel, W. *Magn. Reson. Chem.* **1993**, *31*, 287-292.
5. Scott, K.; Keeler, J.; Can, Q.N.; Shaka, A.J. *J. Magn. Reson.* **1997**, *125*, 302-324.
6. Doddrell, D.M.; Pegg, D.T.; Bendall, M.R. *J. Magn. Reson.* **1982**, *48*, 323-327.
7. Karplus, M. *J. Am. Chem. Soc.* **1963**, *85*, 2870-2871.
8. Wemmer, D.E *Concepts in Magnetic Resonance* **1989**, *1*, 59-72
9. Thomas, W.A. *Prog. NMR Spectrosc.* **1997**, *30*, 183-207.

Chapter Three

Kinetic Studies Relating to the Extended Pinacol Rearrangement of Thiele Cage Diols

3.0.0 – Contributions

All compounds were synthesized by Austin Burman.

All kinetics experiments were run by Austin Burman.

All computational work was done by our collaborators, Zhipeng Pei and Dr. Gino DiLabio, at the University of British Columbia, Okanagan.

Thermodynamic quantities (entropy, enthalpy, and free energy of activation) and the relative rates for the diols were calculated by Julia Levy and Austin Burman using the kinetics data acquired by Austin.

3.1.0 – Constructing a Hammett Series for Measuring the Extended Pinacol Rearrangement

In the initial manuscript, it was proposed that the rearrangement of diol **63** proceeds either through a concerted mechanism or a stepwise mechanism.[1] The concerted mechanism provides a clear reasoning for the observed diastereoselectivity of the transformation, though we anticipated a high barrier of activation for the transformation. Thus, the stepwise mechanism (**Scheme 26**) was proposed, seeming more likely with the generation of a carbocation at either hydroxyl substituent following protonation. The problem with the stepwise mechanism is that it would be more likely to form four possible diastereomers instead of the single diastereomer that is observed. Considering our proposed mechanism for the formation of **69** from Chapter Two, it would seem there are other factors, separate from the formation of the carbocation, that would provide the single diastereomer.

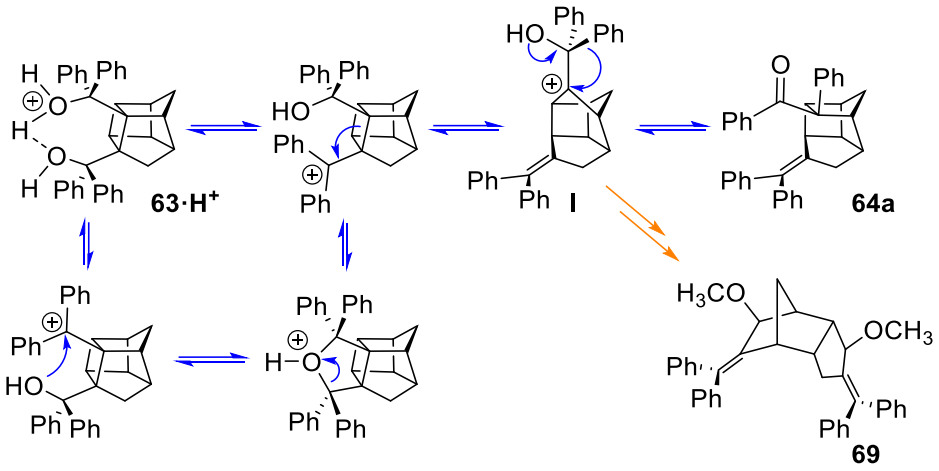

Scheme 26 Mechanism for the production of major product **64a** and minor product **69** from diol **63**. Products **64a** and **69** diverge in the mechanism from carbocation intermediate **I**.

To gain insight into the mechanism for the rearrangement of Thiele cage diols, we selected a series of analogues (**Figure 10**) to synthesize based on their aryl substituent's ability to stabilize a carbocation formed at the benzylic position. We expected that with electron-rich aryl substituents, a carbocation intermediate would be stabilized relative to the carbocation formed during the rearrangement of **63**. Greater stability of the carbocation would result in a faster relative rate of reaction for the consumption of the starting material. For electron-deficient substrates, we expect the relative rate of reaction to be slower due to a destabilization of the carbocation from electron-withdrawing effects, impeding the formation of the intermediates. Should the rate of reaction for electron-deficient species be greater than those of electron-rich species, it would be concluded that the reaction does not pass through a carbocation intermediate. If the carbocation is not generated, then it is more likely that the reaction goes through a concerted pathway that avoids carbocation intermediates. With these considerations, we selected four diols (in addition to diol **63**) upon which to focus our studies: diols **66**, **71**, **72**, and **73**, as shown in **Figure 10**.

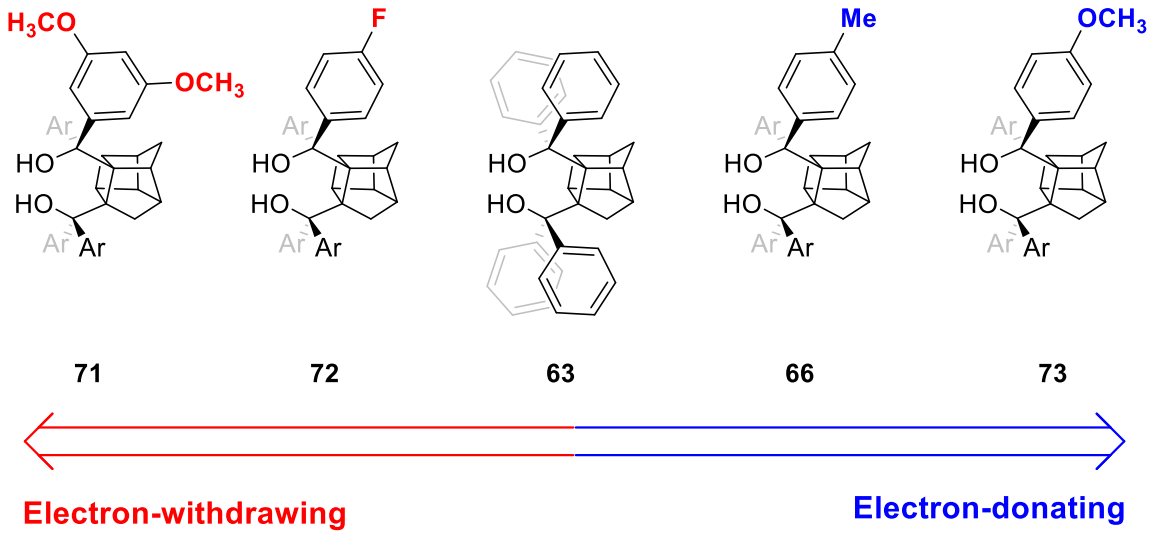

Figure 10 The electron-deficient and electron-rich diols arranged by overall electron density of the aromatic moieties with respect to each other. The more electron-deficient aryl moieties are on the left and the more electron-rich aryl moieties are on the right, with the parent tetraphenyl Thiele cage diol being neutral.

In a previous publication from our group,[1] compounds **73** and **75** were isolated and reacted with sulfuric acid in methanol to determine if they rearrange to generate the major rearrangement product (**Figure 11**). Diol **73** contains strong electron donating substituents on each of its aryl groups (σ_p = −0.27) and was found to undergo the rearrangement rapidly to generate product **74**.[2] To contrast diol **73**, diol **75** bears a strong withdrawing substituent (σ_p = 0.54) and was found to not rearrange under strong acidic conditions.[2] Considering the σ-values of both substituents and their ability to rearrange, we selected substrates **66** (σ_p = −0.17), **71** ($\sigma_{3,5}$ = 0.24), and **72** (σ_p = 0.06), in addition to **63** and **73** to construct our Hammett series. Compounds **71** and **72** were selected as the withdrawing effects of their aryl substituents are weaker than that of **75** and the diols were expected to rearrange with sufficient heating and a strong enough acid. The fluoro substituents of **72** and the di-meta-methoxy substituents of **71** are both inductively withdrawing, though the aryl substituents of **72** are less so due to the mesomeric effect of fluorine.[3] Similarly, diol **66** was chosen due its less electron-rich properties compared to the substituents of **73** since the CH_3-substituents donate electron density through hyperconjugation.[4] Diol **66** was also used to determine the minor side product discussed in Chapter Two with the CH_3 substituents serving as NMR handles.

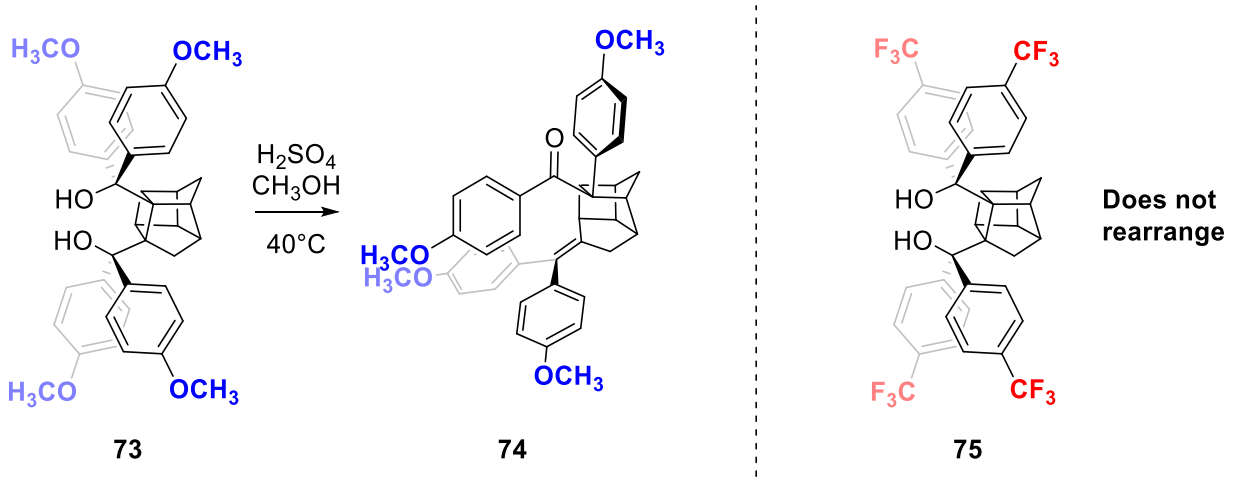

Figure 11 Comparison of functional groups and the ability of diols to rearrange under acidic conditions. While **73**, a diol with electron-rich aryl substituents, can rearrange readily when treated with sulfuric acid, **75** was not observed to rearrange. The substituents of the aryl groups would affect the stabilization of the carbocation, with *p*-OCH_3 stabilizing a carbocation and *p*-CF_3 destabilizing a carbocation.

3.2.0 – Computational Analysis of the Extended Pinacol Rearrangement of Diol 63

Earlier in Chapter 1, we proposed the potential mechanisms for the rearrangement product, either a stepwise (**Scheme 27**) or concerted (**Scheme 28**) mechanism of reaction. With our collaborators in the DiLabio group, we used computational studies to predict barriers for activation in the forward and reverse direction for several of the steps in the proposed mechanisms. The geometry optimizations and frequency calculations were performed at M06-2X/631G(d,p)/SMD level of theory, with chloroform as a solvent, using Gaussian 16.[5-7] The (local) minimum-energy structures were confirmed by a lack of imaginary frequency vibrations, and transition-state structures were confirmed by the presence of exactly one imaginary frequency. The thermal contributions (1M, 298K) were further re-calculated using Grimme's quasi rigid-rotor oscillator (Q-RRHO) approximation with the Shermo 2.38 package.[8,9] Barrier heights were calculated for the tetraphenyl substrate **63·H$^+$** in **Scheme 27**. The first step of the reaction starting from **63·H$^+$** was envisioned to involve the protonation of either the top or bottom-faced hydroxyl substituent. The calculated barrier height for the forward reaction was found to be 66.3 kJ/mol, which is more than 3-fold greater than the barrier height for the reverse reaction at 20.6 kJ/mol. The difference in barrier heights for the forward and reverse reaction may be why the overall reaction requires a strong acid, with weaker acids failing to promote the reaction. Protonation of the OH group results in the formation of either carbocation **A** or **B**. The barrier of activation for the formation of **A** is not shown, as there were difficulties in identifying and calculating the transition state of the transformation. It is assumed that the energy barriers in the forward and reverse reaction to form **A** are similar to those for the reaction to form **B**. The carbocation that is generated is then set up to rapidly interconvert between **A**, **B**, and **C**. From **B** to **C** the forward reaction's energy barrier is small (35.8 kJ/mol) with the reverse barrier being slightly smaller in magnitude (33.8 kJ/mol). Similarly, for the conversion of **A** to **C**, the forward reaction has a barrier of 33.7 kJ/mol, with the energy barrier of the reverse reaction differing slightly at 26.1 kJ/mol. From **A** toward rearrangement product **64a** in the ring-opening mechanism, the barrier of the transition state is low at 18.4 kJ/mol with the resulting product having a local minimum of −30.6 kJ/mol. Though the barrier for the ring-opening reaction from **B** to potential product **64c** is similar to that of **A** to **64a** at 19.6 kJ/mol (taken from the difference between the reactant free energy level and

that of the transition state for the given transformation), the calculated geometries shown in **Figure 12** of **A**, the transition state, and **64a** show how the prearrangement of the migratory aryl substituent influences the stereochemical outcome of the transformation. Additionally, since the energy level of the transition state from **A** to **64a** is lower than that of **B** to **64c** (based on the difference between the transition states – i.e. $\Delta\Delta G^{\ddagger}$), the formation of **64a** is favoured based on the Curtin-Hammett principle. The small reaction barriers to the formation of **C** and either carbocation are likely due to the proximity of the hydroxyl substituents to the carbocation. The rapid interconversion of the species as well as formation of reservoir compound **65** will likely show peak broadening and be represented by a single resonance as a consequence of overlapping signals in the ^{1}H-NMR that differs from **64a** and **63**. **Figures 13** and **14** better illustrate the energy level differences between the reservoir intermediates **A**, **B**, and **C**, as well as paths from diol to the rearrangement product **64a**.

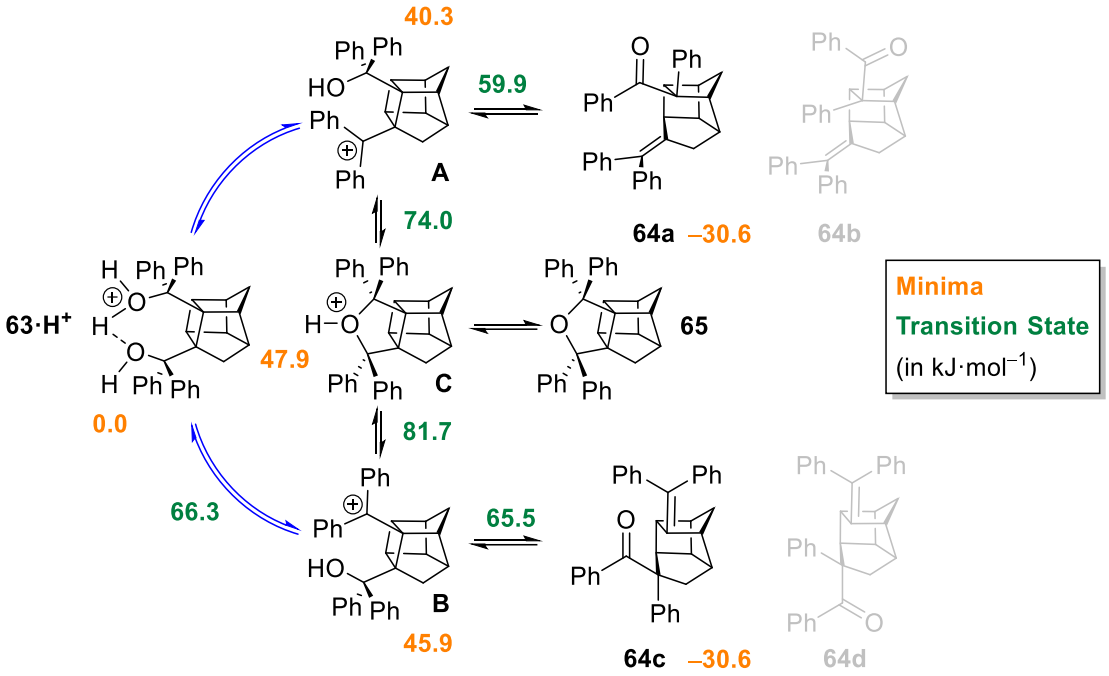

Scheme 27 The proposed stepwise mechanism for the rearrangement of Thiele cage diol **63** with local minima energies in orange and transition state energy barriers in green, both in kJ·mol^{-1}.

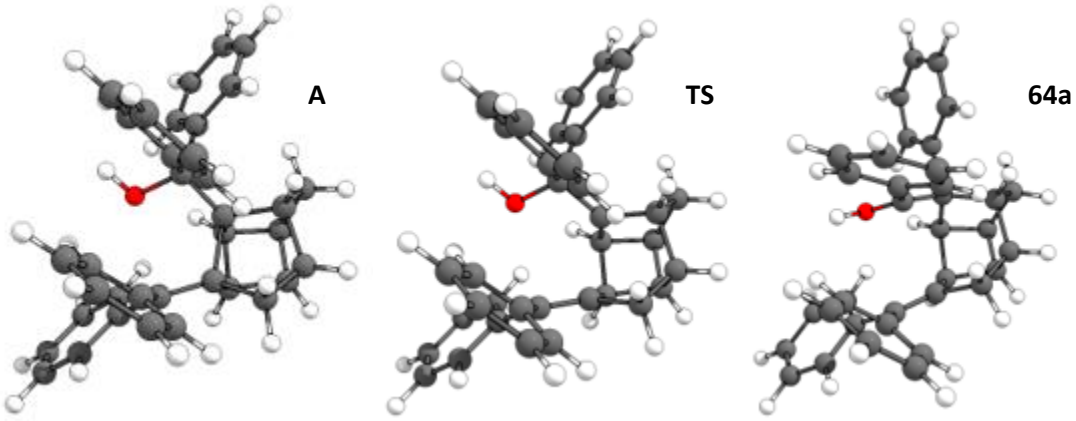

Figure 12 Calculated geometries for **A**, the transition state (**TS**) for the rearrangement reaction, and the product **64a** during the ring-opening transformation of the reaction of diol **63**. Note the parallel nature of the forward-facing aryl groups, suggesting a π–π interaction between the two substituents, and a prearrangement of the migrating aryl substituent on the top-face of the molecule.

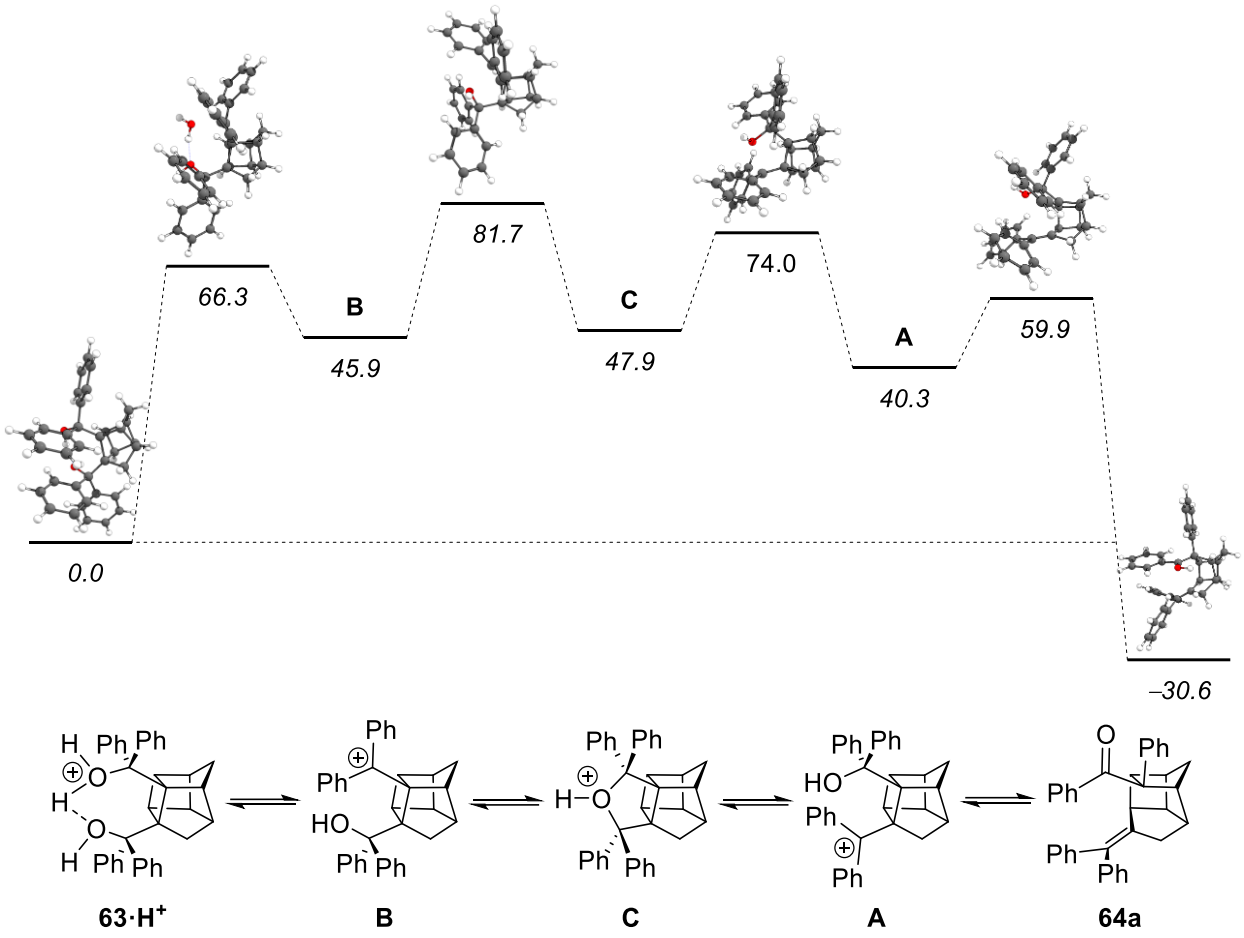

Figure 13 Relative free energies of intermediates **A**, **B**, and **C**, the product, and the energies of the transition states between each species. Energies are in kJ·mol^{-1}.

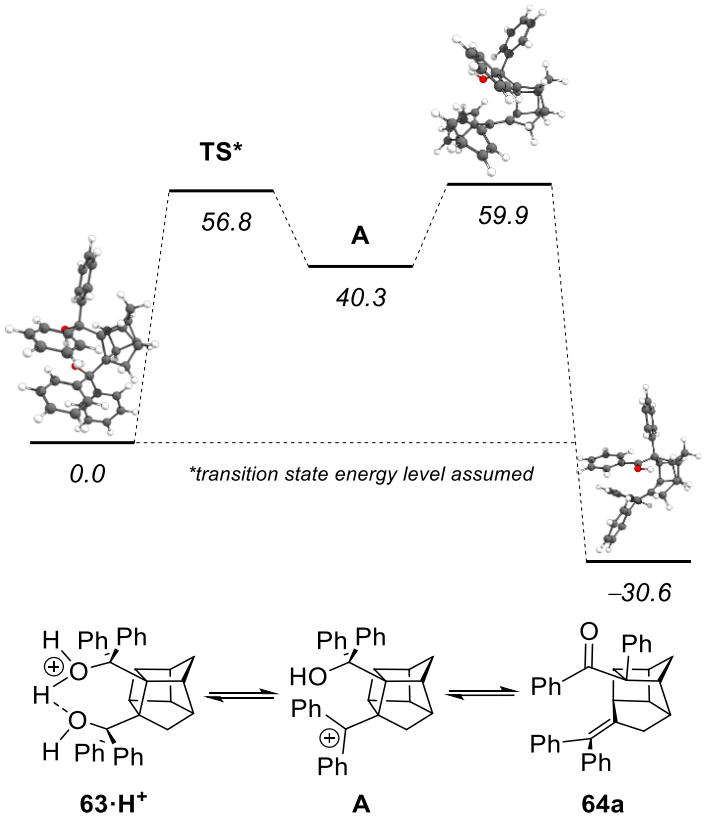

Figure 14 Relative free energies of intermediate **A**, the product, and the energies of the transition states between each species. Energies are in kJ·mol^{-1}.

3.2.1 – Structural Considerations for the Extended Pinacol Rearrangement

In our previous manuscript, a crystal structure for **63** was obtained (**Figure 15**).[1] To compare, our collaborators calculated the lowest energy conformer of diol **63** (**Figure 16**). In both images, it appears as though there is a π-π stacking interaction between two of the phenyl substituents. Though there is free rotation of C2–C11 and C5–C12, π-π interaction of these aryl groups likely affects the geometry of the molecule during the rearrangement reaction. The interaction results in the arrangement of one of the phenyl substituents "up", in the appropriate position for migration. The migratory phenyl substituent is antiperiplanar to the bond (C2–C5) that breaks during the rearrangement, with a calculated dihedral angle of 177.42° and a determined angle of 177.04° from the crystal structure.[1] Interestingly, the position of the phenyl group also explains the observed resonance of the nearby methylene proton at −0.65 ppm in the ^{1}H-NMR spectra of **63**. An observed upfield shift of the proton from typical alkyl chemical shifts is likely caused by the proton sitting within the magnetic field of the aryl substituent, experiencing greater shielding due to the anisotropic effect. Based on the geometry of the substituents, it is likely that the π-π interaction of the aryl groups may play a role in the formation of the reservoir compound **65**. During the rearrangement, following formation of the carbocation, the molecule may be held in a "clasped" position, bringing the remaining OH group close to the carbocationic center.

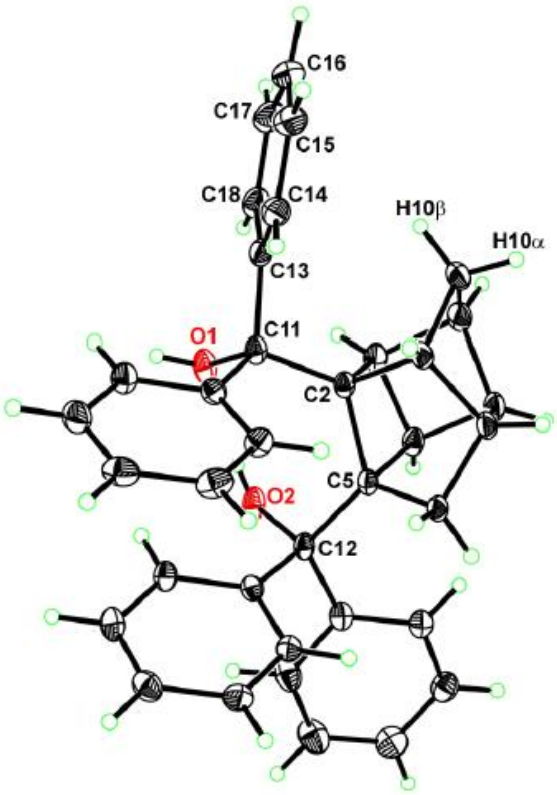

Figure 15 The crystal structure of diol **63**. From the crystal structure, the dihedral angle of C13-C11-C2-C5 was found to be 177.04(8)°.

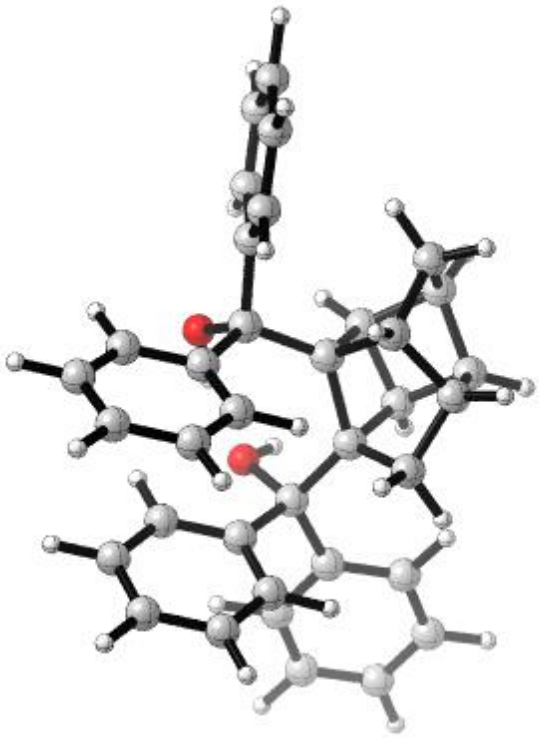

Figure 16 Computational determination of lowest energy conformation for tetraphenyl Thiele cage diol **63**. As seen on the left-hand side of the structure, there appears to be π-π stacking of the two aryl substituents, prearranging the migrating aryl antiperiplanar (θ=177.42°) to the breaking bond.

For the concerted mechanism, the proposed transition state was difficult to pinpoint, though estimates show the energy for the transition state is around 293.4 kJ·mol^{-1}. When compared to the barriers of the reactions proposed in the stepwise mechanism, the energy required to reach the transition state of the proposed concerted mechanism is much greater in magnitude and makes it seem highly improbable. When considering the observation of reservoir compound **65** and side product **69** from Chapter 2, it is difficult to envision a pathway for either of those products to be formed from the concerted mechanism. Considering the concerted transition state relative energy, the likely mechanism for the formation of the isolated side product, and the computationally-determined relative energies of the transformations for **63** to **64a**, it is unlikely that the overall transformation proceeds through a concerted mechanism. There is a possibility that, for some substituents, there is a slight divergence of mechanism with certain processes occurring in a concerted fashion, but ultimately it is highly likely that the mechanism proceeds through a carbocation intermediate.

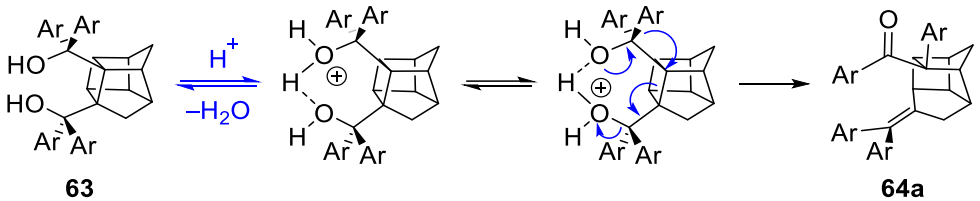

Scheme 28 The proposed concerted mechanism for the rearrangement of Thiele cage diol **63.**

3.3.0 – Computational Analysis of the Hammett Series

We see a trend with the electron-rich diols, **66** and **73**, where there is slight decrease in the barrier energy from starting material **F** toward the carbocation **A** with an increased electron density of the aryl substituents (**Table 3**). When we consider that there is also an increase in the barrier height for the reverse reaction, from **A** to **F**, we can see that there is a stabilization of the carbocation intermediate **A**. This stabilization also translates to a higher barrier height from **A** to product **D** for more electron-rich diols, due again to the lower local minima relative to the other diols. Considering the magnitude of the energy barriers themselves, the required energy for the migration step in the stepwise mechanism (i.e. from **A** to **D**) is much lower in energy compared to the calculated concerted pathway. With the electron-deficient diols, we see similar barrier heights for diol **72** compared to **66**, differing only by 2-4 kJ·mol^{-1} for a given transition. The Hammett constant for a para-fluoro substituent is not very divergent from phenyl ($\sigma_{p\text{-}F}$=0.06 vs. σ_H=0.00),[13] so fluctuations in calculated barrier energies are expected. Fluorine, as an aryl substituent, is overall destabilizing for carbocations, however, there is a small degree of electron donation into the conjugated system due to ideal overlap of fluorine's outer-shell 2p orbitals and the 2p orbitals of the π system of the phenyl group. For diol **71**, we see the greatest barrier height from **F** to **A** at 62.0 kJ·mol^{-1} with the barrier of the reverse reaction being the smallest at 0.6 kJ·mol^{-1}. The small reverse barrier of activation for diol **71** suggests a greater instability of the carbocation **A**, with diol **F** being more favourable. Considering relative energies between the reservoir intermediates **A**, **B**, and **C** (**Table 4**), the transformation of **71** appears to favour **A**, over **B** or **C**, likely due to the tiny barrier for the reverse reaction to **F**. We would expect then that, at least at lower temperatures, formation of the reservoir and the rearrangement product for **71** will be disfavoured and the reaction will be slower when compared to the relative rates of reaction for the other diols. For each substituent, we see that **C** is disfavoured overall, but more so for electron-rich substituents, likely owing to the greater stability of the carbocation in these species compared to the electron-deficient aryl substituents. It should be noted that the non-protonated form of **C** for diols with electron-rich substituents forms rapidly during the reaction and likewise would contribute to **C** being disfavoured. Conversion of non-protonated **C** to **D** for compound **73** was observed to require longer reaction times or elevated temperatures.

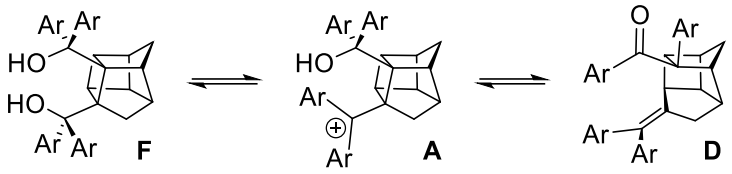

Substituent	F to A	A to F	A to D
3,5-diOCH$_3$ (**71**)	62.0	0.6	20.8
p-F (**72**)	51.5	15.0	22.5
H (**63**)	56.8	10.9	19.6
p-CH$_3$ (**66**)	53.4	15.8	26.6
p-OCH$_3$ (**73**)*	52.0	38.5	40.7
Barrier energy in kJ·mol^{-1}			

*All barriers from F to A and A to F are from calculated barriers for F to B and are assumed to be equivalent, with the exception of compound **73**.

Table 3 The calculated dehydration barriers of (**A** to **F** and **F** to **A**) diols **63**, **66**, and **73** and subsequent ring opening barriers toward formation of the rearrangement products (in kJ·mol^{-1}).

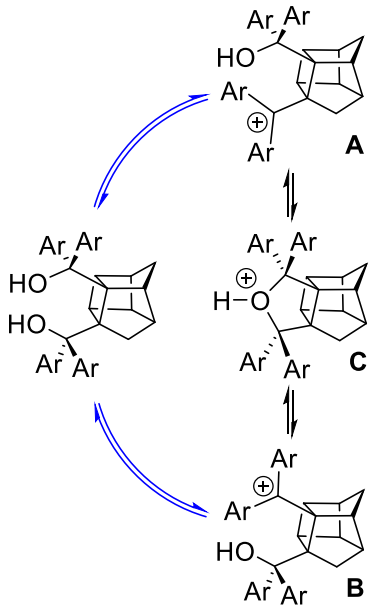

Substituent	A	B	C
3,5-diOCH$_3$ (**71**)	0.0	13.4	13.7
p-F (**72**)	0.0	2.8	17.7
H (**63**)	0.0	5.7	7.7
p-CH$_3$ (**66**)	0.0	4.6	15.6
p-OCH$_3$ (**73**)	0.0	6.9	44.2
Relative energy in kJ·mol^{-1}			

Table 4 The relative free energies of the reservoir intermediates, for the rearrangement of diols **63**, **66**, **71**, **72** and **73**, to one another in kJ·mol^{-1}.

3.4.0 – Synthesis of Thiele Cage Diols

The namesake of our compounds, the Thiele cage diols, comes from the precursor: Thiele's ester (**76**). Synthesized using methods reported by Dive and coworkers and optimized in our lab by Dr. Jun Chen, Thiele's ester **76** is prepared as a white solid in 64% yield from sodium cyclopentadienylide (**Scheme 29**).[10] The precursor cage **77** (**Scheme 30**) is synthesized through a photochemical [2+2]-cycloaddition of the alkenyl moieties of **76** in acetone with 253-nm light. The initial synthesis of **76** required long reaction times (>1 day) to produce it on a gram scale. By reducing the concentration from 0.20 M to 0.020 M, compound **77** was produced as a colourless oil with higher yield (63% vs 55%) at shorter reaction times (12 hours vs 3-4 days). The combination of lower concentration and shorter reaction times allows for a shorter turnover of batches to produce more cage **77** in the same amount of time as higher concentrations and longer reaction times (Around 1.5 grams from 3 to 4 batches versus 0.75 grams from a single pot reaction in the same amount of time).

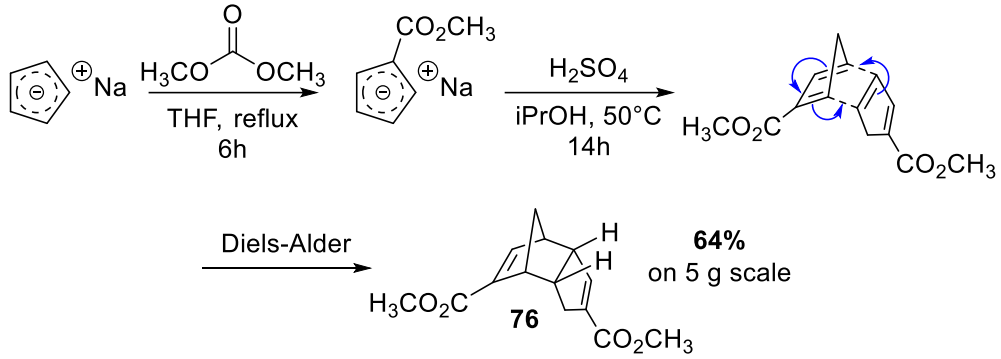

Scheme 29 Synthesis of Thiele's ester **76** from sodium cyclopentadiene and dimethyl carbonate.

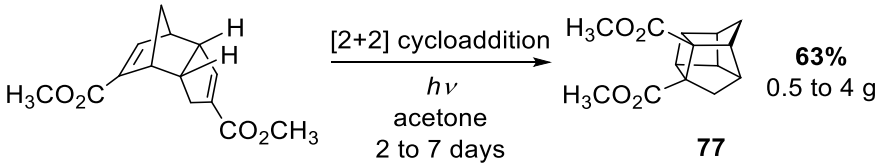

Scheme 30 Synthesis of Thiele cage **77** from Thiele's ester through photochemical [2+2]-cycloaddition.

Each of the Thiele cage diols (**Table 5**) was then synthesized from **77** by addition of either organolithium reagents or Grignard reagents. Diols **63** and **73** were previously prepared with organolithium reagents with 80% and 74% yields respectively.[1] For diols **66**, **71**, and **72**, commercial Grignard reagents were used. In the case of diols **71** and **72**, the mixture needed to be heated to 50°C overnight to ensure the reaction went to completion. A combination of steric congestion around the resultant quaternary alcohols and electron-deficiency of the aryl groups (resulting in lower nucleophilicity of the organometallates) are the likely reasons why additional energy is needed for completion of the reaction for **71** and **72**.

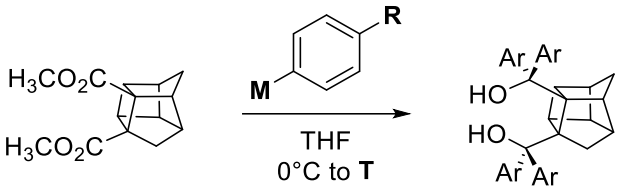

#	R	M	T	Yield
63	H	Li	RT	80%
73	OCH_3	Li	RT	74%
66	CH_3	MgBr	RT	56%
72	F	MgBr	50°C	43%

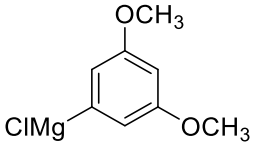

71 74%

Table 5 Reaction conditions and yields for the synthesis of Thiele cage diols **63**, **66**, **72**, and **73**.

3.5.0 – Kinetic Study Optimization

To measure the progress of the reaction, we decided to utilize ^{1}H-NMR spectroscopy by measuring the concentration of each species through the integration of key resonances, that represent each species, over time. Though each of the species in solution shares several similar resonances and overlaps in certain regions, we were able to identify some resonances representative of four different species present in solution. In **Figure 17**, the key peaks representing different protons for the species from the reaction of **63** are highlighted and expanded to show clear baseline separation from nearby peaks. For the rearrangement product, the resonance representing the *ortho* protons of the back-facing aryl group is found at around 6.20 ppm as a doublet. The side product is represented by the resonance at 6.05 ppm, with the resonance corresponding to the *ortho* protons of **Aryl D** (front facing aryl substituent on the Western half of the molecule). The resonance at 1.75 ppm represents the proton of the methylene pointing up on the reservoir compound. We speculate that this peak is likely representative of the sum of species **A**, **B**, and **C** from the proposed mechanism shown in **Scheme 27**. The same proton for the reservoir compound is represented for the starting diol at around −0.65 ppm as a doublet. Due to the conformation of the diol as shown in the crystal structure (**Figure 15**), the proton is being shielded and thus the resonance is shifted upfield due to the ring currents from the anisotropic effects of the aryl groups. This upfield doublet served as a key indicator that the product was formed in the synthesis of diols and is different for each diol. Lastly, the progress of the side product (when observed) was measured following the integration of the resonance just upfield of the rearrangement products' representative resonance (~6 ppm).

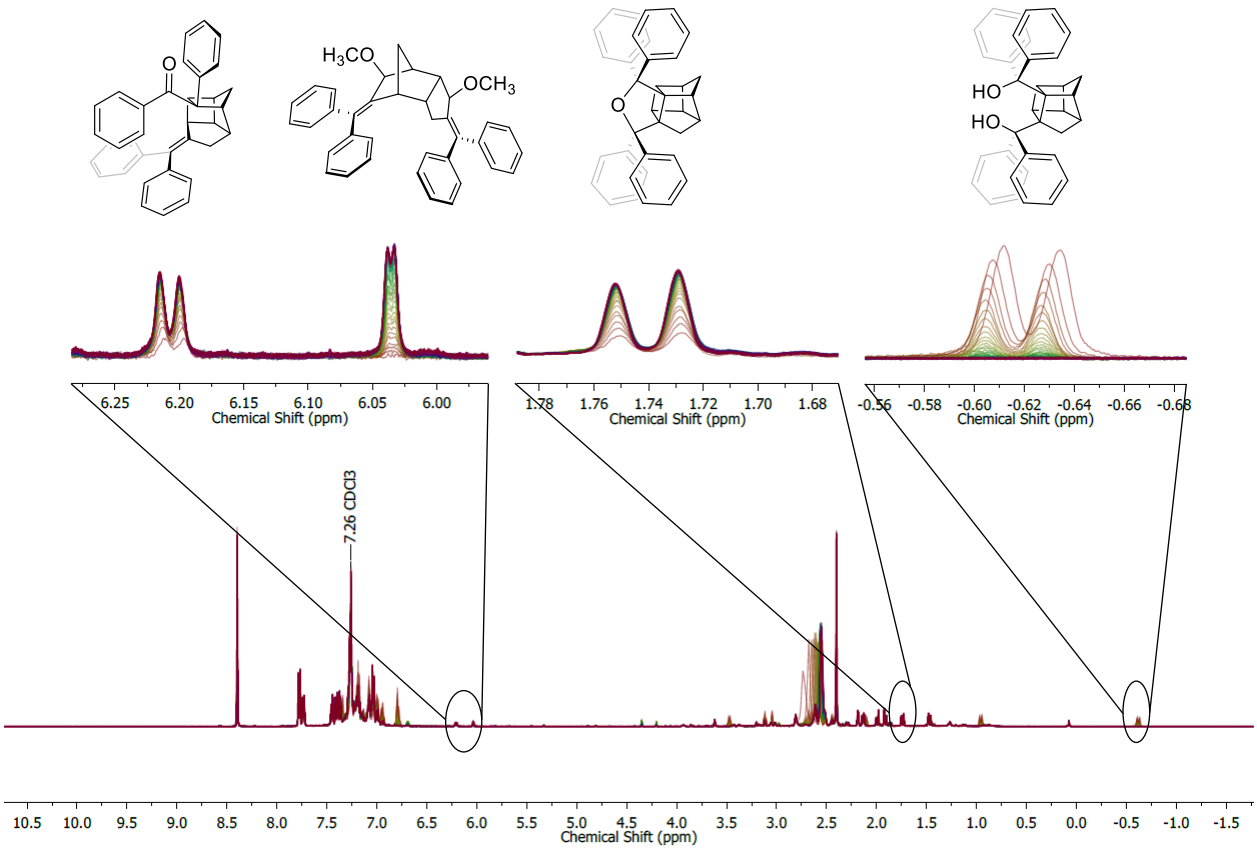

Figure 17 Highlighted resonances for key species in the reaction of diol **63** with *p*-toluenesulfonic acid in 2% methanol-d_4 in chloroform-*d*. The rearrangement product is represented by the resonance at 6.20 ppm, the side product is represented by the resonance at 6.04 ppm, the reservoir compound is represented by the resonance at 1.75 ppm, and the starting material is represented by the resonance at −0.62 ppm.

During the synthesis of the rearrangement products, we noted that formation of the product seemed to be driven by its precipitation out of solution in methanol. When conducting initial studies on monitoring the reactions through quantitative ^{1}H-NMR spectroscopy, a precipitate would form as the reaction progressed in deuterated methanol (methanol-d_4). The starting material, reservoir compound, and product are soluble in deuterated chloroform (chloroform-*d*), however the reaction of the starting diol with a strong acid in chloroform results in decomposition of the material. Further to the problem of decomposition, the initial acid screened, sulfuric acid, was not soluble in chloroform and would slowly settle out of solution over the course of the measurements. To compensate for solubility incompatibilities, we utilized a mixed solvent system. By testing a variety of solvent mixtures, we found that 2% methanol-d_4 in chloroform-*d* was optimal for measuring the reaction. It seems the reaction requires only small amounts of protic solvent for the rearrangement to take place. However, at this point, we noticed that sulfuric acid was still settling out of solution despite the inclusion of a protic solvent. As such, we turned to organic acids that we would expect to be more soluble in the main NMR solvent, chloroform-*d*. While we expected acetic acid to be too weak for the reaction to take place, we thought perhaps trifluoroacetic acid (TFA) might be strong enough. Unfortunately, the reaction was either too slow or did not progress with the use of TFA. To try to increase the strength of TFA in solution, we added a catalytic quantity of hexafluoroisopropanol (HFIP). Addition of HFIP with TFA to the reaction mixture resulted in rapid

decomposition of material (<10 minutes – before the sample was analyzed by ^{1}H-NMR) and was deemed unsuitable for monitoring the reaction. With careful consideration of resonance crowding in the spectra, we settled on the use of *p*-toluenesulfonic acid (PTSA). While resonances representing the aryl protons of PTSA do overlap with some aryl resonances from species present in the reaction, the overlap occurs in regions that were not used for analysis. PTSA is also very soluble in methanol-d_4 and chloroform-*d* and is a strong enough acid (pK_a = −2.8) that the reaction progresses at a high enough rate to measure through ^{1}H-NMR.

We then needed to find a suitable internal standard. Benzoic acid was used initially as it is of insufficient acidity to cause the rearrangement to occur but was found to overlap with key areas of the aryl region of some of the diols. A typical internal standard that could be used for ^{1}H-NMR kinetics is 1,3,5-trimethoxybenzene, but we deemed it to be likely incompatible with our system. Since a carbocation intermediate is likely formed, the intermediate may react with the electron-rich trimethoxybenzene through electrophilic aromatic substitution. Instead, we chose an electron-deficient internal standard that has a distinct resonance (singlet at 8.41 ppm with a relative integration of 4) that would not react with other species present – 1,4-dinitrobenzene.

To monitor the reaction, we settled on a single-scan ^{1}H-NMR kinetics sequence. By using a single scan, we can ensure accurate quantification of any given species at any time point. Each scan is separated by ~33 seconds, ensuring that the nuclei in our system have relaxed from their excited spin state following excitation.[11] When using multiple scans, each individual scan needs to be separated at long enough time intervals to ensure that the nuclei in the system are fully relaxed to allow for accurate integration of a given resonance. The multiple scans are then collated into a single spectrum. If the timescale of a reaction is short, data may be lost in the time eight or more scans for a single spectrum could be taken and thus the integrations will be inaccurate (for much slower reactions, this is fine since the change of concentration over the two to four minutes it would take for the acquisition of a ^{1}H spectra would be relatively small compared to the overall change over the course of the reaction). With our reaction, we observed rapid disappearance of starting material to the formation of a reservoir species within the first five to twenty minutes (depending on substituents) and so single-scan spectra are more optimal for accurate measurement of the concentration of the diol reagent.

We measured the reaction of each diol at 25, 35, 45, and 52°C. As is standard practice with variable temperature NMR experiments, we were limited to an upper temperature that was 5°C below the boiling point of our solvent. Since chloroform-*d* boils at 61–62°C and methanol-d_4 boils at 64.7°C, we were limited to about 55°C, but reduced the temperature slightly to 52°C to allow for any temperature fluctuations.[12] To compensate for our mixed solvent system, we limited our upper temperature to 52°C, providing an additional security window in the event of any temperature fluctuations in the spectrometer. One artefact we observed while running variable temperature NMR experiments was that the first scan following initiation of the reactions was skewed, with measured concentrations of analytes far exceeding the amount of actual material present in the sample. While we attempt to mitigate thermal equilibration of the sample by preheating it to the temperature of the spectrometer, minor fluctuations in temperature still affect the line widths of some peaks, such as that of our internal standard.[13] Following the first scan, however, the system is thermally equilibrated and fluctuations in integrations due to thermal changes are minimal.

3.6.0 – Kinetic Analysis of the Extended Pinacol Rearrangement

With our method and diols in hand, we set out to determine the enthalpy and entropy of activation of the rearrangement reaction, in order to determine the nature of the mechanism, and whether or not a carbocation intermediate is formed, by observing the trends of functional groups on the rates and energies of the reaction. To discuss the dynamics of the reaction, we defined each of the observable species in the reactions as such: diols **63**, **66**, **71**, **72**, and **73** are referred to generally as the *starting diol*, the final product of the reaction is the *rearrangement product*, the tetrahydrofuranyl substrate is referred to as the *reservoir compound*, and the recently isolated opened-cage structure is the *side product* (each shown in **Figure 18**). In each of the reaction profile plots from 25 to 52°C, the starting diol is presented in blue, the rearrangement product is presented in violet, the reservoir is presented in green, and the side product, when present in the reaction profile, is presented in orange.

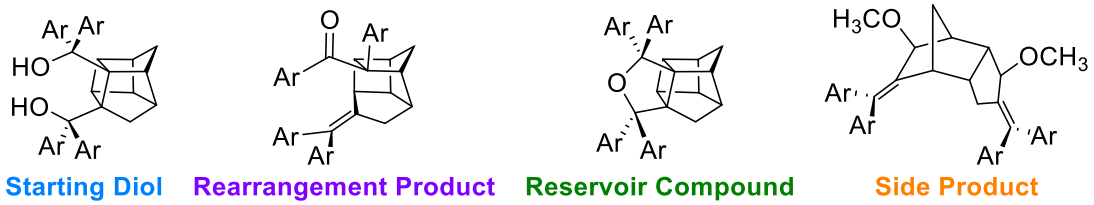

Figure 18 The naming convention of each substrate observed in the kinetic plots.

3.6.1 – Kinetic Profiles at 25°C

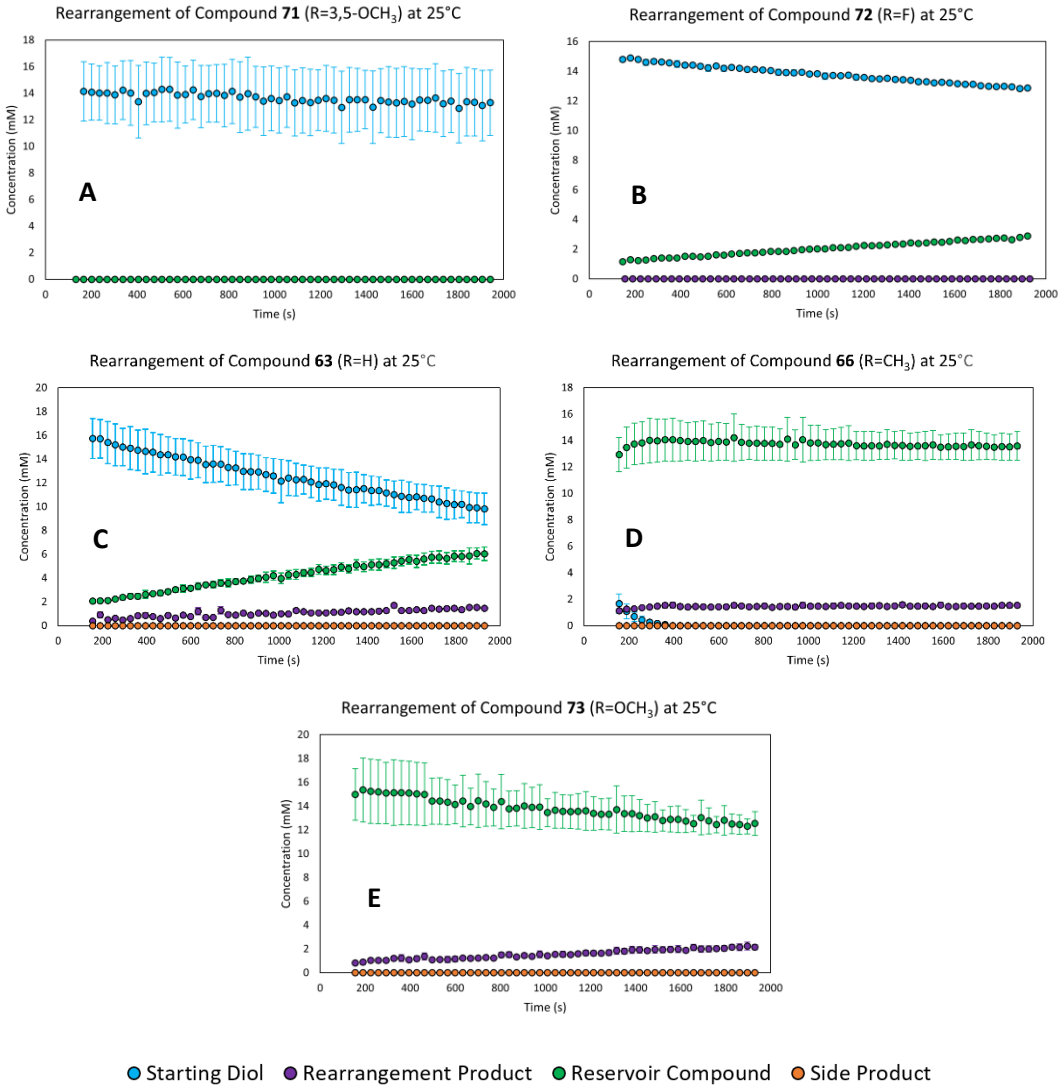

Figure 19 Reaction profile of diols **63**, **66**, **71**, **72**, and **73** at 25°C over 30 minutes with starting diol in blue, its corresponding reservoir compound in green, and the rearrangement product in violet. Error bars shown represent standard deviation between three replicates. Species not observed in a given reaction mixture are presented as "zero values" and, in some cases, overlap with other zero-value data points (e.g. the rearrangement product and side product in the reaction of **72** at 25°C were not observed and the data points overlap with one another).

Starting with 25°C, diols **63** (the parent tetraphenyl-diol: **Figure 19C**), **66** (*para*-CH_3: **Figure 19D**) and **73** (*para*-OCH_3: **Figure 19E**) were both consumed faster than diols **71** (3,5-diOCH_3: **Figure 19A**) and **72** (*para*-F: **Figure 19B**) over the course of 30 minutes. For **63**, the concentration of diol decreased to ~10 mM after 30 minutes while the reservoir compound increased proportionally to the decrease in diol. Some amounts of the rearrangement product were formed over the reaction time, but at this temperature, the formation was limited. For **73**, there is no starting diol remaining by the time of the first scan (~2.5 minutes), with most of the material present being the reservoir. Over the 30-minute reaction, some rearrangement product forms (up to ~2 mM), but like the phenyl analogue, formation is limited at 25°C. For **63** and **73**, it is possible that some of the diol is immediately being converted to the rearrangement

product, passing through the carbocation intermediate, while the remainder of the material forms the reservoir compound. Even at this temperature, we begin to see the conversion of the reservoir of **73** to the rearrangement product slowly over time. For the more electron-deficient diols, **71** and **72**, there are no observable quantities of the rearrangement product present. At this temperature, we observed the slow consumption of **72** to form the corresponding reservoir compound, while **71** remains mostly unchanged. We can already observe the effects of electron-deficient systems on the rate of reaction at a lower temperature. Even with weaker electron-withdrawing effects on the aryl substituents, reaction of the diol with acid to form even the reservoir compound is slow, suggesting the presence of carbocation destabilized by the electron-withdrawing substituent. With stronger electron-withdrawing effects, the reaction itself is shut down with little to no consumption of material observed. When considering the electron-donating substituents, it would follow suit that the donation of density from the aryl substituents into the carbocation would be presented as the fast rate of consumption observed for **63** and **73**. From these two diols, we can see that the formation of the rearrangement product starting from the reservoir compound is likely the rate determining step of the overall transformation. When considering **66**, there are only small quantities of the starting diol present in the first few scans of the reaction. After that point, the formation of rearrangement from the reservoir is limited. At 25°C, there is little to no side product formed for any of the rearrangements, with only trace amounts noticeable in the baseline for diols **63** and **66**.

3.6.2 – Kinetic Profiles at 35°C

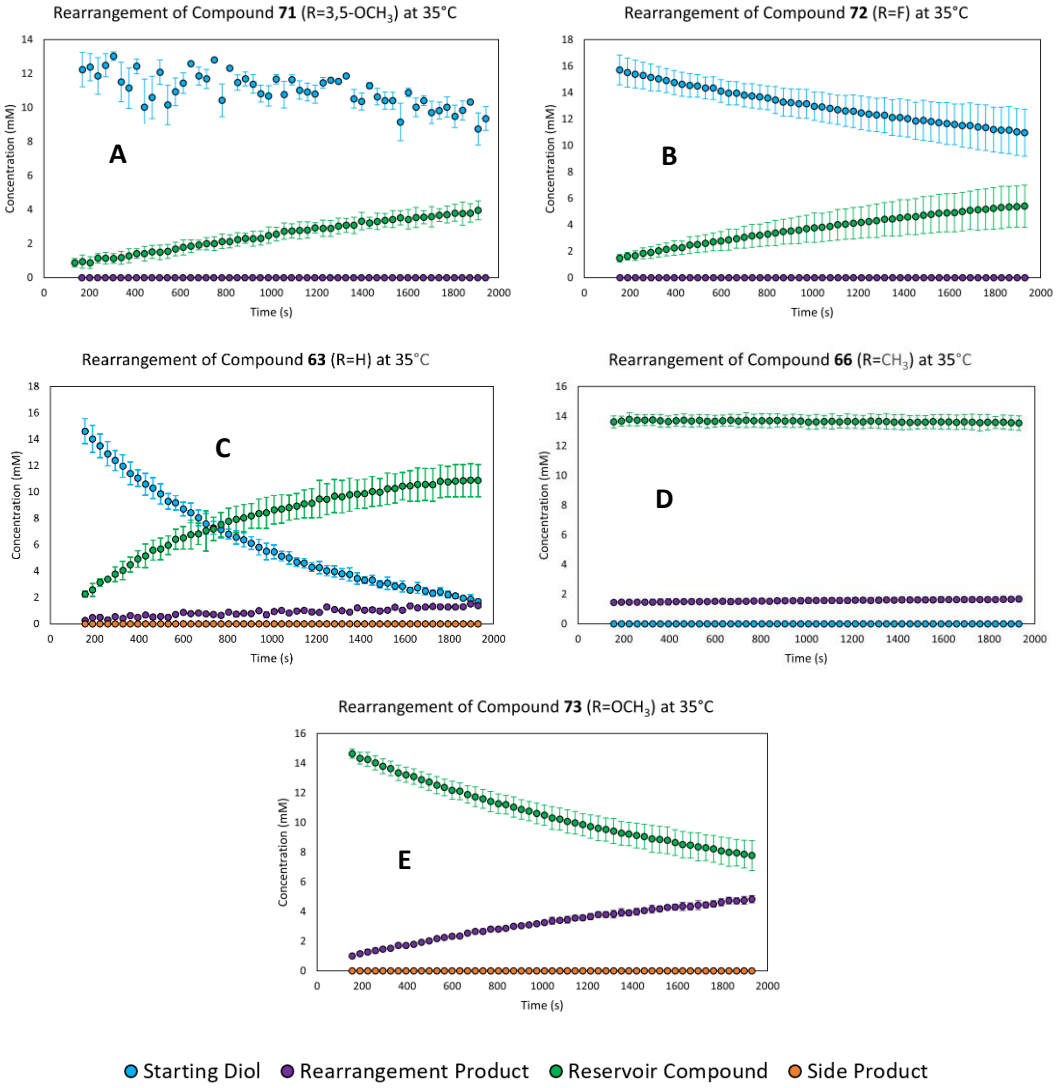

Figure 20 Reaction profile of diols **63**, **66**, **71**, **72**, and **73** at 35°C over 30 minutes with starting diol in blue, its corresponding reservoir compound in green, and its corresponding rearrangement product in violet. Error bars shown represent standard deviation between three replicates. Species not observed in a given reaction mixture are presented as "zero values" and, in some cases, overlap with other zero-value data points (e.g. the rearrangement product and side product in the reaction of **72** at 25°C were not observed and the data points overlap with one another).

At 35°C, the rate of starting diol consumption increased in each reaction, with notable conversion of diol **71** to its respective reservoir compound (**Figure 20**). For diols **63** and **72**, there was an increase in the conversion of starting diol to reservoir, however, **72** showed little to no formation of the rearrangement product at this temperature. Diol **73** showed rapid conversion of the reservoir to the corresponding rearrangement product, while diol **66** showed little change in the rate of reaction of reservoir to product.

3.6.3 – Kinetics at 45°C

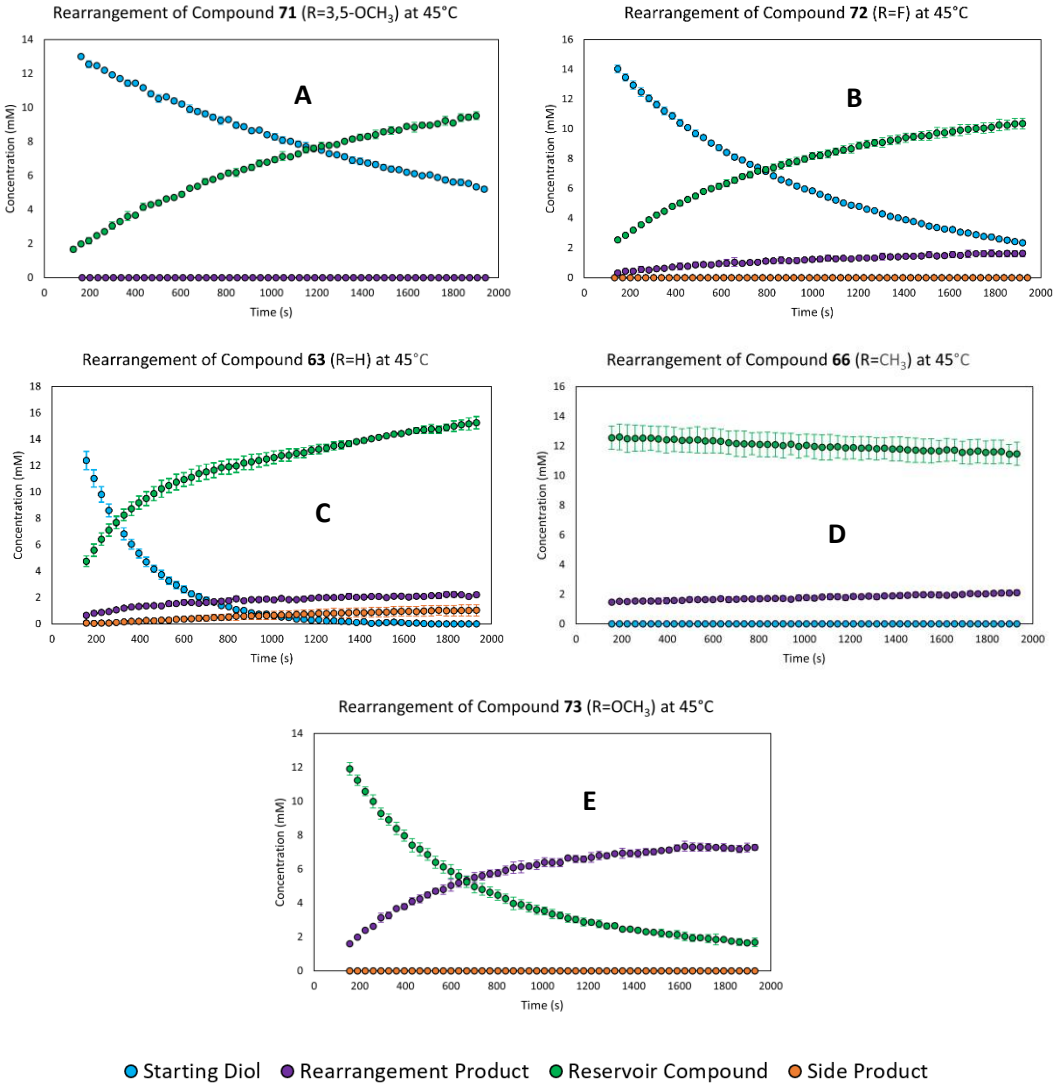

Figure 21 Reaction profile of diols **63**, **66**, **71**, **72**, and **73** at 45°C over 30 minutes with starting diol in blue, its corresponding reservoir compound in green, and its corresponding rearrangement product in violet. Error bars shown represent standard deviation between three replicates. Species not observed in a given reaction mixture are presented as "zero-values" and, in some cases, overlap with other zero-value data points (e.g. the rearrangement product and side product in the reaction of **72** at 25°C were not observed and the data points overlap with one another).

As we go up in temperature to 45°C, so do the rates of conversion for diols **63**, **71**, and **72** to their respective reservoir analogue (**Figure 21**). One of the most significant changes at this temperature is the appearance of side product in the reaction of **63**. By the end of the measurement time, the amount of side product present was roughly 50% of the amount of rearrangement product. We also began to see small quantities of the side product in the reaction of **66**, though it is difficult to get an accurate measurement due to a low signal-to-noise ratio from the low concentration of product present.

3.6.4 – Kinetics at 52°C

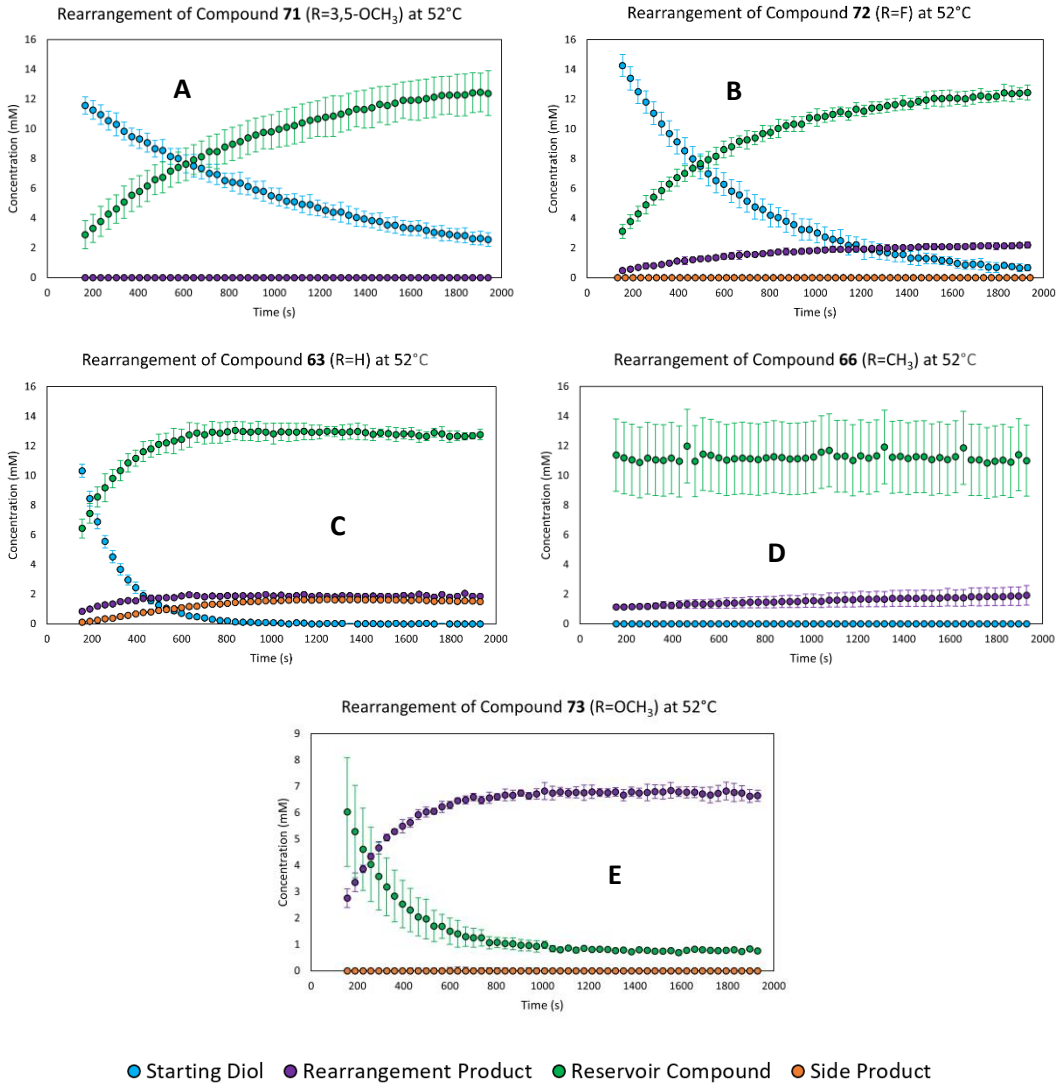

Figure 22 Reaction profile of diols **63**, **66**, **71**, **72**, and **73** at 52°C over 30 minutes with starting diol in blue, its corresponding reservoir compound in green, and its corresponding rearrangement product in violet. Error bars shown represent standard deviation between three replicates. Species not observed in a given reaction mixture are presented as "zero-values" and, in some cases, overlap with other zero-value data points (e.g. the rearrangement product and side product in the reaction of **72** at 25C were not observed and the data points overlap with one another).

For 52°C, the largest difference from earlier temperatures is in the reactions of diol **63** and **73**. With phenyl diol **63** we saw an increased rate of production of the side product, with the concentration being nearly equivalent to the amount of rearrangement product formed after ~30 minutes (1.5 mM of side product versus 1.87 mM of rearrangement product at 32.2 minutes). With stabilization of the carbocation by the *para*-methoxy substituent on the aryl moieties of **73**, the equilibrium would be shifted in such a way that more carbocation is present, allowing for decomposition to the side product. Diol **73** shows quick conversion of reservoir to the rearrangement product over 30 minutes. As can be seen in **Figure 22**, the reaction appeared to stall out at a concentration lower than what was initially reacted. From the previous publication, the isolated yield of the rearrangement product that corresponds to **73**

was isolated in ~50% yield, so the loss of material observed in the reaction trace is expected based on the isolation.[1] The loss of material is likely due to non-isolable decomposition products (the samples were dark brown following measurements). It should be noted that for diol **66**, there was trace amounts of the side product that was noticeable but difficult to measure accurately.

3.7.0 – Activation Parameters of the Extended Pinacol Rearrangement

From the traces previously shown, we took the natural logarithm of the concentration of diol for **63**, **71**, and **72** over time in seconds (**Figure 23**), showing a first order rate of reaction with respect to the consumption of diol. The rates of reaction for the three diols at 25, 35, 45, and 52°C were derived from the slope of these graphs, shown in **Table 6**. As expected, based on the carbocation destabilizing effects of electron-withdrawing groups, the rate of reaction decreases for the consumption of diol with more electron-deficient aryl substituents. When we take the natural logarithm of the rates over temperature (in Kelvin) and plot them against the inverse temperature (T^{-1}), we obtain our Eyring plots (**Figure 24**).[14] It is from these plots that we derive the enthalpy and entropy of activation. Diol **63** was calculated to have an enthalpy of activation of 92.38 kJ·mol^{-1} and an entropy of activation of −2.92 J·mol^{-1}·K^{-1}. The determined values of enthalpy and entropy of activation for **71** are 82.66 kJ·mol^{-1} and −49.65 J·mol^{-1}·K^{-1} respectively, while **72** has an enthalpy of activation of 89.38 kJ·mol^{-1} and an entropy of activation of −22.85 J·mol^{-1}·K^{-1}. From these values overall, the enthalpy of activation for the electron-deficient species is lower in magnitude than that of the phenyl diol while the loss in entropy is greater. The difference in entropy of activation appears to indicate that we may have a difference of initial steps for the mechanism: a S_N1-like pathway versus a S_N2-like pathway. Based on the entropy of the consumption of diols **71** and **72**, there is an associative mechanism that could result in a great loss of entropy.[15-17] As shown in **Scheme 4**, following protonation of either hydroxyl group, the remaining hydroxyl group could donate density into the substitution center, displacing the oxonium leaving group generated, in an S_N2-like fashion. A concerted substitution reaction would generate the reservoir compound directly from the diol, resulting in a greater loss of rotational freedom, while avoiding going through a disfavoured/destabilized carbocation intermediate. For **72**, while deficient enough to prevent the carbocation at lower temperatures, the diol is more likely to form the carbocation and ultimately rearrangement, albeit at a slower rate than the phenyl (more than 3-fold slower). For **71**, little to no rearrangement product is observed, and likely requires much longer reaction times to generate the rearrangement product. For more electron-rich species, since the carbocation is stabilized by the surrounding aryl substituents, it readily formed and can either proceed through the pinacol rearrangement or continue along the S_N1 pathway to generate the tetrahydrofuranyl reservoir. This reservoir can then react with the acid in the system to regenerate the carbocation and form the rearrangement product. In diol **63**, there is a small loss of entropy that could be explained by the loss in rotational freedom from the π–π stacking, even in the transition state, as shown in **Figures 15** and **16** that pre-arranges the migratory aryl group for the transformation.

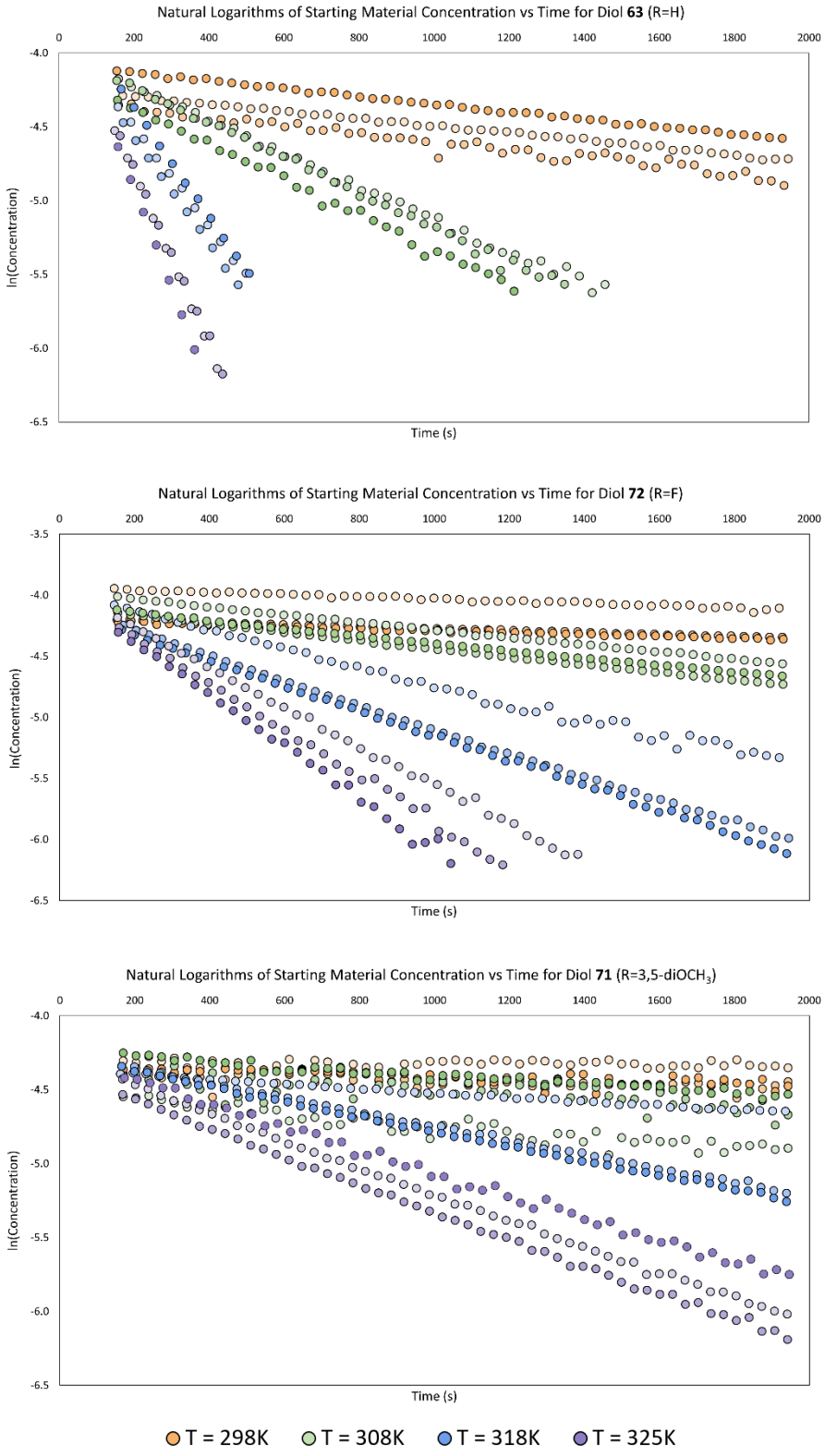

Figure 23 Plots of the natural logarithm of diol concentration over time in seconds for diols **63**, **71**, and **72**, in triplicate.

Table 6 Relative rates of reaction for the consumption of starting diol for substrates **63**, **71**, and **72**.

	Average rate constant (10^{-5} s^{-1}) at T (in K)			
Substrate	**298K**	**308K**	**318K**	**325K**
63 (R=H)	25.94 ± 0.76	116.37 ± 1.98	353.92 ± 3.81	614.98 ± 8.94
72 (R=F)	8.39 ± 0.28	31.27 ± 0.29	90.23 ± 1.12	187.12 ± 2.91
71 (R=3,5-diOCH$_3$)	---*	15.64 ± 2.02	37.52 ± 0.36	86.04 ± 0.94

*Due to little to no change in concentration of diol, the rate constant for **71** at 298K was not determined.
All error presented as standard error.

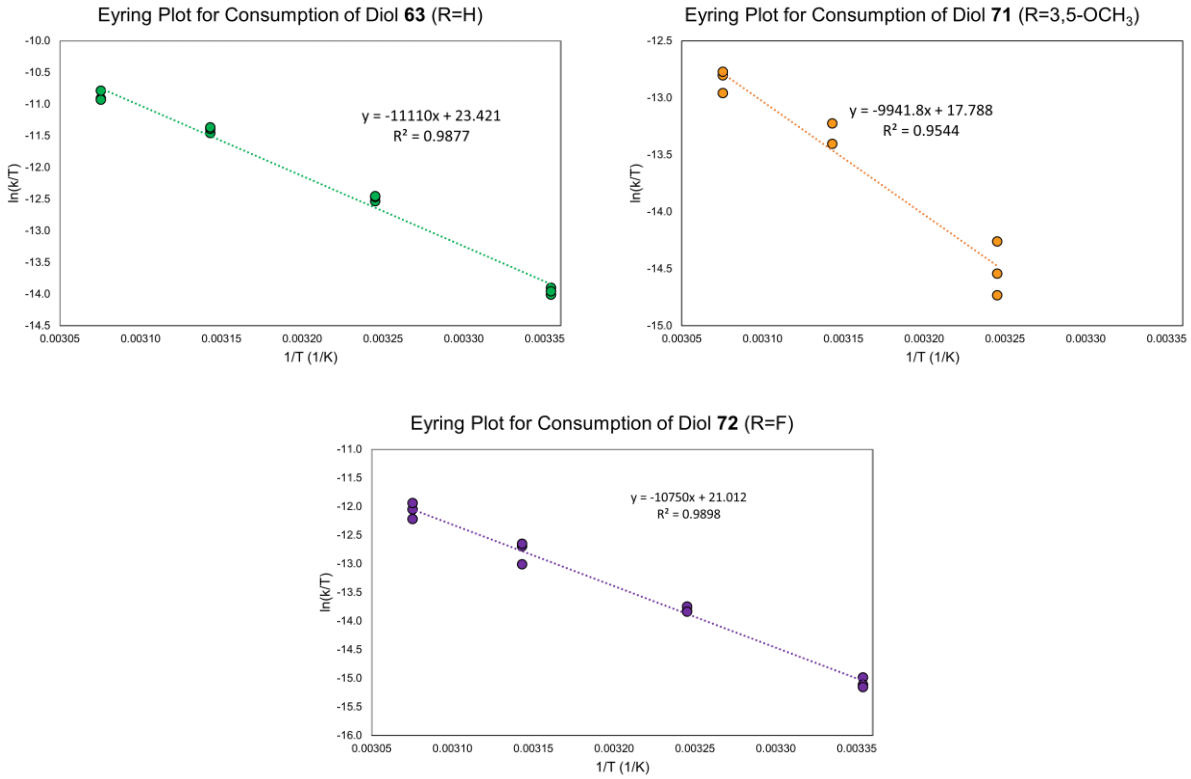

Figure 24 Eyring plots for the consumption of diols **63**, **71**, and **72**.

Table 7 Experimental values for enthalpy ($\Delta H^{\ddagger}$) and entropy ($\Delta S^{\ddagger}$) of activation for the consumption of starting diol for substrates **63**, **71**, and **72**.

	$\Delta H^{\ddagger}$ ($kJ \cdot mol^{-1}$)	$\Delta S^{\ddagger}$ ($J \cdot mol^{-1} \cdot K^{-1}$)
63 (R=H)	92.29 ± 3.26	−2.82 ± 10.46
72 (R=F)	89.30 ± 2.86	−22.98 ± 9.18
71 (R=3,5-diOCH$_3$)	82.24 ± 6.44	−49.65 ± 20.34

For diol **73**, since it was not possible to measure the disappearance of diol for each of the temperatures, we were not able to obtain rates of reaction and thus enthalpy or entropy of activation for the consumption of diol to form reservoir. From a qualitative perspective, however, we can see that the electron-rich **73** reacts much faster, likely due to the strong stabilization of the carbocationic intermediate formed. Unlike the other diols, we can accurately measure the consumption of the reservoir to the formation of the carbocation and, ultimately, the formation of the rearrangement product. From this change in concentration, we take the natural logarithm and plot against time to linearize the plot and derive the rate from the slope of the plots (**Figure 25**). From the rates of reaction, we generated the Eyring plot shown in **Figure 26** that were then used to derive the enthalpy of activation and entropy of activation. For this part of the reaction, the enthalpy of activation is 99.26 ± 7.65 $kJ \cdot mol^{-1}$ and there is a gain in entropy of 9.14 ± 24.54 $J \cdot mol^{-1} \cdot K^{-1}$. A small gain of entropy indicates a dissociative mechanism, likely the ring-opening of the tetrahydrofuranyl ring to the carbocation intermediate that can proceed through to the rearrangement product. The correlation plots of the entropy, enthalpy, and Gibbs free energy of activation with the Hammett constants of each substituent for diols **63**, **71**, and **73** are shown in **Figure 27**. The fit of the plot for the entropy and enthalpy of activation shows a trend with the electron-deficient substituents decreasing in entropy and enthalpy with increasing electron-deficiency.

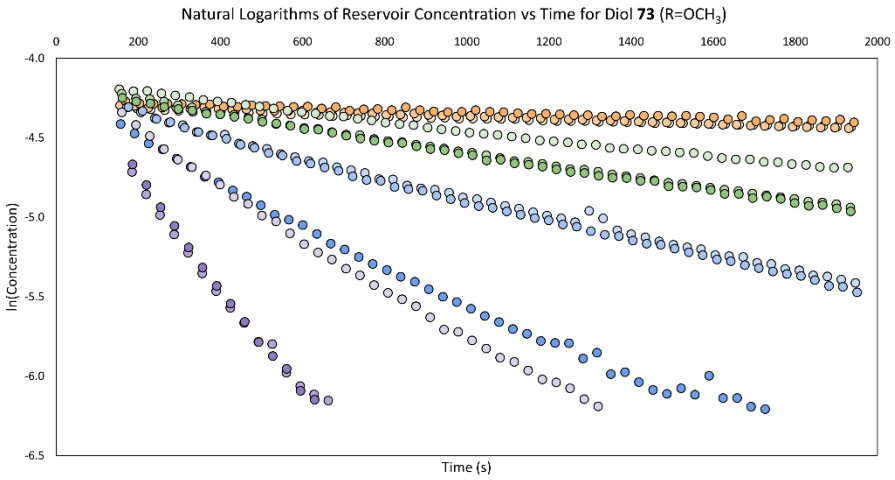

Figure 25 Plots of the natural logarithm of diol concentration over time in seconds for diol **73** in triplicate.

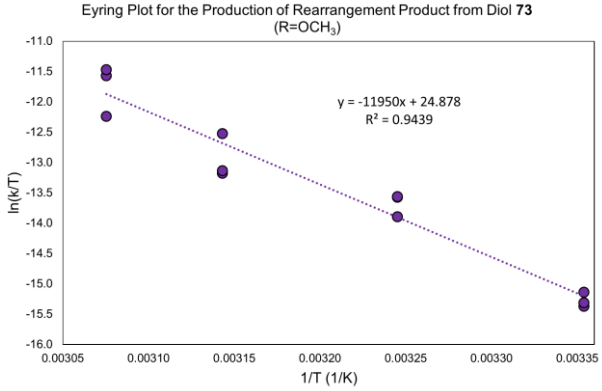

Figure 26 Eyring plot of the consumption of reservoir from diol **73**.

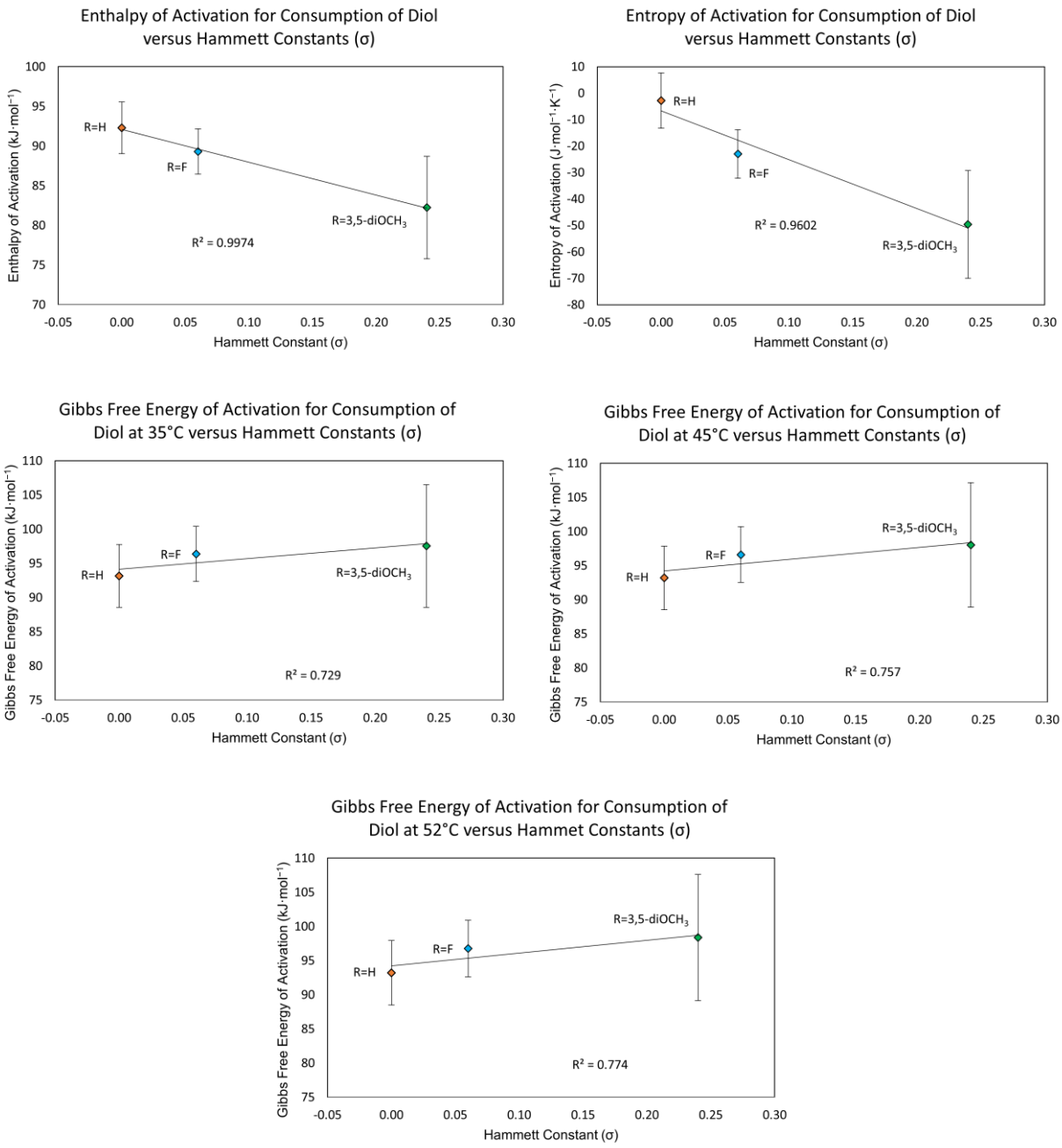

Figure 27 Plots showing the correlation of Hammett constants (σ) for calculated values of entropy ($J \cdot mol^{-1} \cdot K^{-1}$), enthalpy ($kJ \cdot mol^{-1}$), and Gibbs free energy of activation ($kJ \cdot mol^{-1}$) from the consumptions of diols **63** (R=H), **71** (R=3,5-diOMe), and **72** (R=F). The Gibbs free energy Hammett plots for 35°C, 45°C, and 52°C are shown since the enthalpy and entropy of activation for diol **71** could not be determined. The correlation plot for 25°C was omitted since we were unable to determine the rate of consumption for diol **71** at 25°C.

3.8.0 – The Mechanism for the Extended Semipinacol Rearrangement of Thiele Cage Diols

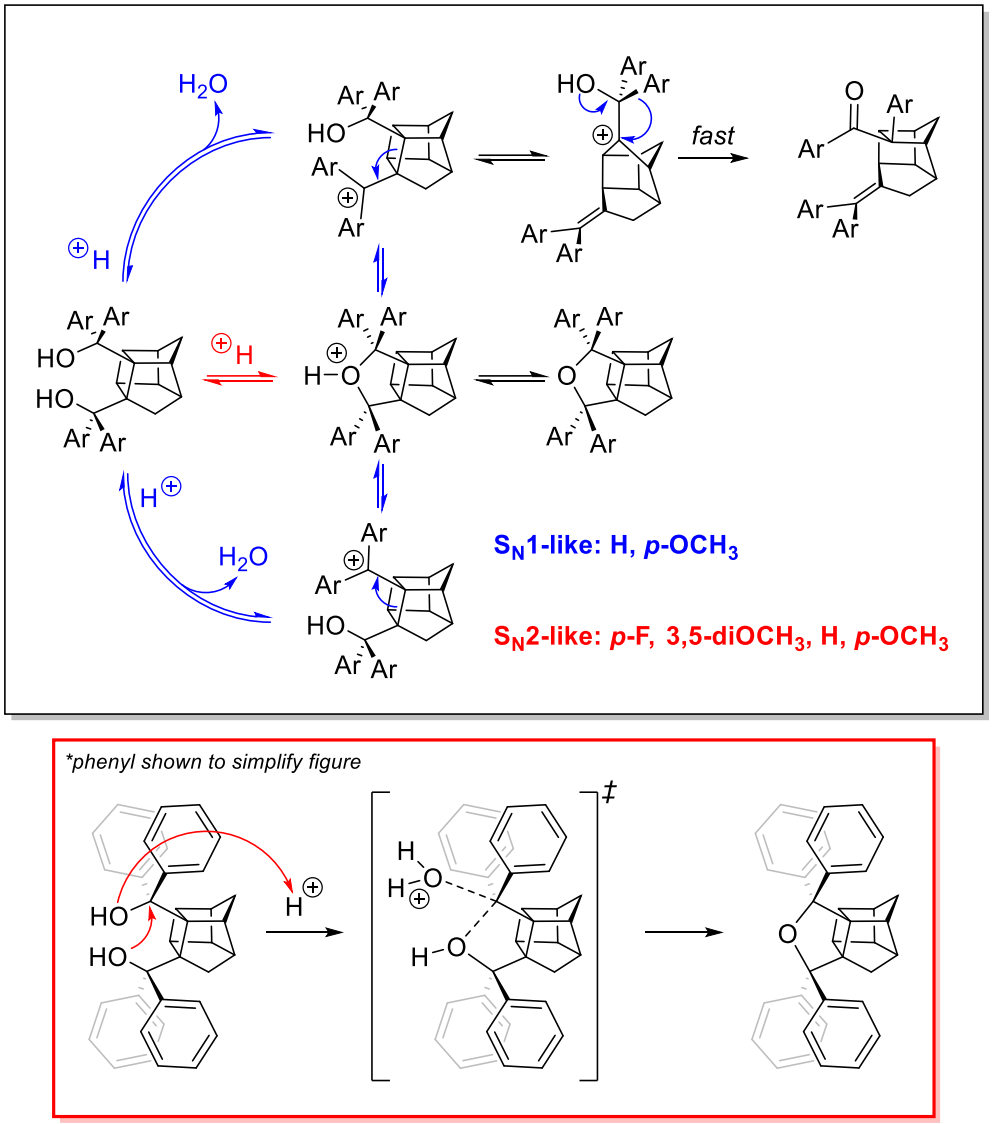

Scheme 31 Complete proposed mechanism including a concerted formation of the tetrahydrofuranyl reservoir directly from the starting material for electron-deficient aryl substituted diols.

In our initial mechanism, we proposed the formation of the carbocation following dehydration of the diol in strong acid. For the more electron deficient species, the rate of consumption of diol is impeded significantly indicating that the carbocation is destabilized. However, at elevated temperatures there is the observable formation of reservoir from diol, with limited formation of rearrangement product for weakly withdrawing aryl substituents, like on diol **72**. With electron-rich species, consumption of the diol is nearly immediate with subsequent formation of the reservoir compound. There are small amounts of rearrangement product formed early in the reaction, likely immediately from the carbocation of the transformation while the remaining amounts are from carbocation formed following protonation of the reservoir compound and ring-opening toward the side and rearrangement products. The absence of rearrangement product for deficient species is likely due to two reasons: any carbocation that is formed is immediately consumed by reaction of the nearby alcohol, forming the reservoir, or formation of the

carbocation is disfavoured and most of the species present remains as the diol. We propose, based on the experimental entropy of activation, that upon protonation of one of the alcohols to the oxonium leaving group, the other alcohol acts as a nucleophile to substitute at the activated center carbinol center. The transition state shown in **Scheme 31** presents an alternate, associative path through the rearrangement process for the diols, particularly the electron-poor diols, that results in immediate formation of the reservoir compound through an S_N2-like mechanism. While the rate of an S_N2 mechanism on a tertiary carbon center is orders of magnitude slower than on secondary or primary carbon centers, it is possible to achieve the substitution provided the electron withdrawing substituents sufficiently destabilize the competing carbocation formation.[18,19] From the common reservoir, and with sufficient energy, the tetrahydrofuranyl core could ring-open to the carbocationic intermediate and progress through the rearrangement like the more electron-rich diols. With that in mind we propose that, for electron-rich species, we expect the reaction to proceed through the extended pinacol rearrangement as previously described beginning with the formation of the carbocation with water leaving after addition of acid. Some of the generated carbocation would form some amounts of rearrangement product immediately and the remainder would form the reservoir. Over the course of the reaction, the reservoir will open up with strong acid to regenerate the carbocation such that there is a small quantity of reservoir available for the rearrangement process. We also observed that, at elevated temperatures for the electron-rich systems, there is a greater quantity of the tricyclic side product produced with little to no side product formed in the reaction of electron-deficient species.

Based on the nature of the formation of the side product and the proposed mechanism for the rearrangement of diol to the main product, it is likely that release of ring strain within the bishomocubane core is a strong driving force that facilitates the forward reaction. Overall, the reaction proceeds through a carbocation intermediate that is the point at which the mechanism splits off, either forming the side product or the rearrangement product. The diastereoselectivity of the primary extended pinacol rearrangement appears to be largely dictated by the π-π stacking interaction of two of the aryl substituents, twisting the geometry of the molecule such that the migrating substituent is antiperiplanar to bond that is breaking, and not by the virtue of an overall-concerted mechanism. Should we desire to design a more-widely applicable system that could undergo a similar rearrangement over $C(sp^3)$-$C(sp^3)$ bonds, the following characteristics should be considered: 1) there should be sufficient strain about the bond that is breaking, likely by means of a polycyclic core, and 2) the migratory substituent is sufficiently carbocation stabilizing.

3.9.0 – References

1. Dao, N.; Sader, J.K.; Oliver, A.G.; Wulff, J.E. *Chem. Commun.* **2019**, *55*, 1600-1603.
2. Hansch, C.; Leo, A.; Taft, R.W. *Chem. Rev.* **1991**, *91*, 165-195.
3. Politzer, P.; Timberlake, J.W. *J. Org. Chem.* **1972**, *37*, 3557-3559.
4. Bolton, J.R.; Carrington, A.; McLachlan, A.D. *Molecular Physics* **1962**, *5*, 31-41.
5. Zhao, Y.; Truhlar, D.G. *Function. Theor. Chem. Acc.* **2008**, *120*, 215-241.
6. Marenich, A.V.; Cramer, C.J.; Truhlar, D.G. *J. Phys. Chem. B* **2008**, *113*, 6378-6396.
7. Gaussian 16, Revision A.03, Frisch, M.J.; Trucks, G.W.; Schlegel, H.B.; Scuseria, G.E.; Robb, M.A.; Cheeseman, J.R.; Scalmani, G.; Barone, V.; Petersson, G.A.; Nakatsuji, H.; Li, X.; Caricato, M.; Marenich, A.V.; Bloino, J.; Janesko, B.G.; Gomperts, R.; Mennucci, B.; Hratchian, H.P.; Ortiz, J.V.; Izmaylov, A.F.; Sonnenberg, J.L.; Williams-Young, D.; Ding, F.; Lipparini, F.; Egidi, F.; Goings, J.; Peng, B.; Petrone, A.; Henderson, T.; Ranasinghe, D.; Zakrzewski, V.G.; Gao, J.; Rega, N.; Zheng, G.;

Liang, W.; Hada, M.; Ehara, M.; Toyota, K.; Fukuda, R.; Hasegawa, J.; Ishida, M.; Nakajima, T.; Honda, Y.; Kitao, O.; Nakai, H.; Vreven, T.; Throssell, K.; Montgomery, J.A., Jr.; Peralta, J.E.; Ogliaro, F.; Bearpark, M.J.; Heyd, J.J.; Brothers, E.N.; Kudin, K.N.; Staroverov, V.N.; Keith, T.A.; Kobayashi, R.; Normand, J.; Raghavachari, K.; Rendell, A.P.; Burant, J.C.; Iyengar, S.S.; Tomasi, J.; Cossi, M.; Millam, J.M.; Klene, M.; Adamo, C.; Cammi, R.; Ochterski, J.W.; Martin, R. L.; Morokuma, K.; Farkas, O.; Foresman, J.B.; Fox, D.J. Gaussian, Inc., Wallingford CT, 2016.

8. Grimme, S. *Chem . – A Eur. J.* **2012**, *18*, 9955-9964.
9. Lu, T.; Chen, Q. *Comput. Theor. Chem.* **2021**, *1200*, 113249.
10. Chen, J.; Kilpatrick, B.; Oliver, A.G.; Wulff, J.E. *J. Org. Chem.* **2015**, *80*, 8979-8989.
11. Wei, R.; Dickson, C.L.; Uhrín, D.; Lloyd-Jones, G.C *J. Org. Chem.* **2021**, *86*, 9023-9020.
12. Budavari, S.; O'Neill, M.J.; Smight, A.; Heckelman, P.E. *The Merck Index*, an Encyclopedia of Chemicals, Drugs and Biologicals – Eleventh Edition, Merck Co., Inc. Rahway, NJ, 1989.
13. a) Gottlieb, H.E.; Kotlyar, V.; Nudelman, A. *J. Org. Chem.* **1997**, *62*, 7512-7515. b) Fulmer, G.R.; Miller, A.J.M.; Sherden, N.H.; Gottlieb, H.E.; Nudelman, A.; Stoltz, B.M.; Bercaw, J.E.; Goldberg, K.I. *Organometallics* **2010**, *29*, 2176-2170.
14. Wynne-Jones, W.F.K; Eyring, H. *J. Chem. Phys.* **1935**, *3*, 492-502.
15. Poë, A.; Sekhar, V.C. *J. Am. Chem. Soc.* **1984**, *106*, 5034-5035.
16. Pondit, A.K.; Das, A.; Banerjea, D. *Transition Met. Chem.* **1991**, *16*, 324-327.
17. Bunrit, A.; Dahlstrand, C.; Olsson, S.K.; Srifa, P.; Huang, G.; Orthaber, A.; Sjöberg, P.J.R.; Biswas, S.; Himo, F.; Samec, J.S.M. *J. Am. Chem. Soc.* **2015**, *137*, 4646-4649.
18. Shibatomi, K.; Soga, Y.; Narayama, A.; Fujisawa, I.; Iwasa, S. *J. Am. Chem. Soc.* **2012**, *134*, 9836-9839.
19. Zhang, Y.-Q.; Poppel, C.; Panfilova, A.; Bohle, F.; Grimme, S.; Gansauer, A. *Angew. Chem. Int. Ed.* **2017**, *56*, 9719-9722.

Chapter Four

Experimental Procedures and Supplementary Data

General Methods. Unless stated otherwise, all reactions were performed in flame-dried glassware equipped with rubber septa under an inert argon atmosphere. Organic solutions were concentrated at 30 to 50°C in vacuo by rotary evaporation. THF was freshly distilled over sodium and benzophenone. Unless stated otherwise, all organometallic reagents were purchased from Sigma-Aldrich and were used as received. Solvents and air-sensitive solutions were transferred via stainless-steel cannula or via plastic syringe equipped with a stainless-steel needle. Thin layer chromatography was performed on MACHEREY-NAGEL pre-coated ALUGRAM® SILG/UV_{254} TLC plates (0.20 mm silica gel 60 with 254 nm fluorescent indicator). TLC plates were visualized under UV light (254 nm) and developed by staining and heating with $KMnO_4$. Flash column chromatography was performed on silica gel (60 Å, 40-63 µm, Silicycle SiliaFlash® F60).

All NMR spectra for characterization were recorded at ambient temperature (298 K). The ^1H NMR and ^{13}C NMR spectra for compounds **66**, **68**, **69**, **71**, and **72** were recorded at 500 and 126 MHz, respectively, on a Bruker AVANCE NEO 500 spectrometer equipped with a BBF probe. The ^1H and ^{13}C NMR spectra for compounds **63**, **73**, and **77** were recorded at 300 and 76 MHz, respectively, on a Bruker AVANCE 300 spectrometer equipped with a 5 mm QNP probe. ^1H chemical shifts (δ) are reported in parts-per-million (ppm) relative to tetramethylsilane and referenced to the solvent peak ($CDCl_3$, δ 7.26; CD_2Cl_2, δ 5.32; $(CD_3)_2CO$, δ 2.05). NMR data is presented as follows: chemical shift, multiplicity (s = singlet, d = doublet, dd = doublet of doublets, t = triplet, q = quartet, m = multiplet, tdd = triplet of doublet of doublets, bs = broad singlet, app = apparent), coupling constants (*J*, reported in Hz), integration. All ^{13}C-NMR spectra are proton-decoupled ($^{13}C\{^1H\}$). ^{13}C chemical shifts (δ) are reported in parts-per-million (ppm) relative to tetramethylsilane and referenced to the solvent peak ($CDCl_3$, δ 77.16; CD_2Cl_2, δ 53.84; $(CD_3)_2CO$, δ 29.84). All ^{19}F NMR spectra are proton-decoupled ($^{19}F\{^1H\}$). ^{19}F chemical shifts (δ) are reported in parts-per-million (ppm) and are uncorrected. Prior to recording NOESY spectra, samples were sparged by bubbling argon through the NMR tube for several minutes.

Infrared spectra were obtained using a Perkin-Elmer ATR spectrometer and a Perkin-Elmer FTIR Spectrometer Two via thin film on a salt (NaCl) plate. IR wavenumbers (v) are reported cm^{-1}. Accurate masses were obtained by electrospray ionization high resolution mass spectrometry (HRMS) using a Thermo Scientific™ Exactive™ Plus Orbitrap Ultimate 3000 LC-MS system. Melting points were measured using a Gallenkamp melting point apparatus and are uncorrected.

General Procedure A: Preparation of Thiele Cage Diols. A flame-dried round bottom flask under inert Ar atmosphere was charged with Thiele cage ester **77** and THF (to a concentration of 0.07 to 0.10 M; typically, 0.36 mmol in 4 mL THF). To this solution was added the desired commercial organometallic reagent solution at 0°C dropwise over 5 minutes. The reaction mixture was warmed to room temperature overnight (10-14 hours), then cooled to 0°C. The mixture was quenched with the addition of saturated solution of NH_4Cl (5 mL) and diluted with distilled water (5 mL) and Et_2O (10 mL). The two phases were separated, and the aqueous phase was the extracted with Et_2O (3 x 10 mL). The combined organic phases were washed with brine (1 x 20 mL), dried over Na_2SO_4, then concentrated *in vacuo* to afford the crude diol (typically as a foamy solid). Each diol was purified via flash column chromatography with hexanes/ethyl acetate as the eluent.

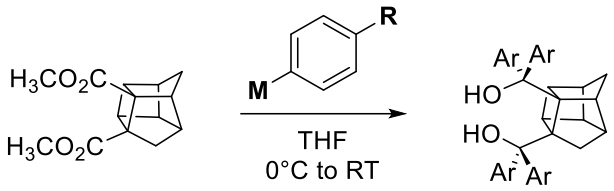

General Procedure B: Single-scan ^{1}H-NMR Kinetics Experiments at Variable Temperature. 1,4-Dinitrobenzene (DNB; δ 8.10) was used as an internal standard for all ^{1}H kinetics experiments. Samples were measured at 500.27 MHz in a Bruker AVANCE NEO 500 Spectrometer at 25, 35, 45, and 52°C. For each temperature, samples were measured in triplicate with a set of 54 single-scan spectra, with each set separated by 34.14 seconds (AQ=2.62144 s, D1=1.50 s, D10=30.00 s) for a total of 30 minutes 12 seconds (plus the time measured from addition of acid solution to a sample to the first scan; typically, around 2 minutes). The spectra were centered (O1P) at chemical shift 4.50 ppm with a spectral width (SW) of 12.49 ppm (from 10.75 to −1.75 ppm).

A stock solution of diol (6.00 mL, 27.7 mM) and a stock solution of DNB (2.00 mL, 127 mM) were prepared in $CDCl_3$. To each NMR tube was added 0.45 mL of diol stock solution and 0.05 mL of DNB stock solution and mixed with a vortex mixer. A stock solution of *p*-toluenesulfonic acid (1.00 mL, 1.44 M) in CD_3OD, of which 0.10 mL was diluted in 0.90 mL $CDCl_3$ for a concentration of 144 mM in a $CDCl_3$/CD_3OD solvent mixture. For faster reacting substrates (*p*-OCH_3, *p*-CH_3, H), a sample was reacted in advance to be used to shim the magnet of the spectrometer. For slower reacting substrates (3,5-diOCH_3, *p*-F), the magnet of the spectrometer was shimmed with an unreacted sample Samples were preheated in a warmed distilled water bath at the respective temperature of the experiment (e.g. samples measured at 45°C were preheated in a 45°C bath). Before addition of the PTSA stock solution, the magnet was shimmed with the appropriate shimming sample and a t=0, single-scan ^{1}H spectrum was collected for the sample being measured. The sample was returned to the distilled water bath, then 0.10 mL of the $CDCl_3$/CD_3OD PTSA mixture was added and mixed (final diol concentration of 0.20 mM in 0.60 mL of 98:2 $CDCl_3$:CD_3OD) with a vortex mixer and quickly inserted into the spectrometer. The final concentrations of each initial material in the tube were 20.8 mM for the diol, 10.4 mM for DNB, and 24 mM for PTSA.

Compound 63

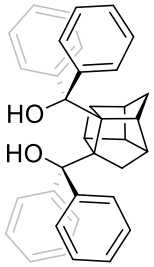

Prepared according to the procedure by Dao et al.,[1] following **General Procedure A**, with commercial (Aldrich) phenyllithium solution (1.8 M in dibutyl ether).

^{1}H NMR (300 MHz, $CDCl_3$): δ 7.40-7.36 (m, 2H), 7.24-6.95 (m, 15H), 6.83-6.78 (m, 3H), 4.65 (bs, 1H), 4.25 (bs, 1H), 3.51-3.46 (m, 1H), 3.15-3.11 (m, 1H), 3.08-3.03 (m, 1H),2.74-2.62 (m, 2H), 2.57-2.54 (m, 1H), 2.47-2.44 (m, 1H), 2.08 (d, *J* = 11.8 Hz, 1H), 0.96 (d, *J* = 11.3 Hz, 1H), −0.65 (d, *J* = 11.3 Hz, 1H).

^{13}C NMR (75 MHz, $CDCl_3$): δ 147.5, 147.2, 146.8, 145.7, 128.1, 127.9, 127.6, 127.3, 127.0, 126.9, 126.8, 126.7, 126.3, 80.4, 80.4, 70.2, 68.8, 53.9, 47.3, 42.7, 42.4, 40.9, 38.9, 38.3.

IR (film): 3390, 3057, 2973, 1639, 1493, 1446 cm^{-1}.

Compound 66

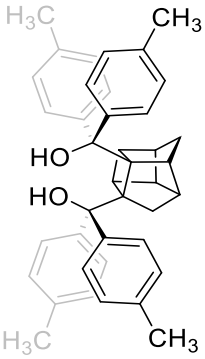

Prepared following **General Procedure A**, with compound **76** (160 mg, 0.645 mmol) commercial (Aldrich) 4-tolylmagnesium bromide solution (1.0 M in THF). Compound **66** was isolated as a crude light yellow solid (563 mg) and was purified by flash column chromatography (hexanes:EtOAc 10:1) as a white solid (200 mg, 0.362 mmol, 56% yield).

^{1}H NMR (500 MHz, CD_2Cl_2): δ 7.26 (d, *J* = 8.4 Hz, 2H), 7.08-7.03 (m, 6H), 6.92-6.86 (m, 4H), 6.81 (d, *J* = 8.0 Hz, 2H), 6.62 (d, *J* = 8.0 Hz, 2H), 4.46 (s, 1H), 4.32 (s, 1H), 3.42-3.39 (m, 1H), 3.04-3.00 (m, 2H), 2.64-2.60 (m, 2H), 2.52-2.51 (m, 1H), 2.42-2.41 (m, 1H), 2.31 (s, 3H), 2.27 (s, 3H), 2.22 (s, 3H), 2.15 (s, 3H), 0.94 (d, *J* = 11.1 Hz, 1H), −0.59 (d, *J* = 11.1 Hz, 1H).

^{13}C NMR (126MHz, CD_2Cl_2): δ 145.1, 144.9, 144.7, 143.8, 136.9, 135.7, 128.8, 128.6, 128.4, 128.3, 128.3, 128.1, 128.0, 127.2, 80.3, 80.2, 47.6, 44.7, 43.1, 42.5, 41.2, 39.4, 38.8, 21.3, 21.1, 21.1, 21.1.

IR (film): 3536, 3245, 3025, 2970, 2921, 1508, 807 cm^{-1}.

Melting point: 183-184°C.

HRMS (ESI+): m/z [M + Na]$^+$ calculated for $C_{40}H_{40}O_2Na$: 575.2921, found: 575.2925.

Compound 68

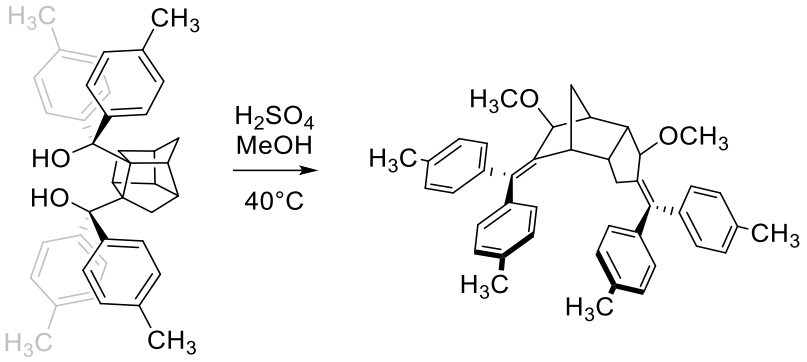

66 **68** (12.8%)

To a 20-mL scintillation vial with solution of **66** (261 mg, 472 mmol) in methanol (5.0 mL) was added sulfuric acid (100 µL, 1.88 mmol) in a solution of methanol (1 mL). The mixture was heated at 40°C overnight for 16 hours, then cooled to 0°C and quenched with saturated $NaHCO_3$ solution to a neutral solution. The mixture was diluted with water (5 mL) and Et_2O (5 mL), then the two phases were separated, and the aqueous layer was further extracted with Et_2O (2 x 5 mL). The combined organic phase was dried with anhydrous sodium sulfate, filtered, then concentrated in vacuo to a crude yellow solid (308 mg). The crude was purified via flash column chromatography (hexanes:EtOAc 4:1) and subsequent preparative TLC (Hexanes:EtOAc 1:1) to provide **68** as a white solid (35.1 mg, 60.4 mmol, 13% yield).

^{1}H NMR (500 MHz, $(CD_3)_2CO$): δ 7.32 (d, *J* = 8.1 Hz, 2H), 7.28 (d, *J* = 7.8 Hz, 2H), 7.21 (d, *J* = 8.2 Hz, 2H), 7.10 (d, *J* = 8.5 Hz, 2H), 7.01 (d, *J* = 7.9 Hz, 2H), 6.97 (d, *J* = 7.8 Hz, 2H), 6.55 (d, *J* = 8.0 Hz, 2H), 4.37 (s, 1H), 4.25 (d, *J* = 2.0 Hz, 1H), 2.94 (d, 1H – found through compound **69**), 2.92 (s, 3H), 2.91 (s, 3H), 2.67-2.54 (m, 4H), 2.38 (s, 3H), 2.32 (s, 3H), 2.27 (s, 3H), 2.25 (s, 3H), 1.81 (d, *J* = 9.3 Hz, 1H), 1.39 (d, *J* = 9.3 Hz, 1H).

^{13}C NMR (126 MHz, $(CD_3)_2CO$): δ 143.1, 141.5, 140.4, 140.2, 140.1, 139.7, 138.4, 137.2, 136.3, 136.1, 135.5, 135.4, 130.0, 129.6, 129.2, 128.7(72), 128.7(66), 128.5, 128.0, 127.7, 82.3, 79.3, 56.6, 54.7, 49.4, 46.1, 44.0, 43.8, 37.5, 33.1, 20.3, 20.2(23), 20.2(23), 20.2(21).

HRMS (ESI+): m/z [M + Na$^+$] calculated for $[C_{42}H_{44}O_2Na]^+$: 603.3234, found: 603.3233.

Compound 69

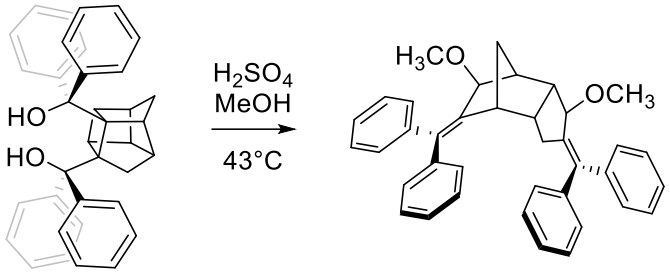

63 **69** (9.1%)

To a 20-mL scintillation vial with a solution of **63** (52.1 mg, 0.105 mmol) in methanol (3.0 mL) was added concentrated sulfuric acid (14.0 µL, 0.263 mmol). Upon addition of acid, the mixture became yellow, then quickly became colourless again. After 2.5 minutes, more methanol (0.5 mL) was added and the reaction was placed into a pre-heated oil bath at 43°C while stirring with the vial loosely capped. The reaction was stirred for 2 hours 50 minutes and cooled to R.T. before quenching with a large excess (~250 mg) of K_2CO_3 while stirring for an additional 10 minutes. The mixture was filtered through cotton and washed with small volumes of MeOH and EtOAc, then concentrated to a crude, off-white solid (72.2 mg). The product was purified via flash column chromatography (gradient eluent – hexanes:EtOAc 20:1 – 10:1 – 5:1) to provide a white solid (~5 mg, 0.010 mmol, 9% yield).

^{1}H NMR (500 MHz, $CDCl_3$): δ 7.43-7.42 (m, 2H), 7.40-7.38 (m, 3H), 7.35-7.32 (m, 3H), 7.25-7.24 (m, 3H), 7.20-7.18 (m, 2H), 7.16-7.13 (m, 1H), 7.13-7.10 (m, 3H), 6.68-6.64 (m, 2H), 4.39 (s, 1H), 4.24 (d, *J* = 1.6 Hz, 1H), 3.01 (d, *J* = 4.4 Hz, 1H), 2.94 (s, 3H), 2.94 (s, 3H), 2.77 (dd, *J* = 17.5, 10.2 Hz, 1H), 2.66 (tdd, *J* =10.1, 4.9, 1.5 Hz, 1H), 2.60 (d, *J* = 5.0 Hz, 1H), 2.56 (dd, *J* = 10.4, 5.2 Hz, 1H), 2.30 (d, *J* = 17.5 Hz, 1H), 1.91 (d, *J* = 9.6 Hz, 1H), 1.44 (d, *J* = 9.2 Hz, 1H).

^{13}C NMR (126 MHz, $CDCl_3$): δ 143.9, 143.0, 142.9, 142.7, 142.1, 142.1, 139.4, 137.9, 130.2, 129.8, 129.4, 128.8, 128.3, 128.2, 127.7, 127.6, 127.0, 126.9, 126.4, 126.4, 82.9, 79.8, 54.7, 56.1, 49.6, 46.0, 44.3, 44.06, 38.2, 33.4.

IR (film): 3057, 3024, 2926, 2815, 1599, 1492, 1443 cm^{-1}.

Melting point: 173-175°C.

HRMS (ESI+): m/z [M + Na^+] calculated for $[C_{38}H_{36}O_2Na]^+$: 547.2607, found: 547.2607.

Compound 71

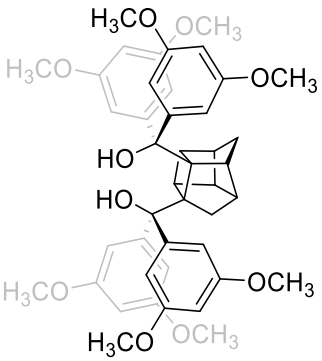

Prepared following **General Procedure A**, with compound **76** (104 mg, 0.420 mmol) and 3,5-dimethoxyphenylmagnesium bromide solution (1.0 M in THF). Compound **71** was isolated as a crude yellow oil (576 mg) and purified by flash column chromatography (Hexanes:EtOAc 10:1) to a yellow solid (230 mg, 74% yield).

^{1}H NMR (500 MHz, $CDCl_3$): δ 6.58 (d, *J* = 2.2Hz, 1H), 6.53-6.45 (m, 5H), 6.35-6.30 (m, 1H), 6.28 (t, *J* = 2.2 Hz, 1H), 6.23 (t, *J* = 2.3 Hz, 1H), 6.12 (t, *J* = 2.1 Hz, 1H), 5.96 (t, *J* = 2.2 Hz, 1H), 3.72-3.70 (m, 6H). 3.70-3.69 (m, 6H), 3.67-3.64 (m, 12H), 3.45 (q, *J* = 4.8 Hz, 1H), 3.09-3.05 (m, 2H), 2.72-2.62 (m, 2H – contains d, *J* = 11.2 Hz at δ2.69), 2.54-2.51 (m, 1H), 2.48 (t, *J* = 4.2 Hz, 1H), 2.09 (d, *J* = 11.2 Hz, 1H), 1.03 (d, *J* = 11.2 Hz, 1H), −0.41 (d, *J* = 11.2 Hz, 1H).

^{13}C NMR (126 MHz, $CDCl_3$): δ 160.3, 159.9, 159.5, 149.7, 149.0, 148.6, 147.9, 106.7, 105.7, 99.8, 98.7, 98.5, 97.9, 80.4, 79.9, 70.3, 69.1, 55.4(41), 55.4(39), 55.1, 54.9, 54.4, 47.0, 44.3, 43.2, 42.1, 41.0, 38.9, 38.5, 31.1.

IR (film): 3429, 2963, 1607, 1458, 1423 cm^{-1}.

Melting point: 93-95°C.

HRMS (ESI+): m/z [M + Na^+] calculated for $[C_{44}H_{48}O_{10}Na]^+$: 759.3140, found: 759.3143.

Compound 72

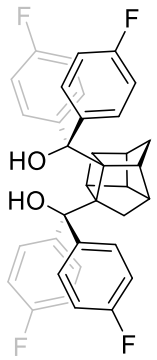

Prepared following **General Procedure A**, with Compound **76** (110 mg, 0.443 mmol) and 4-fluorophenylmagnesium bromide solution (1.0 M in THF). Compound **72** was isolated as a crude, fluffy

yellow solid and was purified by flash column chromatography (Hexanes:EtOAc 10:1) to a white solid (109 mg, 0.192 mmol, 43% yield).

^{1}H NMR (500 MHz, $CDCl_3$): δ 7.18 (dd, J_{HH} = 8.9 Hz, J_{HF} = 5.3 Hz, 2H), 7.06 (dd, J_{HH} = 8.8 Hz, J_{HF} = 5.4 Hz, 2H), 7.03 (dd, J_{HH} = 8.8 Hz, J_{HF} = 5.4 Hz, 2H), 6.97-6.92 (m, 2H), 6.88 (dd – app. t, J_{HH} = J_{HF} = 8.7 Hz, 2H), 6.81 (dd – app. t, J_{HH} = J_{HF} = 8.7 Hz, 2H), 6.61 (dd – app. t, J_{HH} = J_{HF} = 8.6 Hz, 2H), 6.48 (dd – app. t, J_{HH} = J_{HF} = 8.7 Hz, 2H), 5.76 (bs, 1H), 4.24 (bs, 1H), 3.41 (m, 1H), 3.08 (m, 1H), 2.93 (s, 1H), 2.82 (m, 1H), 2.65 (m, 1H), 2.55 (d, *J* = 11.9 Hz, 1H), 2.50 (m, 1H), 2.24 (d, *J* = 11.7 Hz, 1H), 1.02 (d, *J* = 11.4 Hz, 1H), −0.63 (d, *J* = 11.5 Hz, 1H).

^{13}C NMR (126 MHz, $CDCl_3$): δ 162.9, 162.5, 162.4, 160.9, 160.5(52), 160.5(49), 143.7, 143.6, 143.6, 142.8, 142.7, 141.2, 130.1, 130.1, 128.6, 128.5, 114.8, 114.6, 114.3, 114.2, 114.1(12), 114.1(07), 113.8, 113.7, 80.4, 79.5, 69.9, 69.1, 53.5, 47.7, 44.4, 42.4, 42.3, 40.9, 39.0, 38.4.

^{19}F NMR (471 MHz, $CDCl_3$): δ −114.9, −116.2, −116.7, −117.3.

IR (film): 3391, 2975, 2868, 1602, 1506 cm^{-1}.

Melting point: 182-185°C.

HRMS (ESI–): m/z [M – H^+] calculated for $[C_{36}H_{27}F_4O_2]^-$: 567.1953, found: 567.1950.

Compound 73

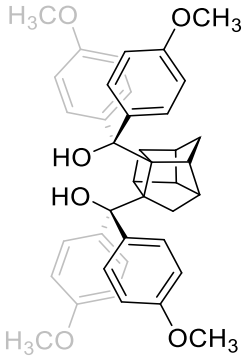

Prepared according to the procedure by Dao et al.[1] with 4-bromoanisole (Aldrich) and n-butyllithium (2.5 M) from Acros.

^{1}H NMR (500MHz, $CDCl_3$): δ 7.21 (d, *J* = 9.0 Hz, 2H), 7.06 (d, *J* = 8.9 Hz, 2H), 7.03 (d, *J* = 8.9 Hz, 2H), 6.95-6.85 (m, 2H), 6.73 (d, *J* = 9.0 Hz, 2H), 6.64 (d, *J* = 9.2 Hz, 2H), 6.47 (d, *J* = 8.8 Hz, 2H), 6.33 (d, *J* = 8.9 Hz, 2H), 3.77 (s, 3H), 3.74 (s, 3H), 3.71 (s, 3H), 3.67 (s, 3H), 3.44-3.39 (m, 1H), 3.12-3.08 (m, 1H), 2.98-2.93 (m, 1H), 2.79-2.71 (m, 1H), 2.60-2.52 (m, 2H), 2.50-2.43 (m, 1H), 2.13 (d, *J* = 11.7 Hz, 1H), 0.97 (d, *J* = 11.1 Hz, 1H), −0.56 (d, *J* = 11.2 Hz, 1H).

^{13}C NMR (126 MHz, $CDCl_3$): δ 158.2, 158.0, 157.5, 157.3, 140.2, 139.8, 138.3, 129.5, 129.3, 129.0, 128.2 ,113.0, 112.5, 112.0, 80.1, 79.6, 70.1, 69.0, 55.2, 54.9, 54.7, 47.4, 42.2, 40.9, 39.0, 38.4.

IR (film): 3315, 2963, 2835, 2864, 1608, 1583, 1509, 1251 cm^{-1}.

Compound 77

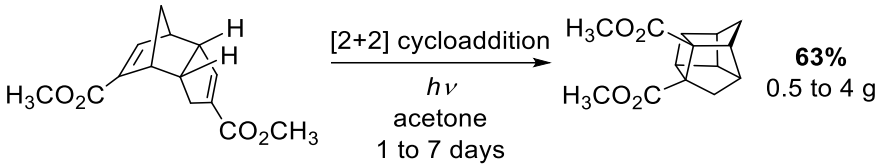

Prepared following literature procedure[1]: A 100-mL quartz round-bottom flask was charged with a solution of Thiele's ester (498 mg, 2.00 mmol) in acetone (50 mL). The solution was irradiated at 254-nm in a photochemical chamber reactor (model RMRM-600 Rayonet) for 14 hours. Following the consumption of all starting material (17 hours), the mixture was concentrated to a yellow residue (~600 mg). As the compound is not easily detected by standard methods (UV at 254 nm or TLC stains), the compound **77** was flowed quickly over silica gel (via flash column chromatography) with 7% EtOAc in hexanes. Fractions collected were allowed to concentrate slightly at ambient temperature and pressure until the appearance of a colourless oil on the lip of the tubes was noted. Fractions with oil were carefully collected and checked by ^{1}H-NMR to confirm their identity, and compound **77** was isolated as a colourless oil (314 mg, 1.27 mmol, 63%).

Note: Larger quantities of **77** could be isolated by increasing the concentration of the solution, but typically require much longer reaction times to observe complete consumption of starting material.

^{1}H NMR (300 MHz, $CDCl_3$): δ 3.68 (s, 3H), 3.65 (s, 3H), 3.15-3.10 (m, 1H), 2.93-2.88 (m, 1H), 2.87-2.84 (m, 1H), 2.79-2.76 (m, 2H), 2.56-2.54 (m, 1H), 2.16 (d, *J* = 11.4 Hz, 1H), 1.74-1.62 (m, 2H), 1.50 (d, *J* = 11.3 Hz, 1H).

^{13}C NMR (75 MHz, $CDCl_3$): δ 173.8, 173.6, 61.1, 59.4, 54.3, 51.9, 51.8, 47.4, 44.3, 43.7, 41.2, 40.9, 39.6, 37.7.

IR (film): 3631, 3548, 3444, 2954, 2861, 1733, 1436 cm^{-1}.

References

1. Dao, N.; Sader, J.K.; Oliver, A.G.; Wulff, J.E. *Chem. Commun.* **2019**, *55*, 1600-1603.

Compound 63

^{1}H NMR Spectrum

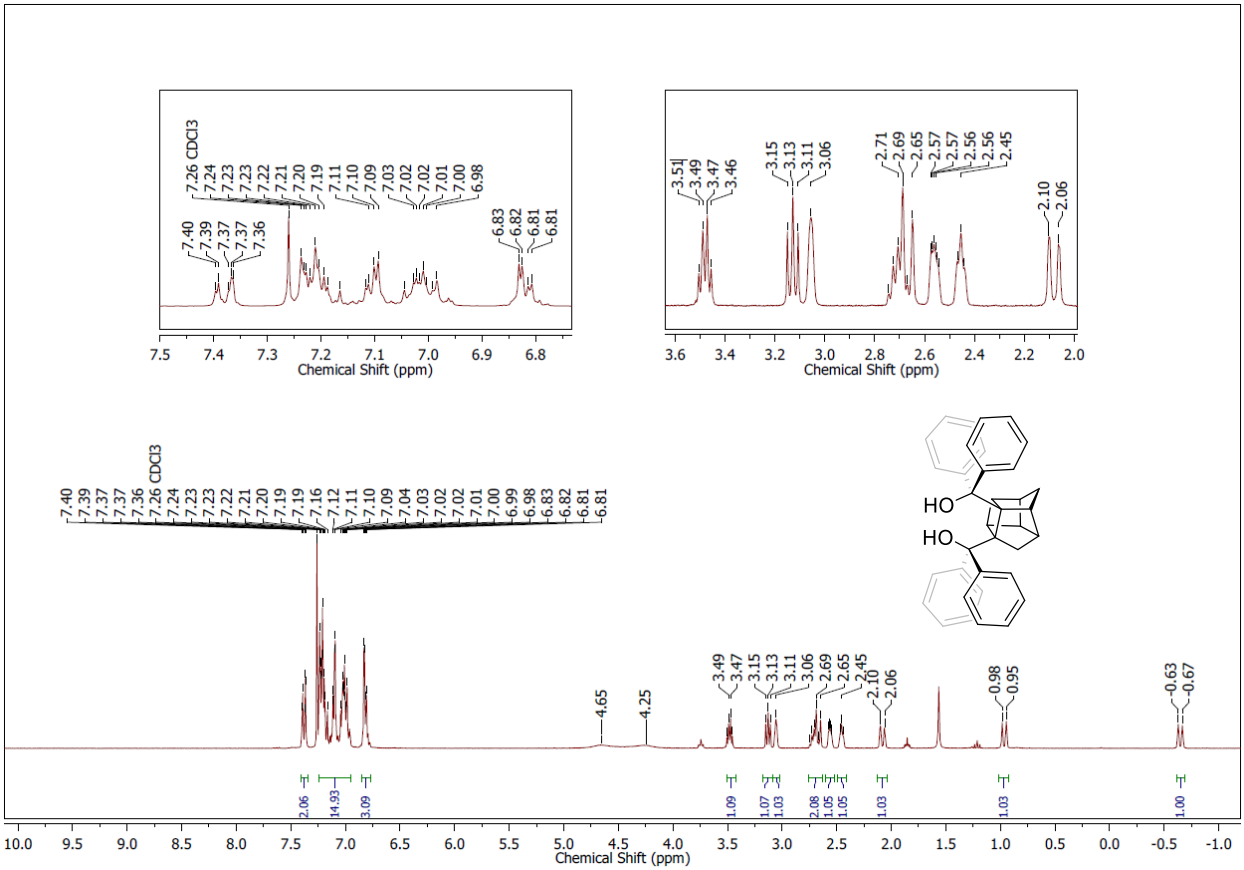

Compound 63

^{13}C NMR Spectrum

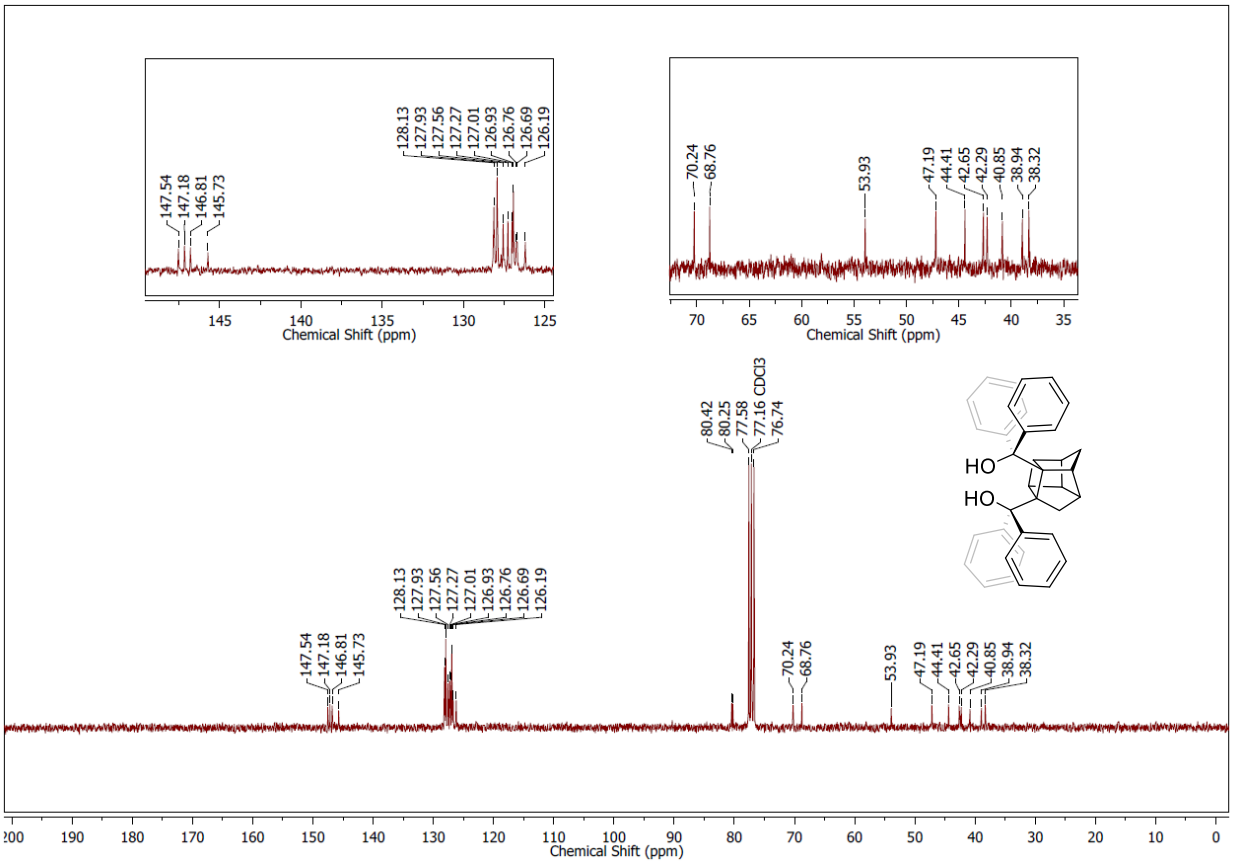

Compound 63

IR Spectrum

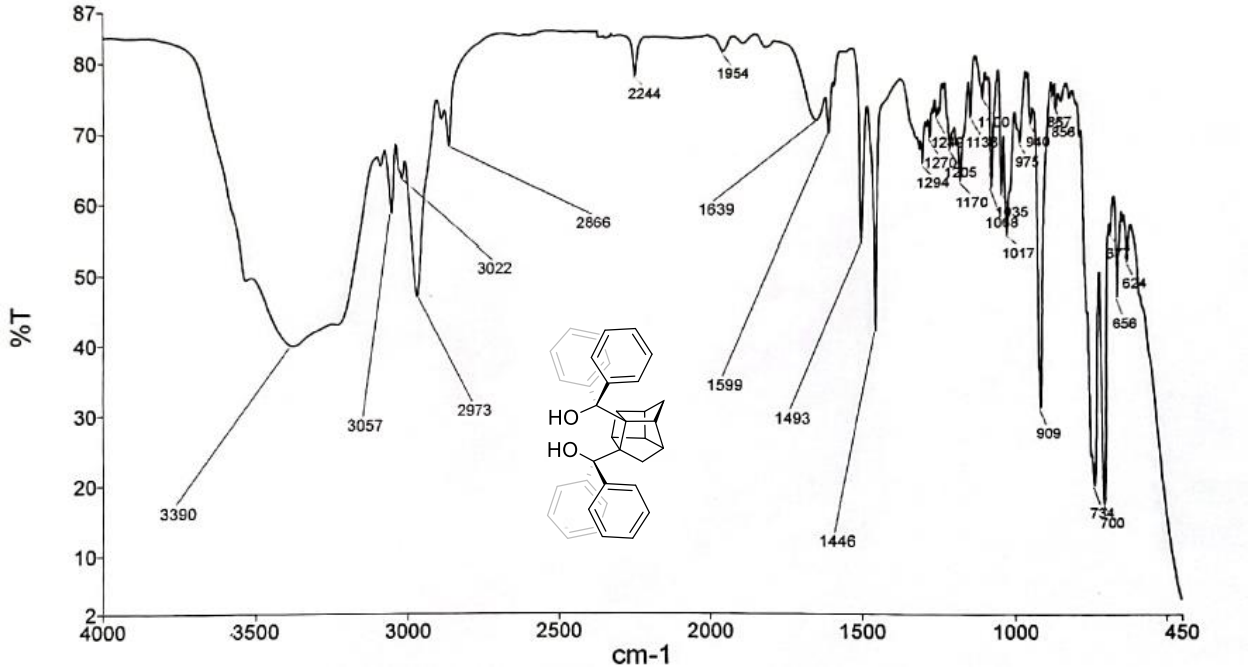

Compound 66

^{1}H NMR Spectrum

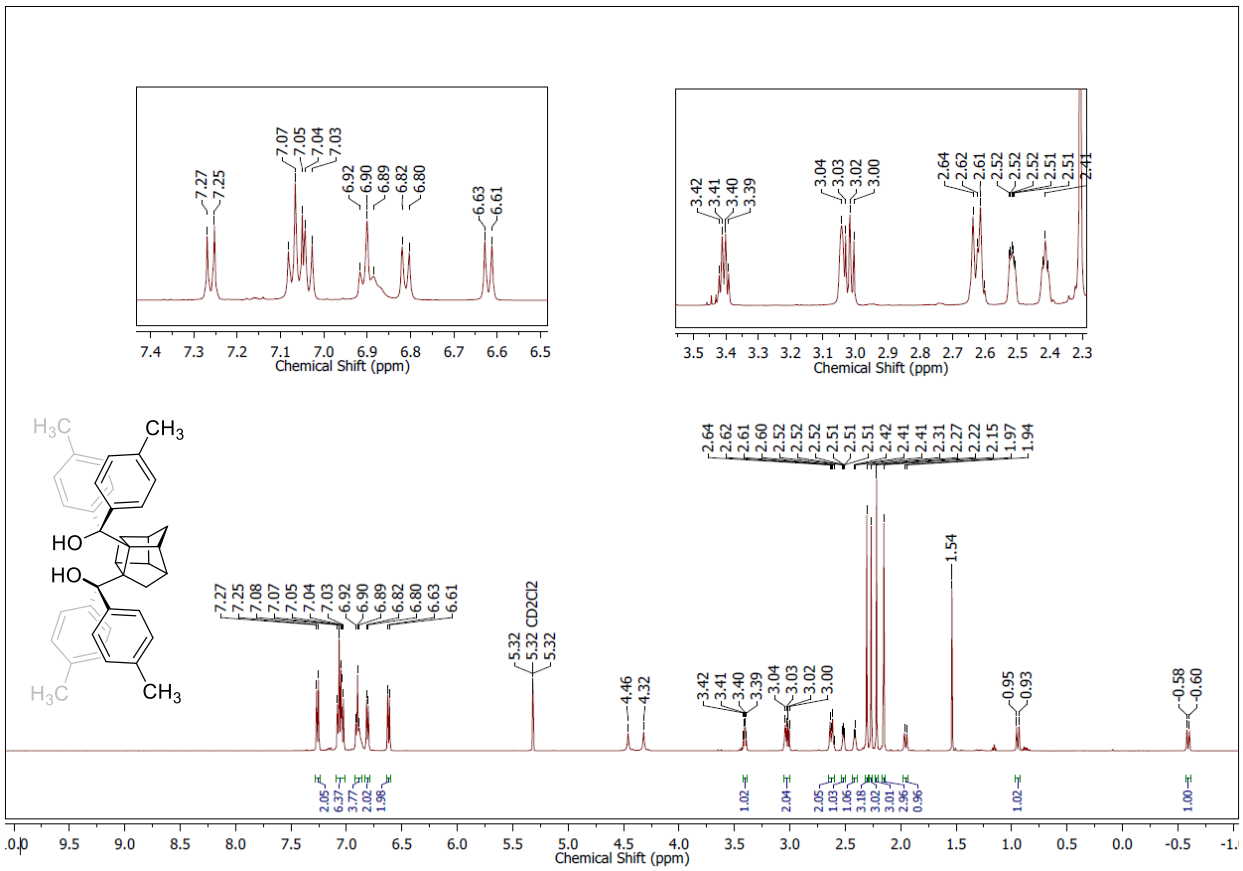

Compound 66

^{13}C NMR Spectrum

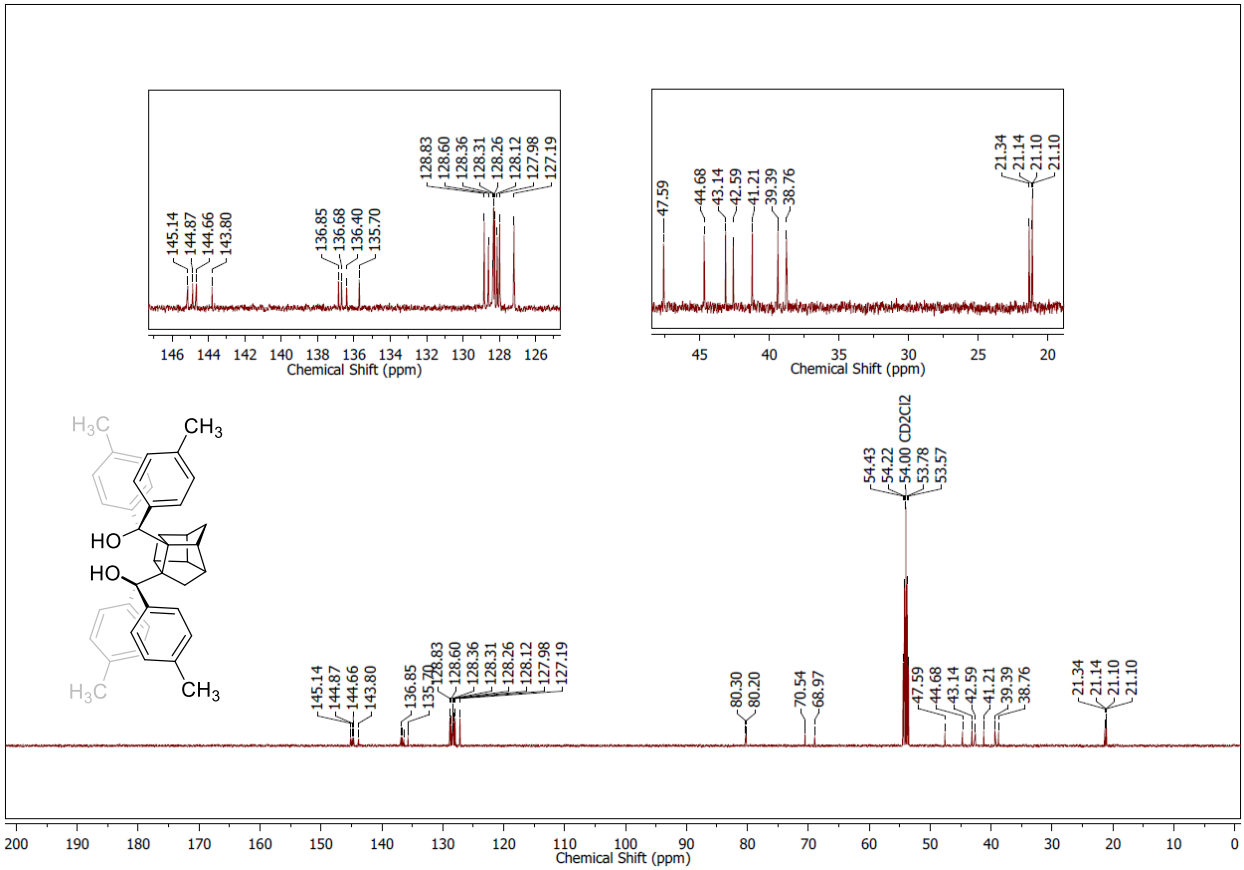

Compound 66

IR Spectrum

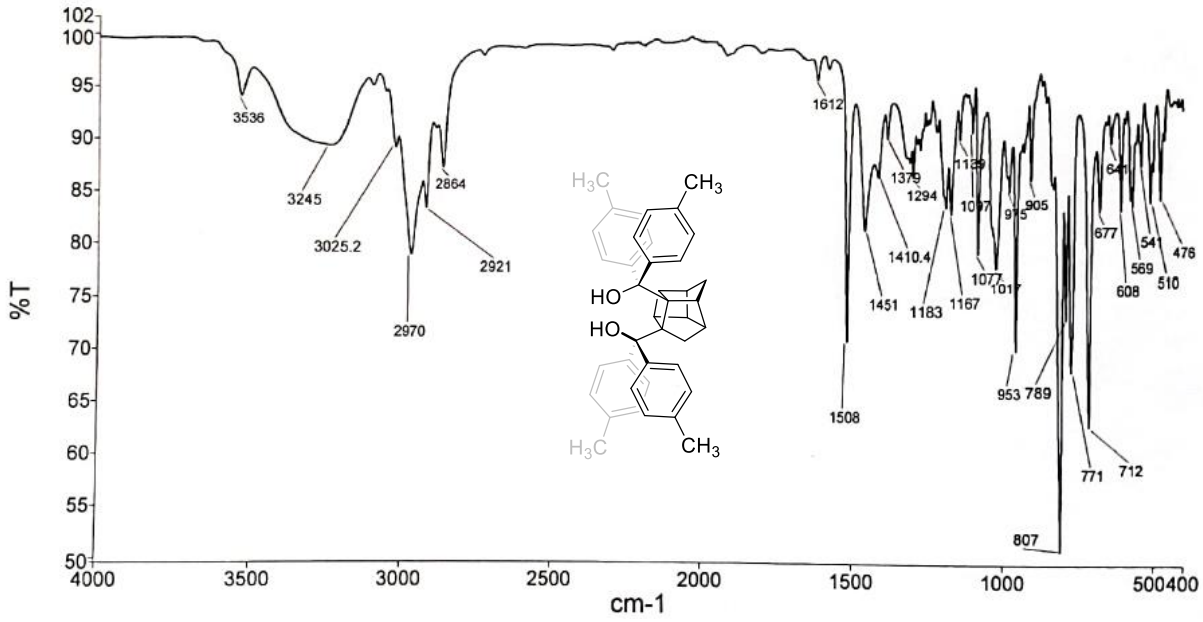

Compound 71

^{1}H NMR Spectrum

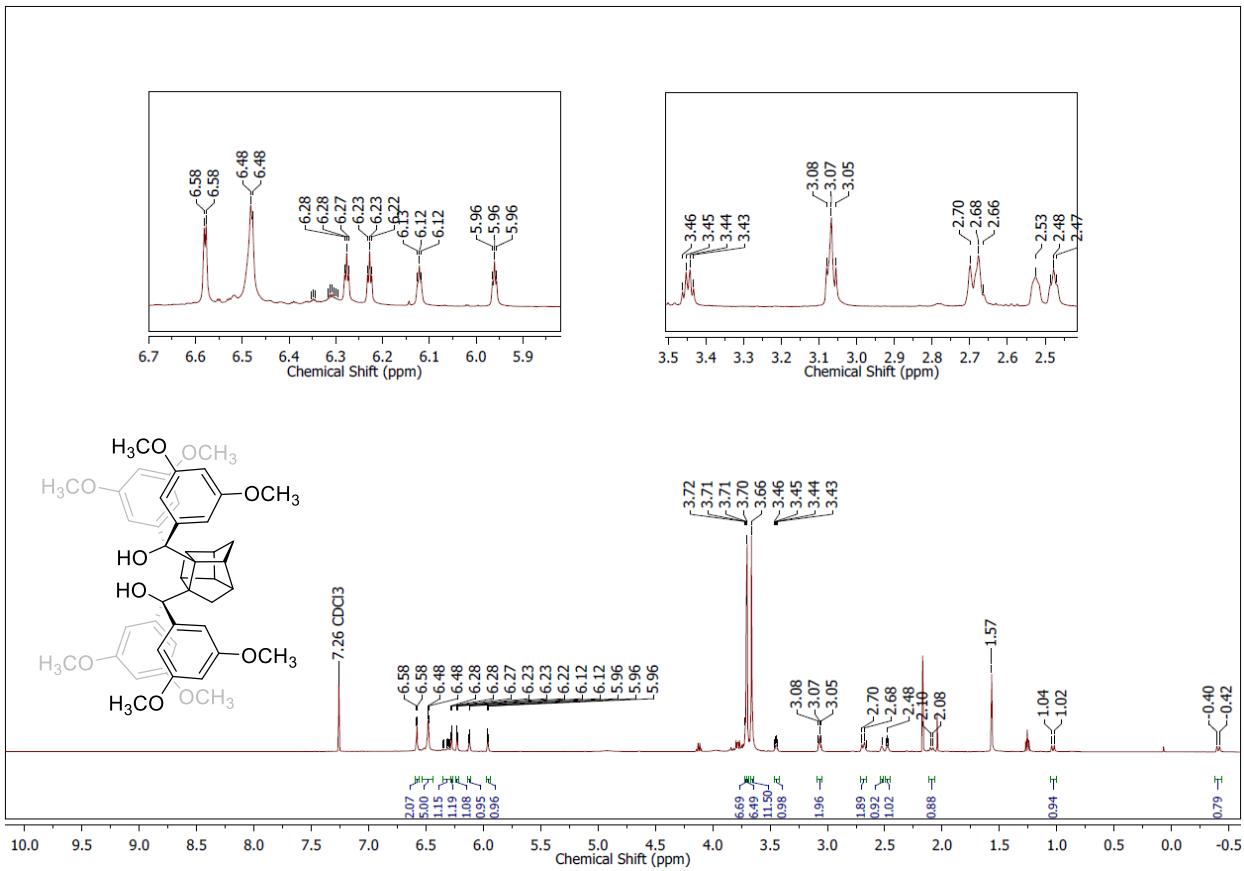

Compound 71

^{13}C NMR Spectrum

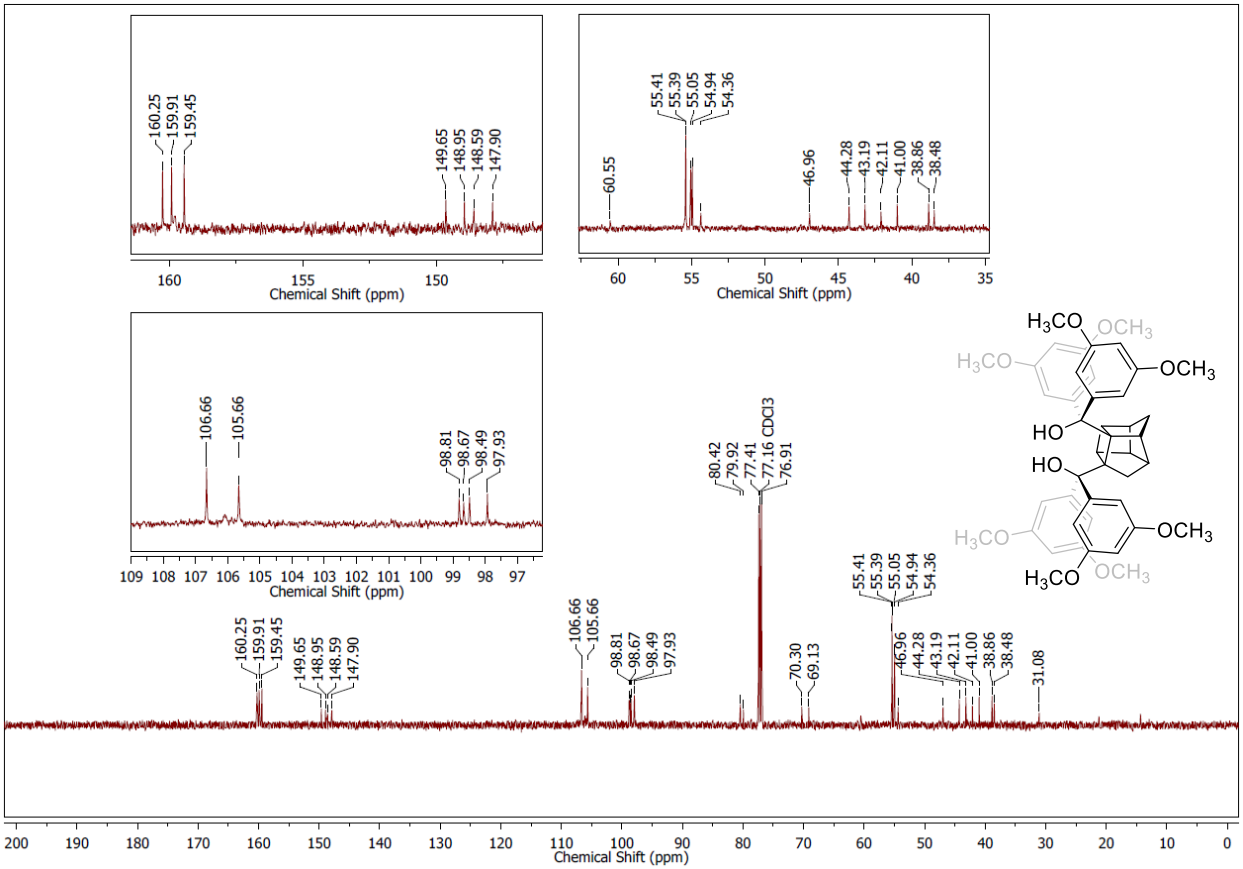

Compound 71

IR Spectrum

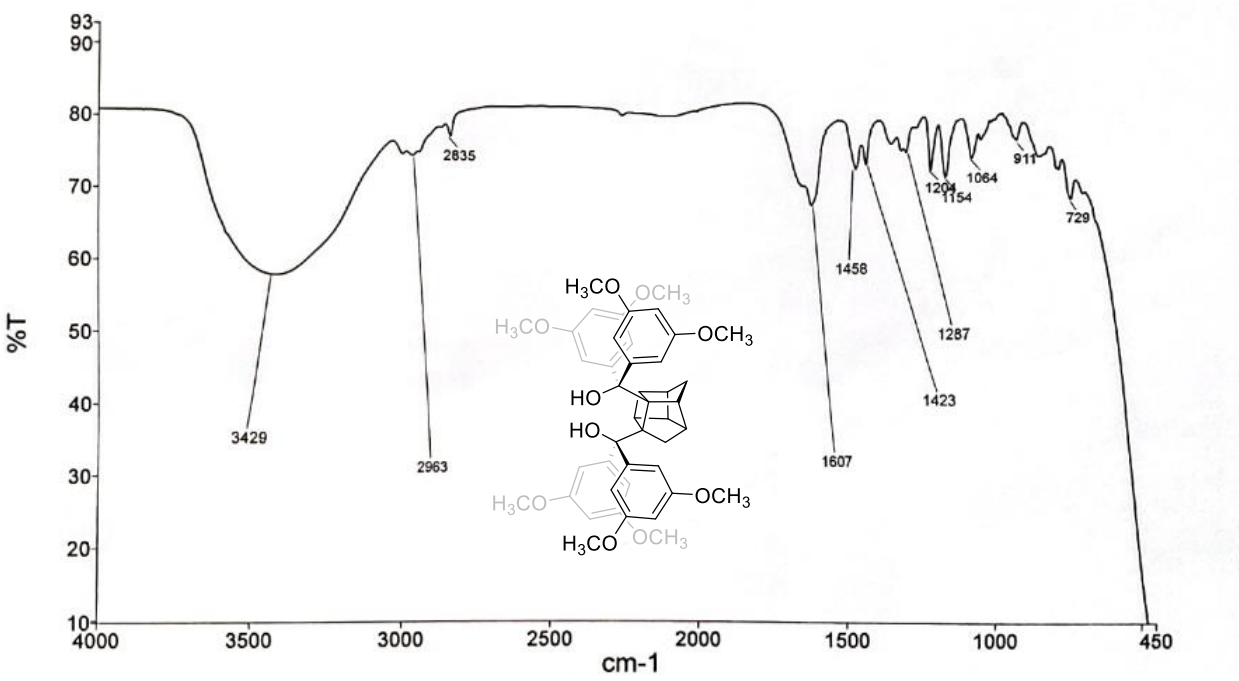

Compound 72

^{1}H NMR Spectrum

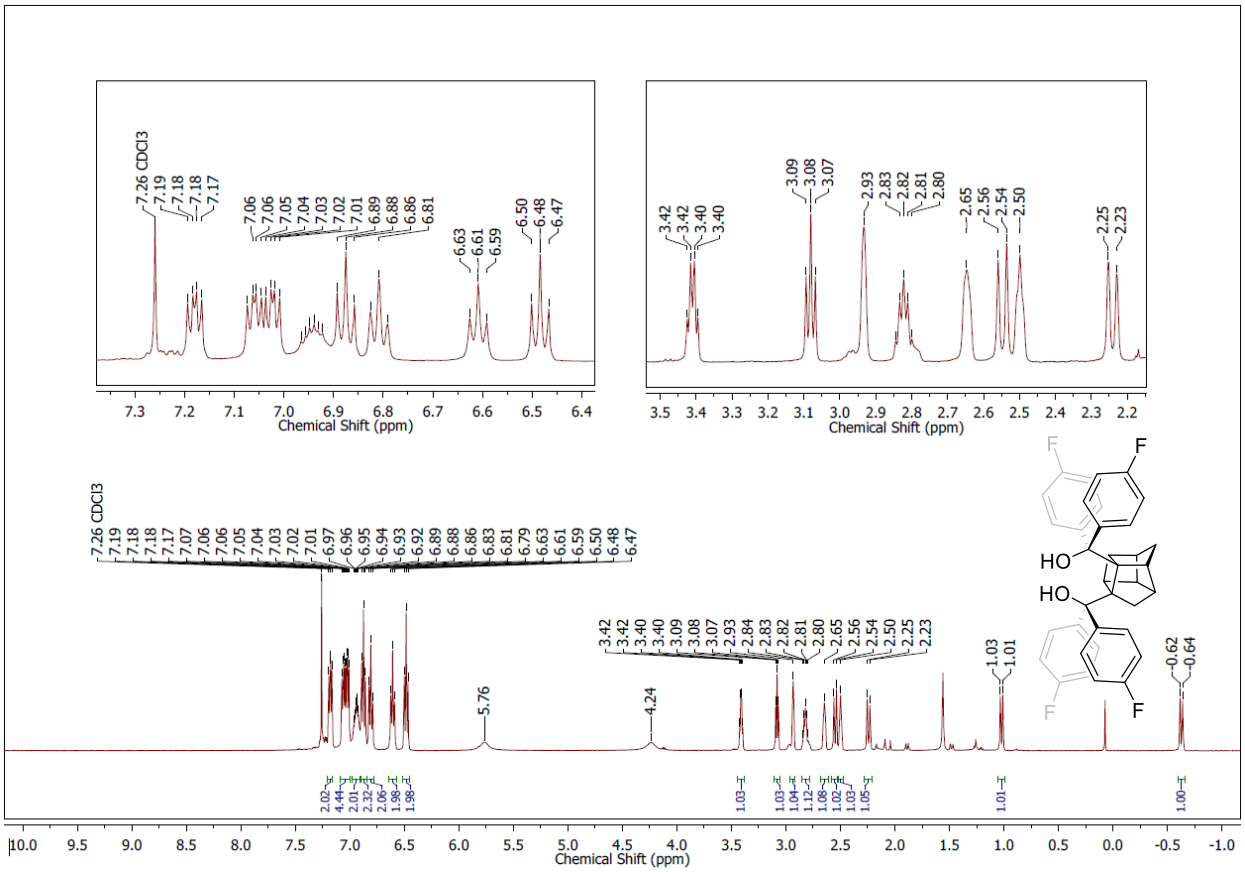

Compound 72

^{13}C NMR Spectrum

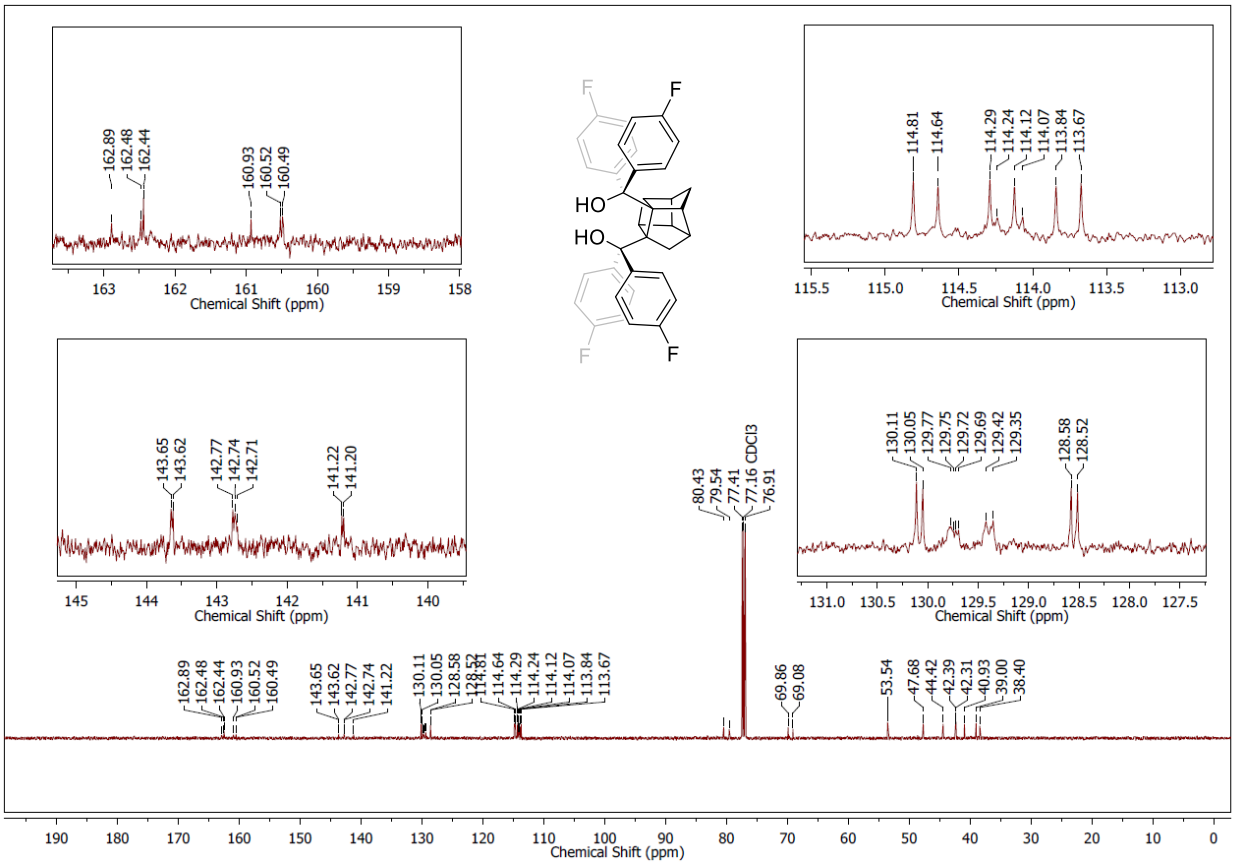

Compound 72

^{19}F NMR Spectrum

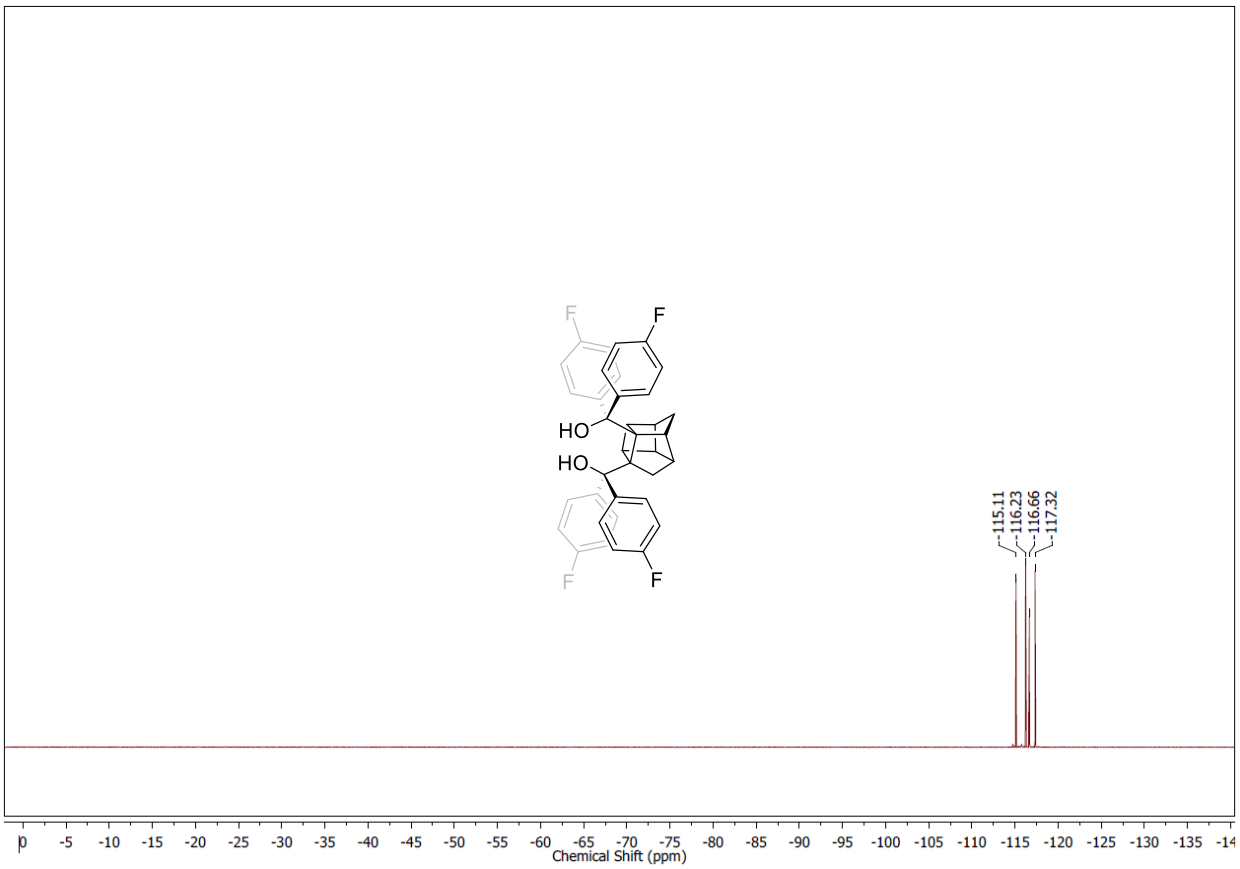

Compound 72

IR Spectrum

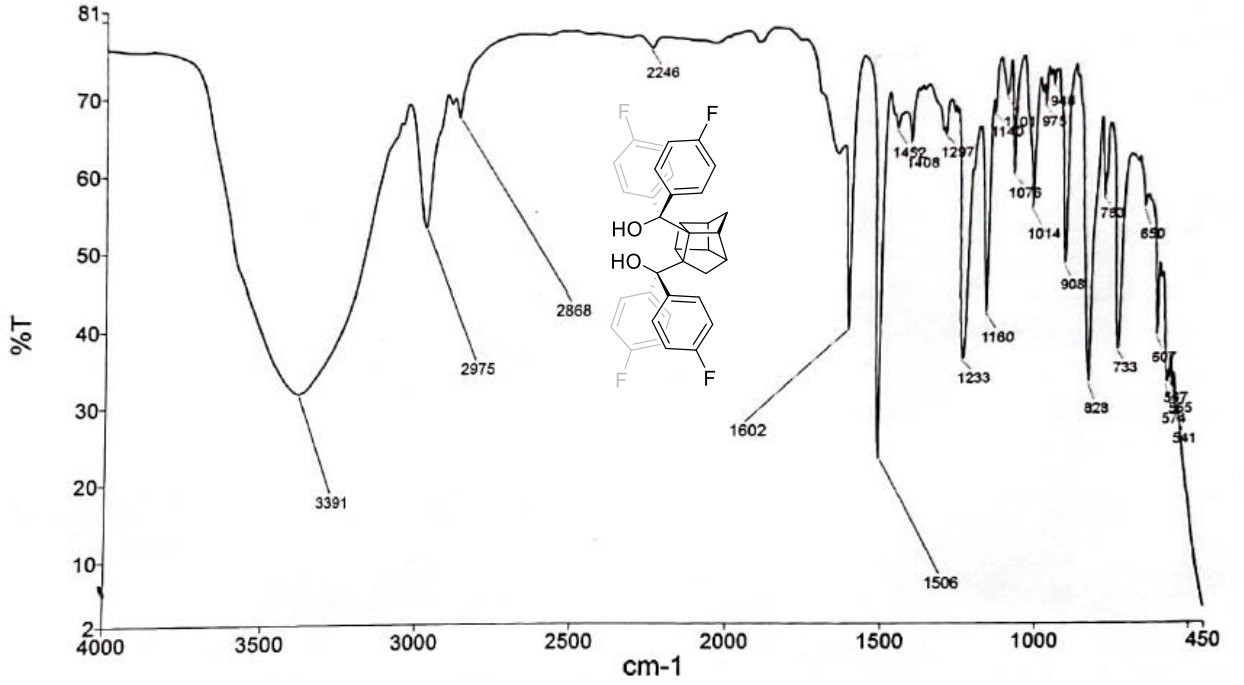

Compound 73

^{1}H NMR Spectrum

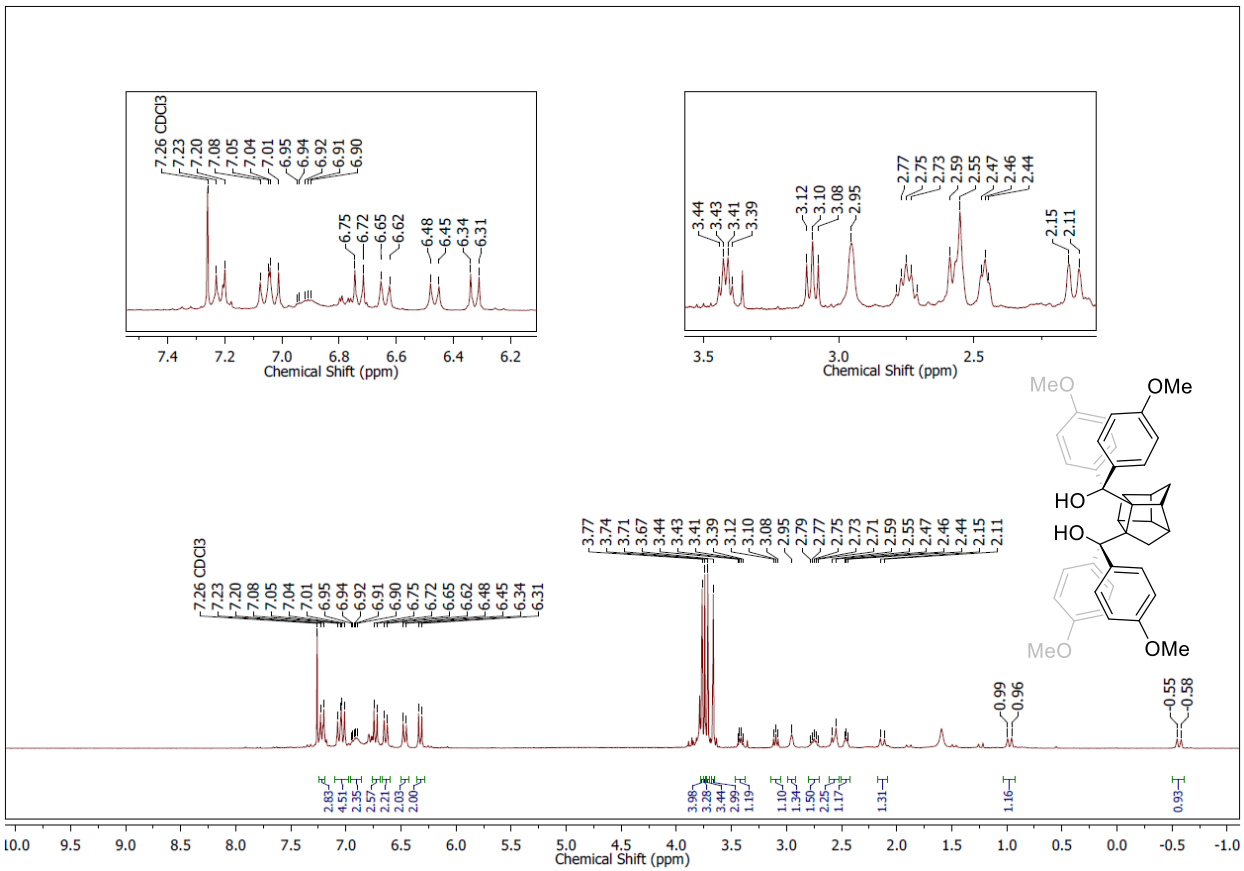

Compound 73

^{13}C NMR Spectrum

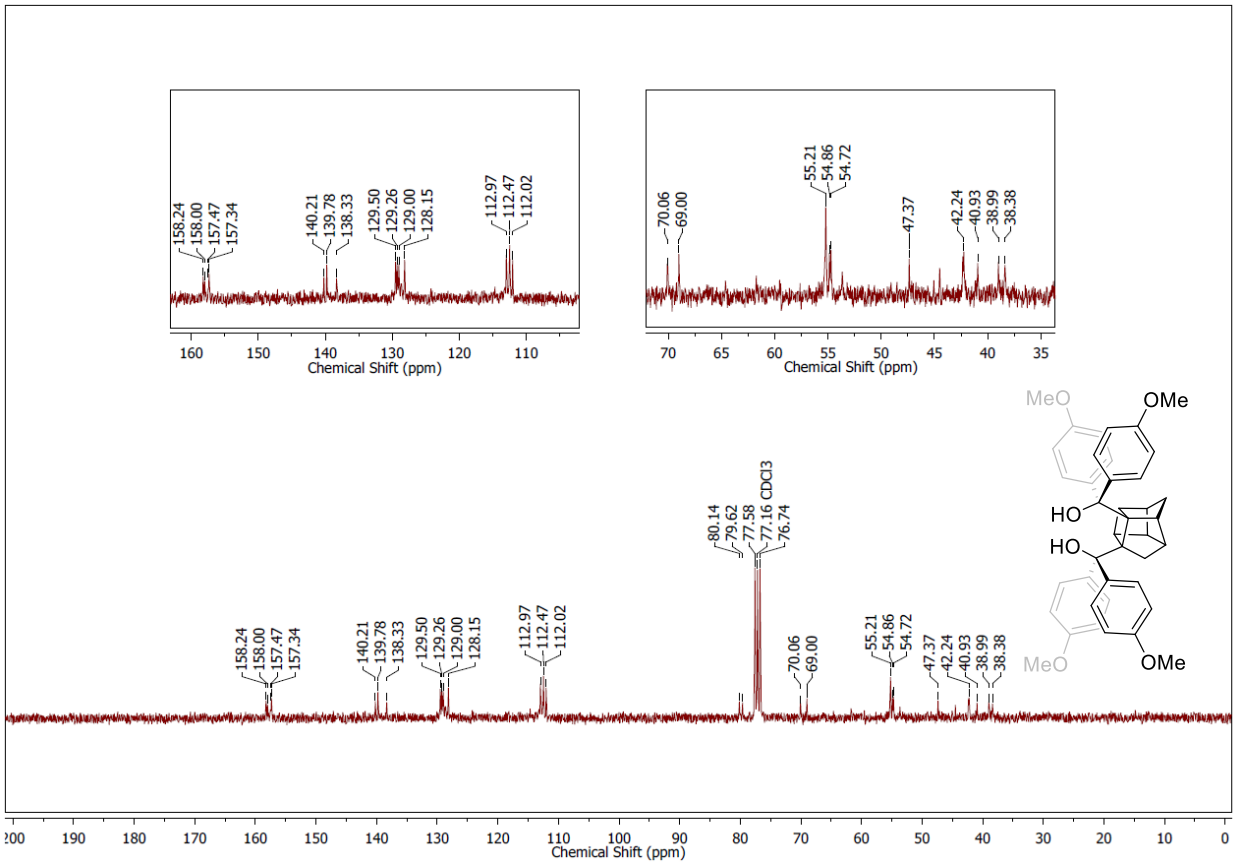

Compound 73

IR Spectrum

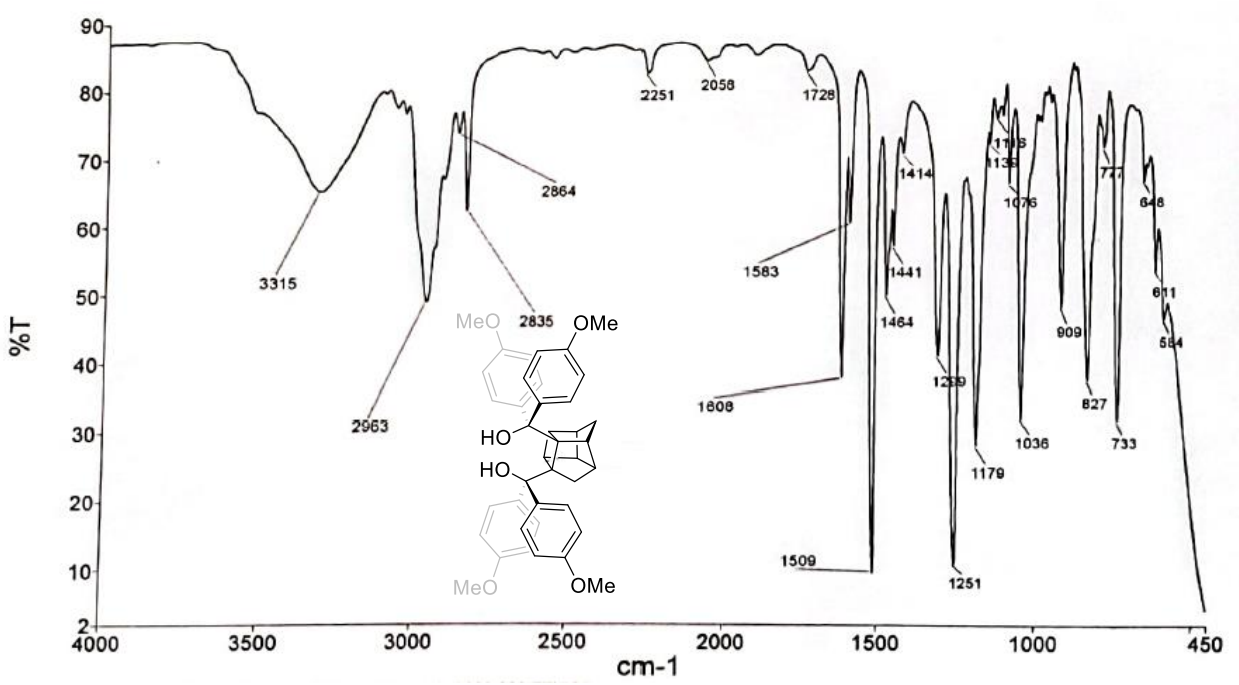

Compound 77

^{1}H NMR Spectrum

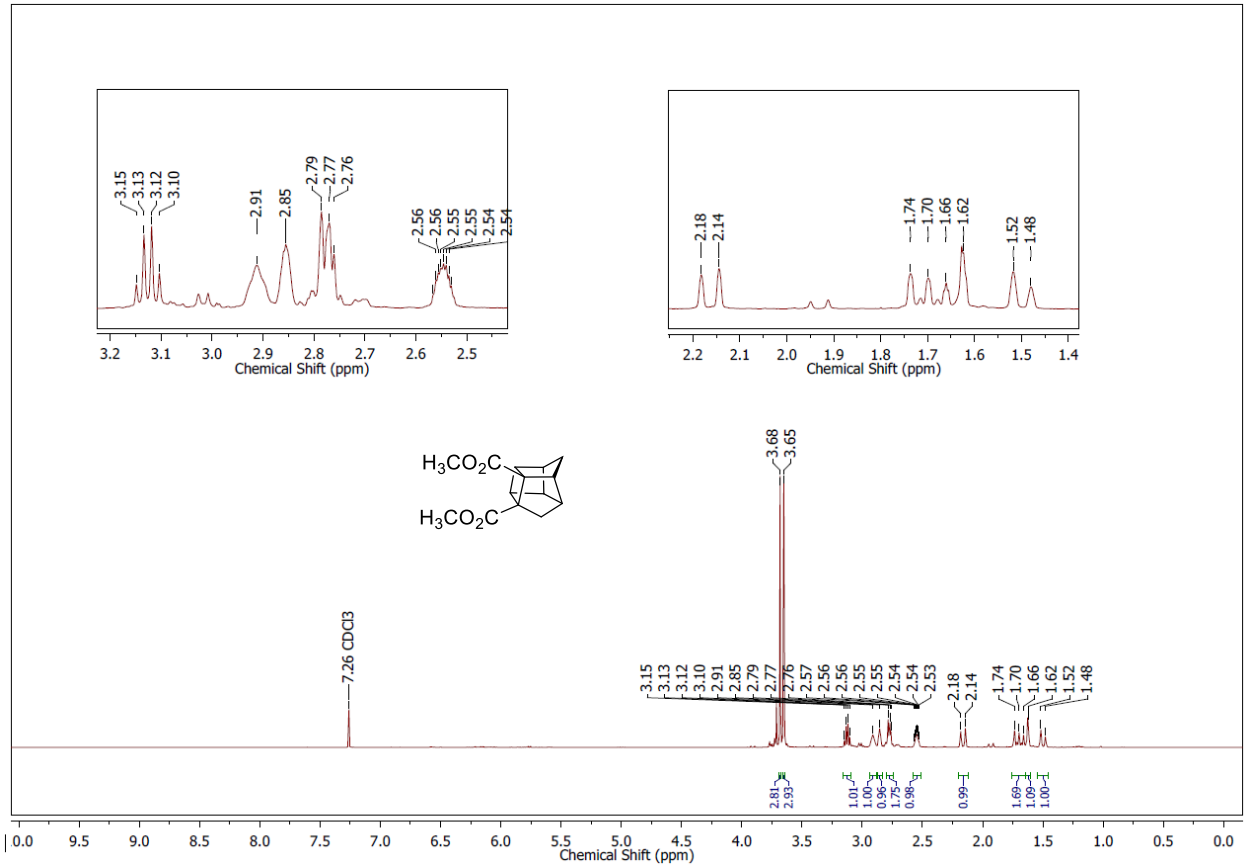

Compound 77

^{13}C NMR Spectrum

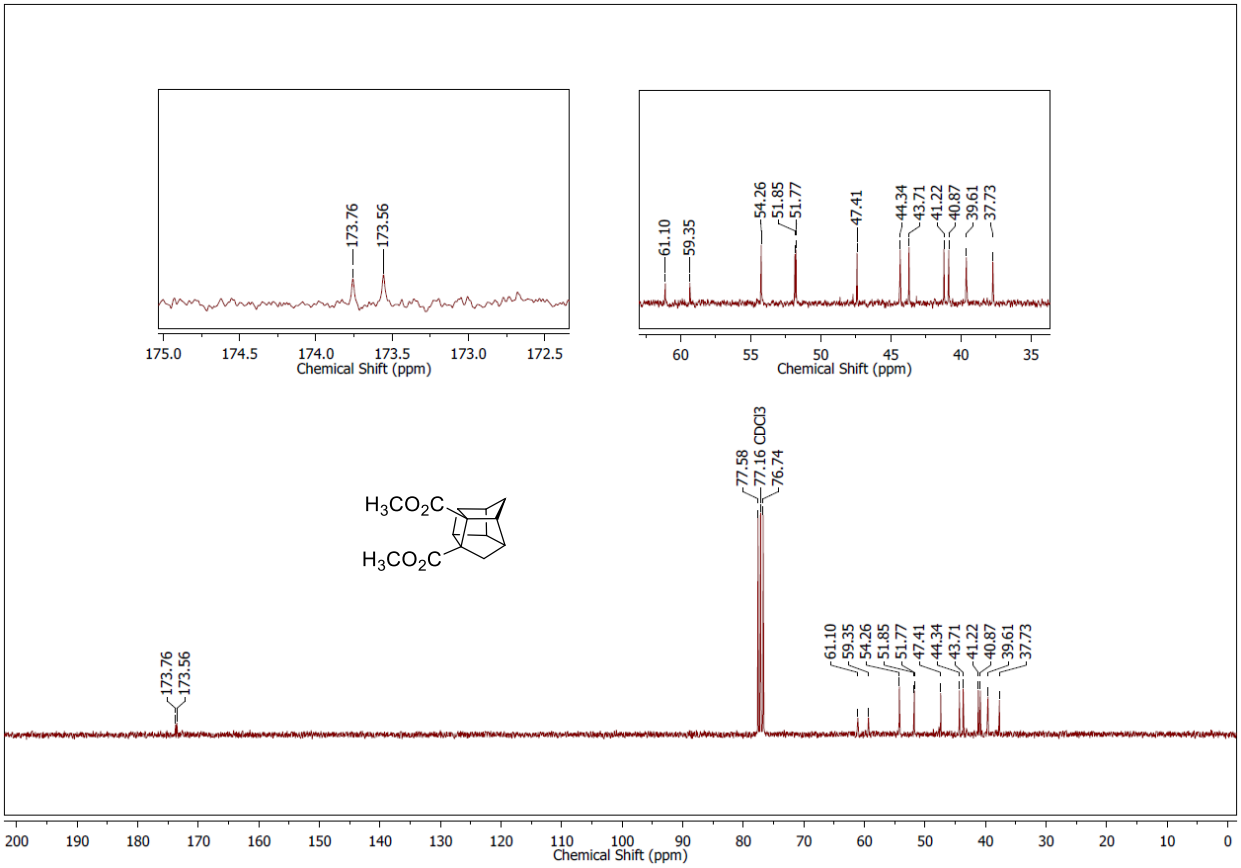

Compound 77

IR Spectrum

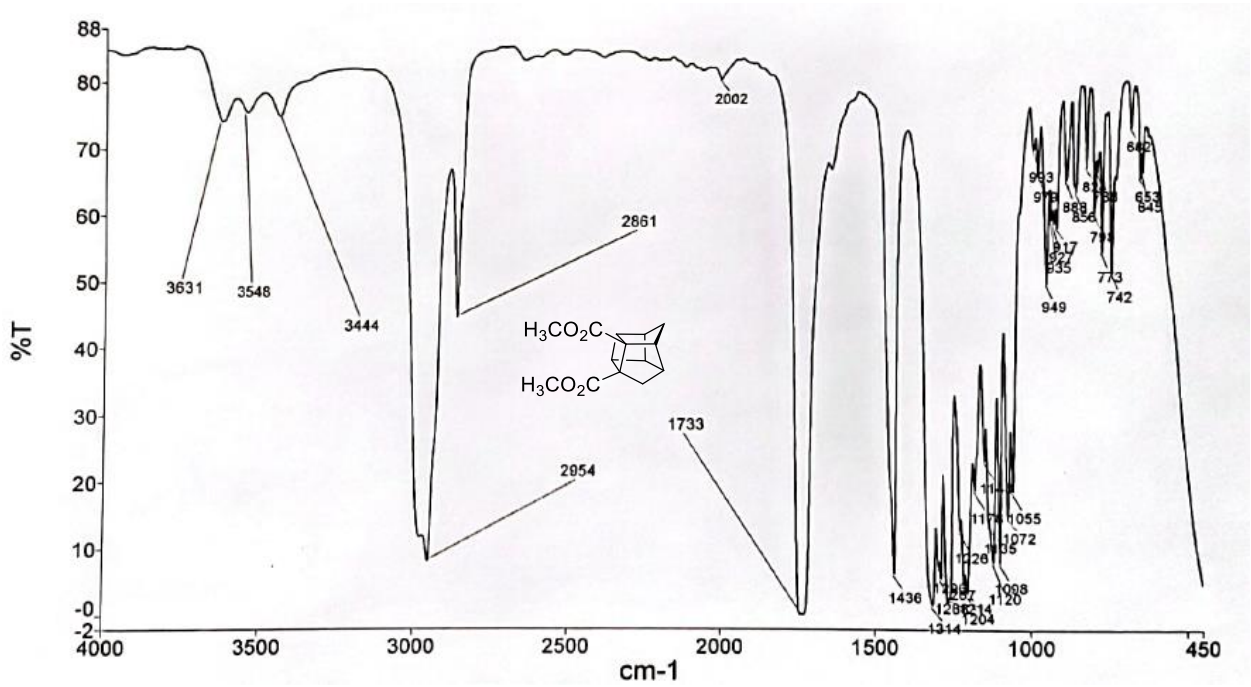

Compound 68

^{1}H NMR Spectrum

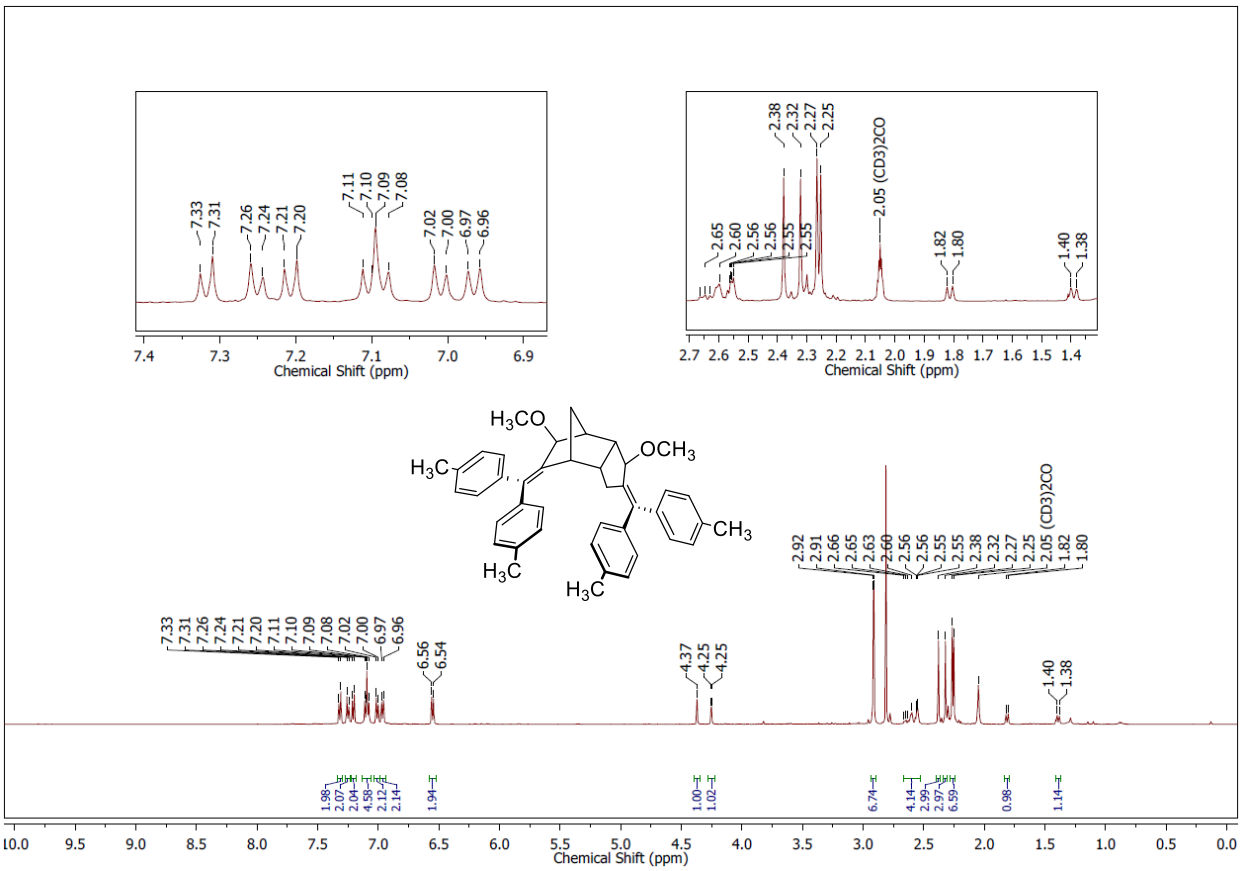

Compound 68

^{13}C NMR Spectrum

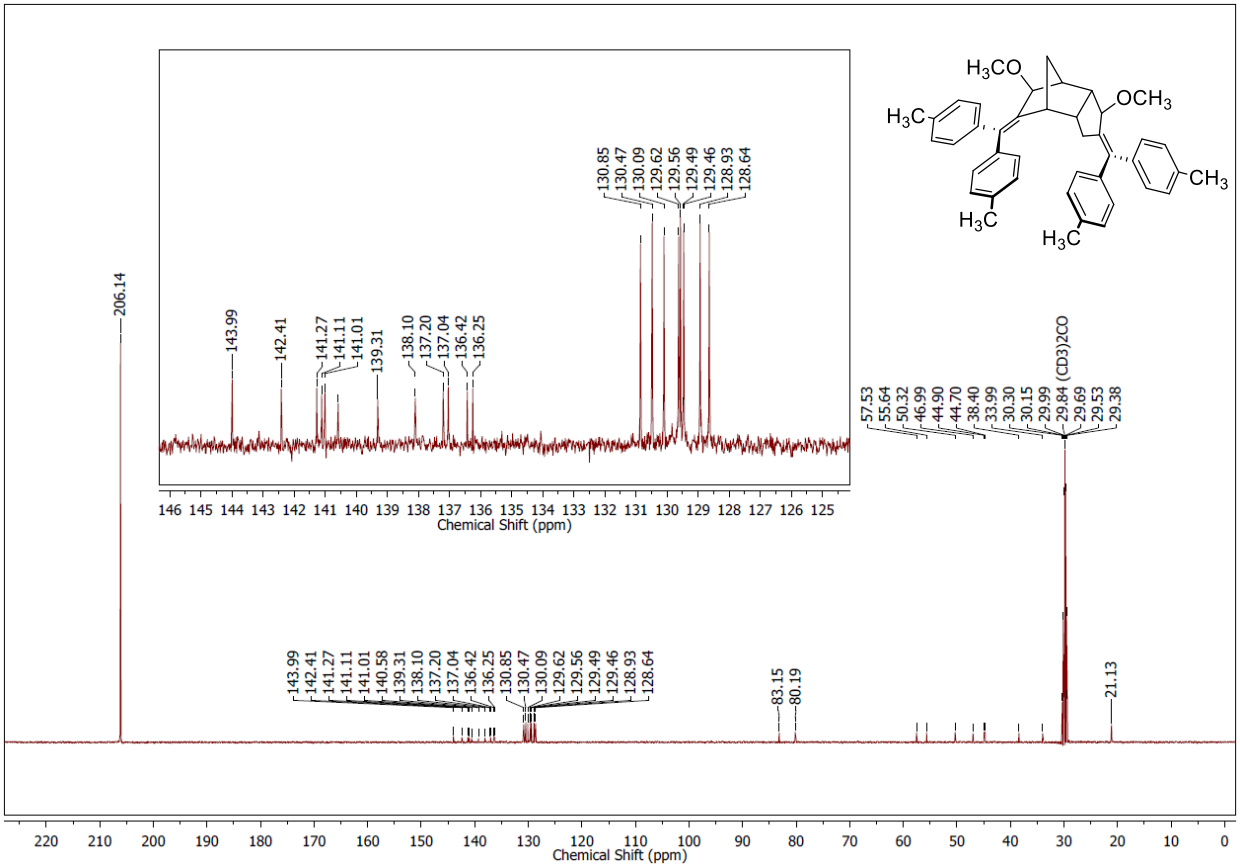

Compound 68

^{1}H-^{1}H COSY NMR Spectrum

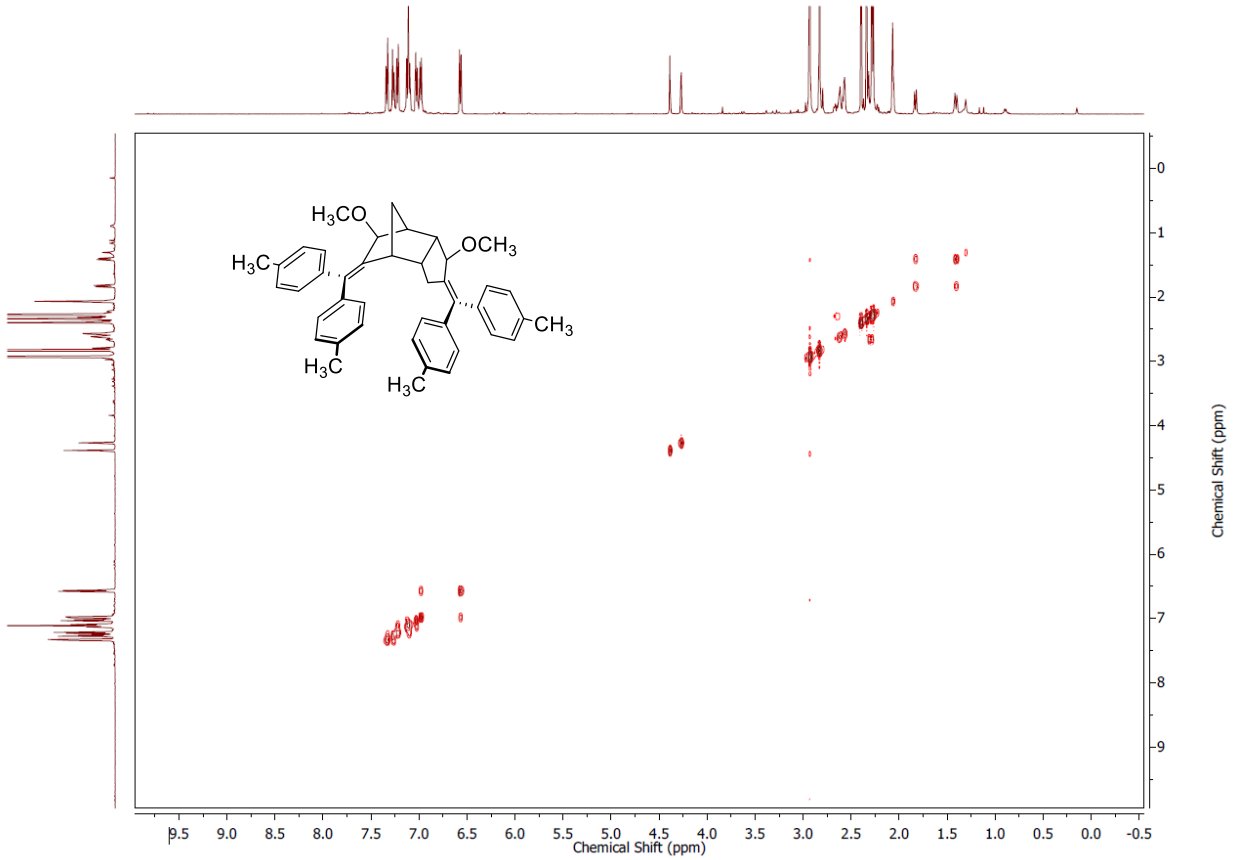

Compound 68

^{1}H-^{1}H COSY NMR Spectrum – Upfield

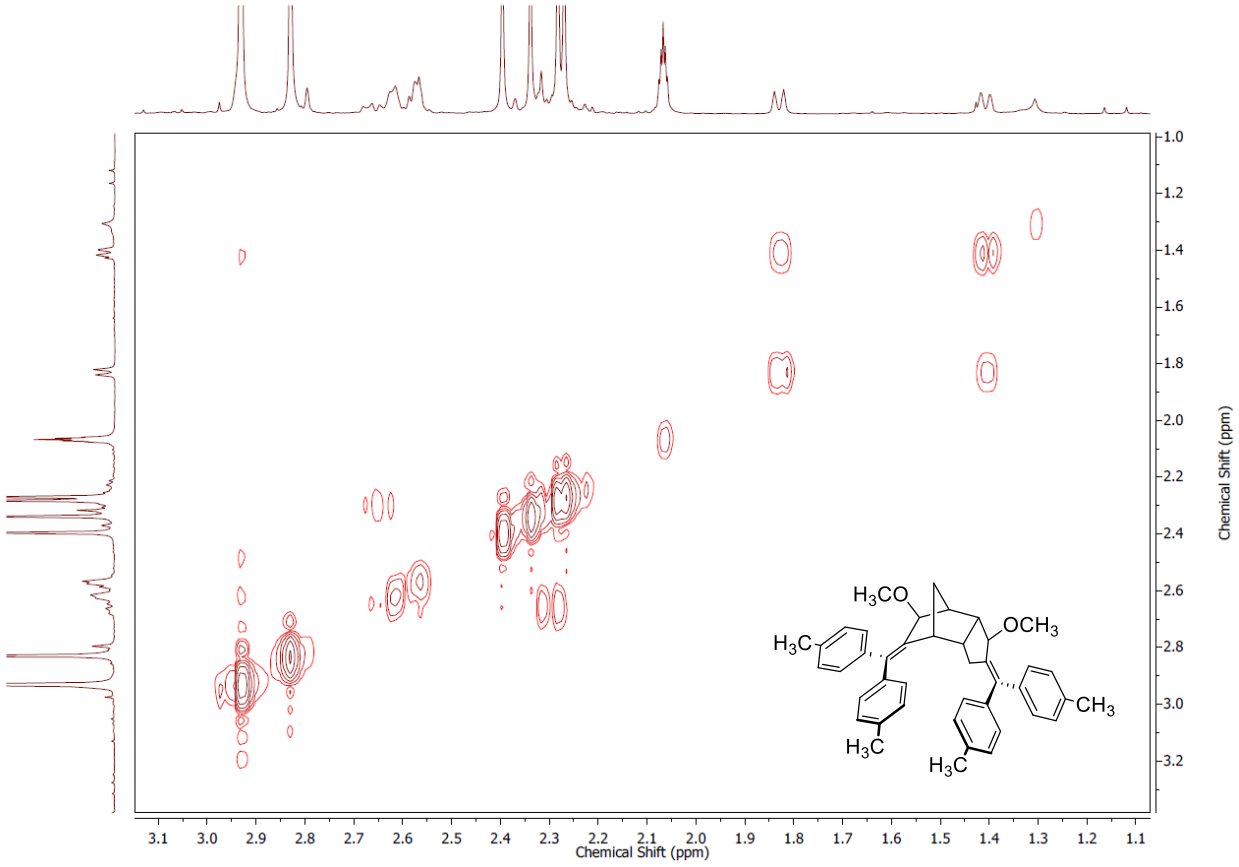

Compound 68

^{1}H-^{1}H COSY NMR Spectrum – Downfield

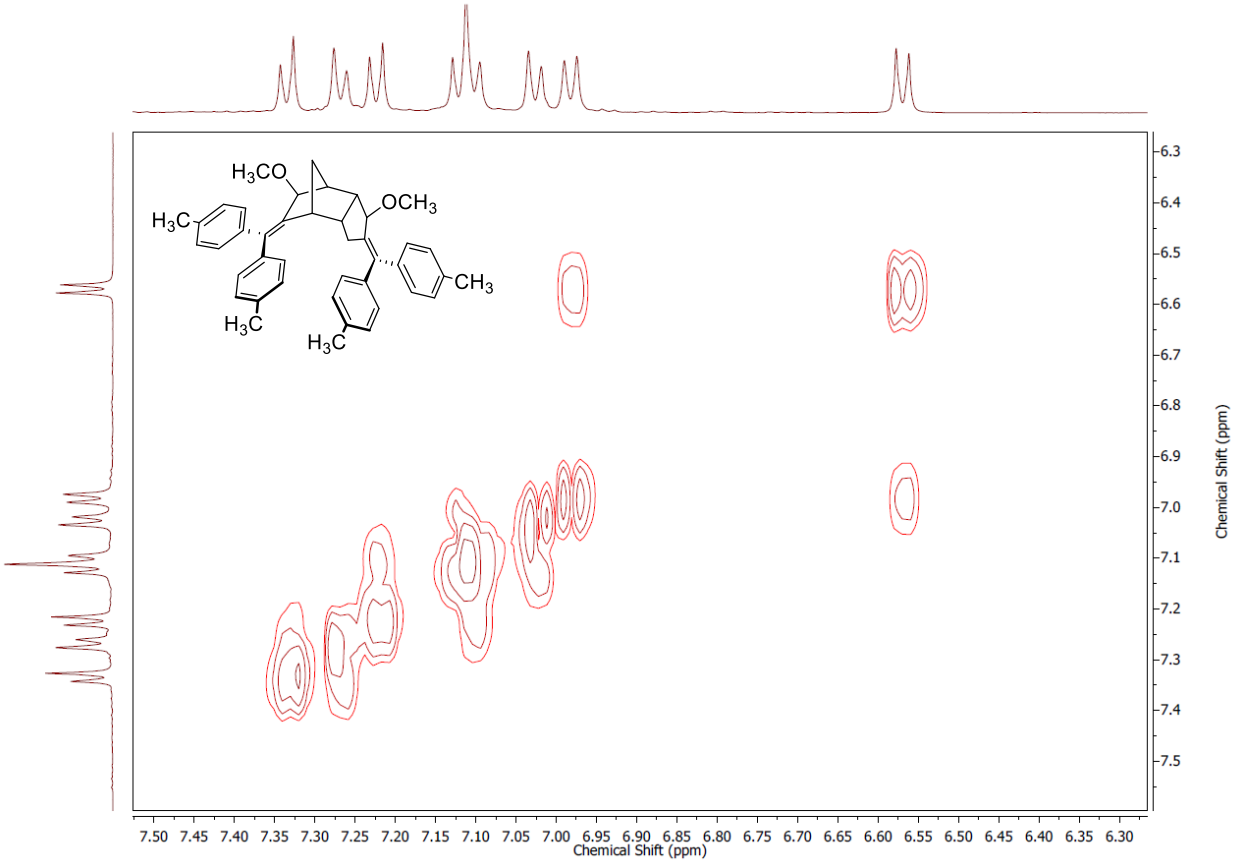

Compound 68

^{1}H-^{13}C HSQC NMR Spectrum

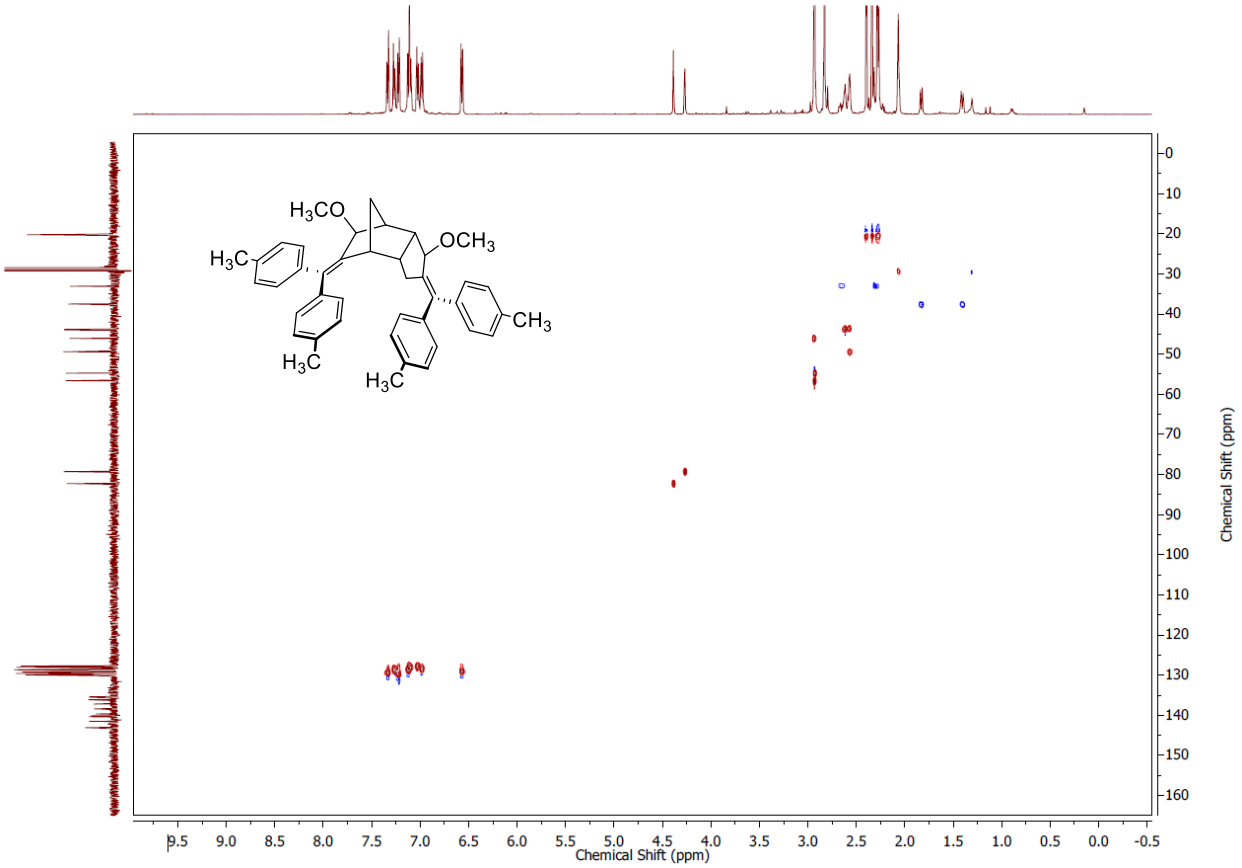

Compound 68

^{1}H-^{13}C HSQC NMR Spectrum – Upfield

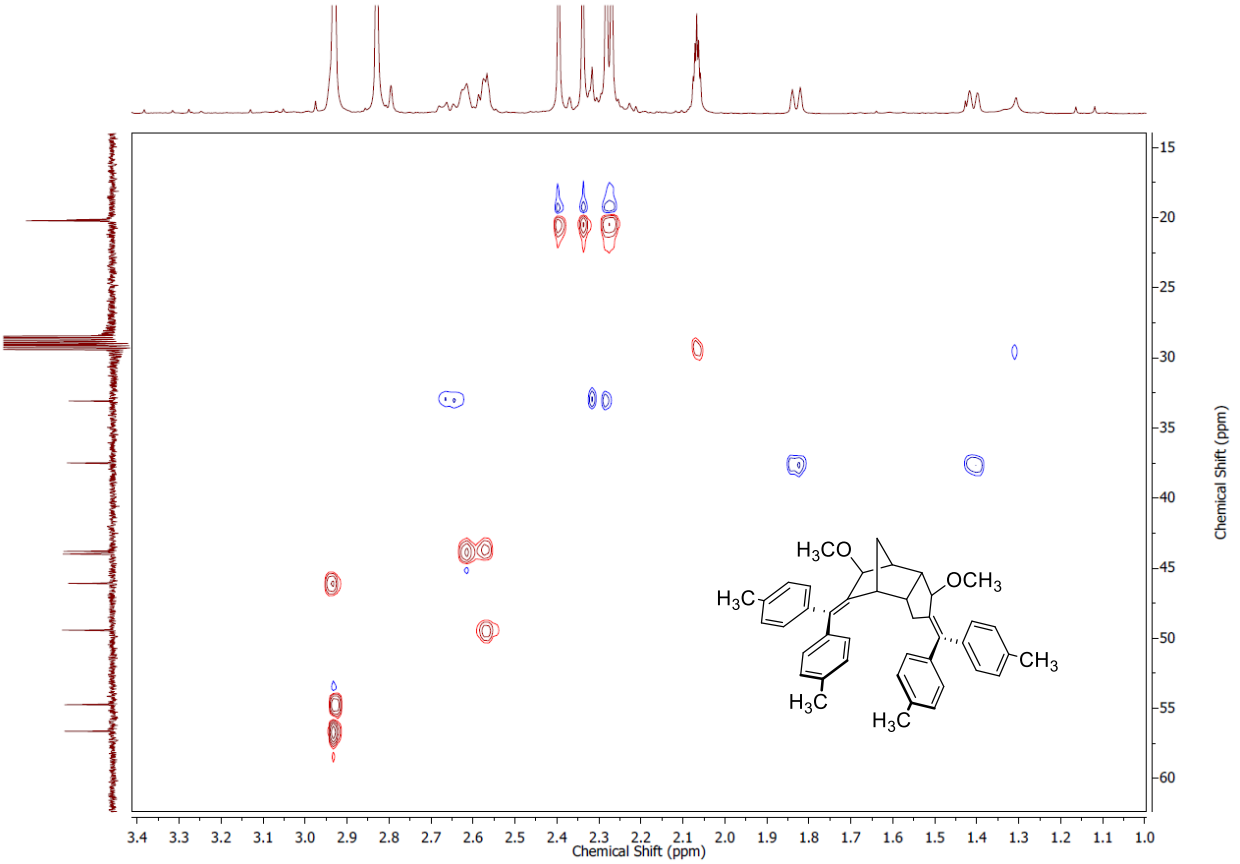

Compound 68

^{1}H-^{13}C HSQC NMR Spectrum – Downfield

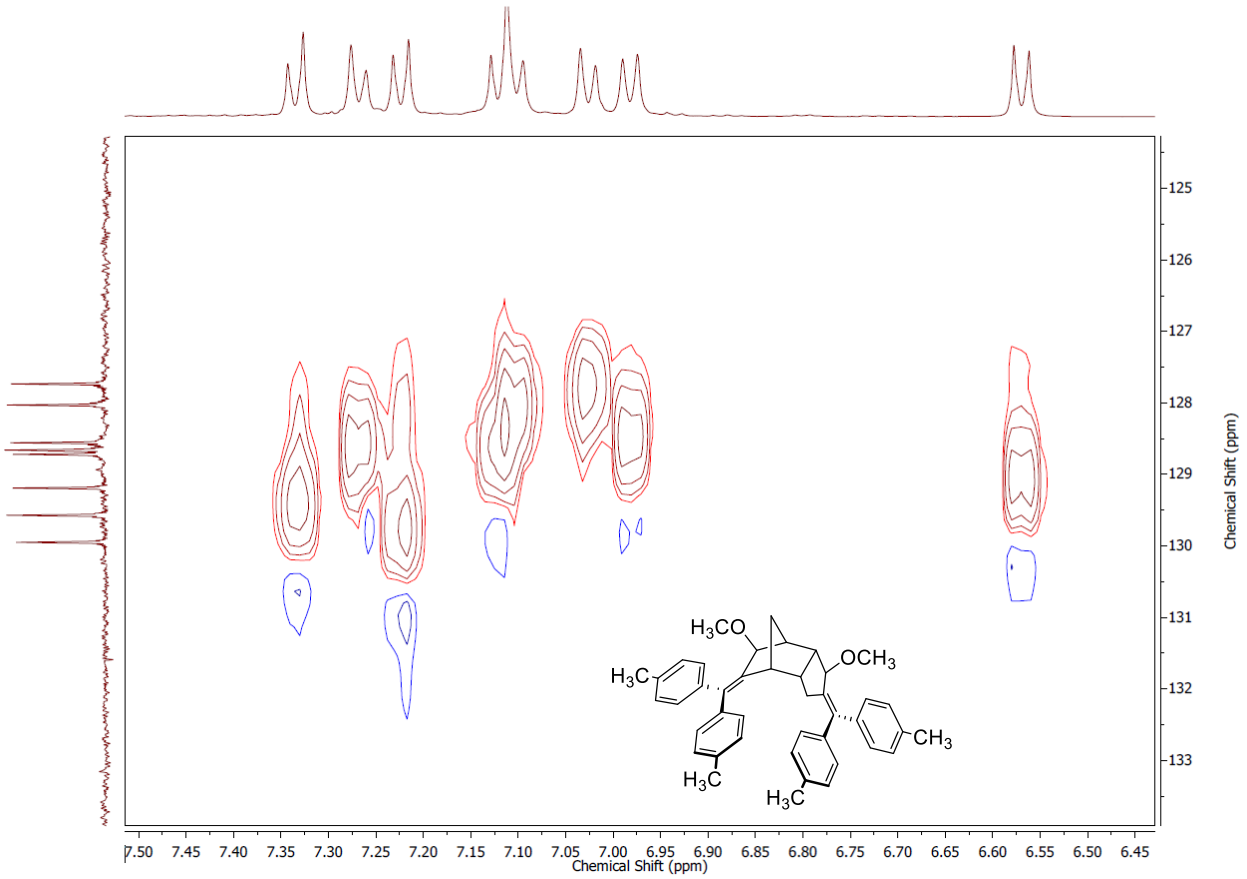

Compound 68

^{1}H-^{13}C HMBC NMR Spectrum

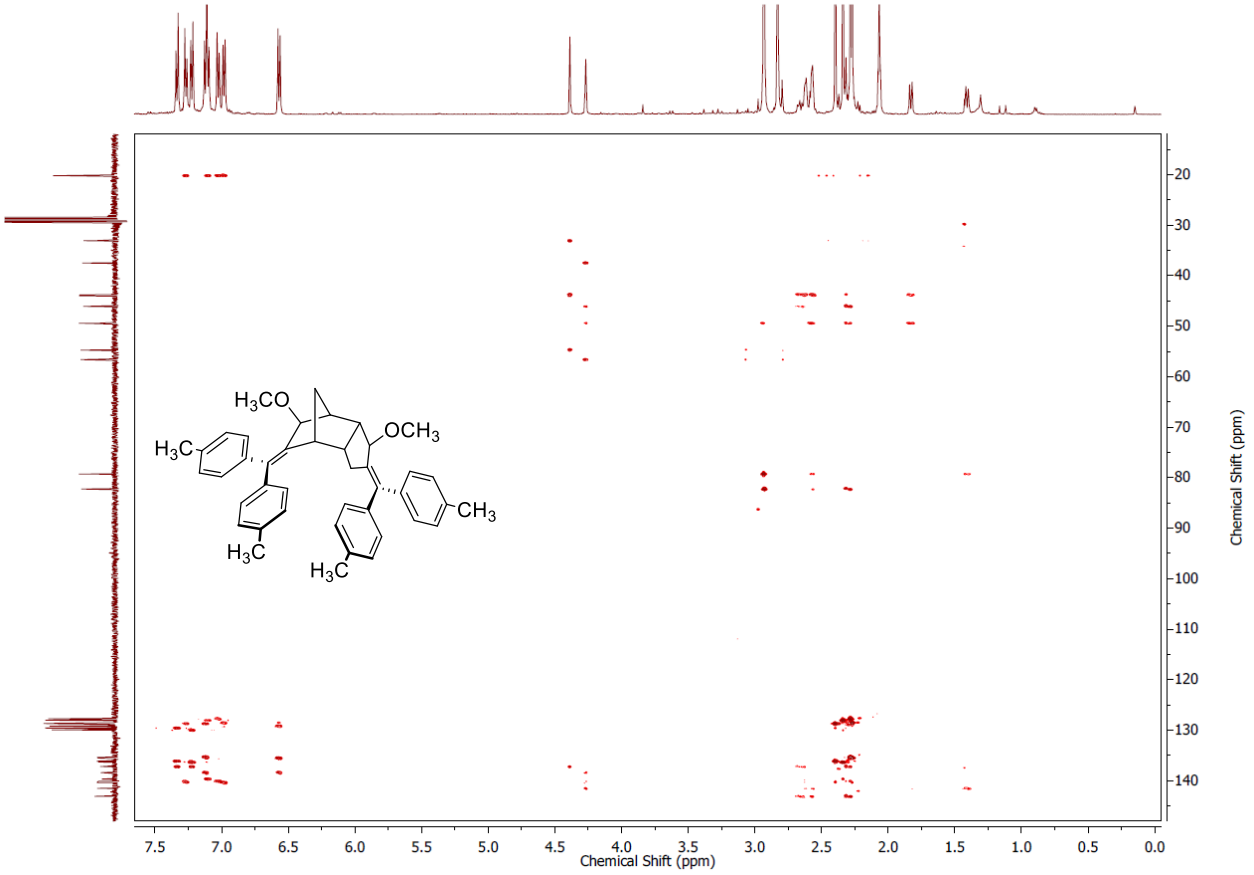

Compound 68

^{1}H-^{13}C HMBC NMR Spectrum – 2.70-1.75 ppm (^{1}H): 54-40 ppm (^{13}C)

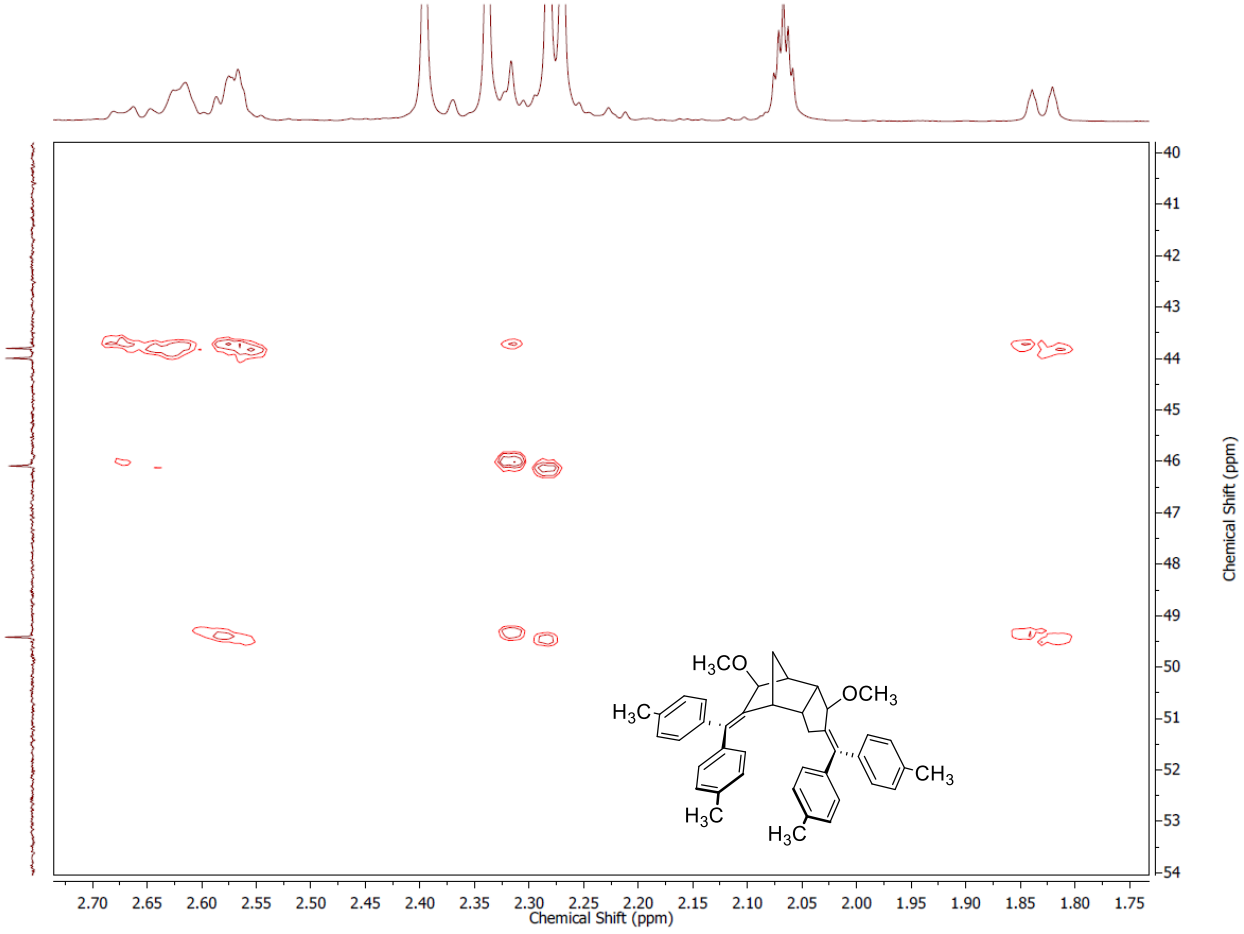

Compound 68

^{1}H-^{13}C HMBC NMR Spectrum – 2.42-2.25 ppm (^{1}H): 130-127 ppm (^{13}C)

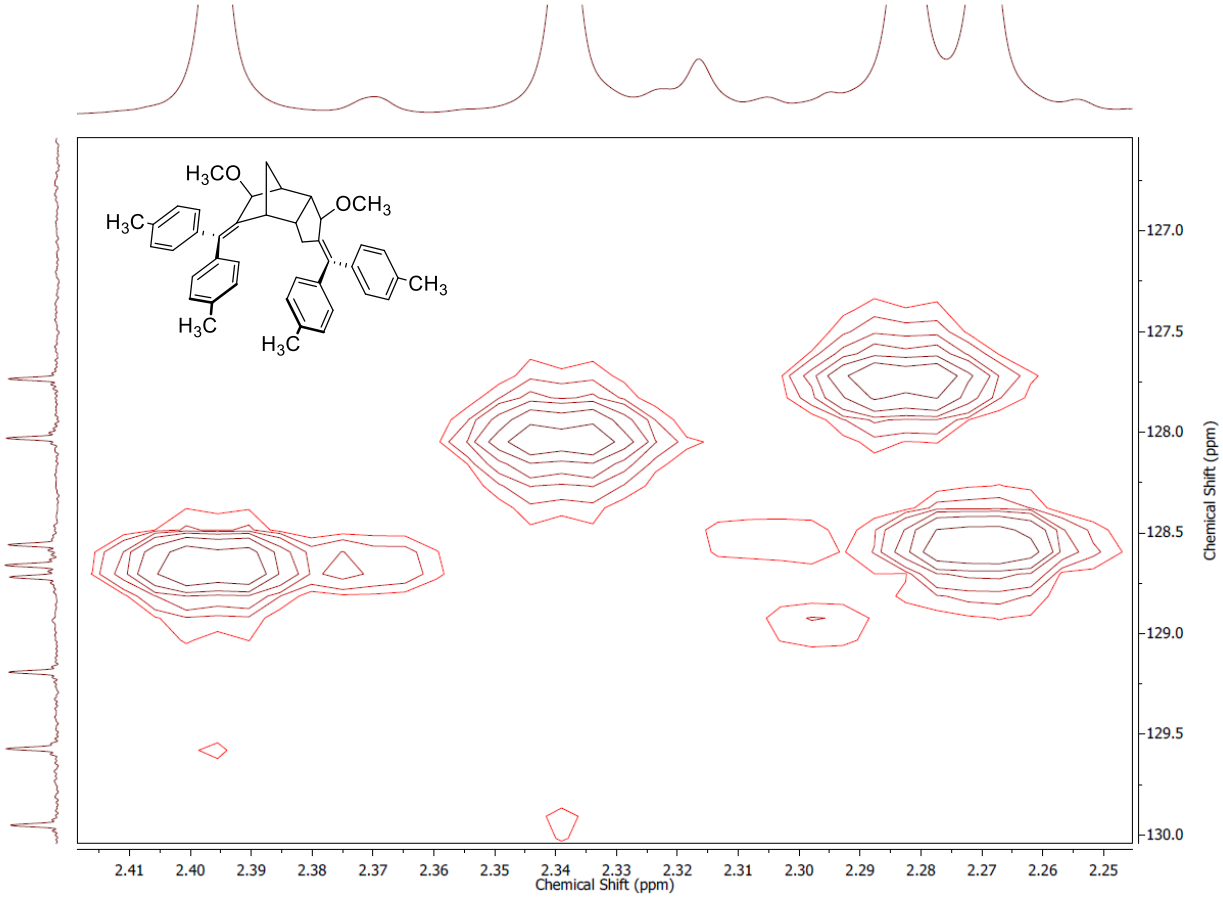

Compound 68

^{1}H-^{13}C HMBC NMR Spectrum – 2.43-2.25 ppm (^{1}H): 145-134 ppm (^{13}C)

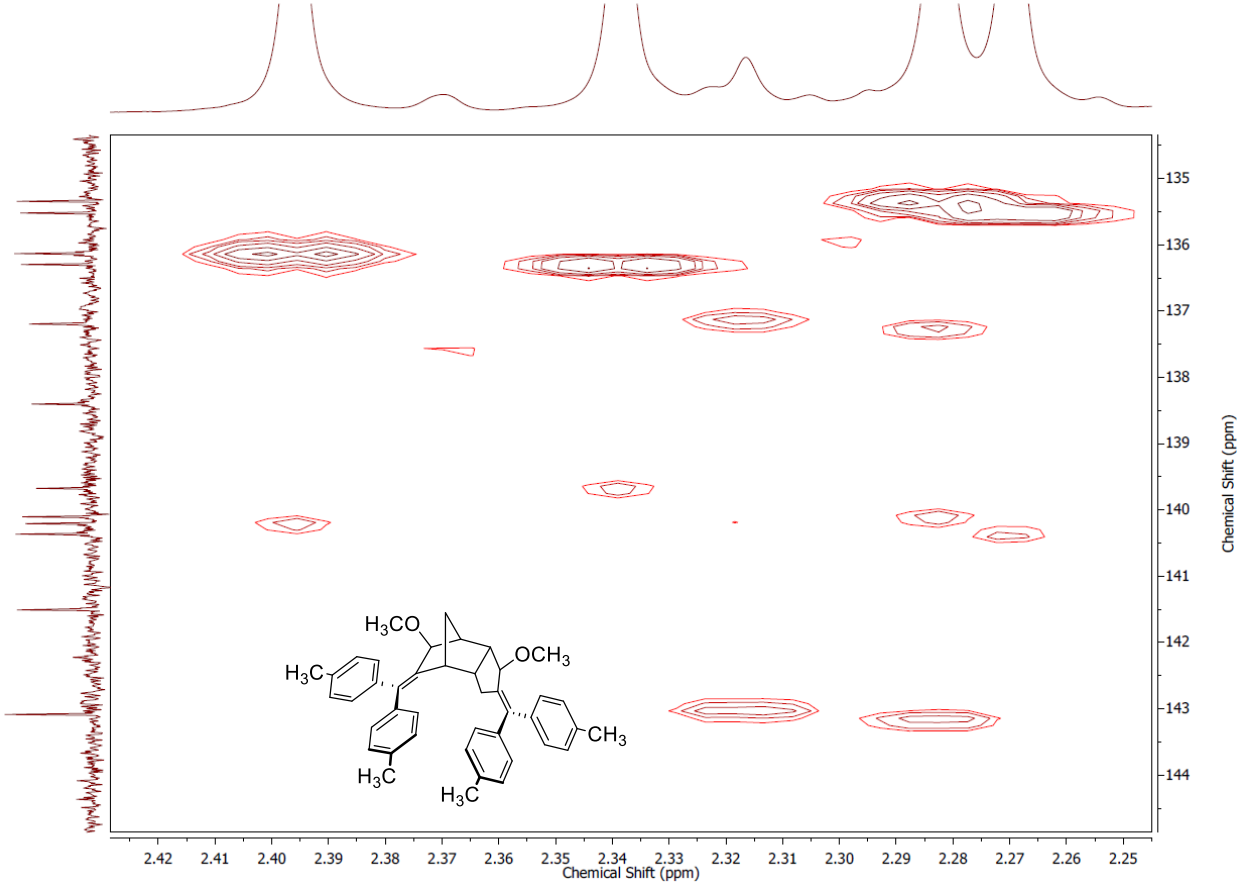

Compound 68

^{1}H-^{13}C HMBC NMR Spectrum – 3.00-2.15 ppm (^{1}H): 87-76 ppm (^{13}C)

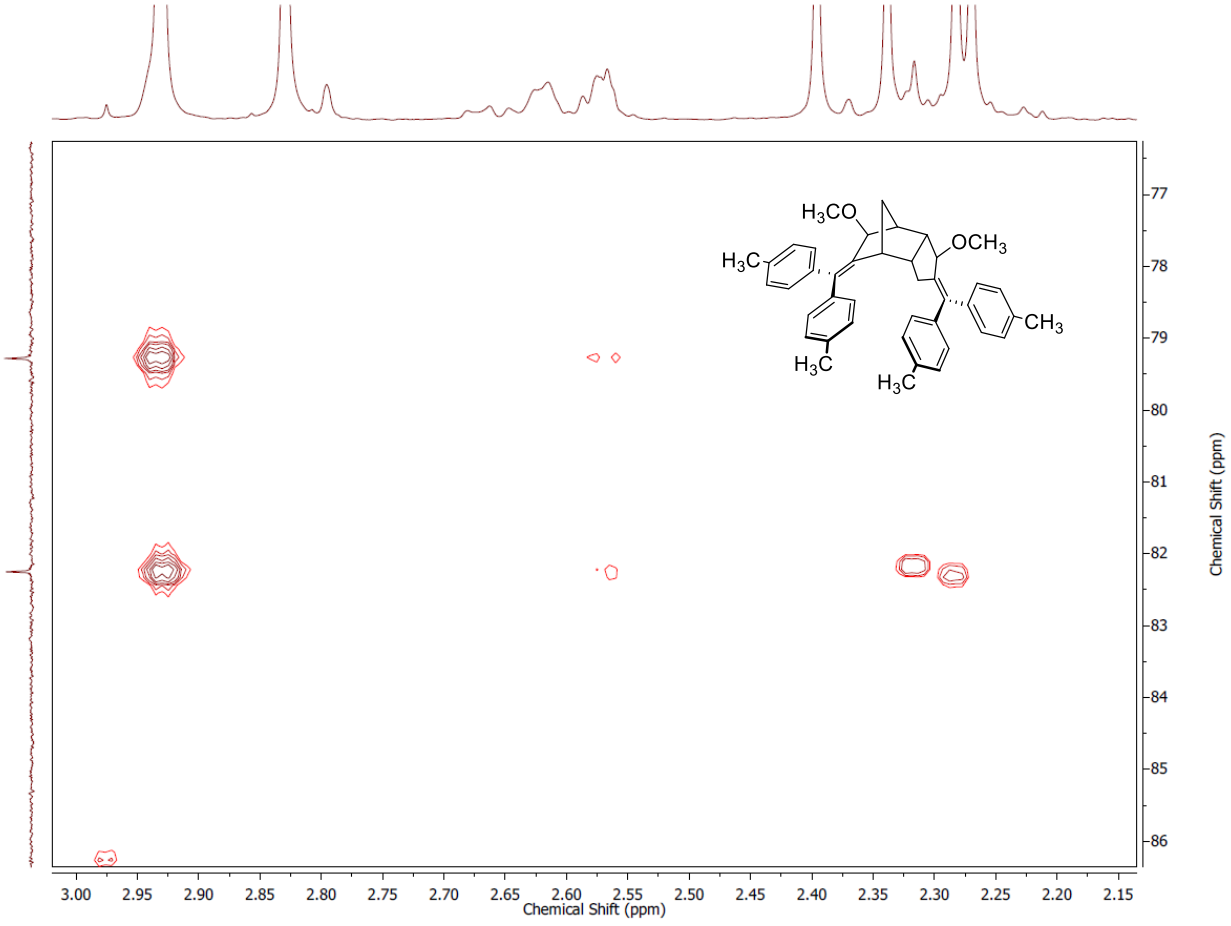

Compound 68

^{1}H-^{13}C HMBC NMR Spectrum – 4.47-4.17 ppm (^{1}H): 60-32 ppm (^{13}C)

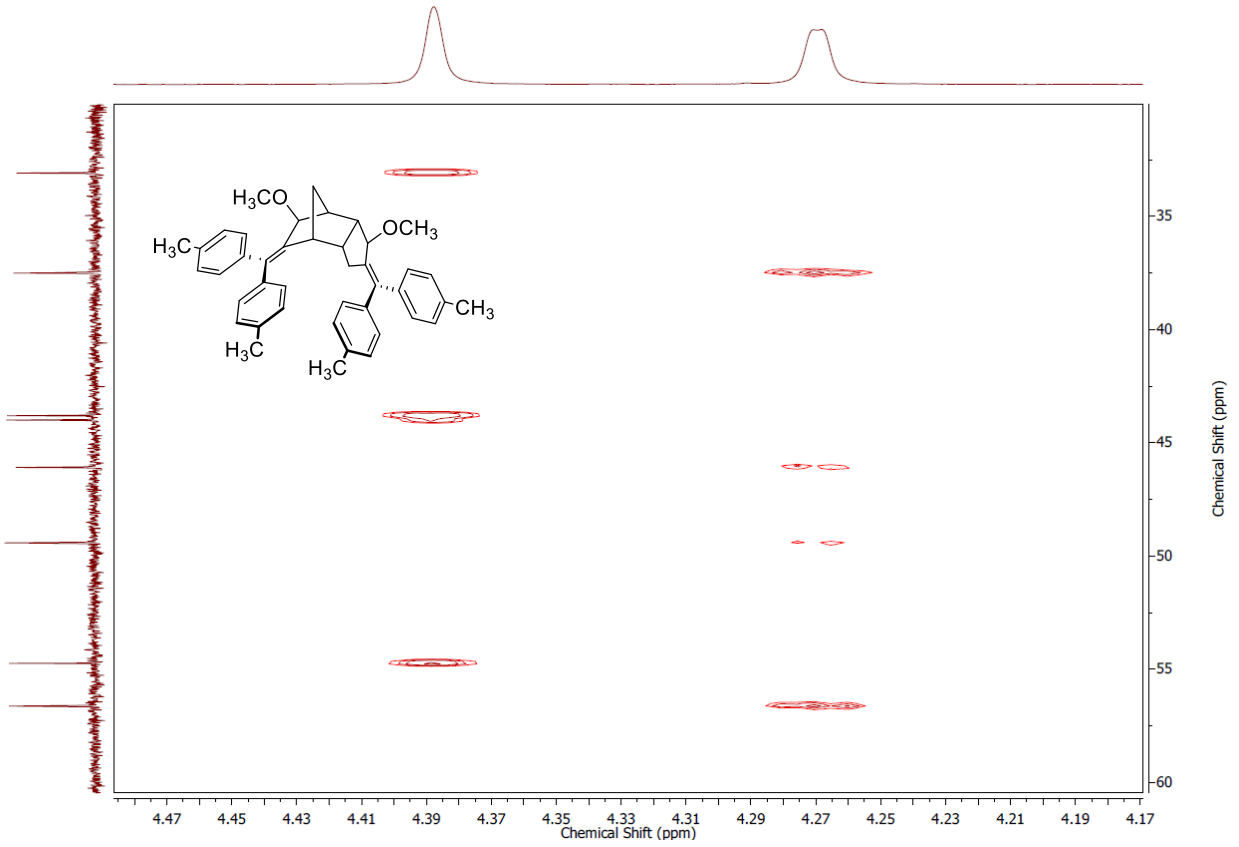

Compound 68

^{1}H-^{13}C HMBC NMR Spectrum – 4.49-4.14 ppm (^{1}H): 145-134 ppm (^{13}C)

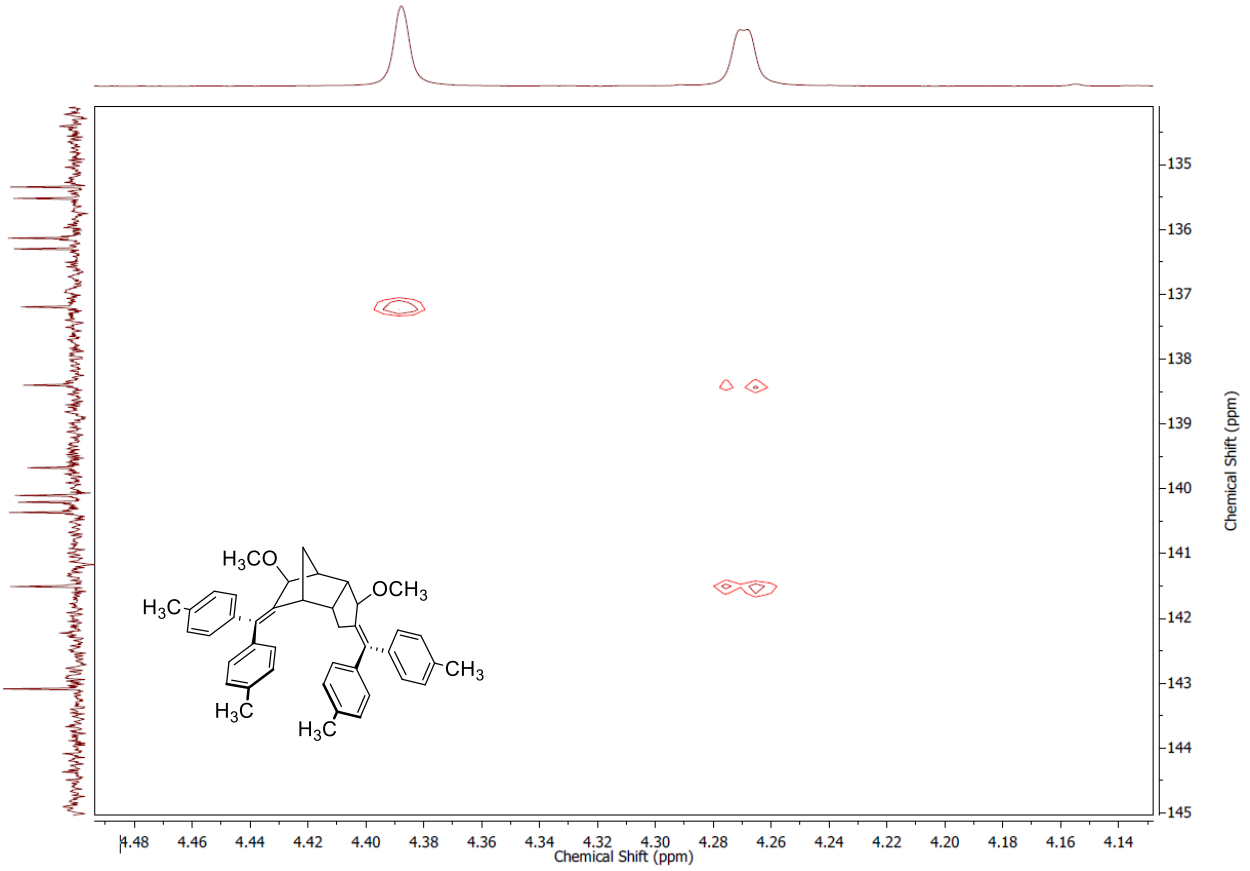

Compound 68

^{1}H-^{13}C HMBC NMR Spectrum – 7.35-6.50 ppm (^{1}H): 131-127 ppm (^{13}C)

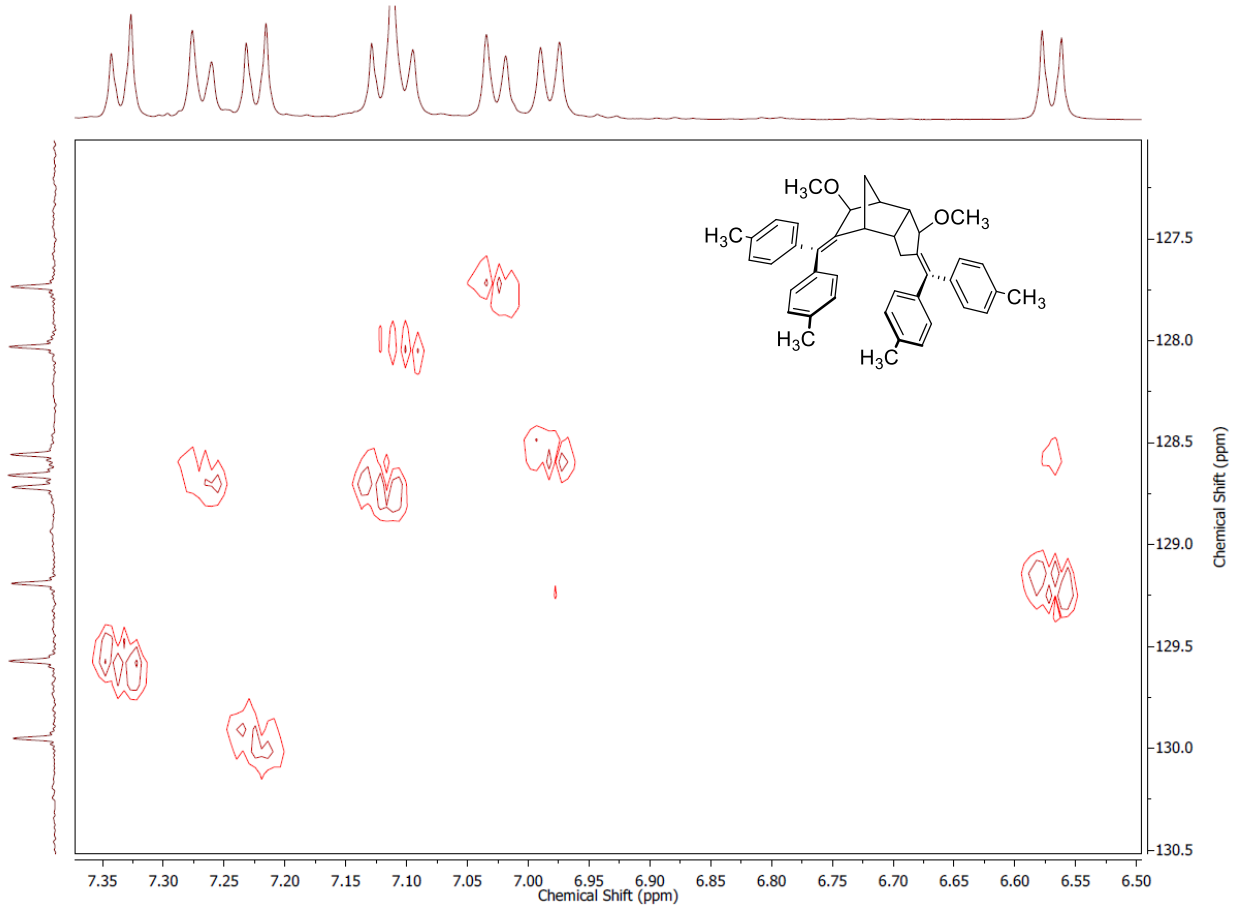

Compound 68

^{1}H-^{13}C HMBC NMR Spectrum – 7.35-6.55 ppm (^{1}H): 142-134 ppm (^{13}C)

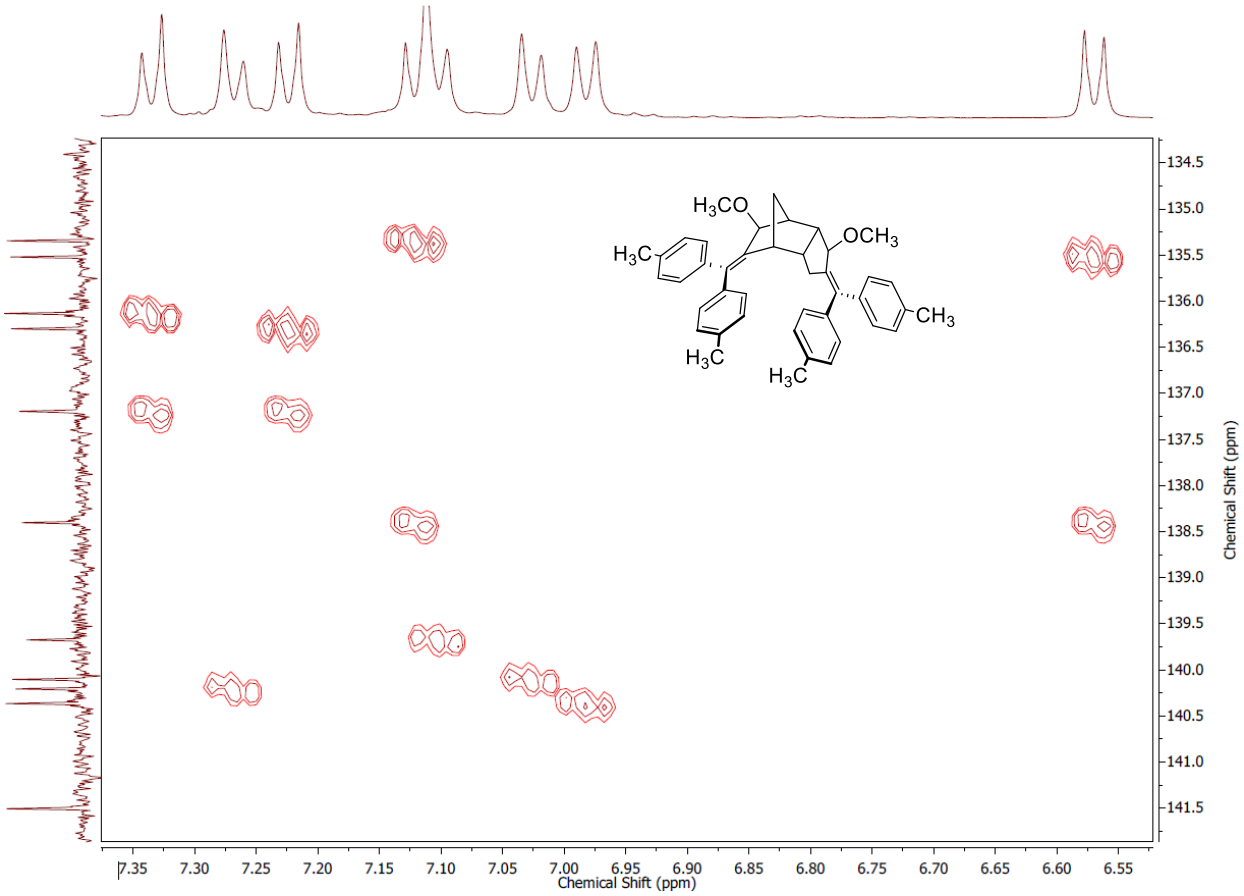

Compound 68

^{1}H-^{13}C HMBC NMR Spectrum – 7.30-6.95 ppm (^{1}H): 21-19 ppm (^{13}C)

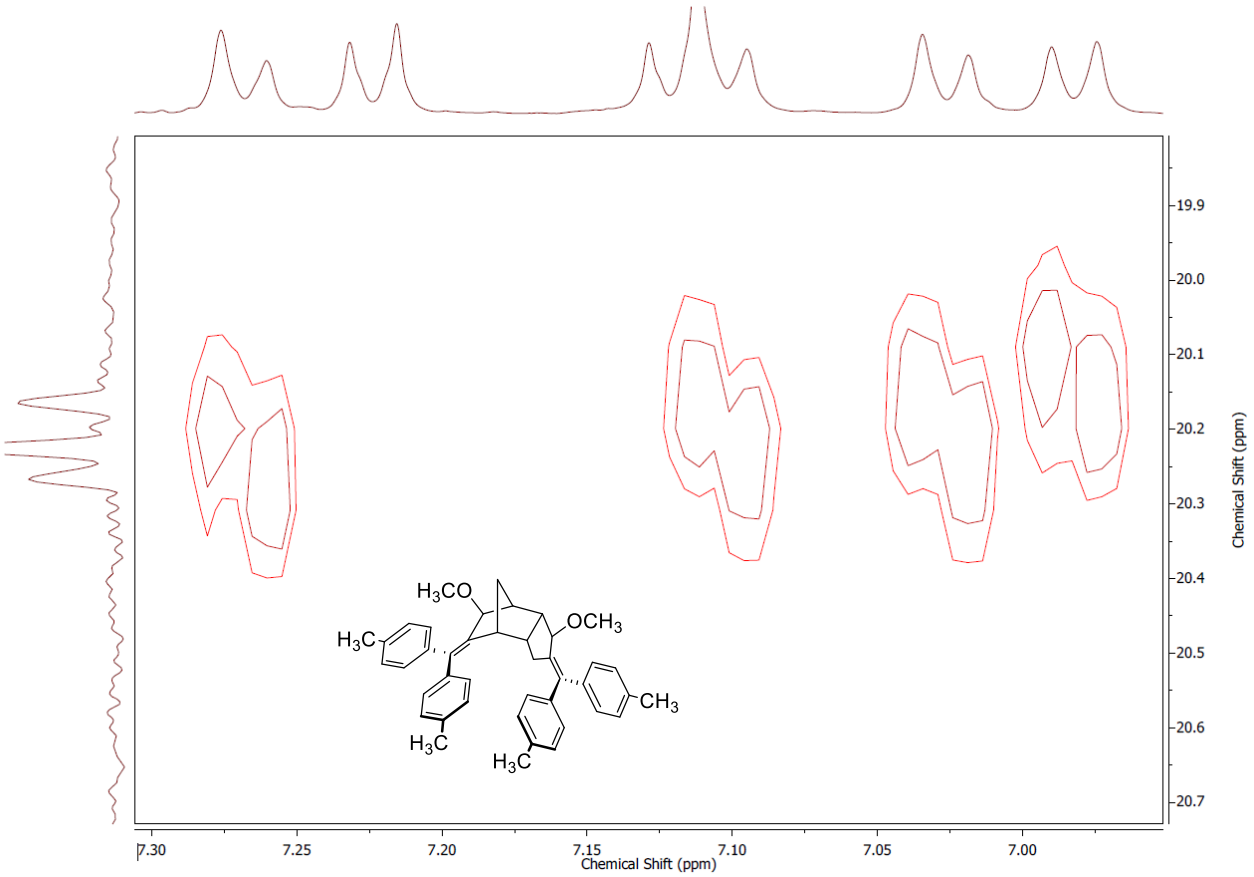

Compound 69

^{1}H NMR Spectrum

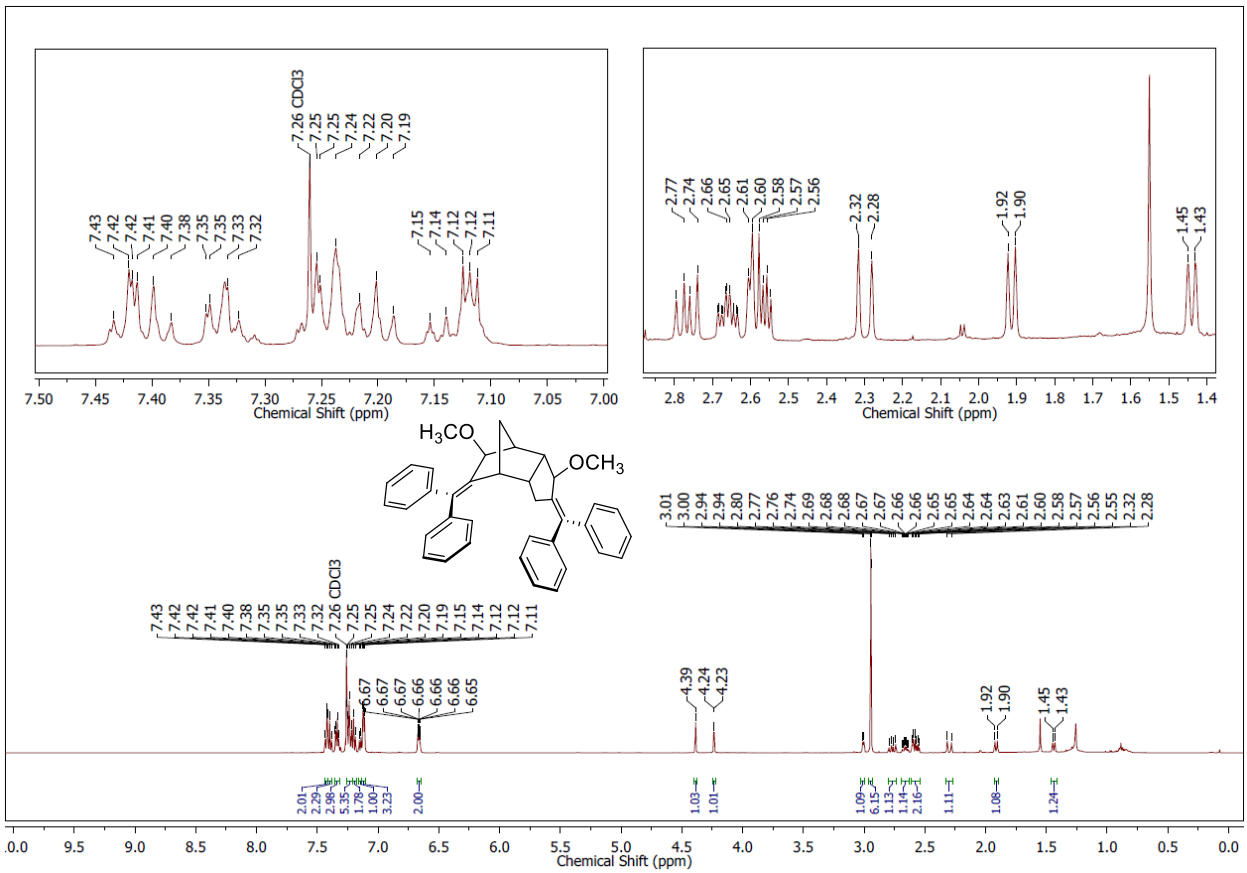

Compound 69

^{13}C NMR Spectrum

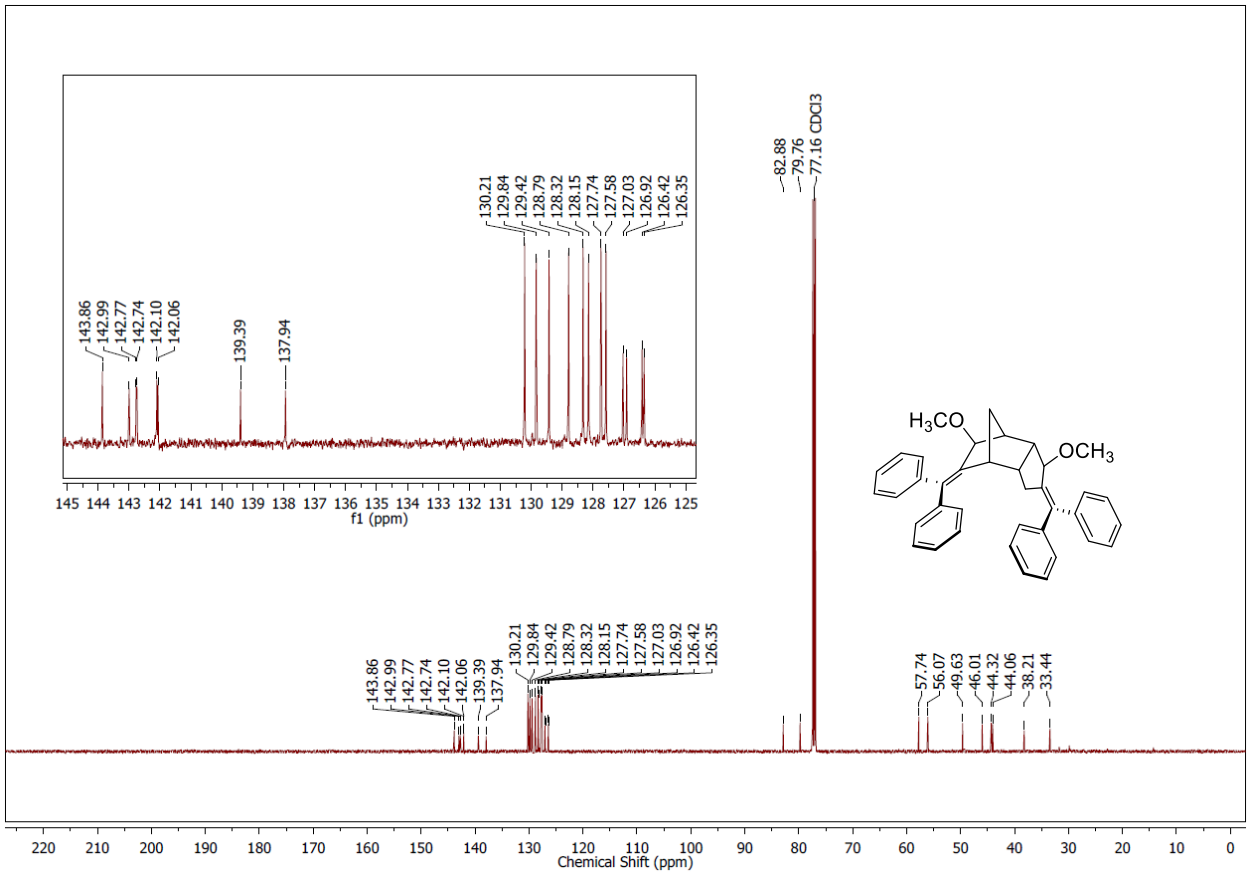

Compound 69

IR Spectrum

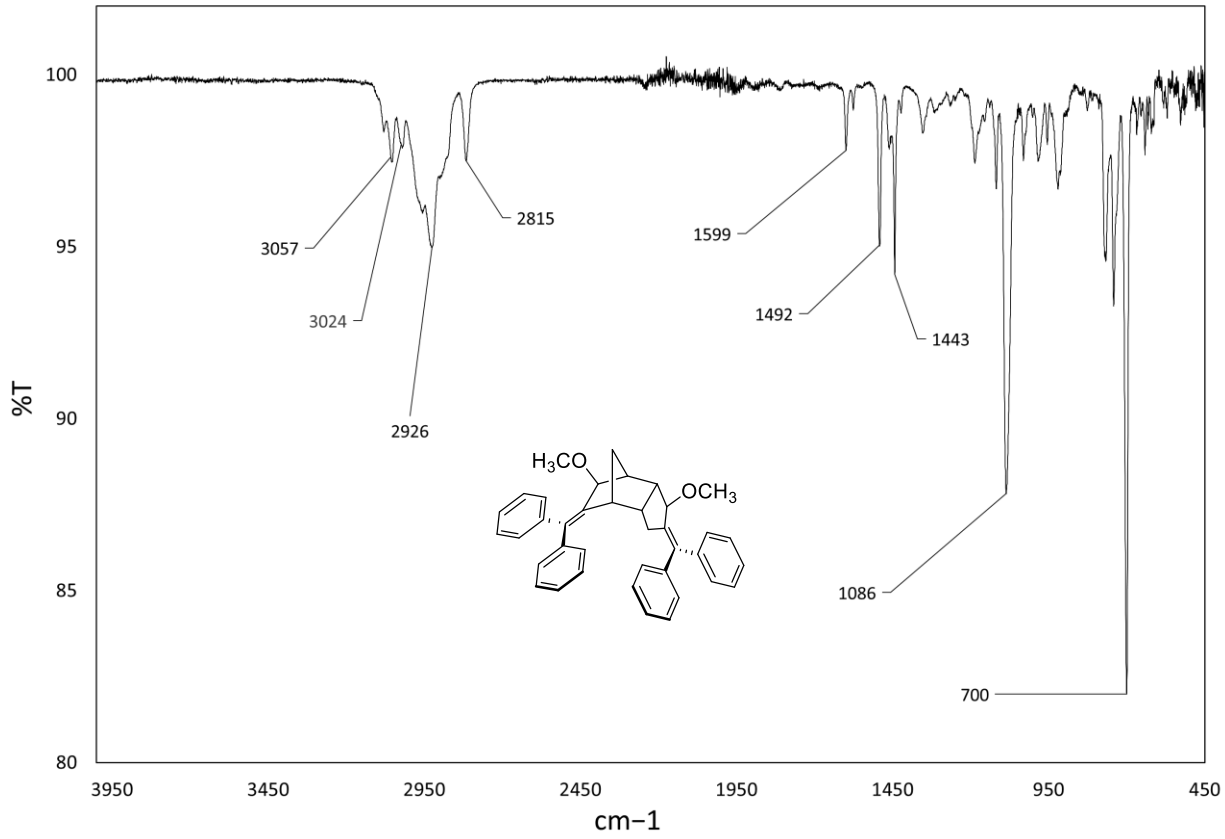

Compound 69

^{1}H-^{1}H COSY NMR Spectrum

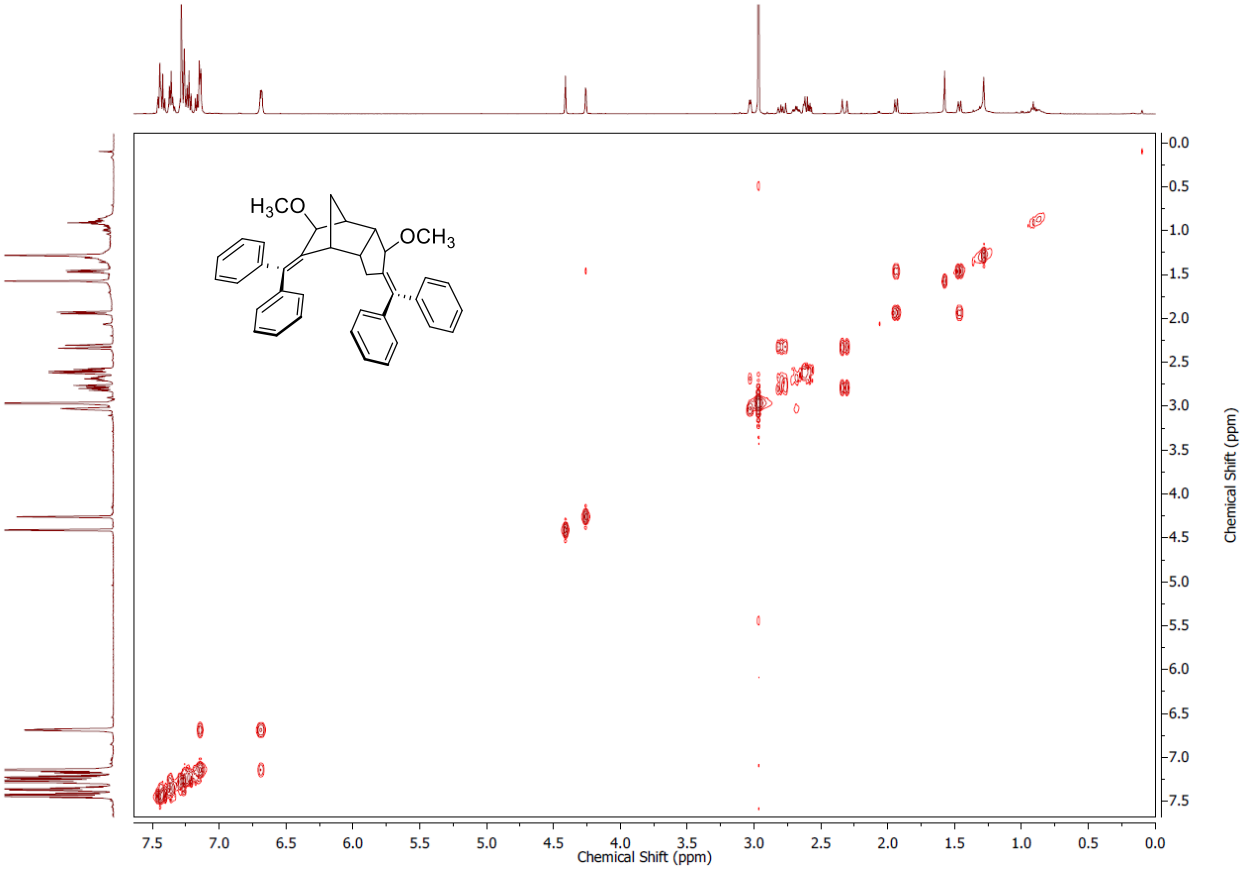

Compound 69

^{1}H-^{1}H COSY NMR Spectrum – Upfield

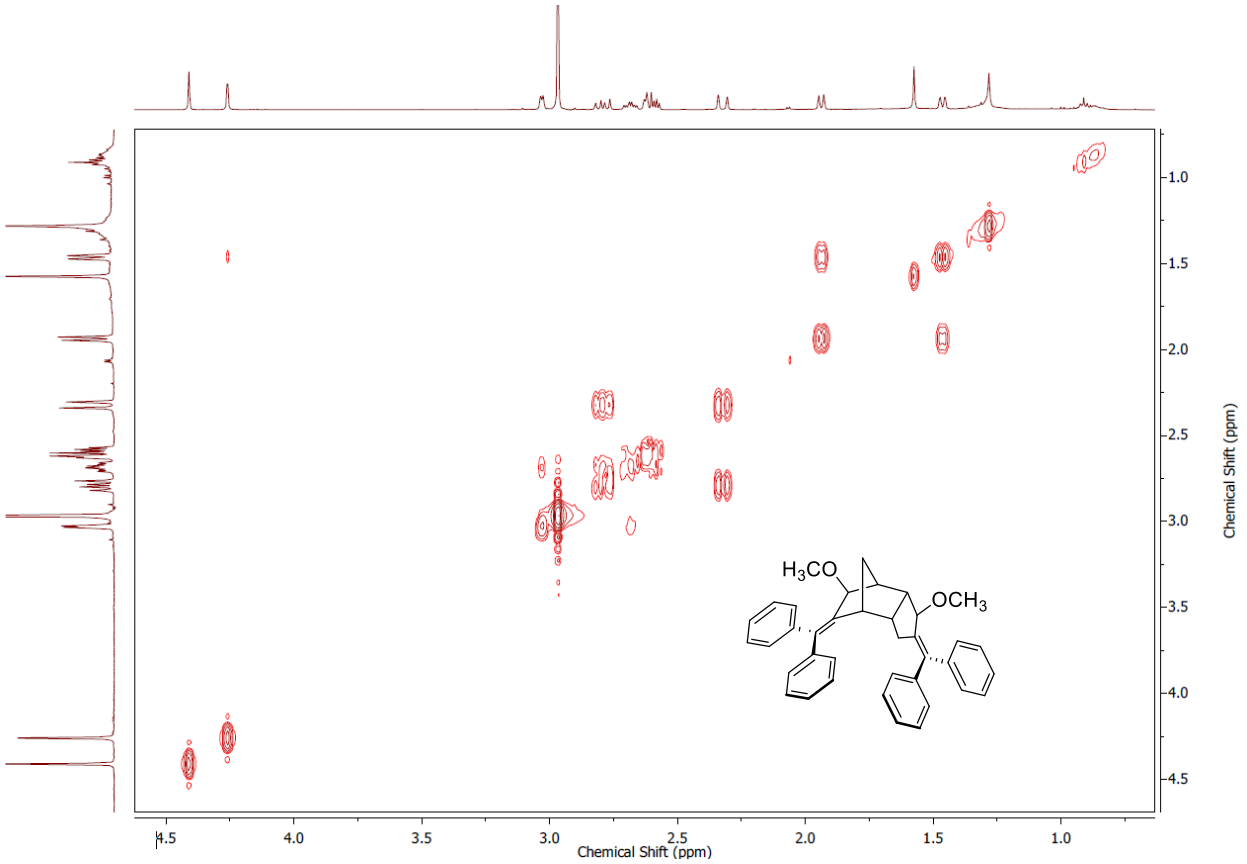

Compound 69

^{1}H-^{1}H COSY NMR Spectrum – Downfield

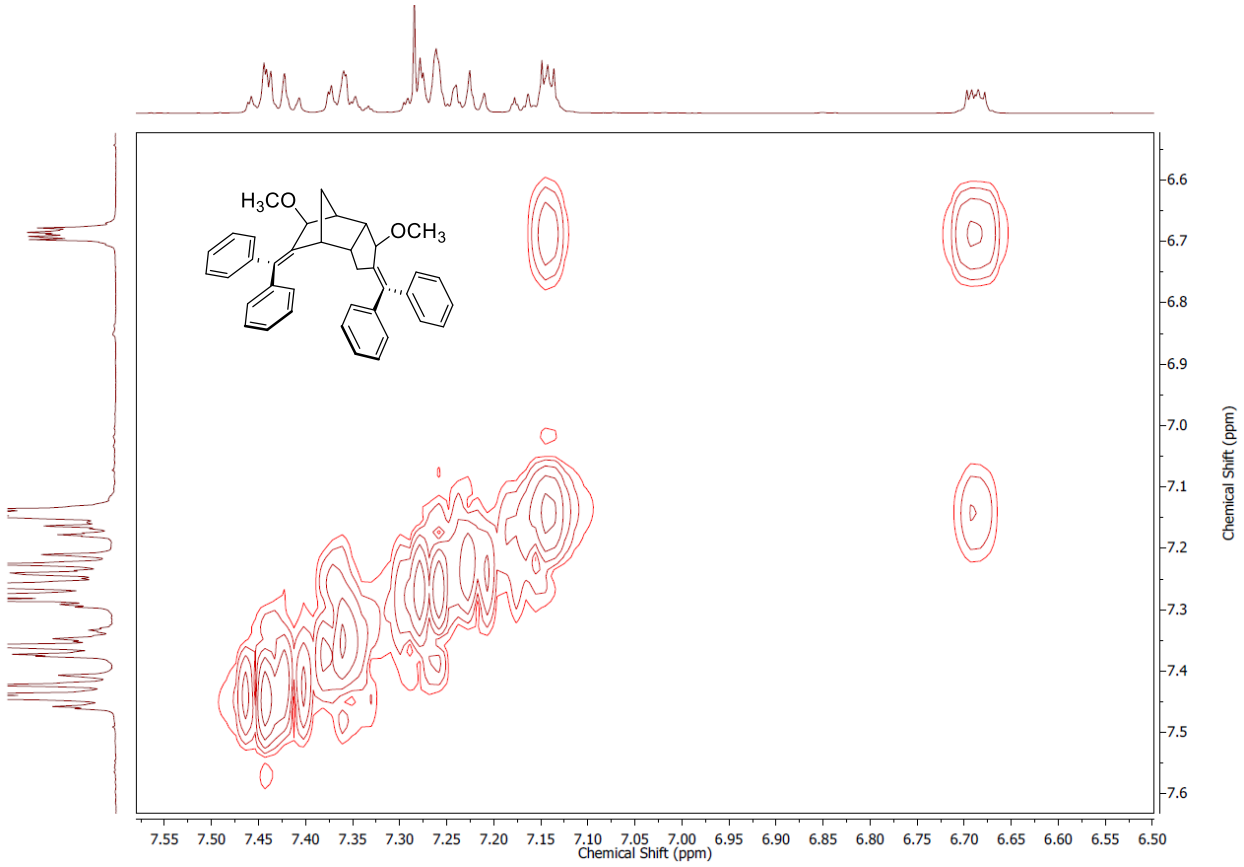

Compound 69

^{1}H-^{13}C HSQC NMR Spectrum

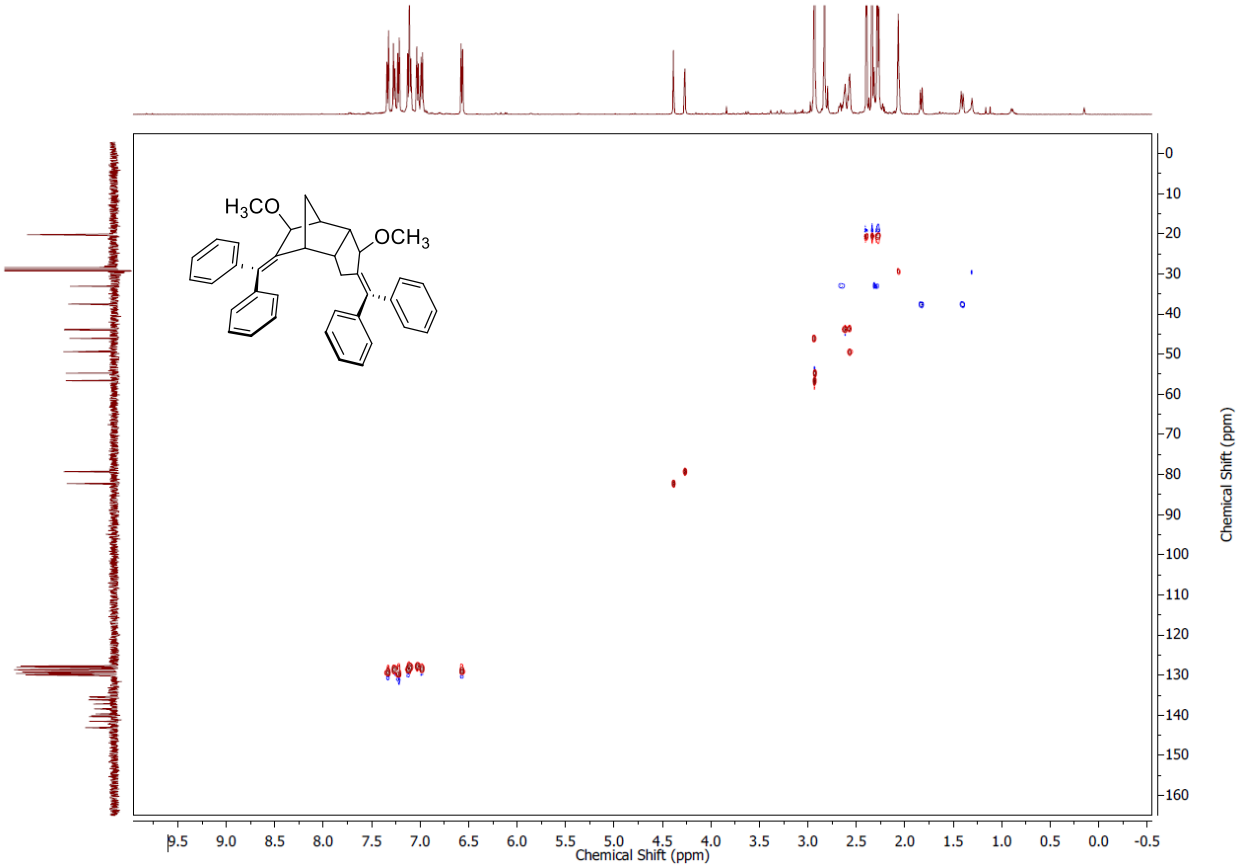

Compound 69

^{1}H-^{13}C HSQC NMR Spectrum – Upfield

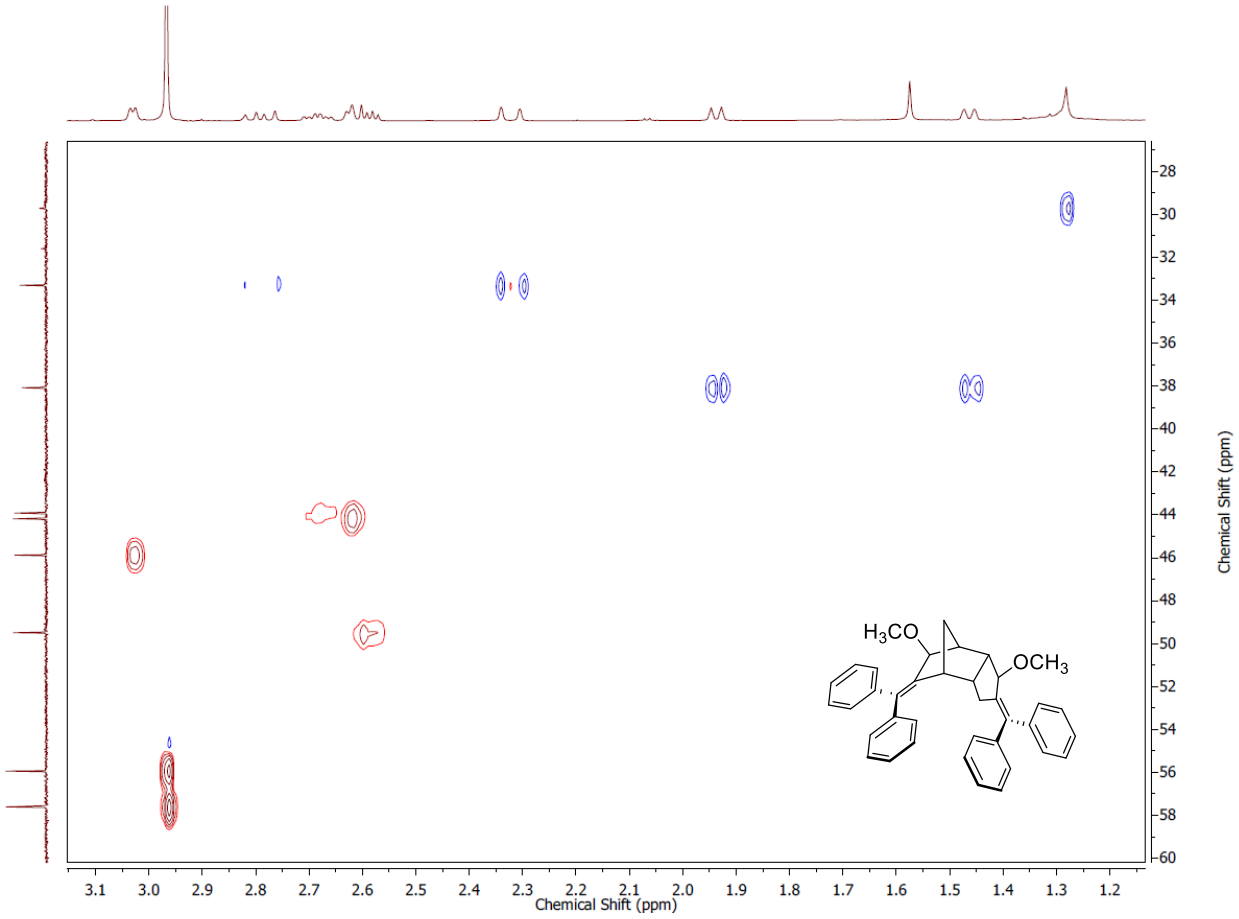

Compound 69

^{1}H-^{13}C HSQC NMR Spectrum – Downfield

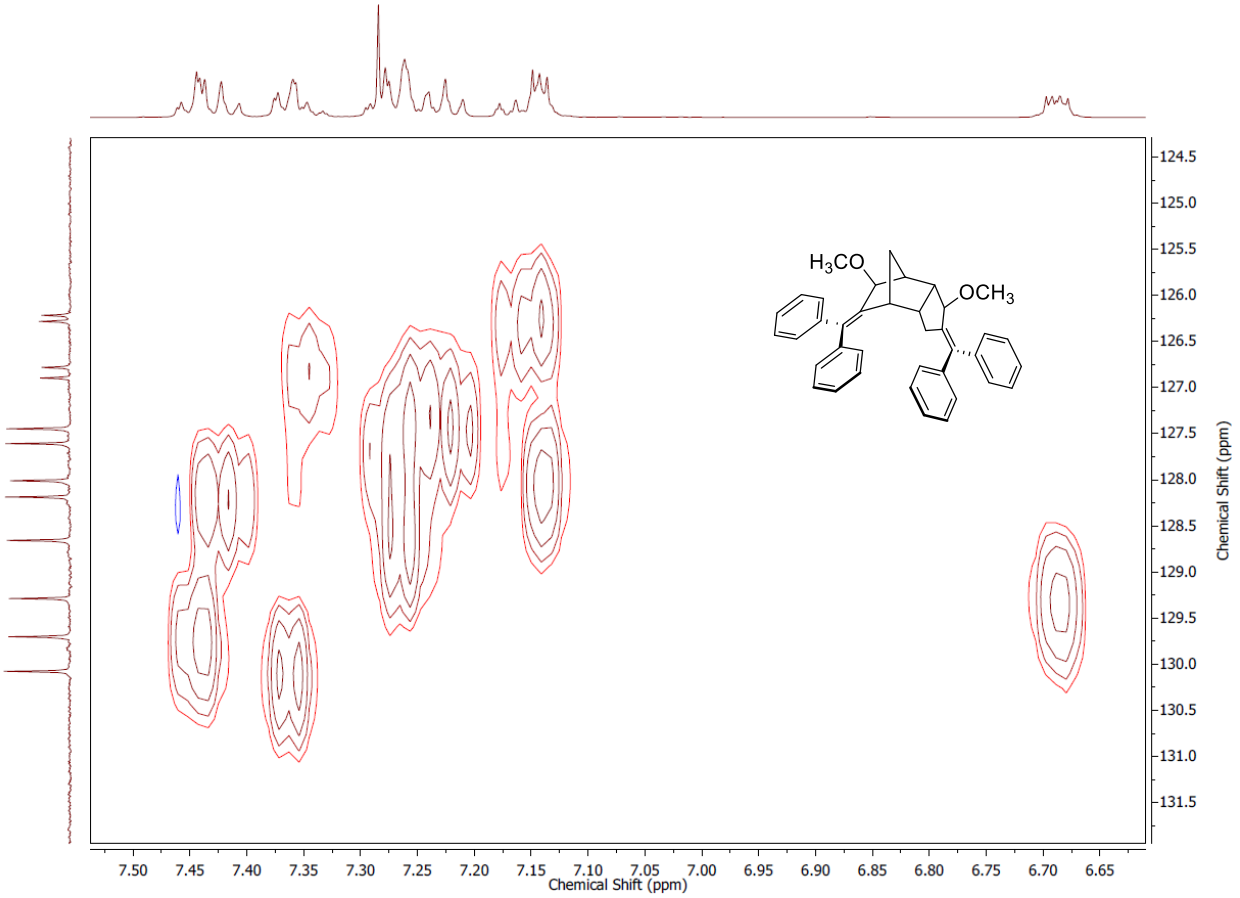

Compound 69

^{1}H-^{13}C HMBC NMR Spectrum

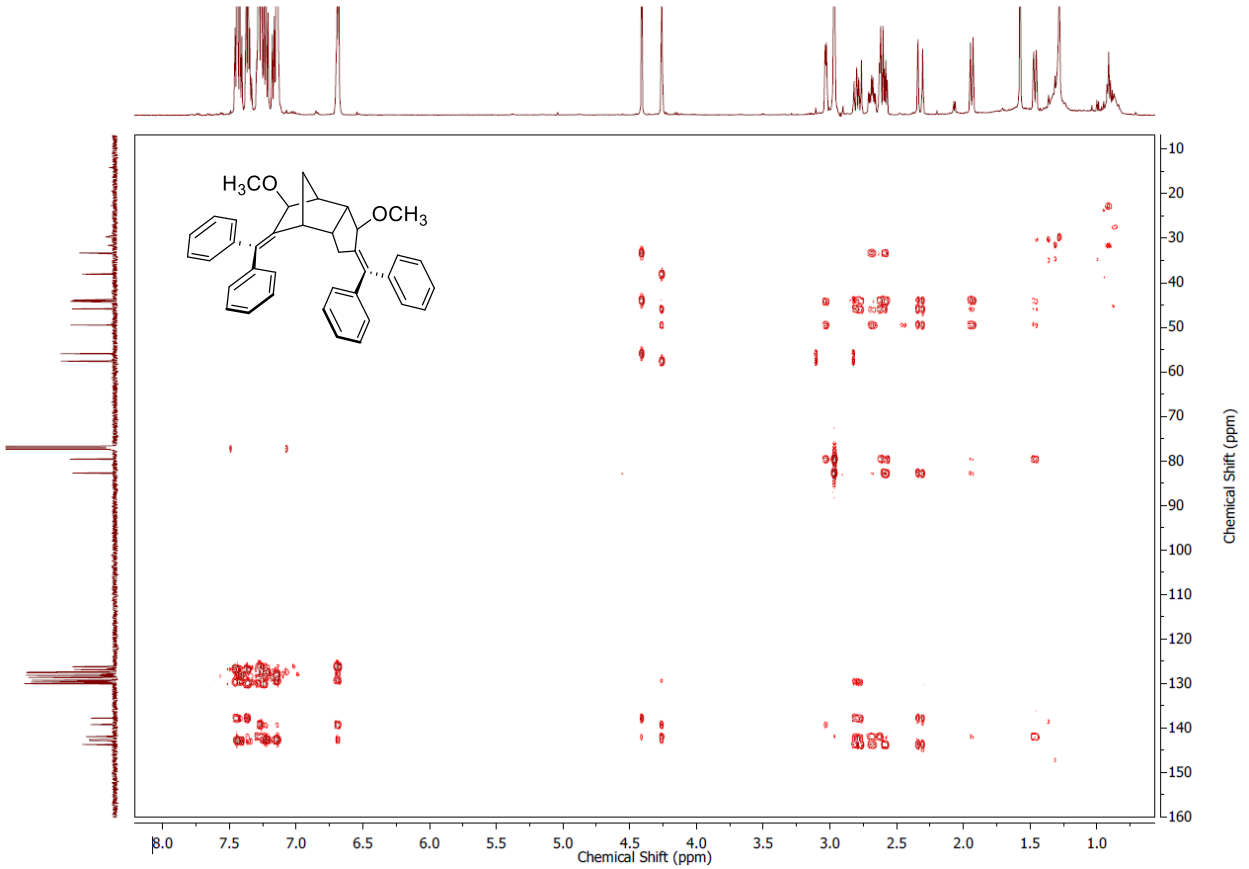

Compound 69

^{1}H-^{13}C HMBC NMR Spectrum – Upfield

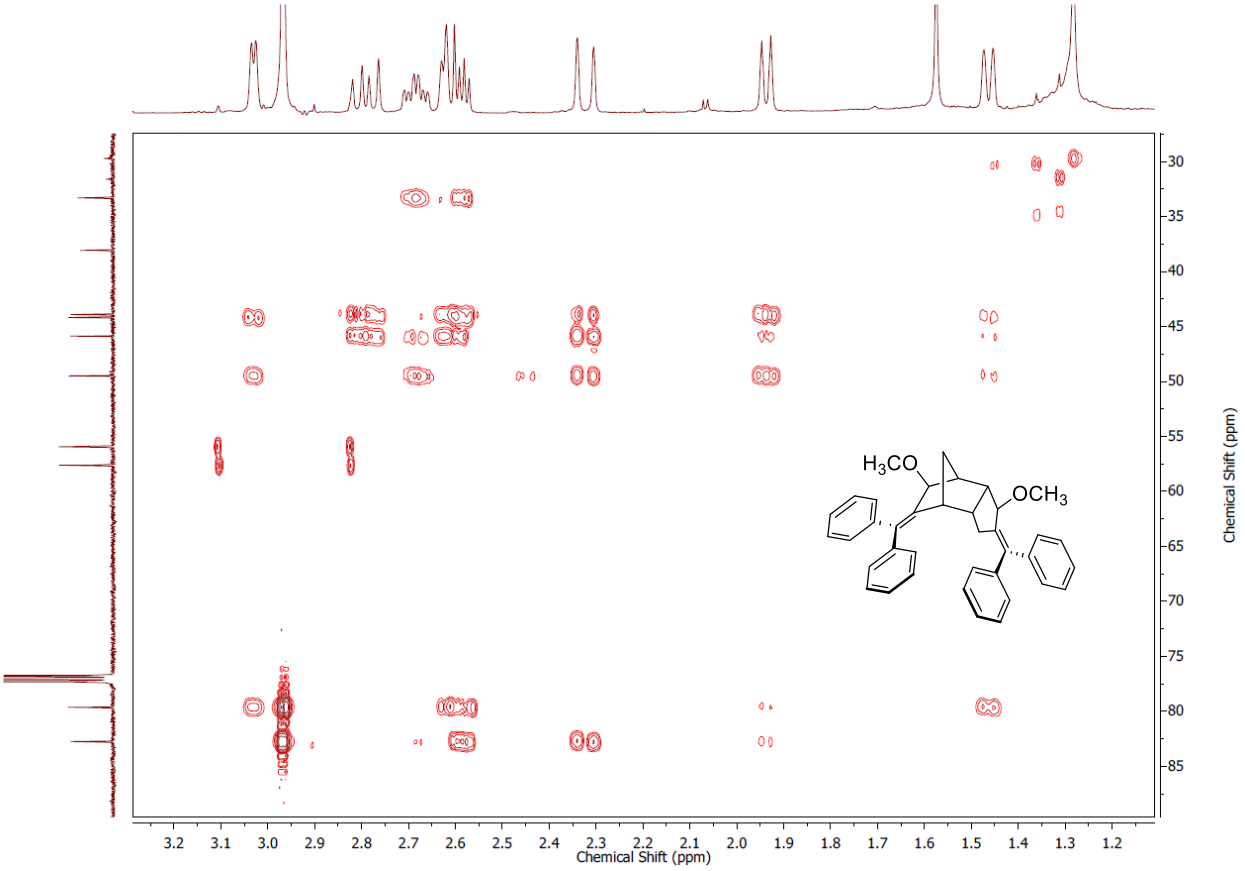

Compound 69

^{1}H-^{13}C HMBC NMR Spectrum – 3.20-1.30 ppm (^{1}H): 150-120 ppm (^{13}C)

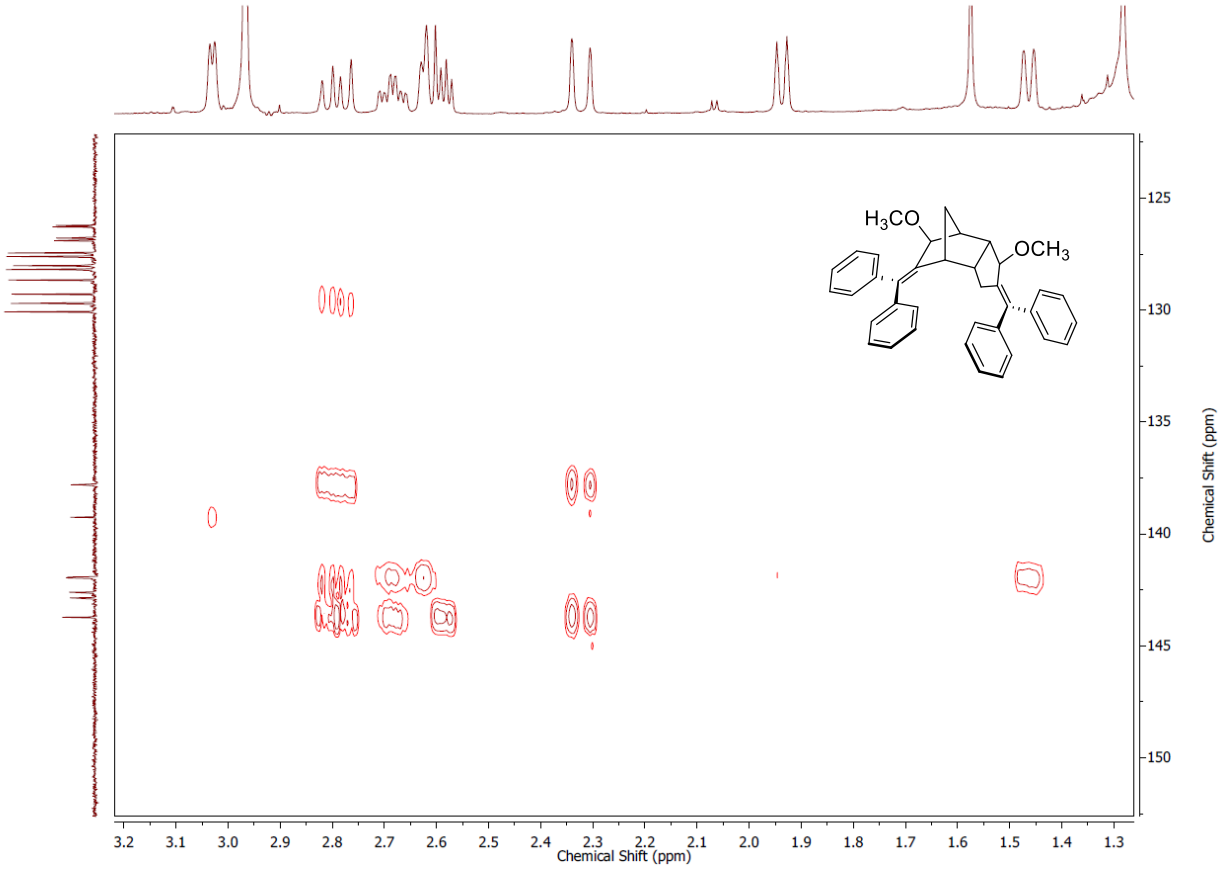

Compound 69

^{1}H-^{13}C HMBC NMR Spectrum – 4.60-4.05 ppm (^{1}H): 62-30 ppm (^{13}C)

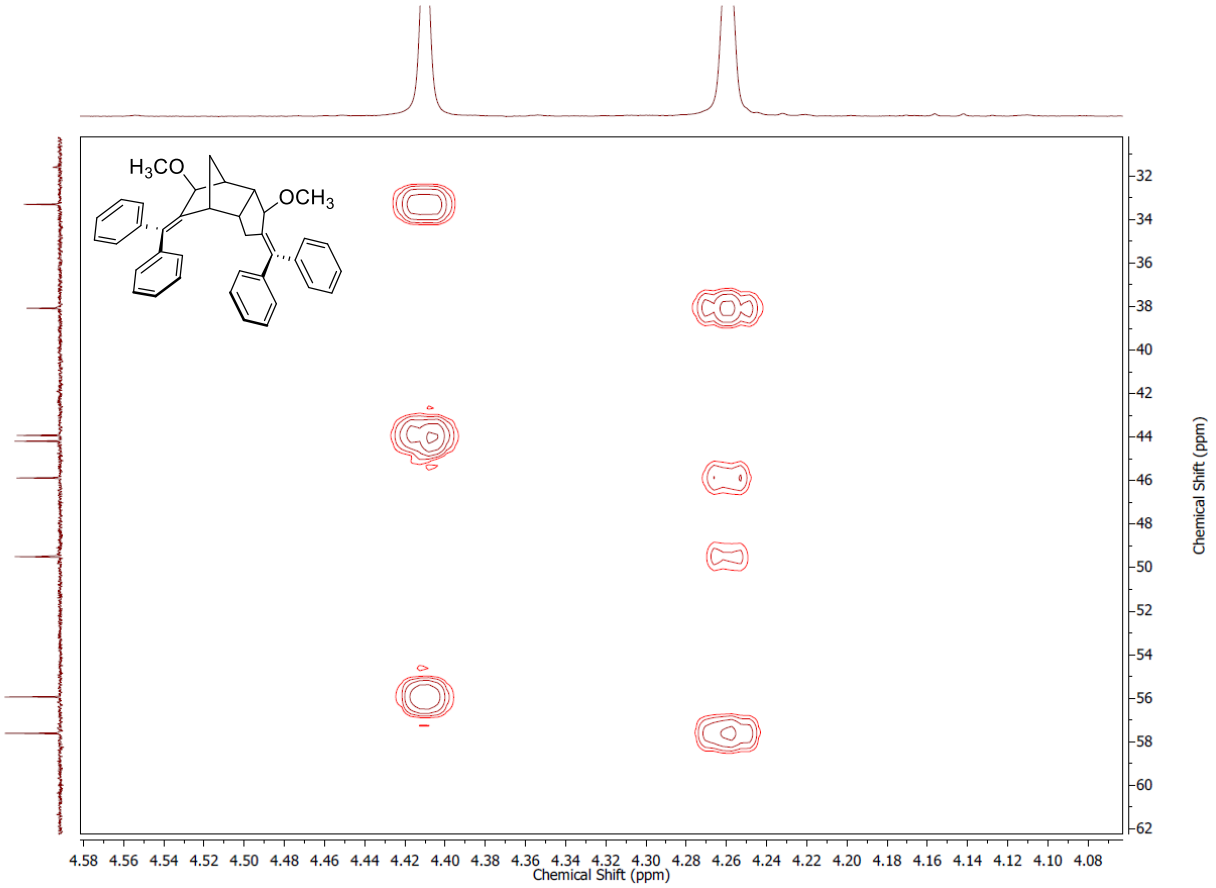

Compound 69

^{1}H-^{13}C HMBC NMR Spectrum – 4.60-4.05 ppm (^{1}H): 154-125 ppm (^{13}C)

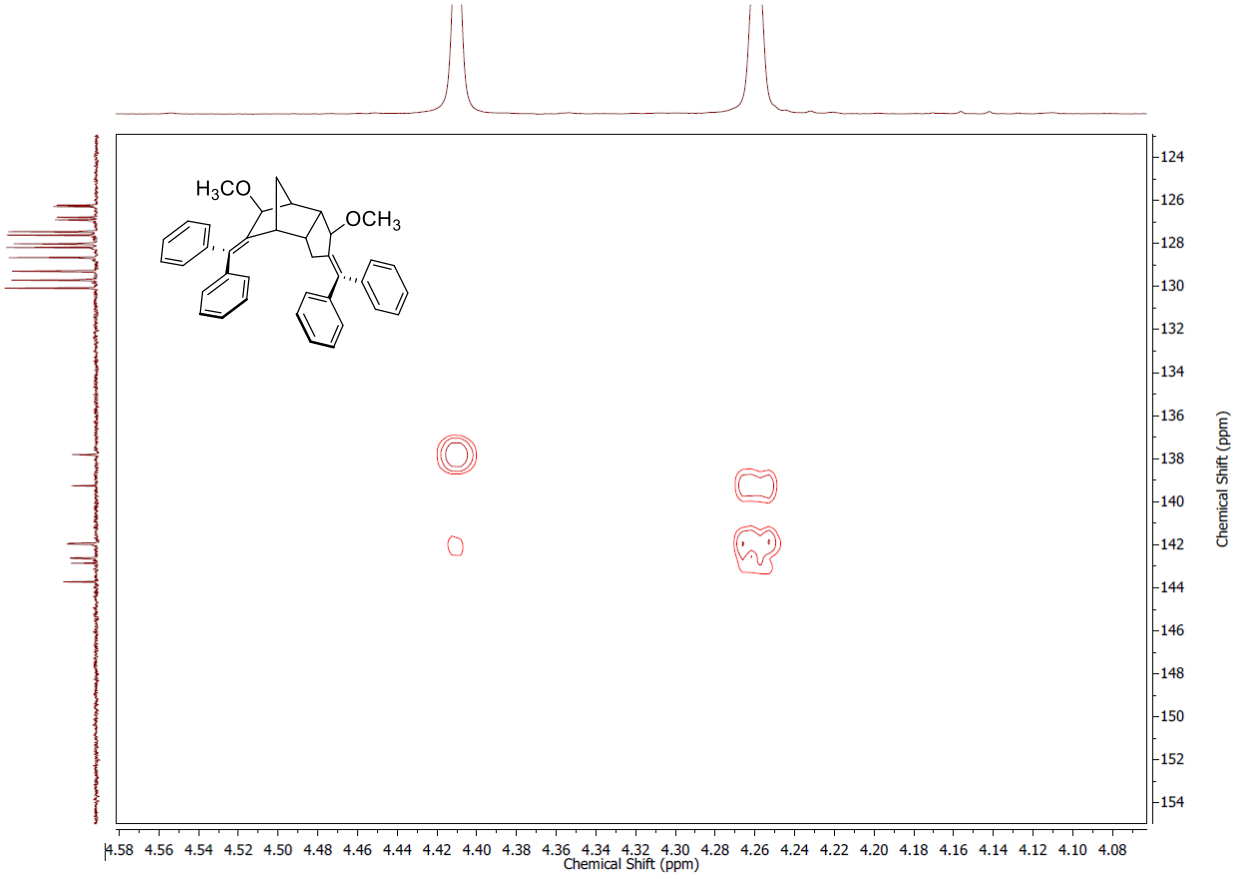

Compound 69

1D-NOE NMR Spectrum – Pulsed Frequency: 6.685 ppm

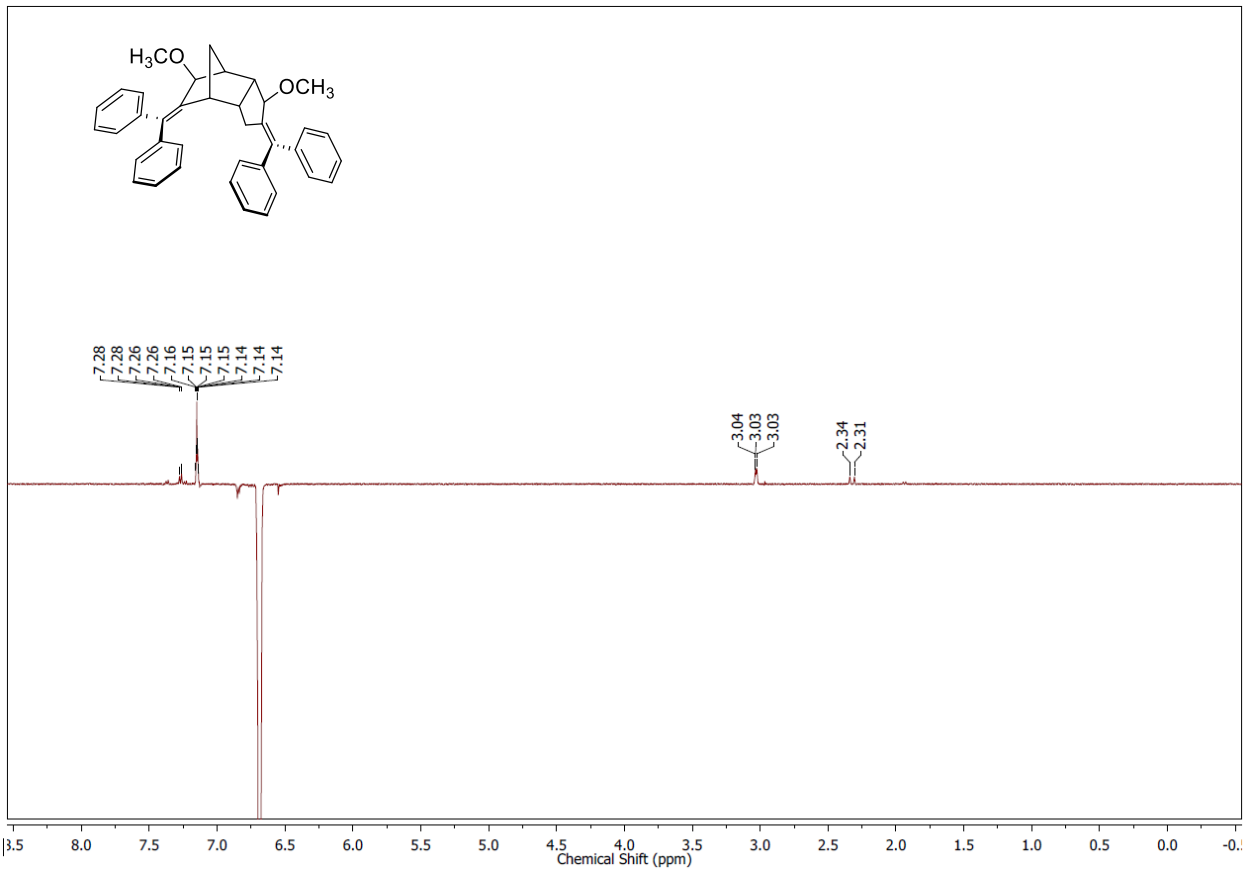

Compound 69

1D-NOE NMR Spectrum – Pulsed Frequency: 4.425 ppm

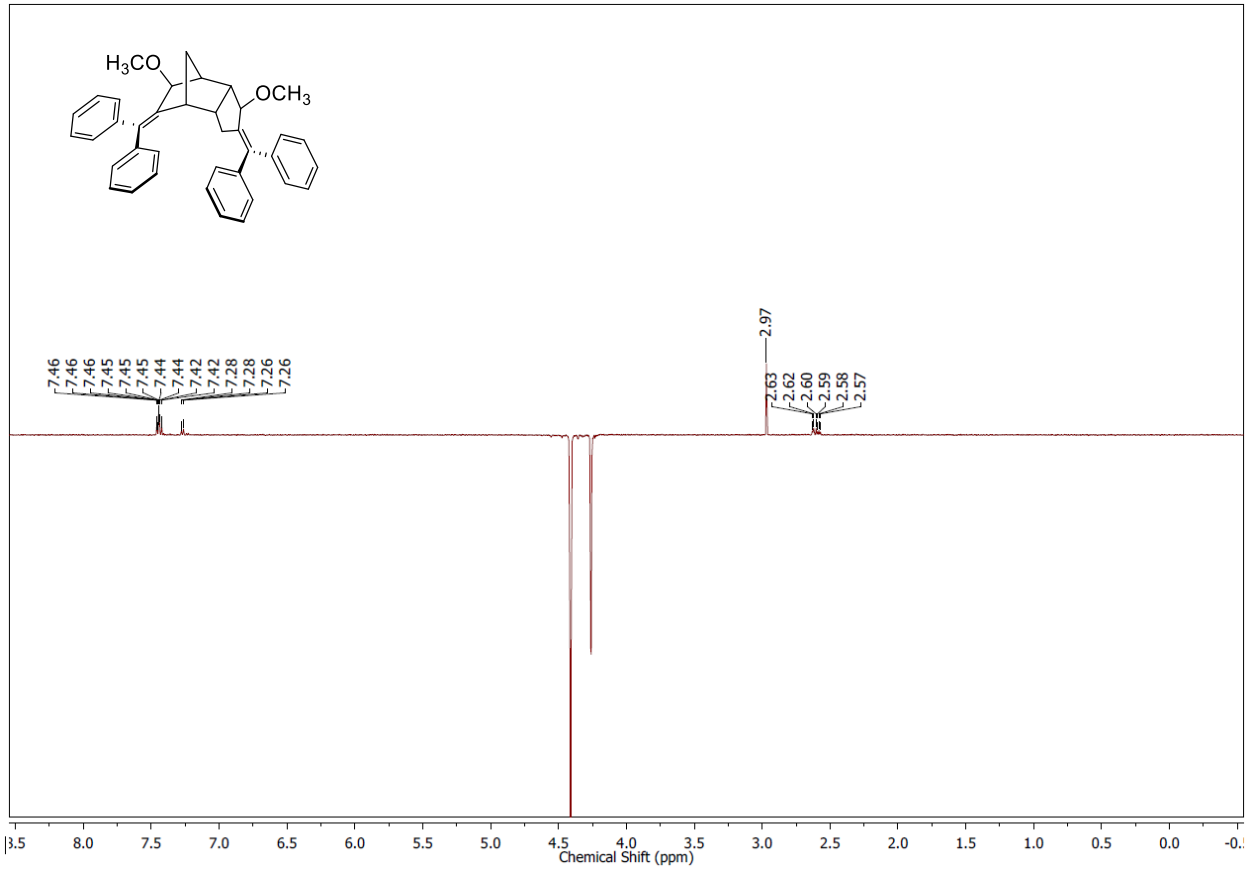

Compound 69

1D-NOE NMR Spectrum – Pulsed Frequency: 4.225 ppm

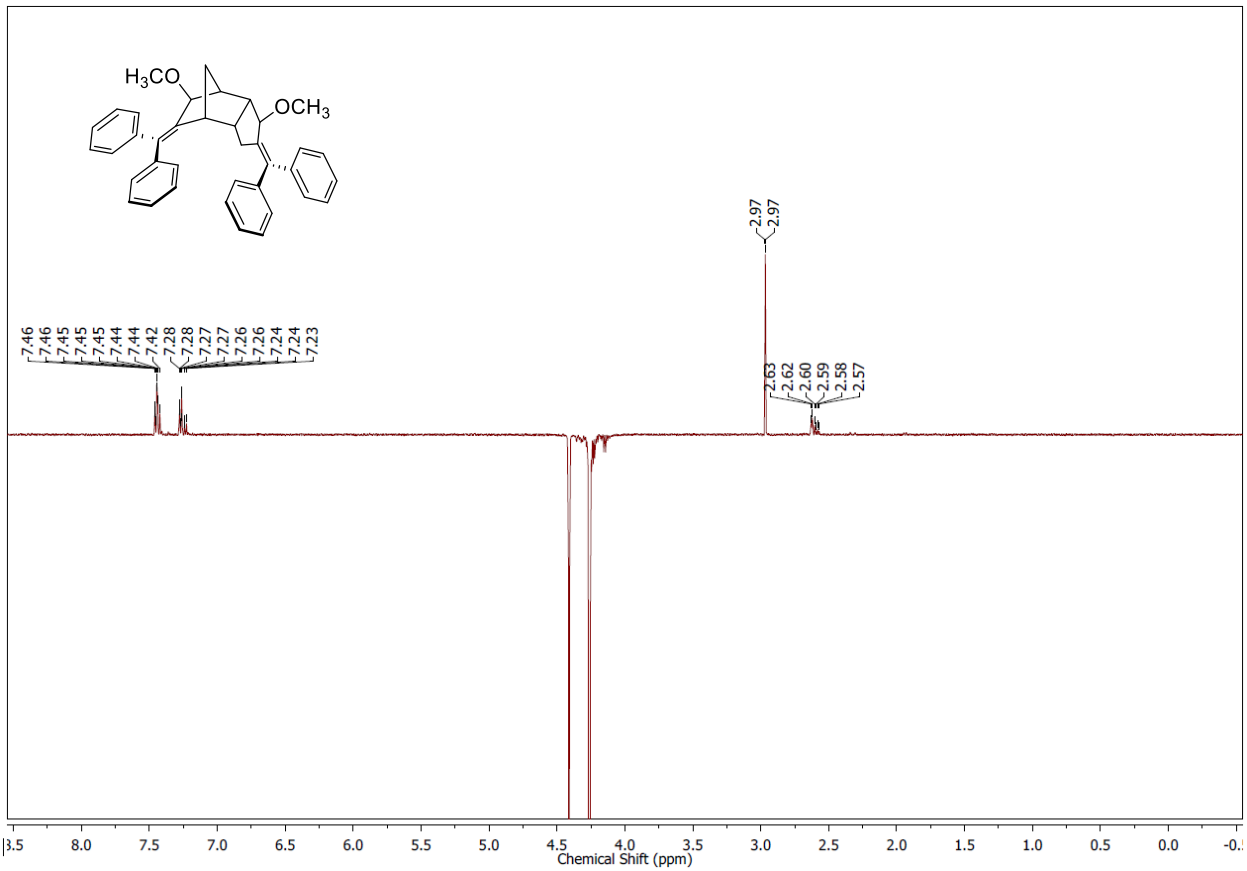

Compound 63 Kinetics Spectra

25°C – Trial 1

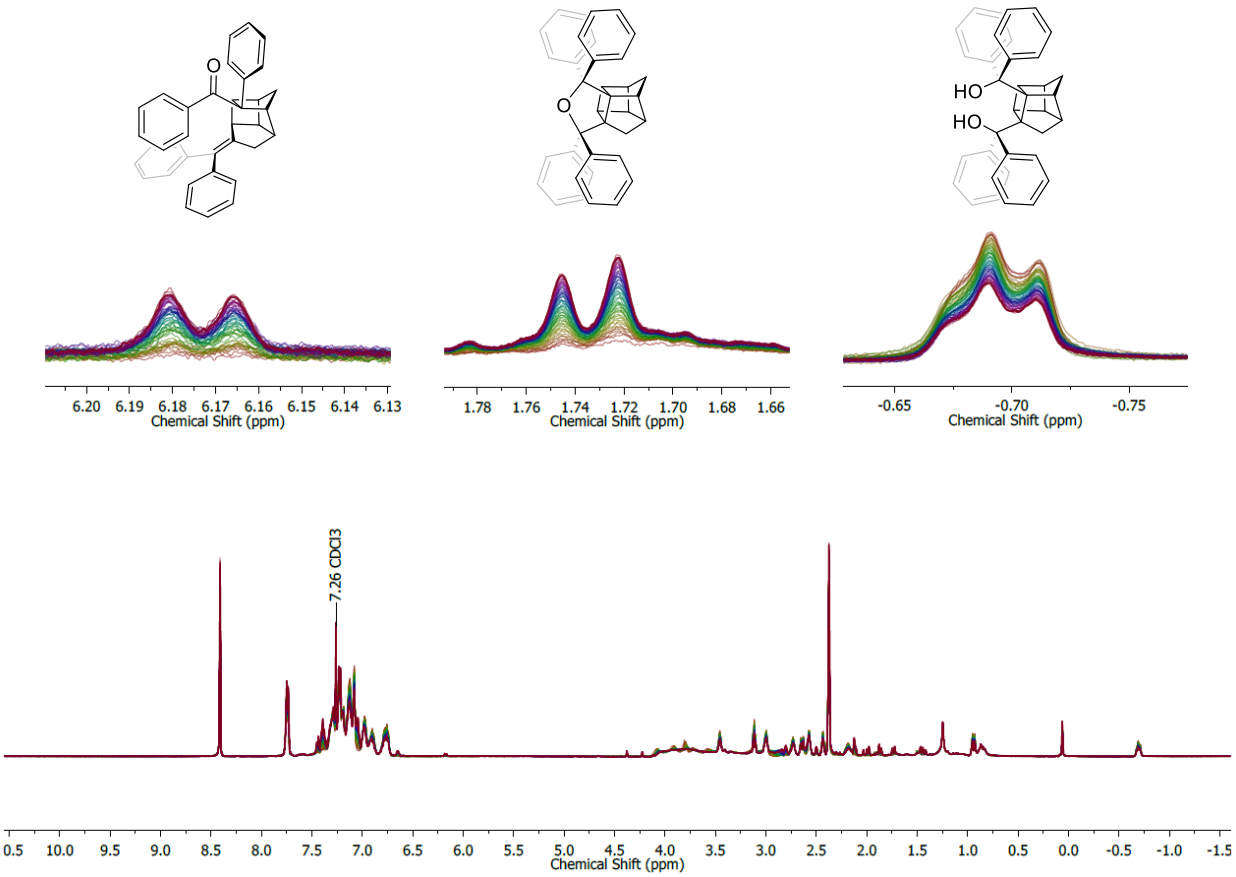

Compound **63** @ 25°C - Trial 1

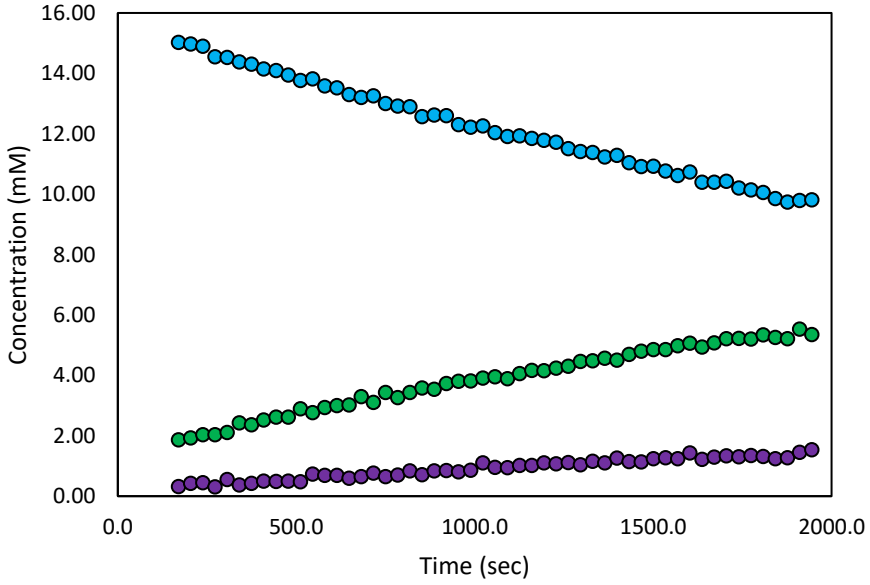

Compound 63 Kinetics Spectra

25°C – Trial 2

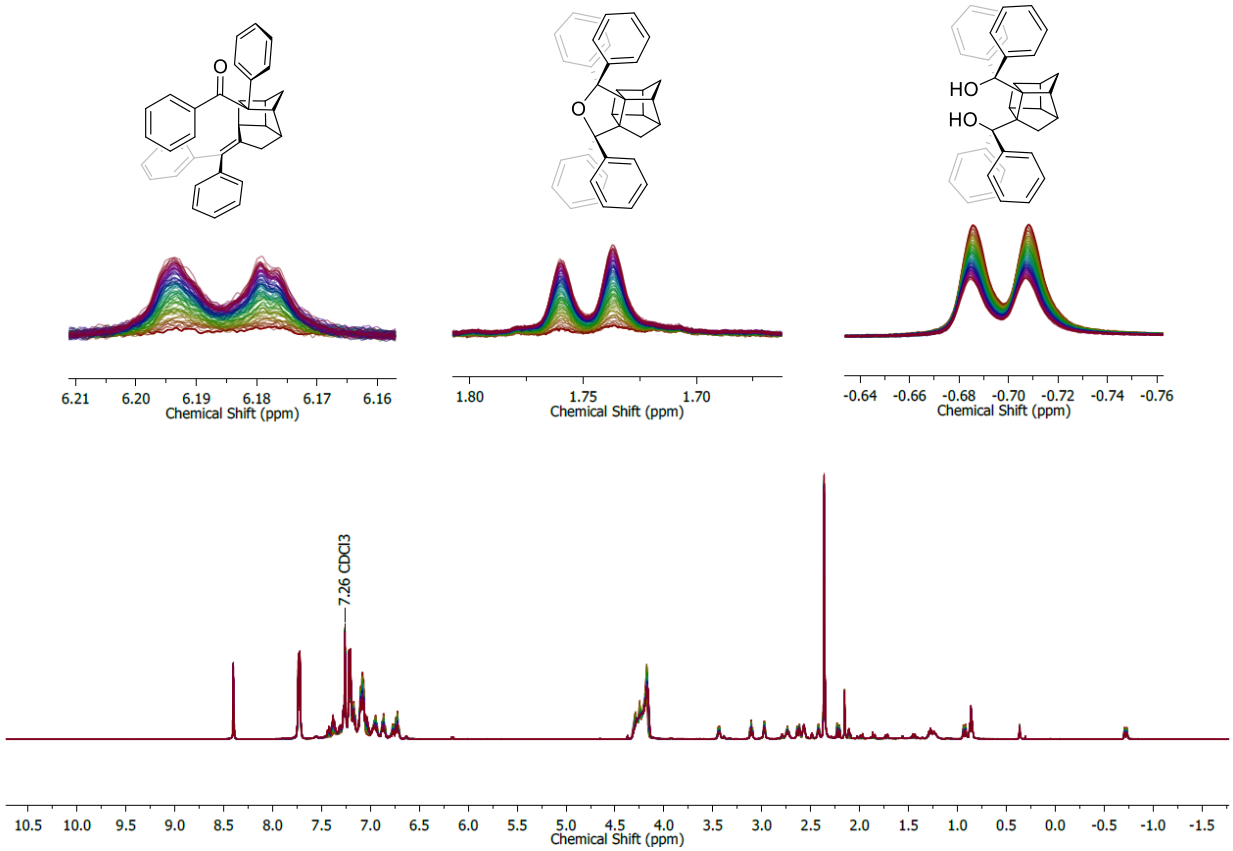

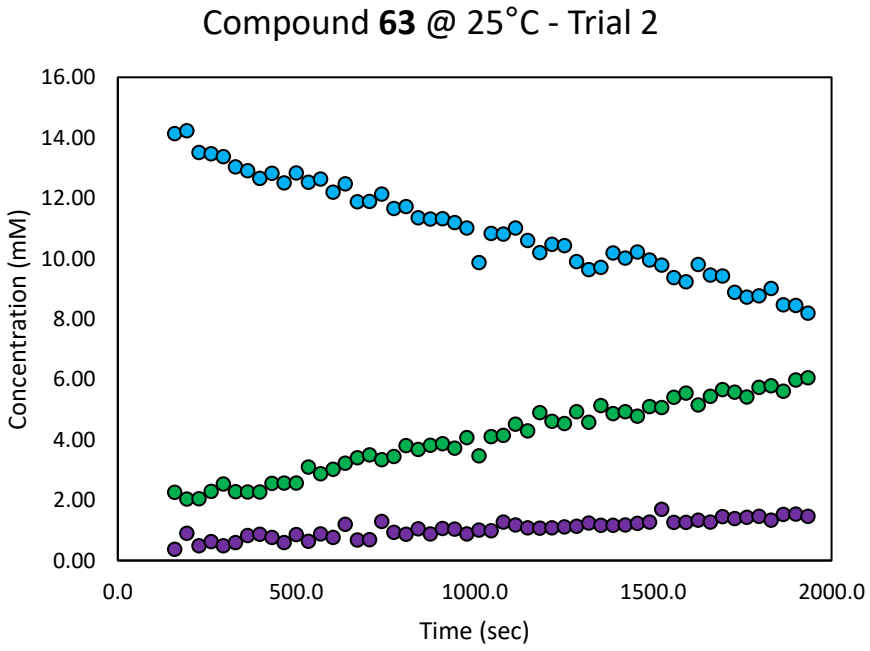

Compound 63 Kinetics Spectra

25°C – Trial 3

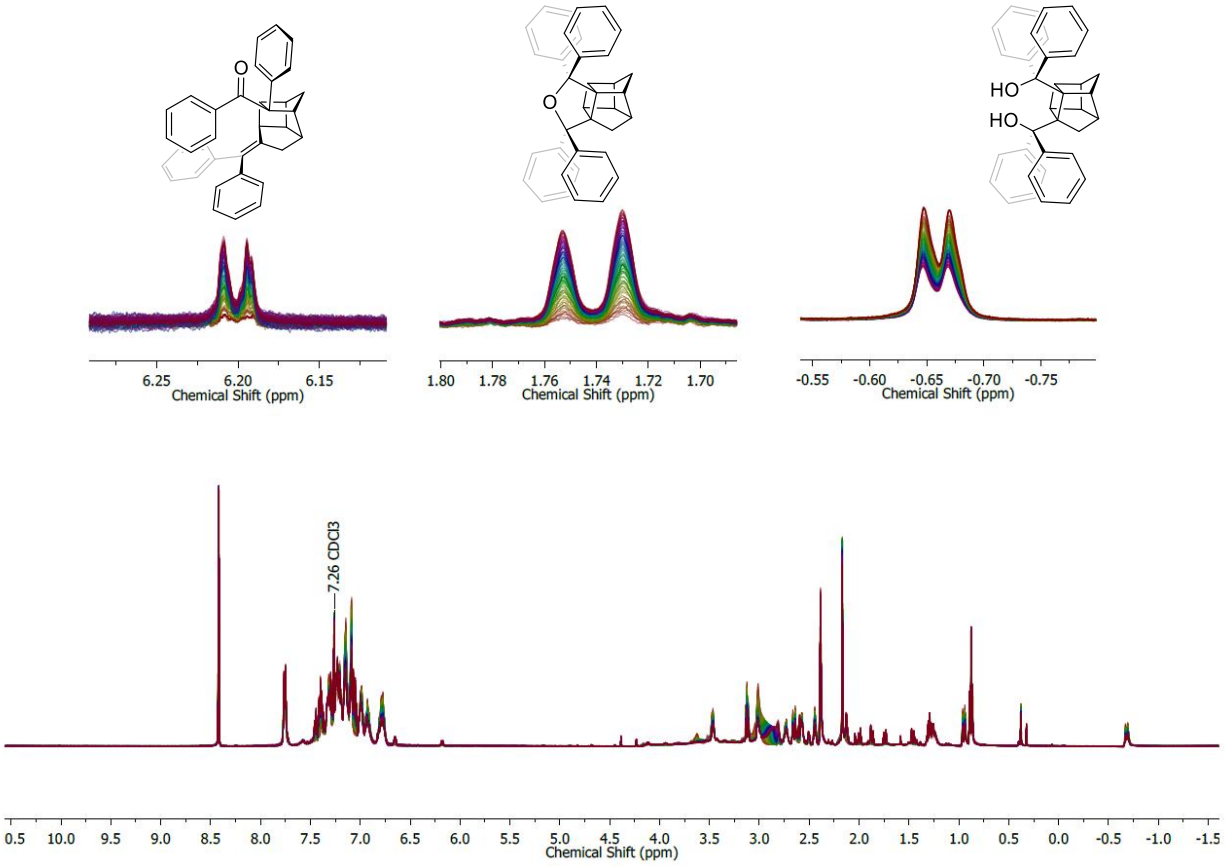

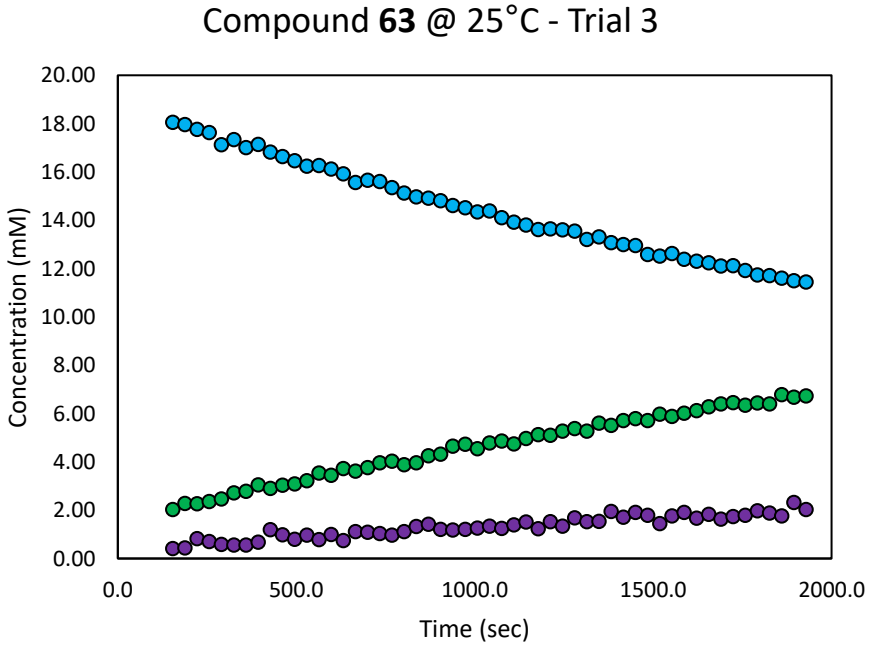

Compound 63 Kinetics Spectra

35°C – Trial 1

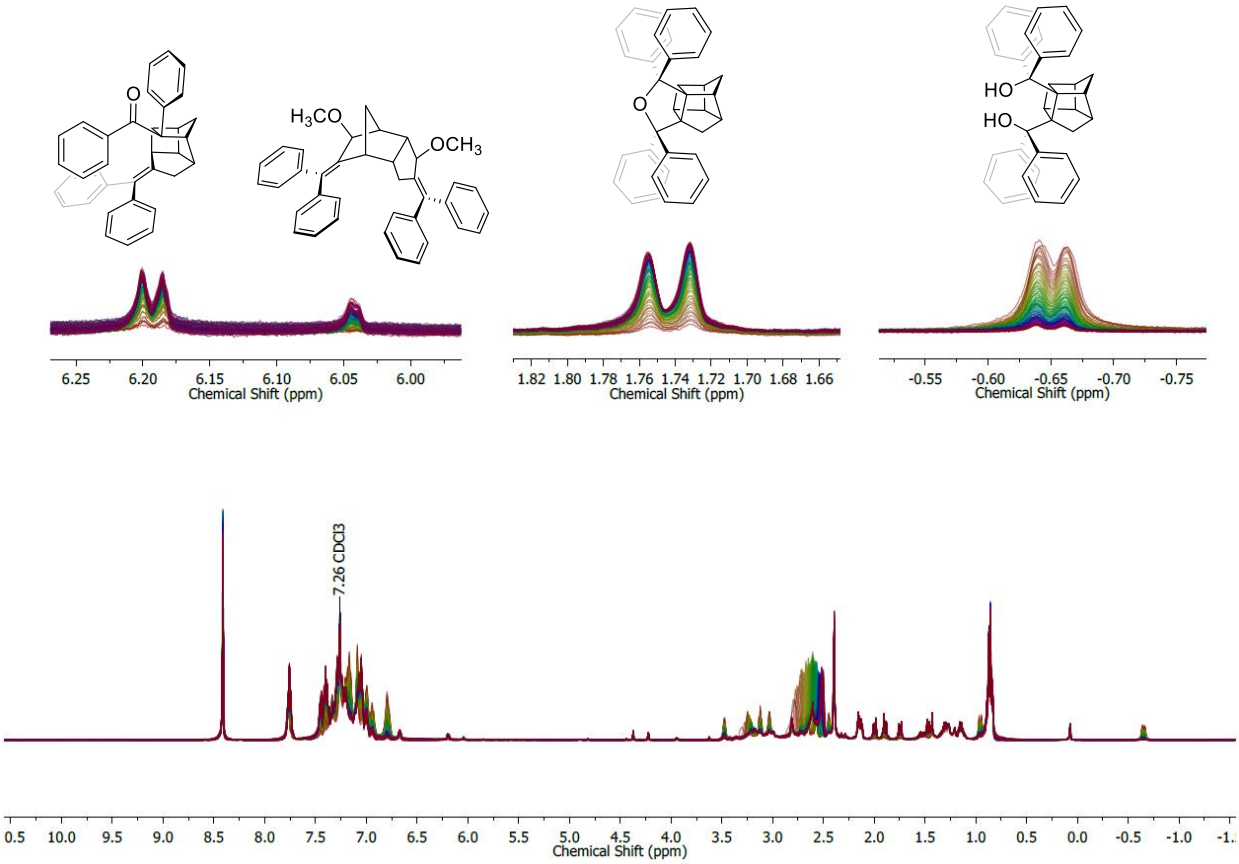

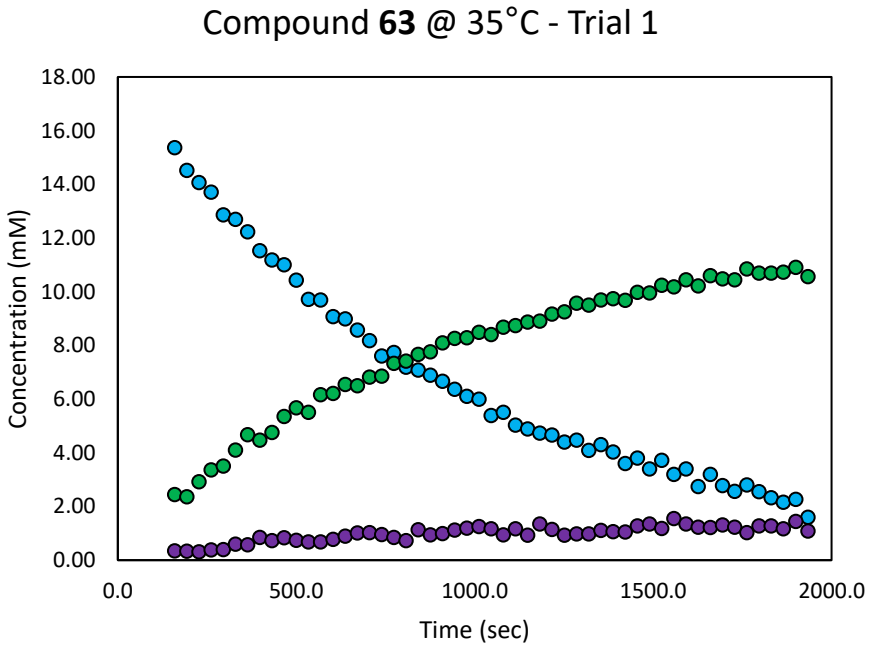

Compound 63 Kinetics Spectra

35°C – Trial 2

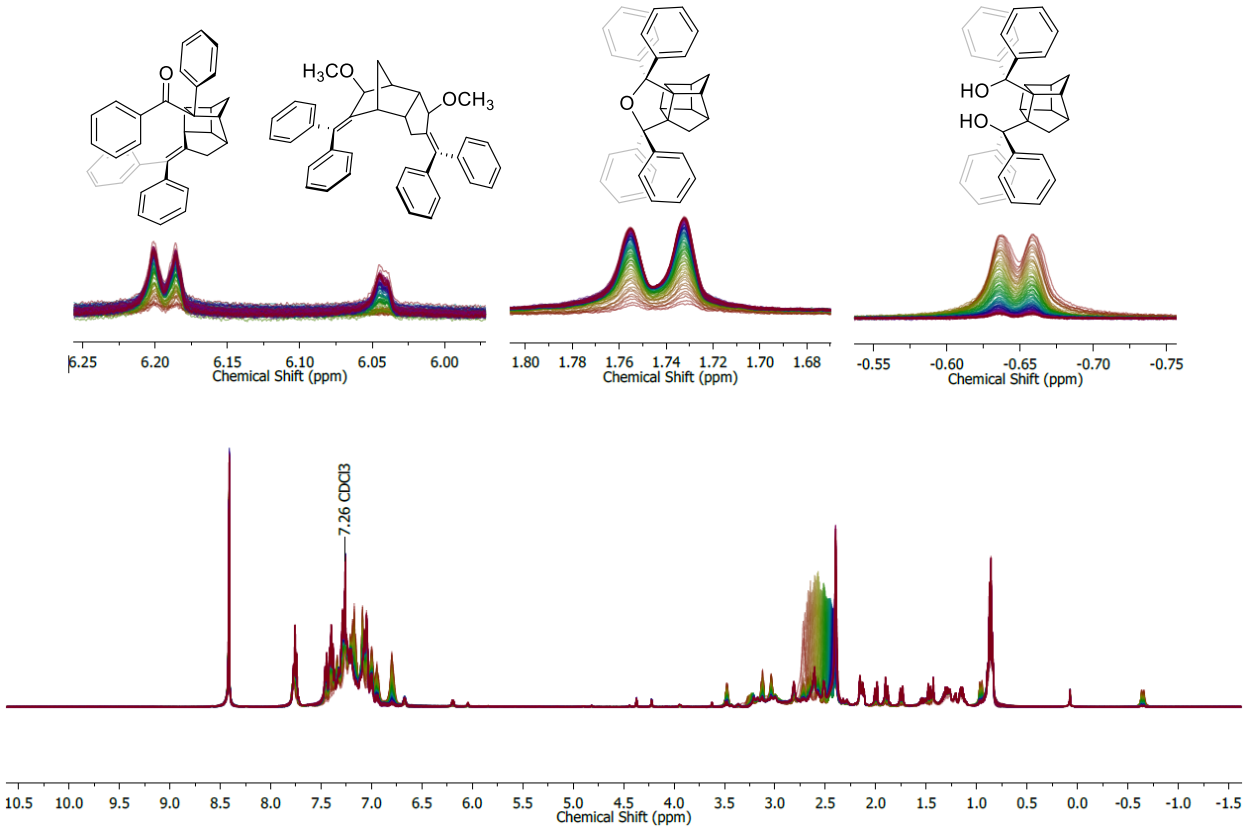

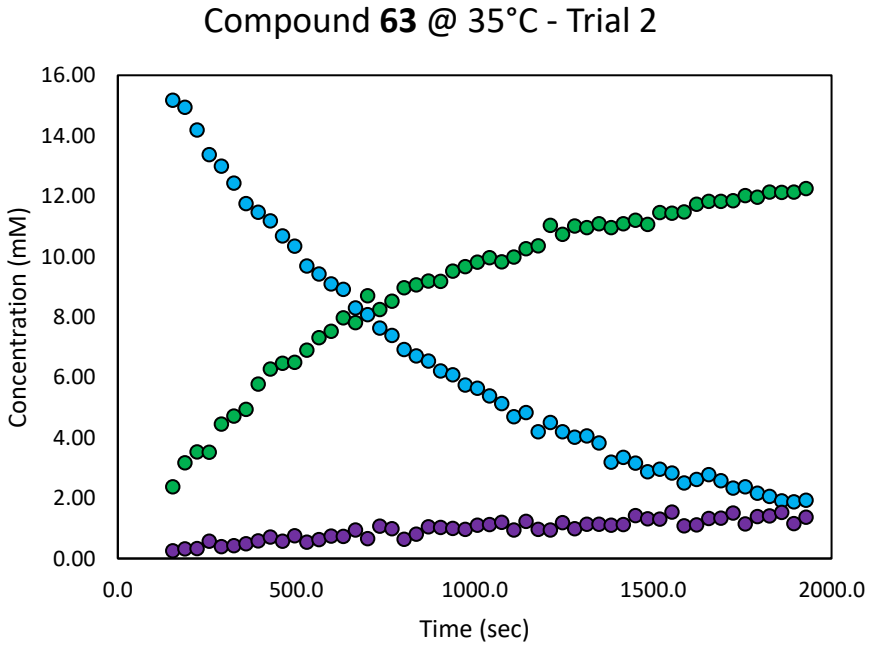

Compound 63 Kinetics Spectra

35°C – Trial 3

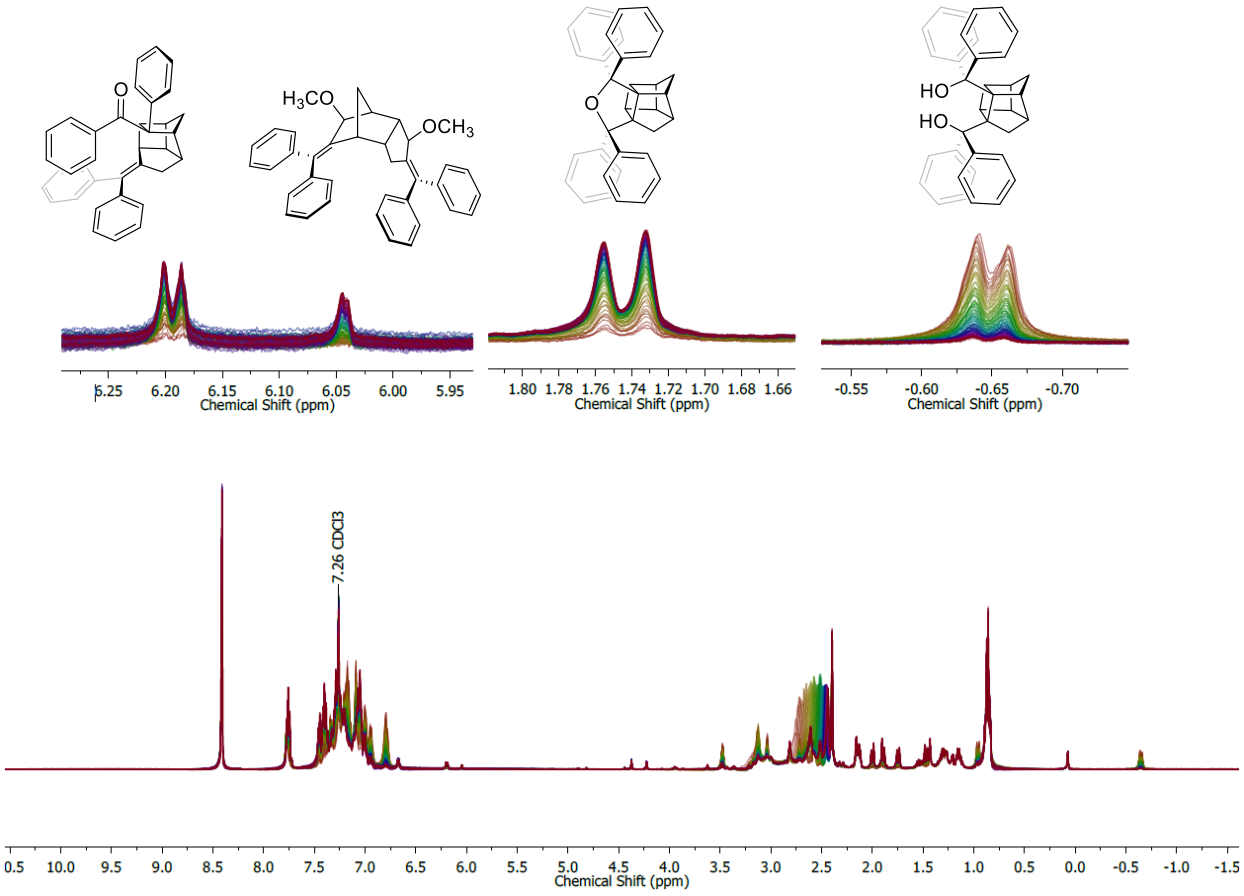

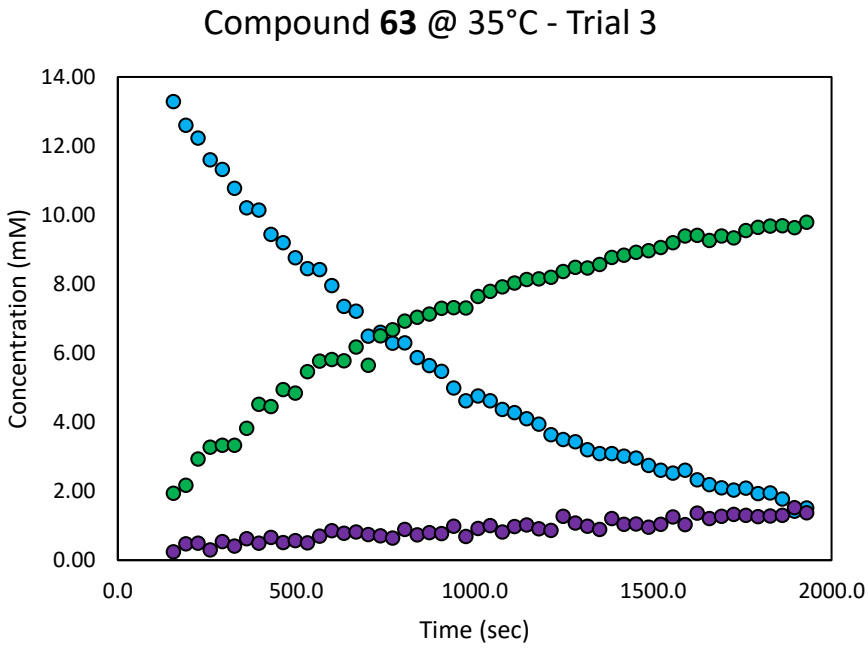

Compound 63 Kinetics Spectra

45°C – Trial 1

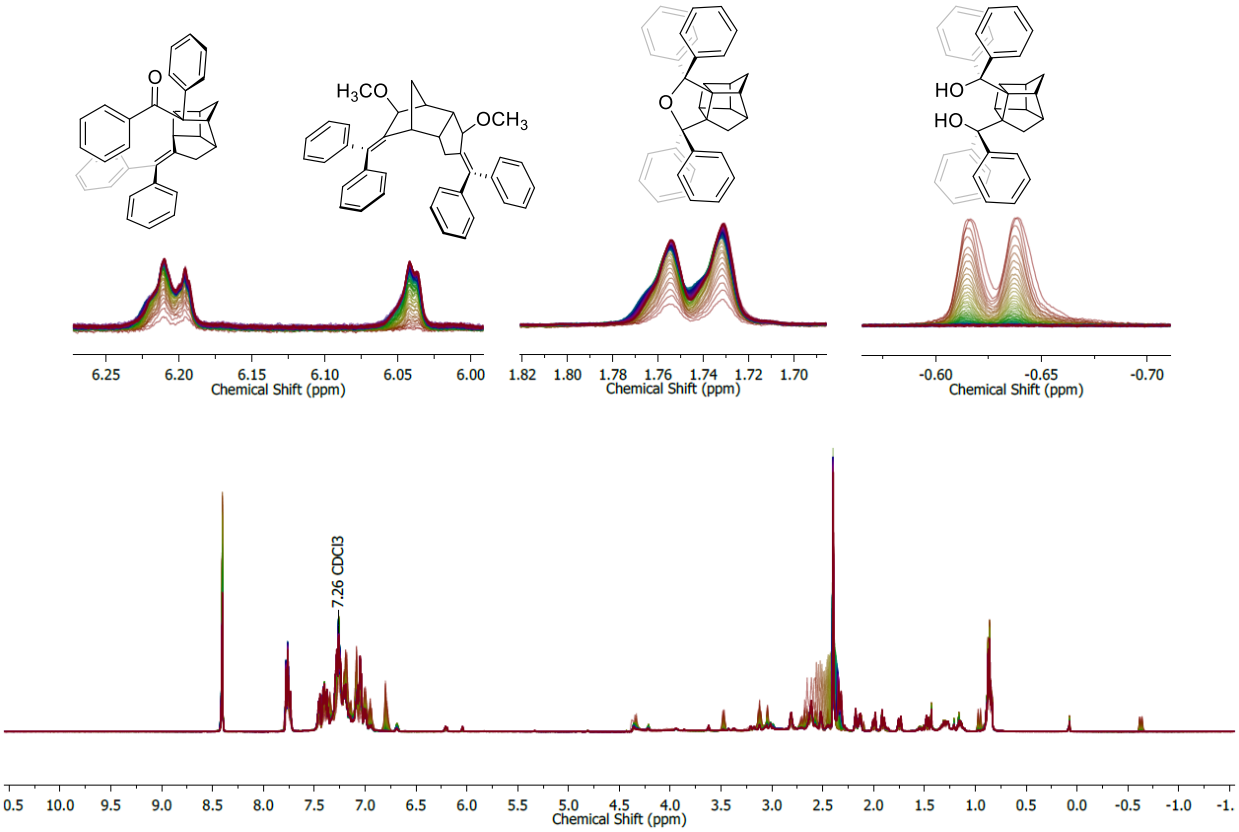

Compound **63** @ 45°C - Trial 1

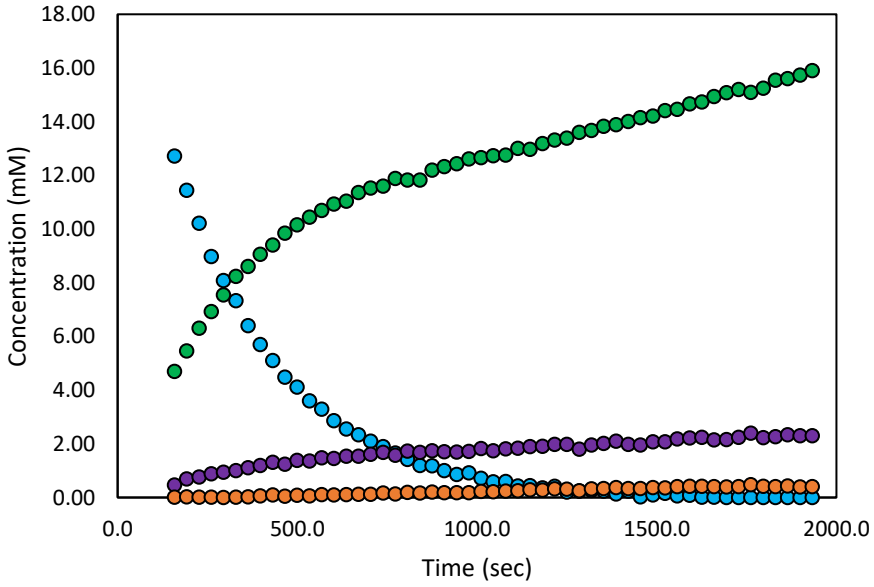

Compound 63 Kinetics Spectra

45°C – Trial 2

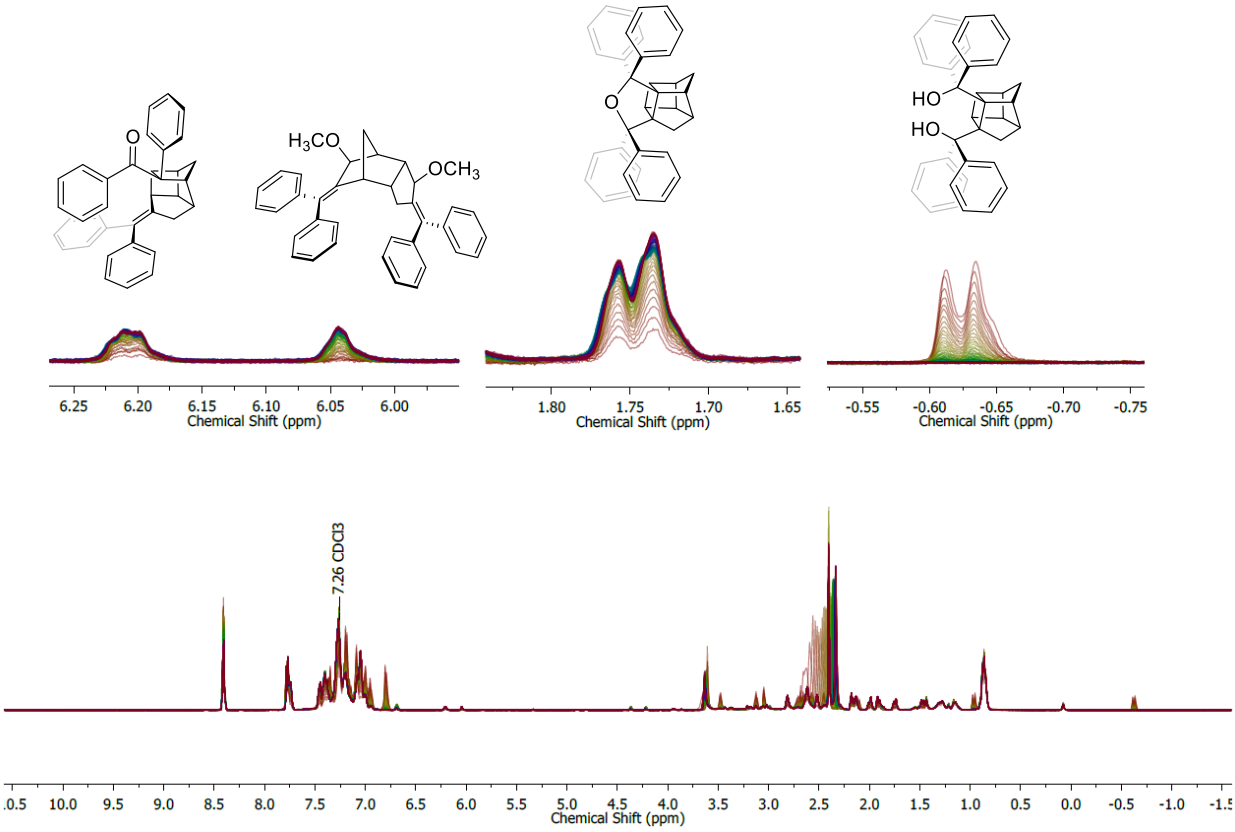

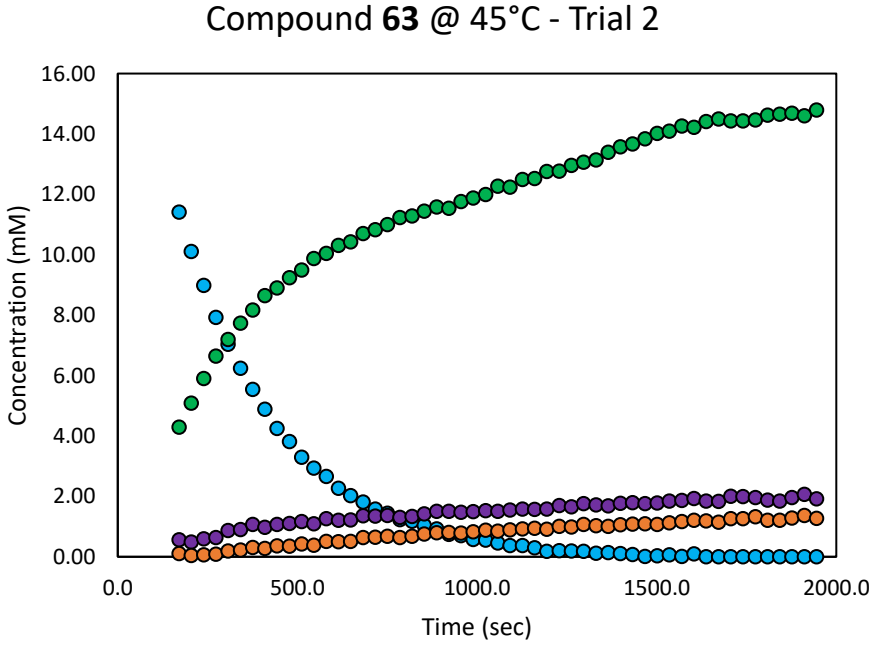

Compound 63 Kinetics Spectra

45°C – Trial 3

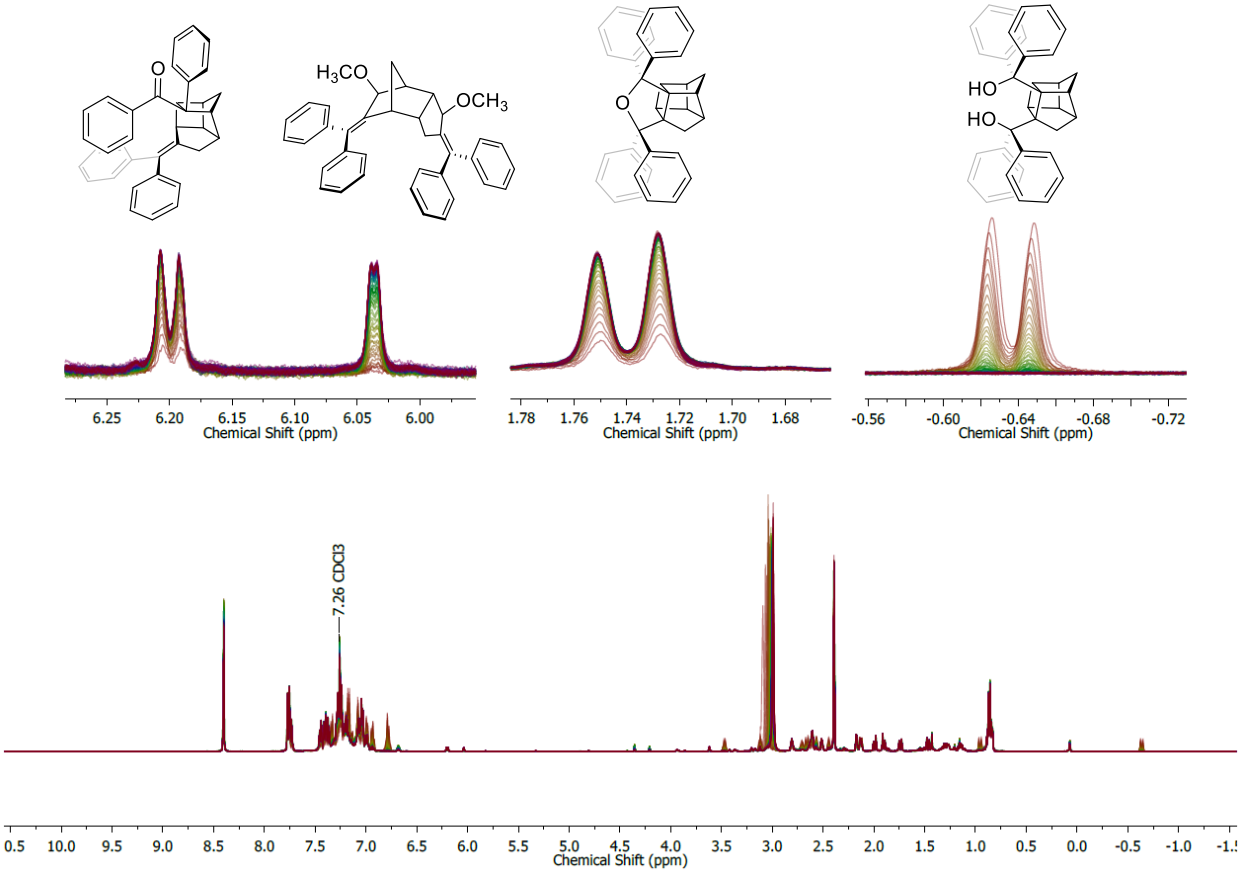

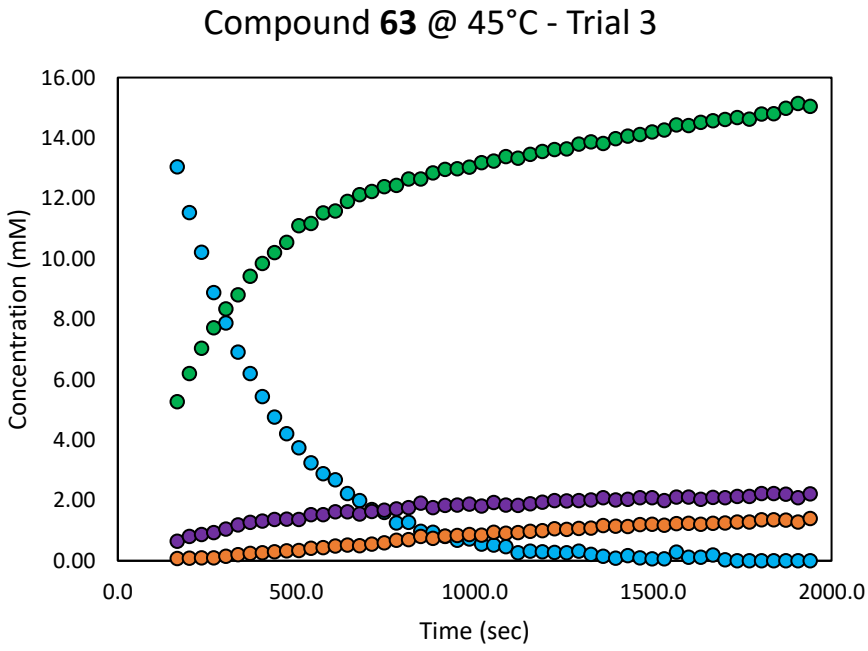

Compound 63 Kinetics Spectra

52°C – Trial 1

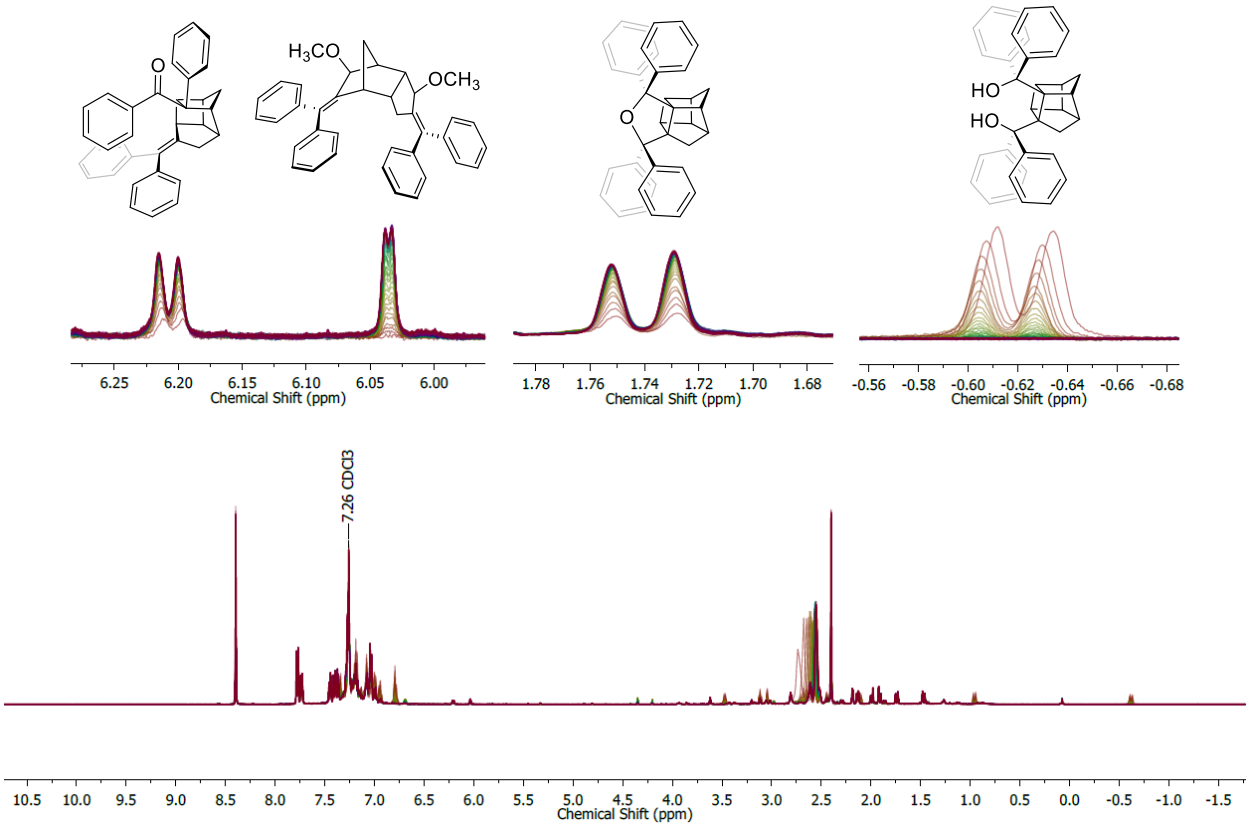

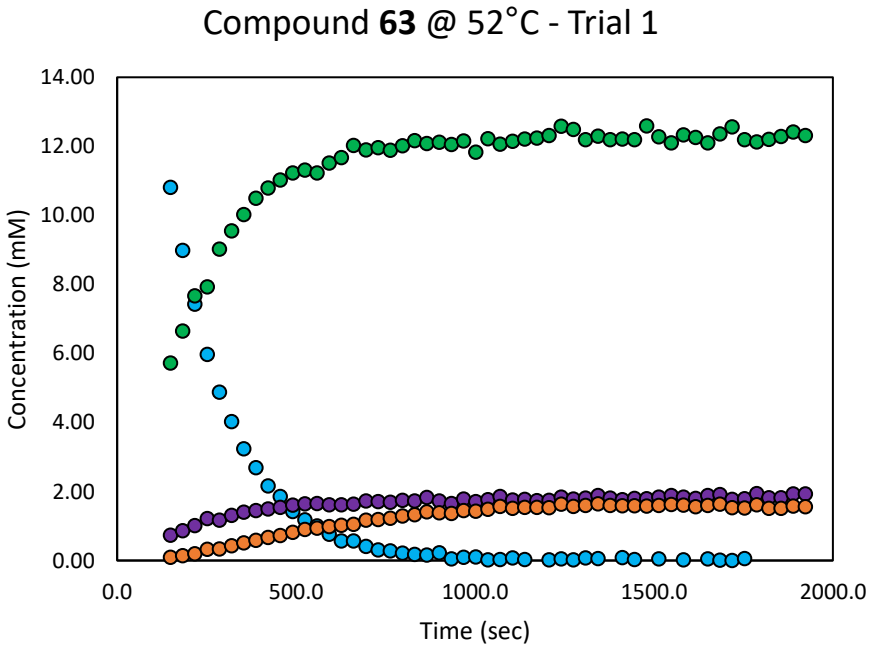

Compound 63 Kinetics Spectra

52°C – Trial 2

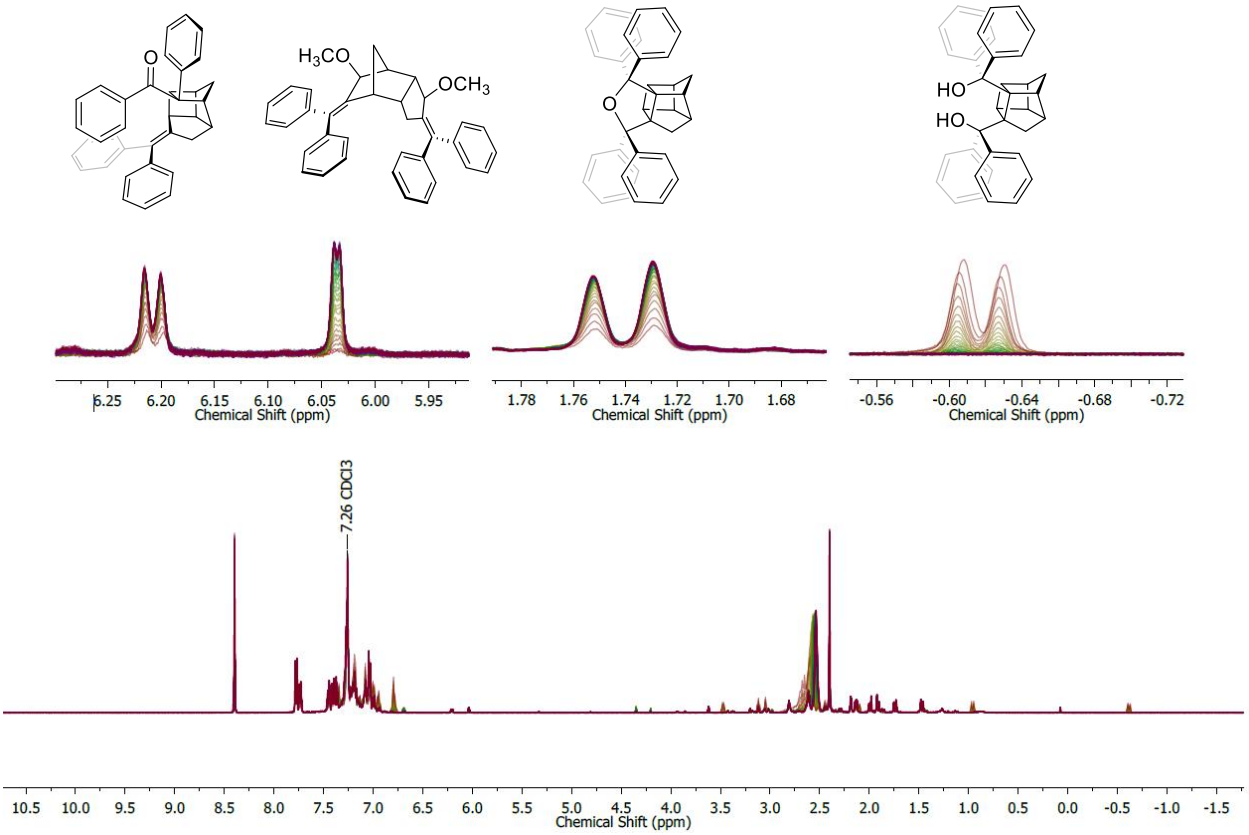

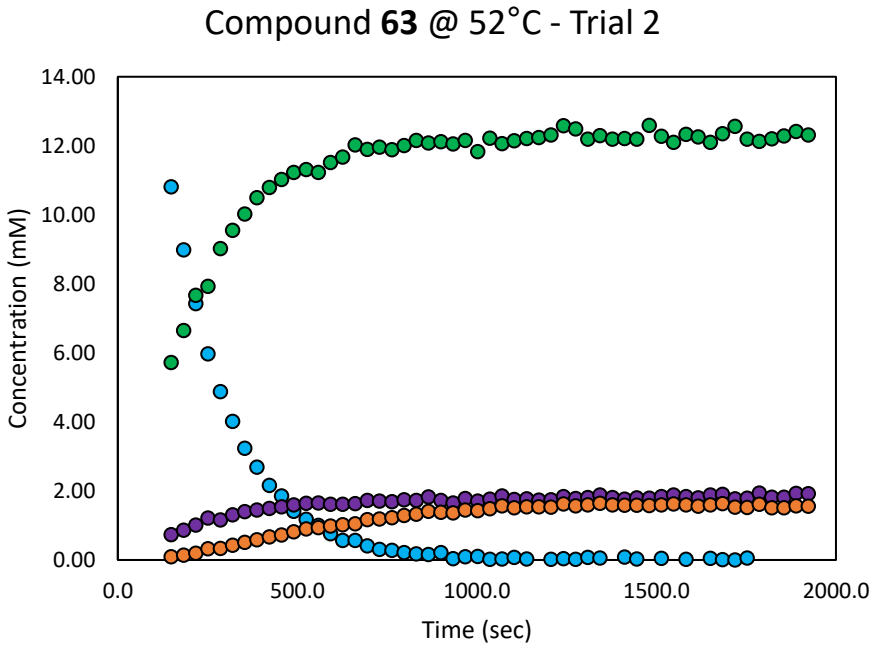

Compound 63 Kinetics Spectra

52°C – Trial 3

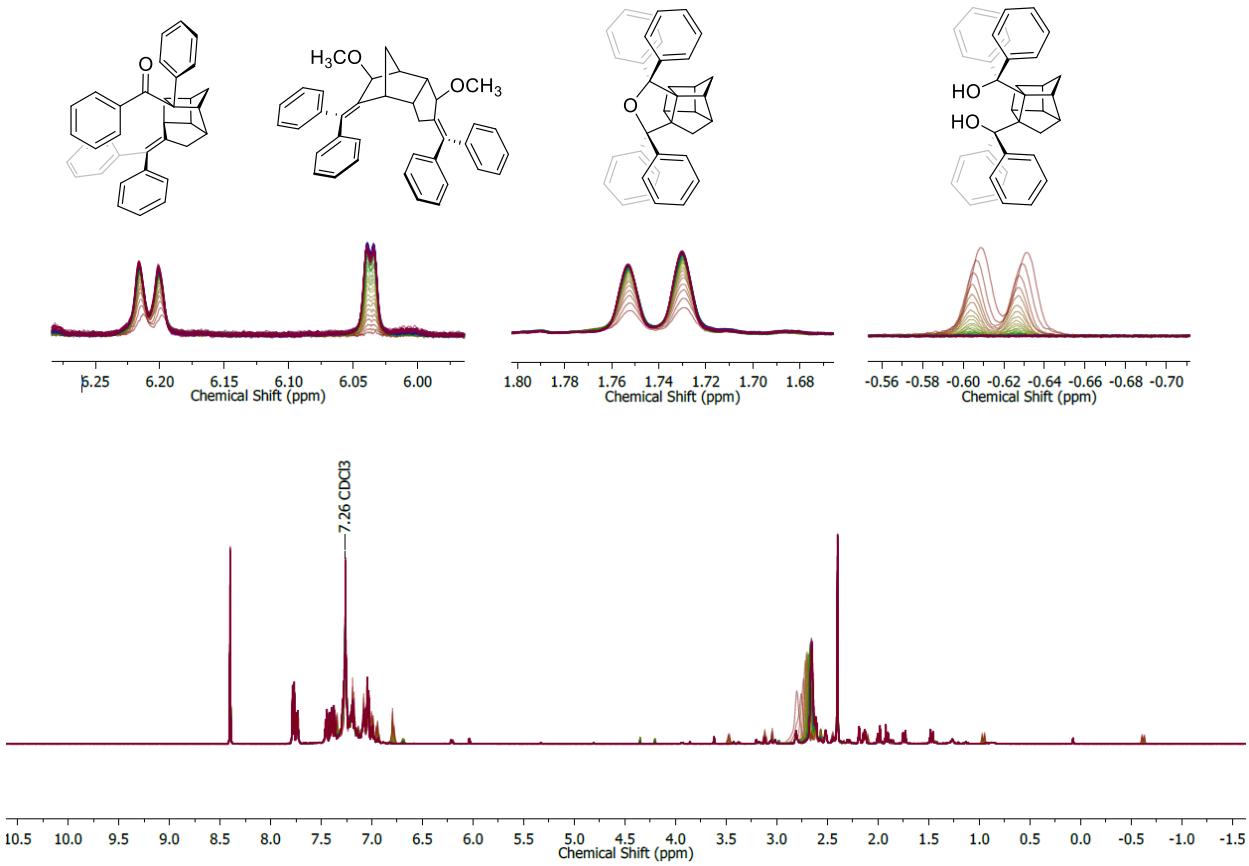

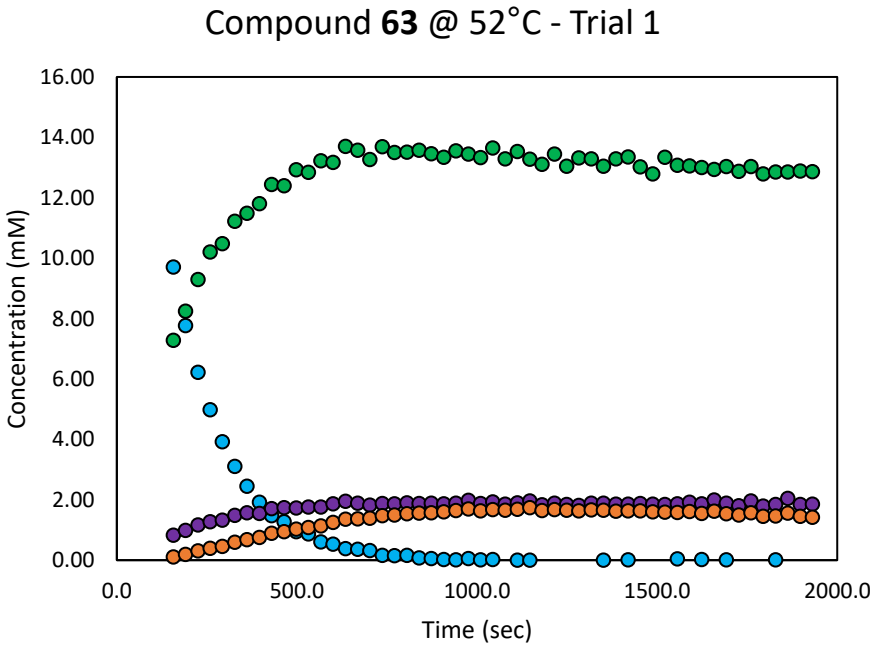

Compound 66 Kinetics Spectra

25°C – Trial 1

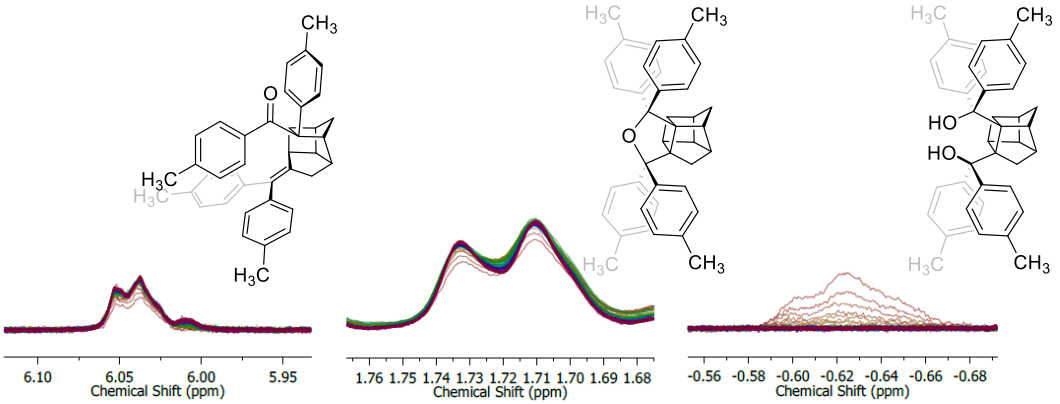

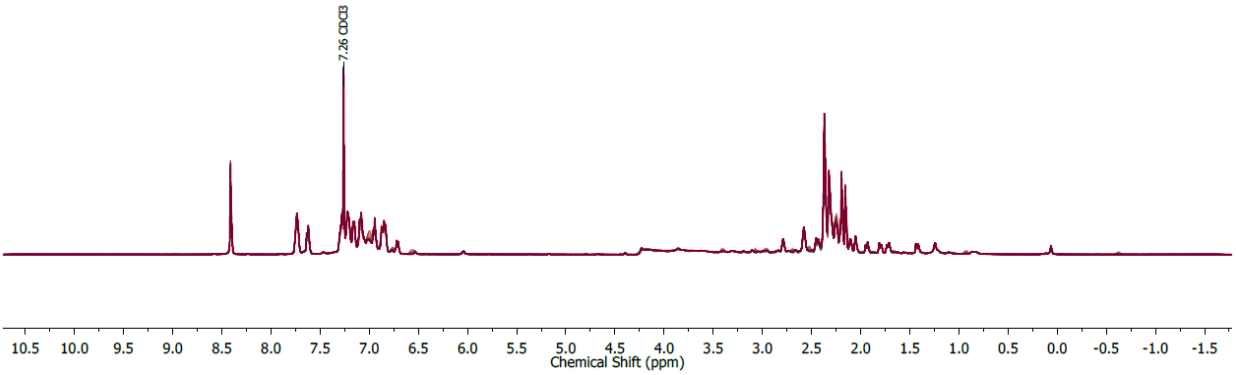

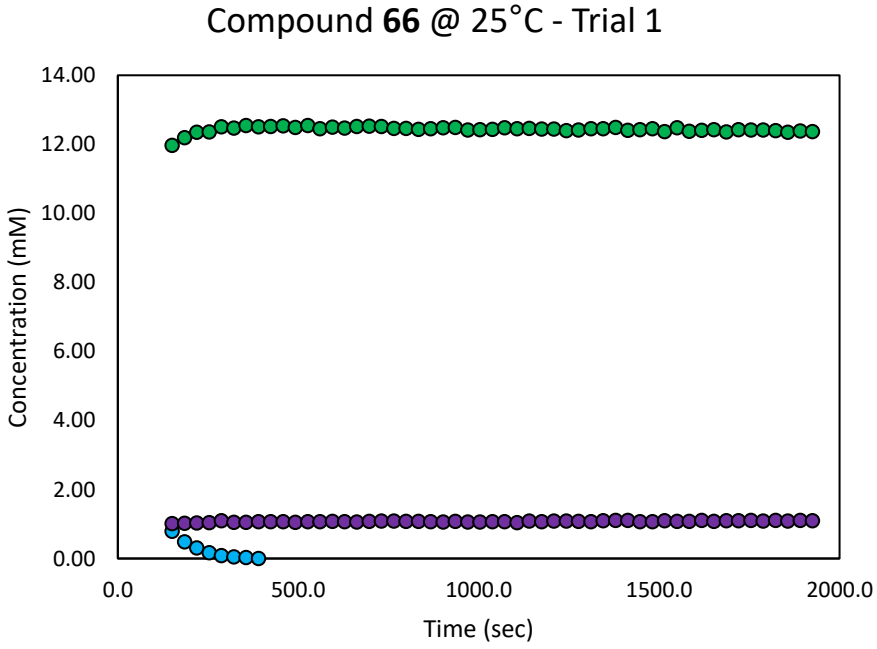

Compound 66 Kinetics Spectra

25°C – Trial 2

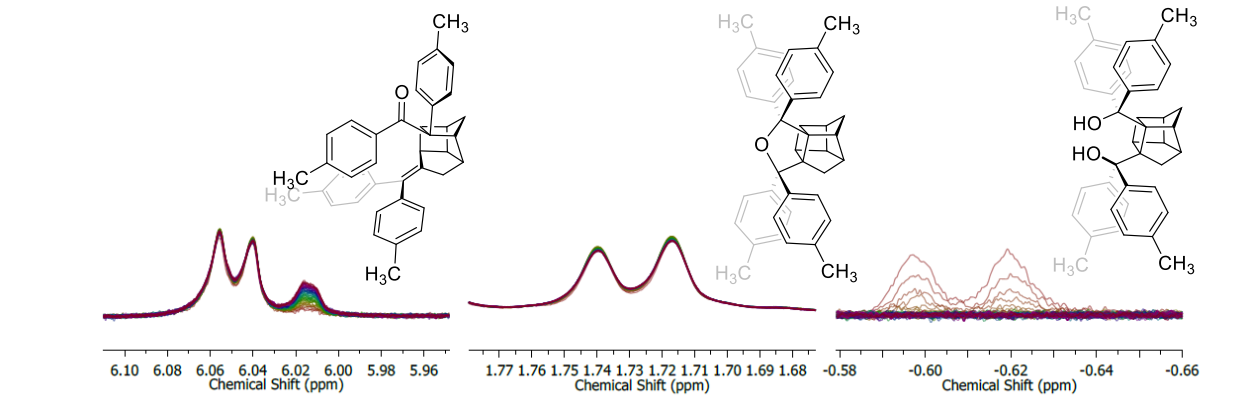

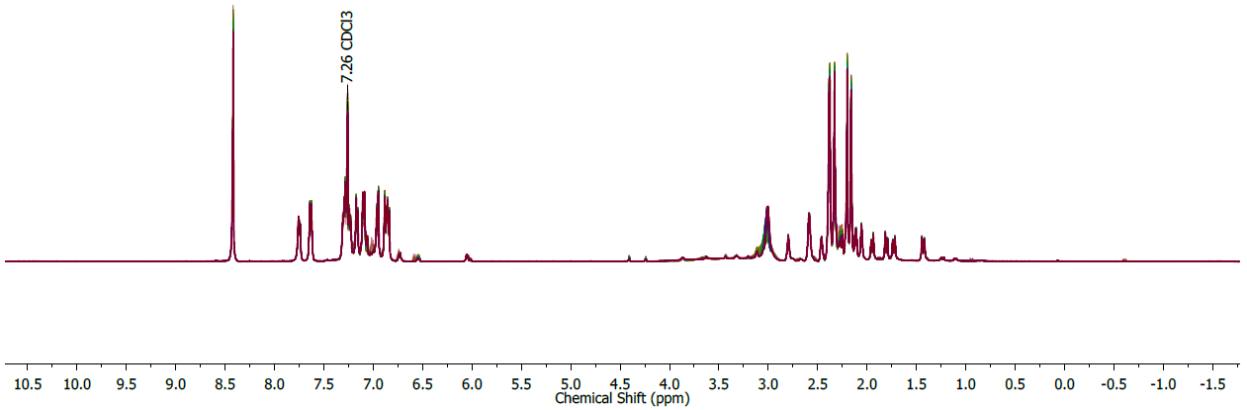

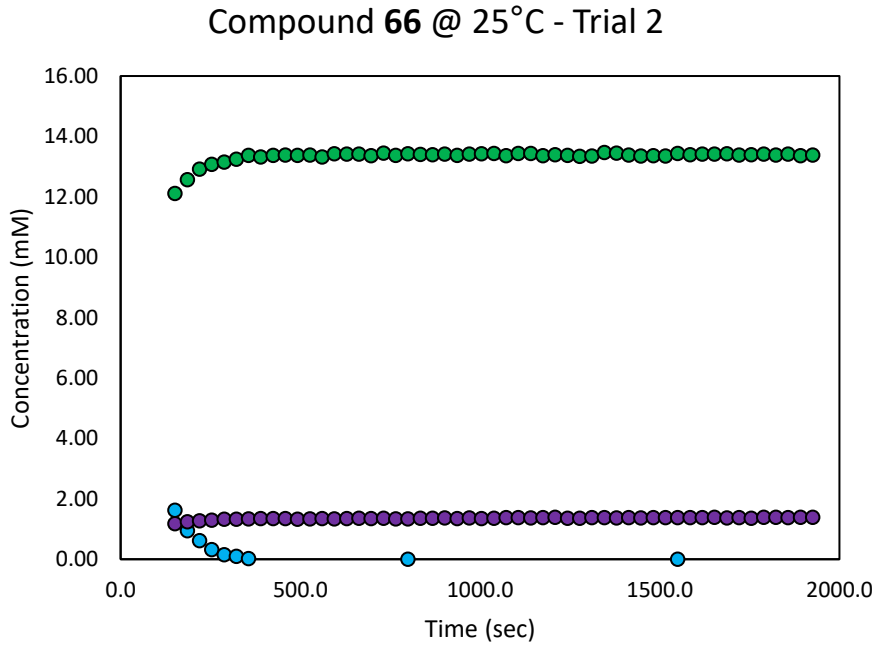

Compound 66 Kinetics Spectra

25°C – Trial 3

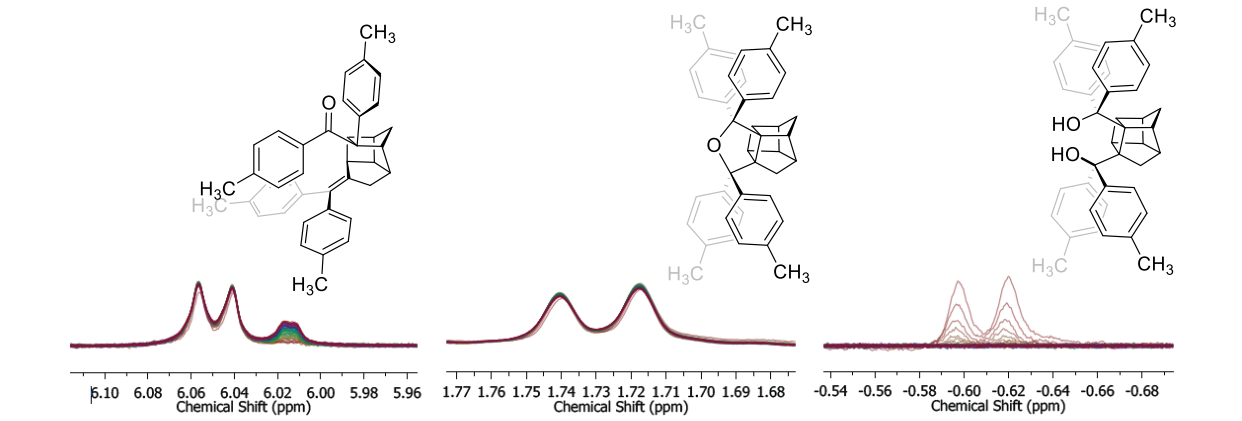

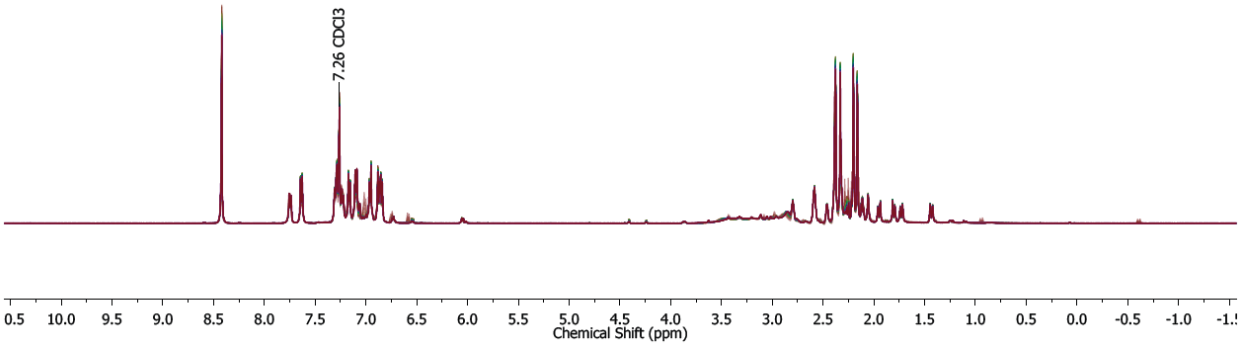

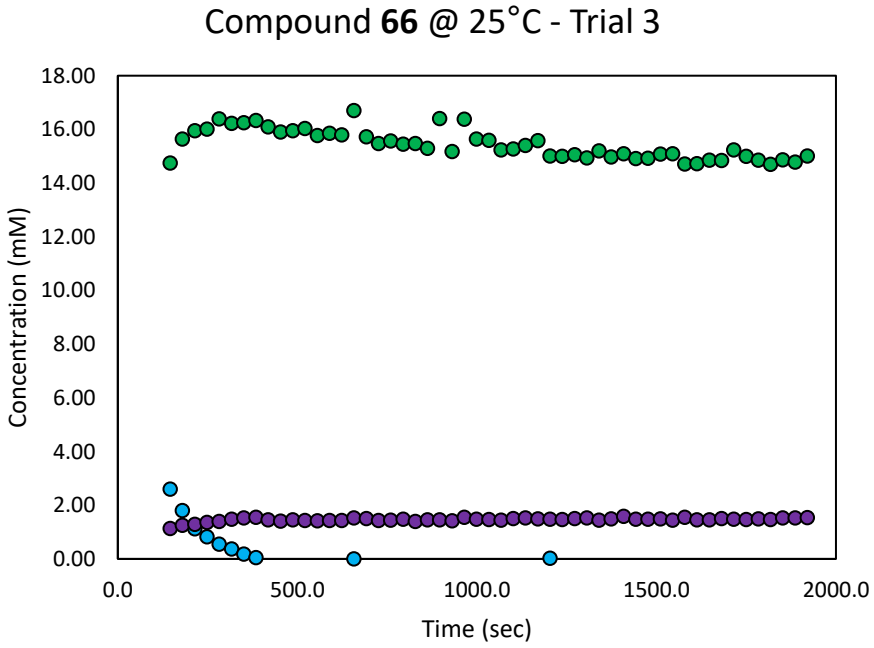

Compound 66 Kinetics Spectra

35°C – Trial 1

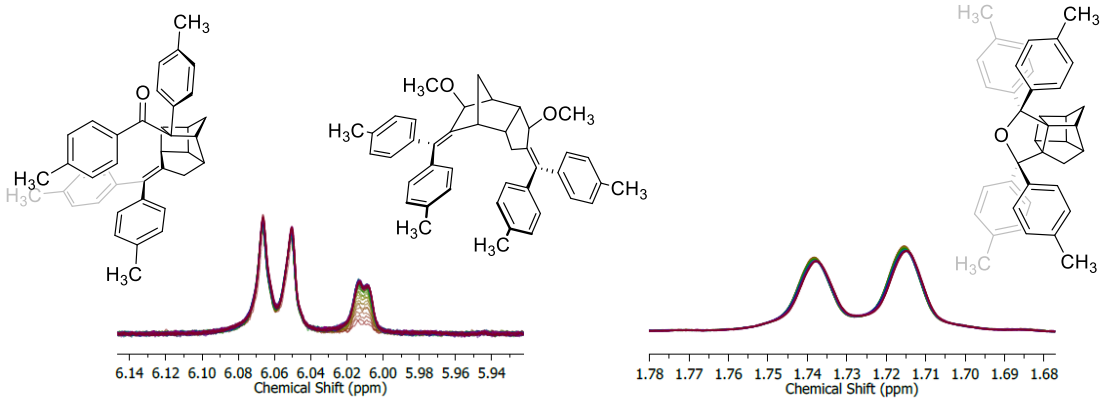

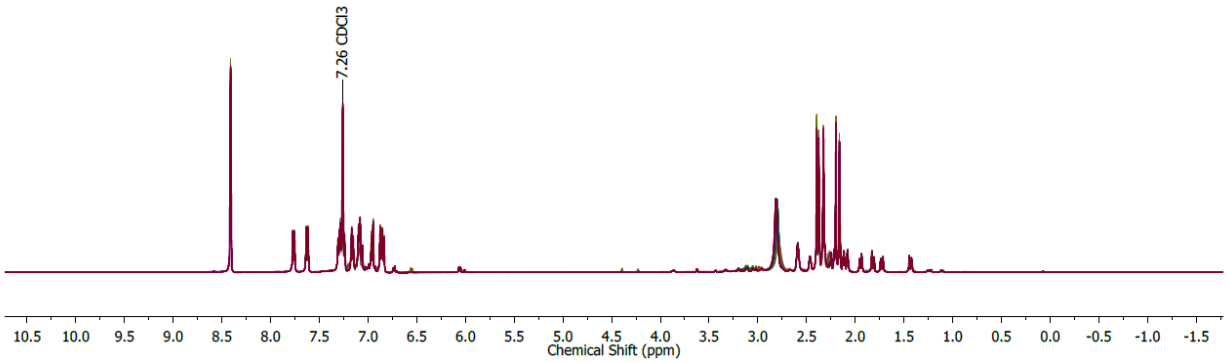

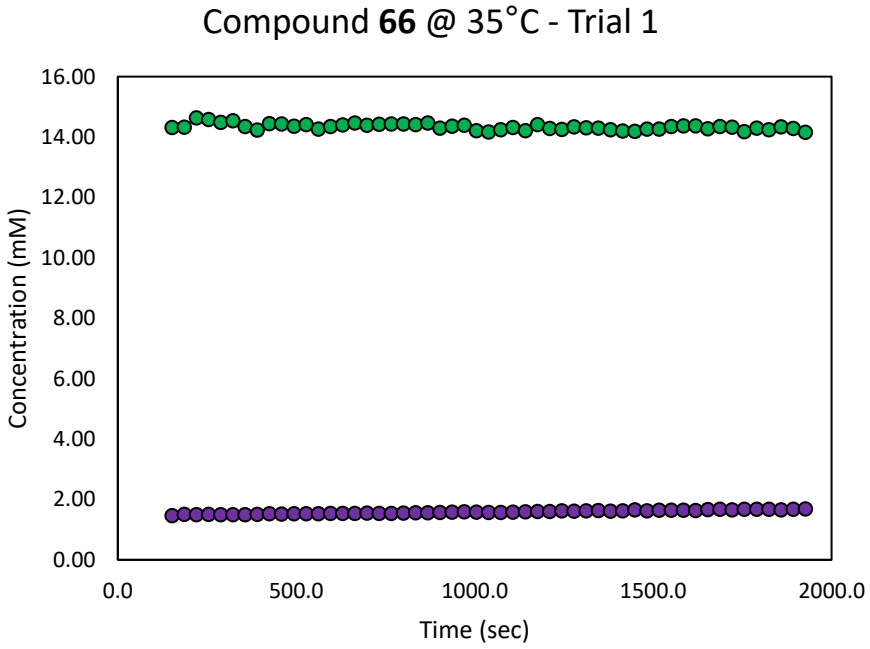

Compound 66 Kinetics Spectra

35°C – Trial 2

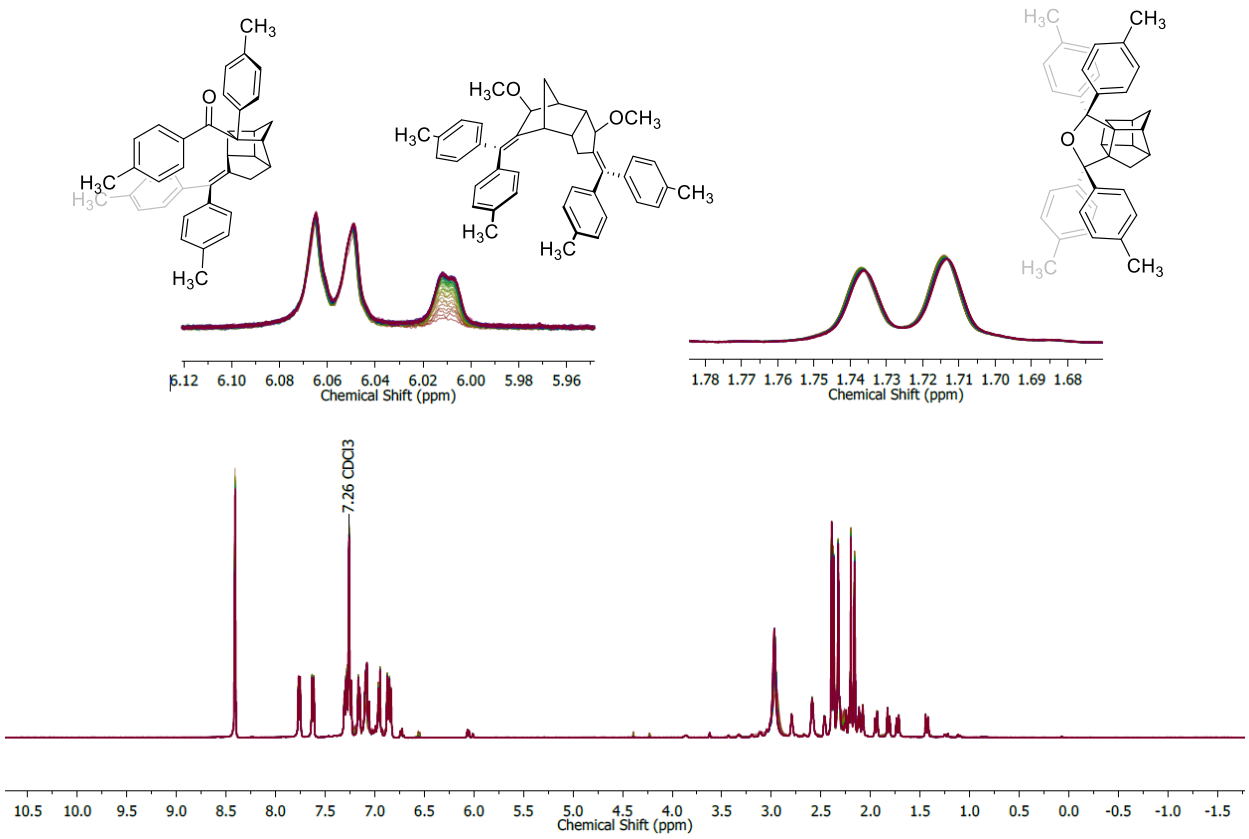

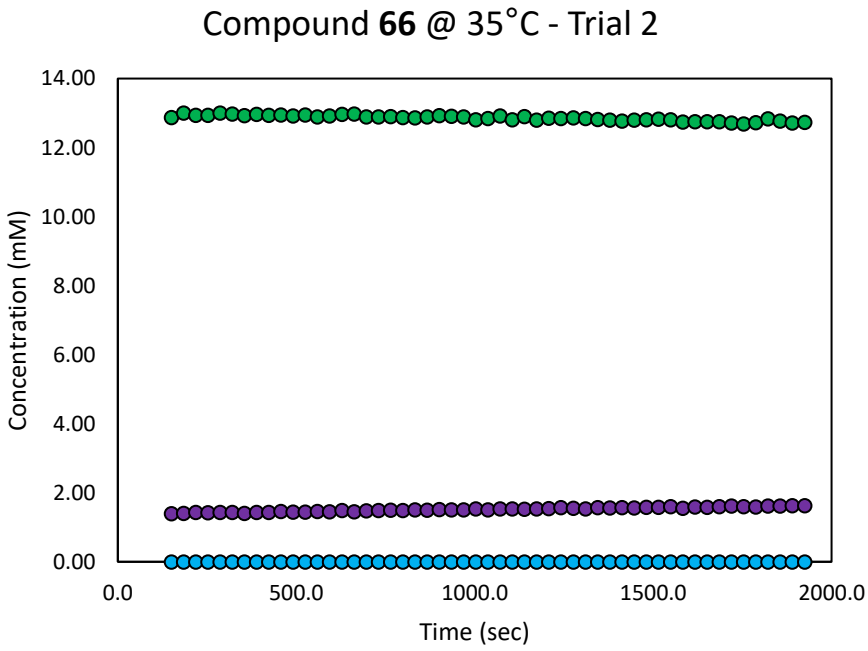

Compound 66 Kinetics Spectra

35°C – Trial 3

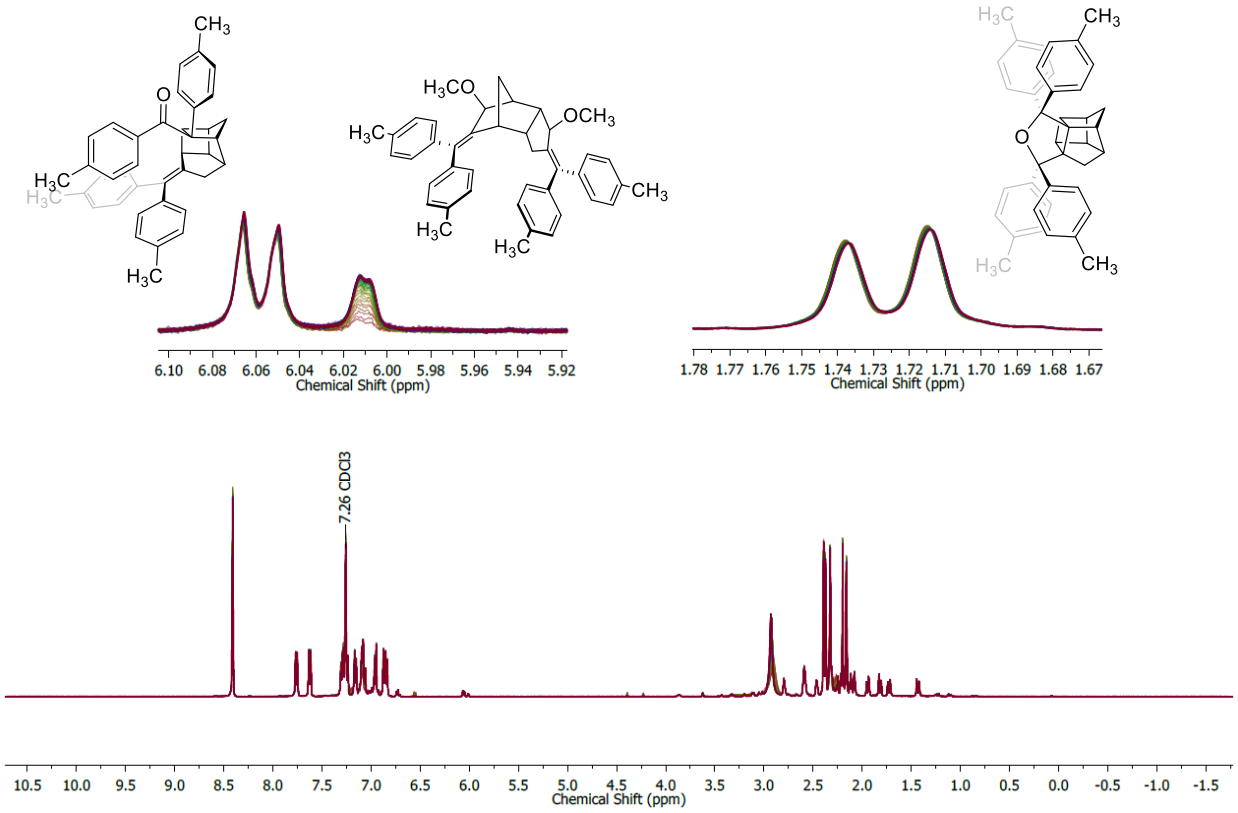

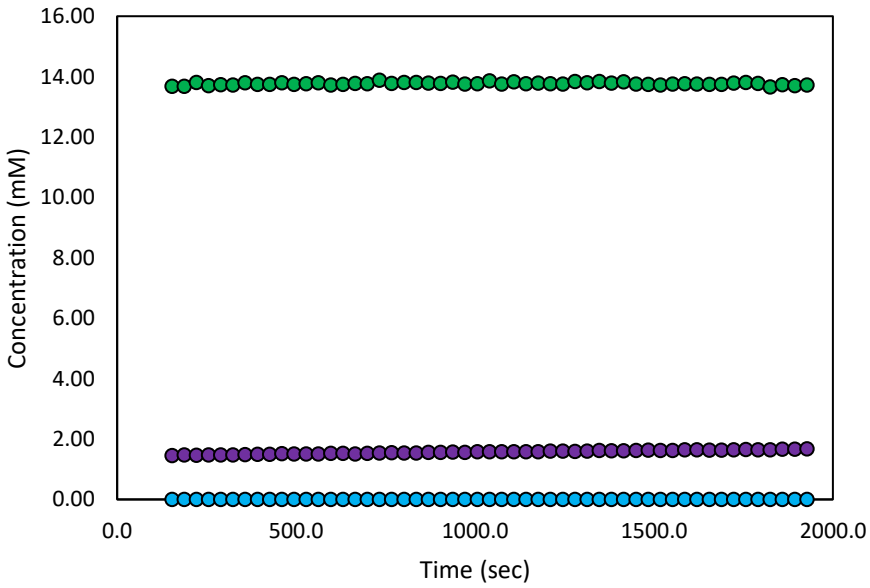

Compound 66 Kinetics Spectra

45°C – Trial 1

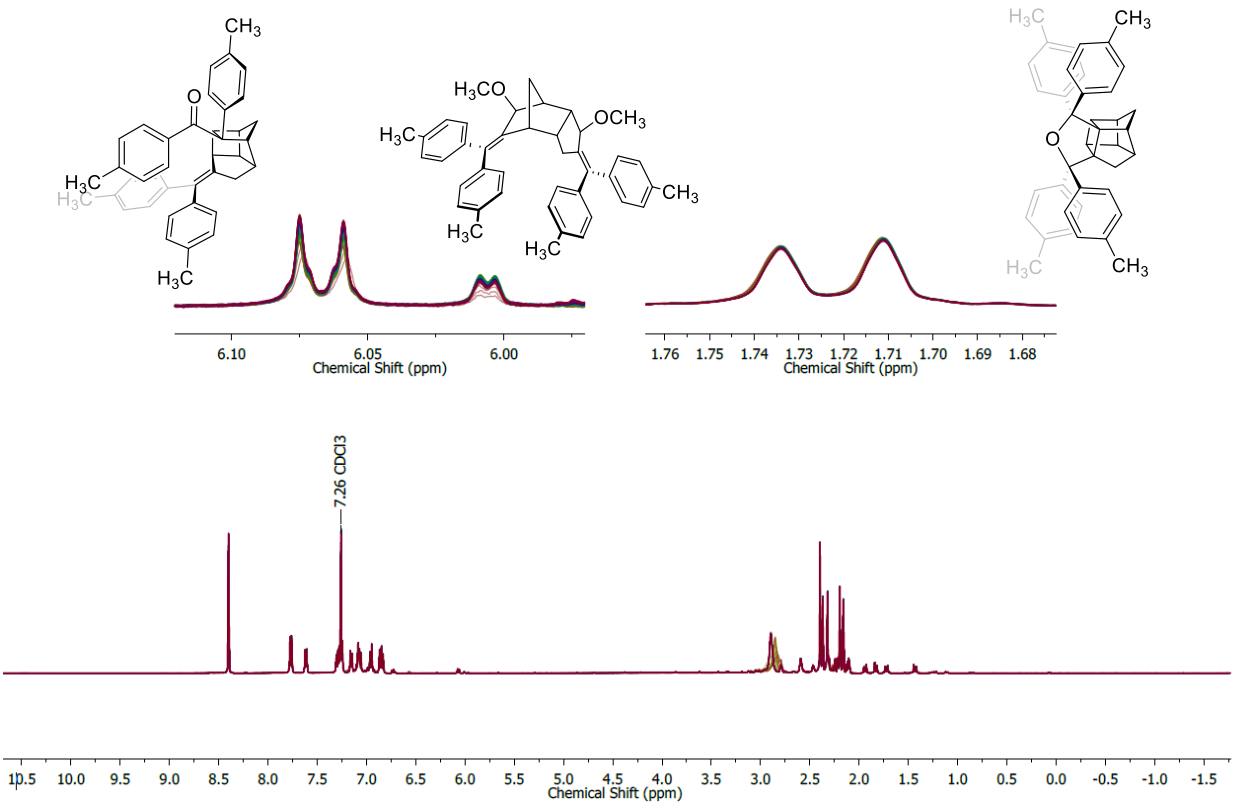

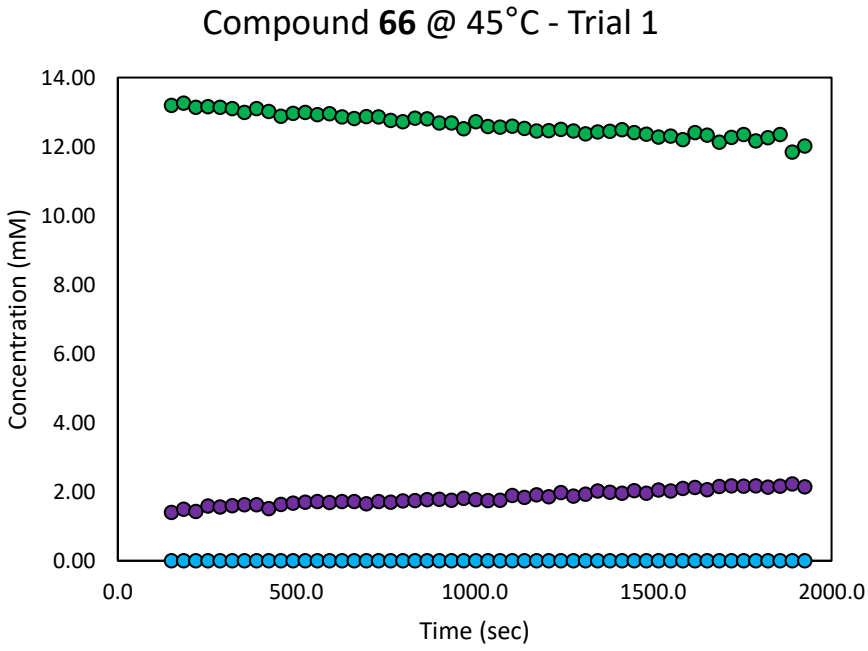

Compound 66 Kinetics Spectra

45°C – Trial 2

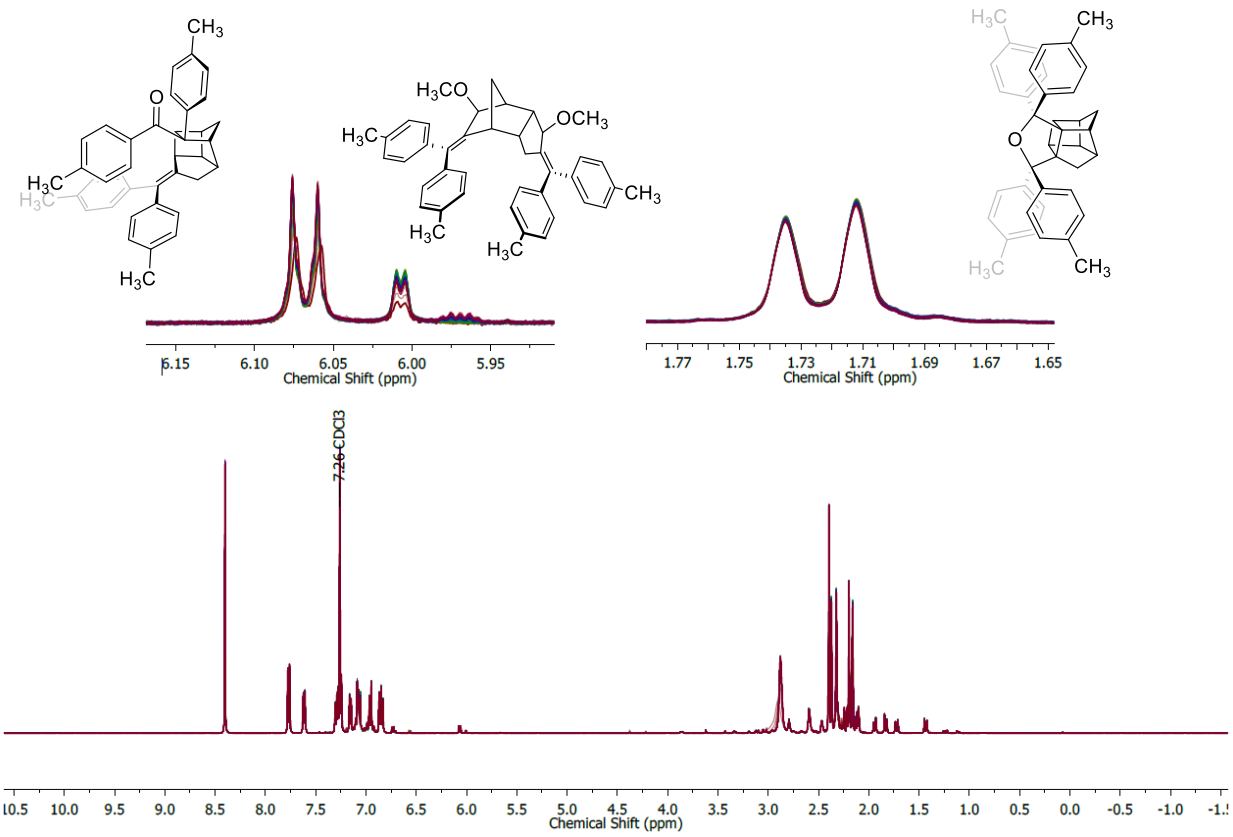

Compound **66** @ 45°C - Trial 2

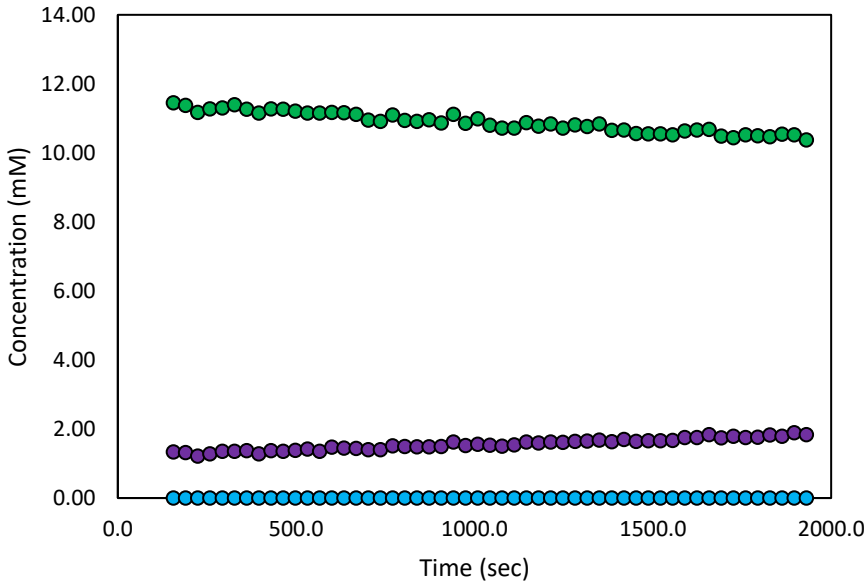

Compound 66 Kinetics Spectra

45°C – Trial 3

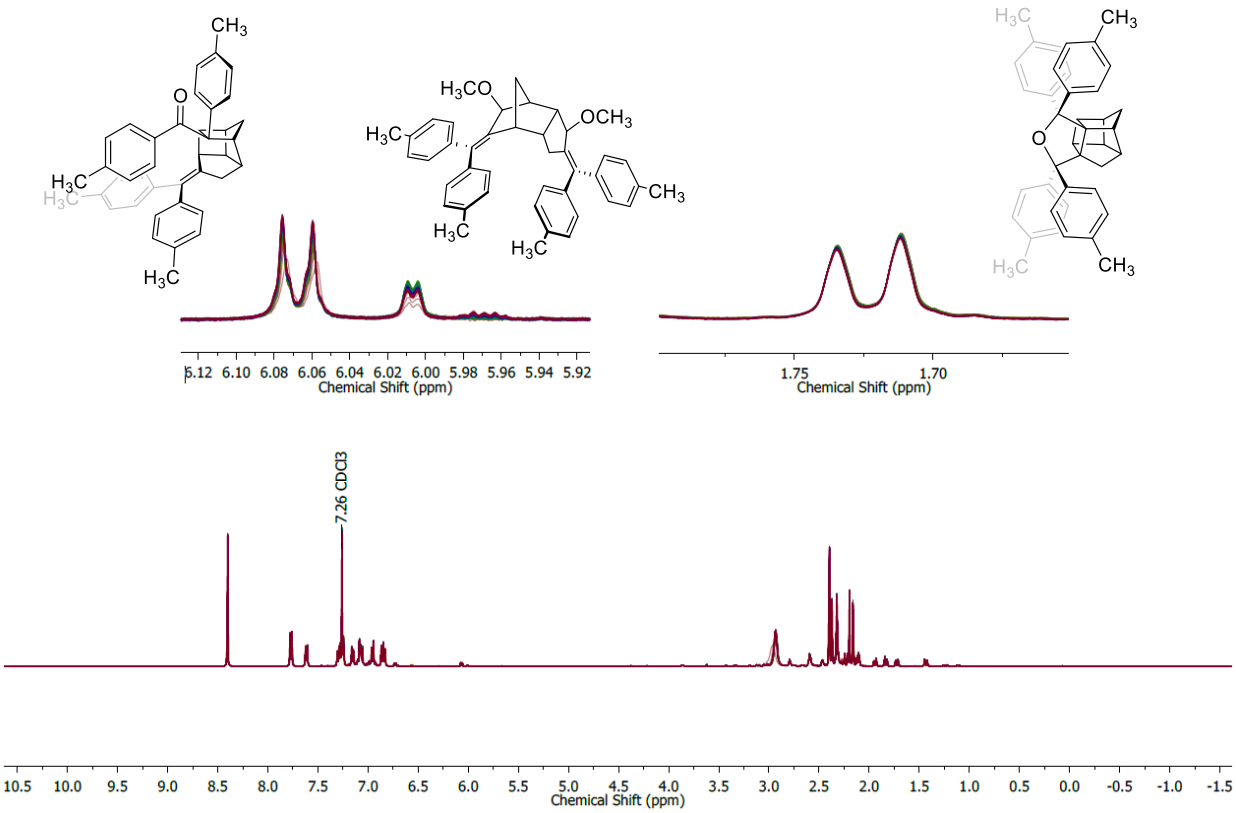

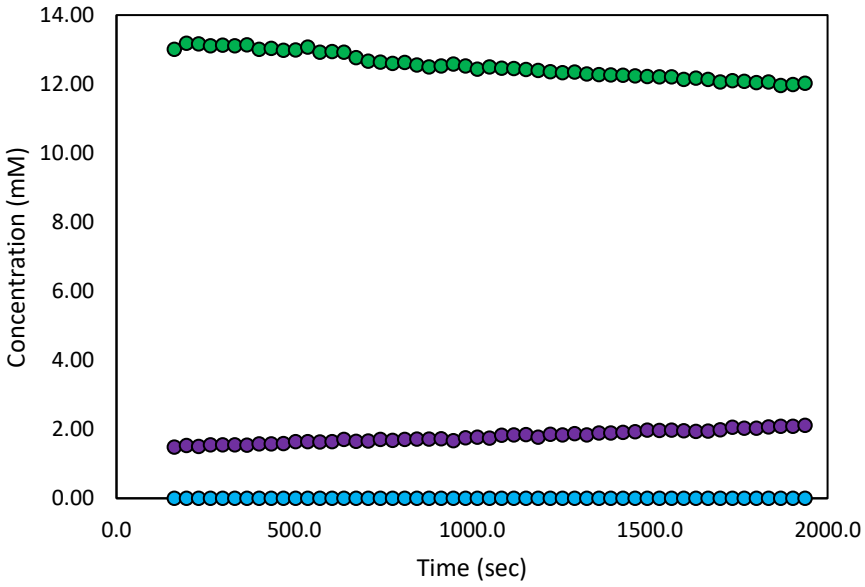

Compound 66 Kinetics Spectra

52°C – Trial 1

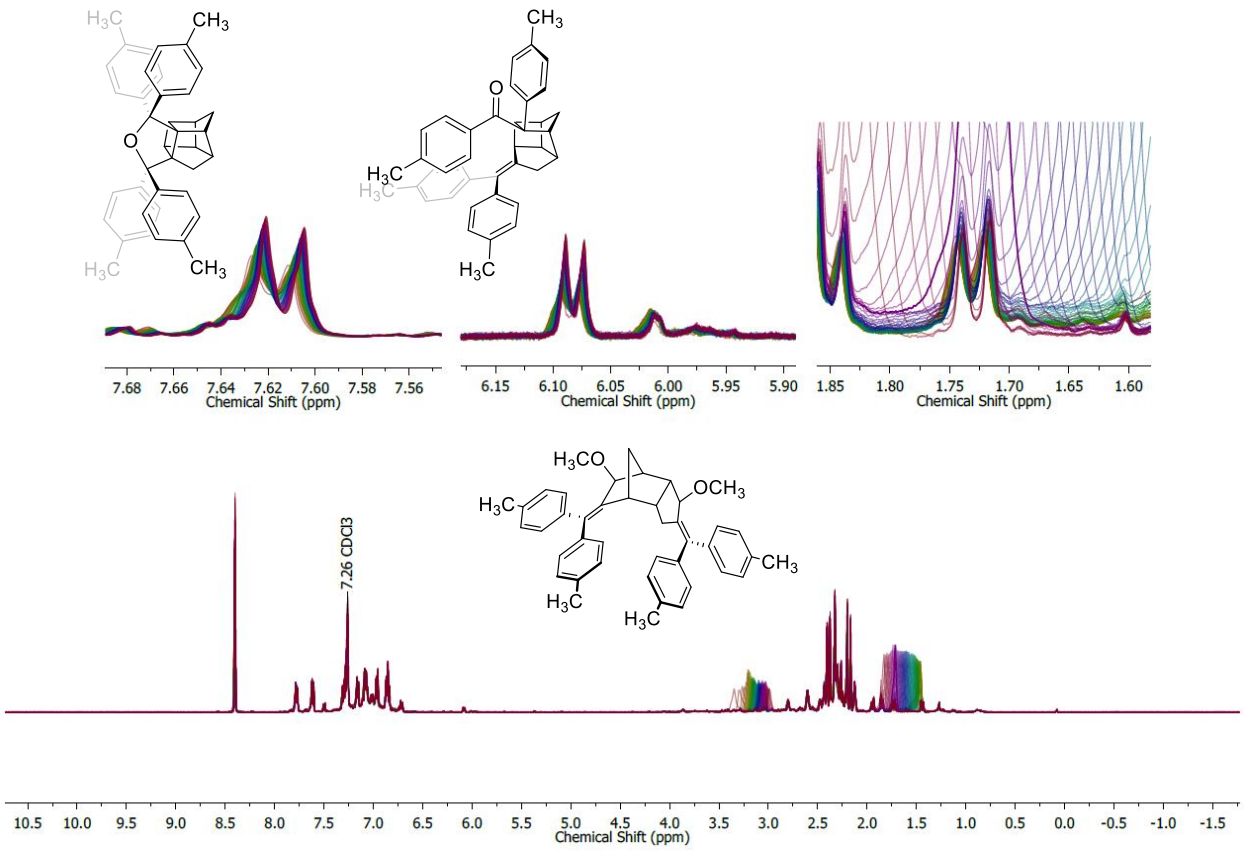

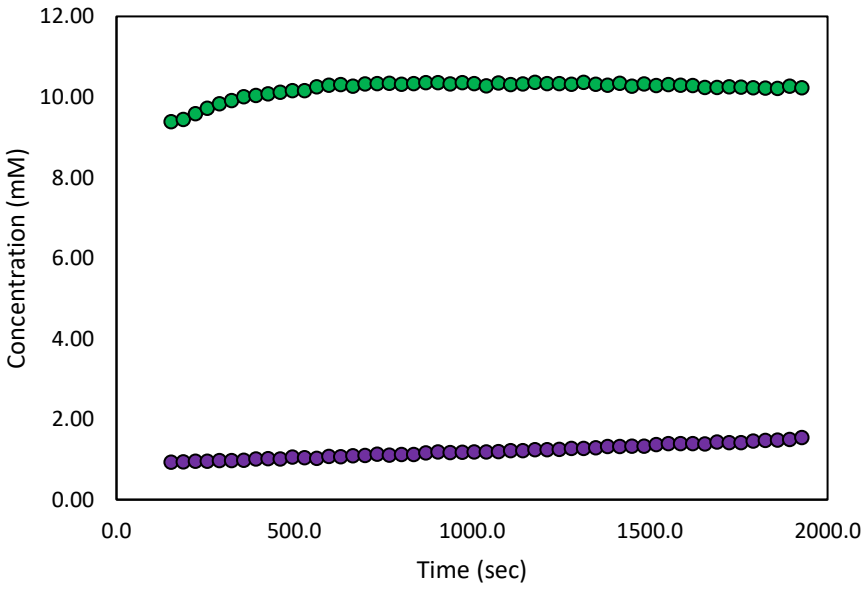

Compound 66 Kinetics Spectra

52°C – Trial 2

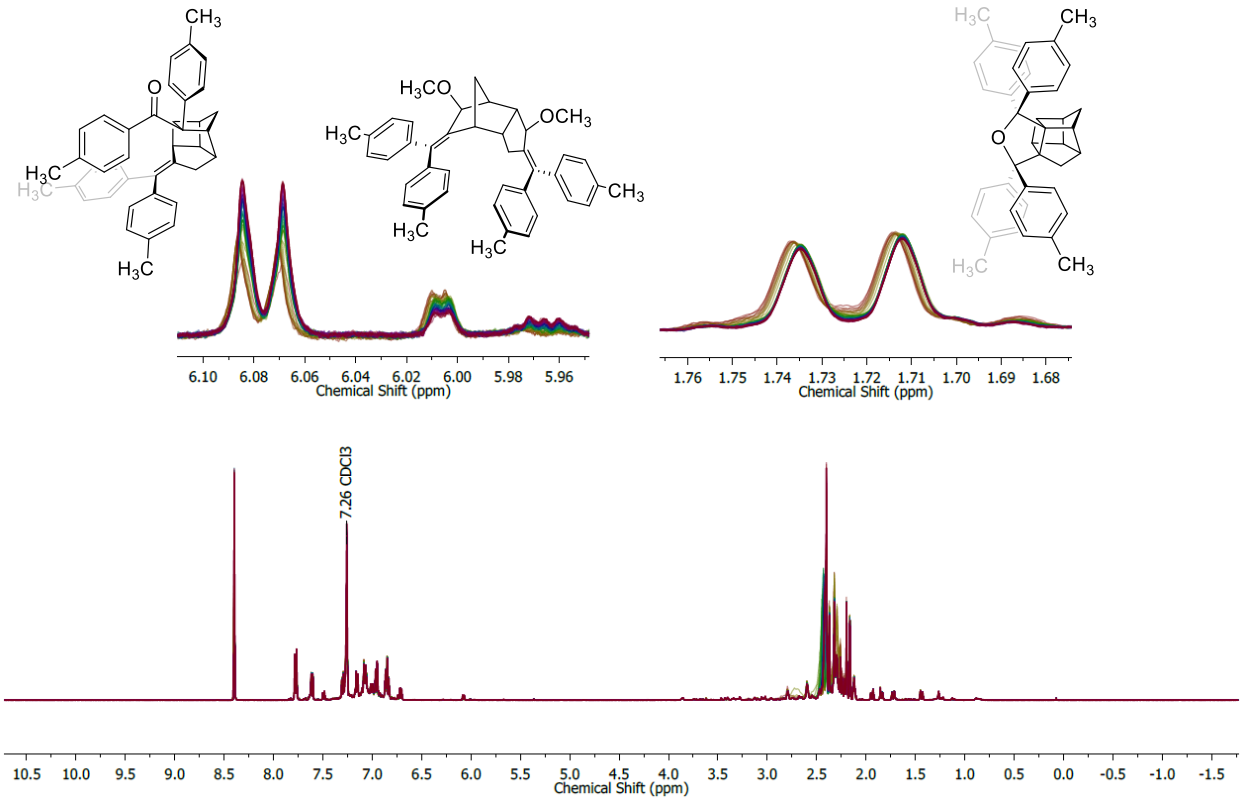

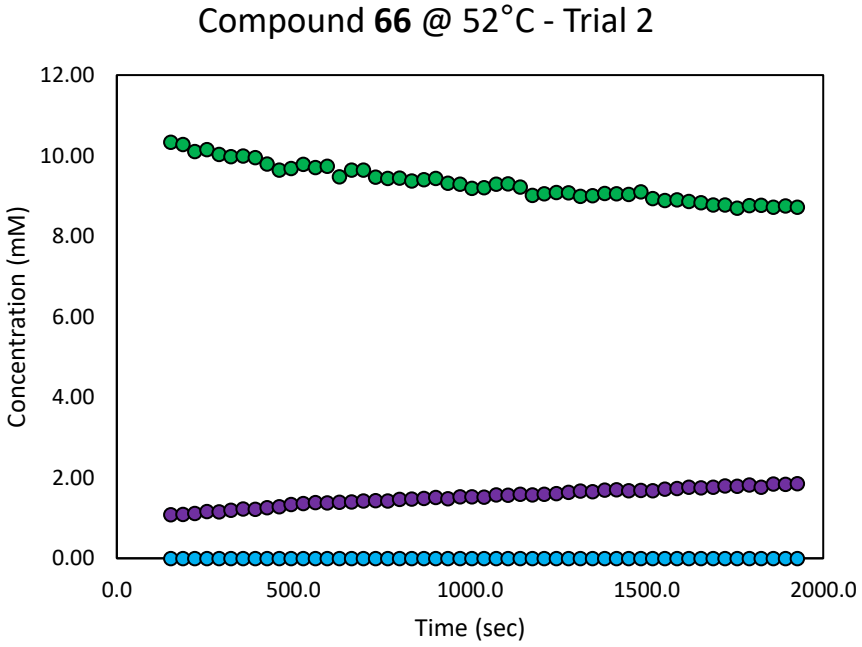

Compound 66 Kinetics Spectra

52°C – Trial 3

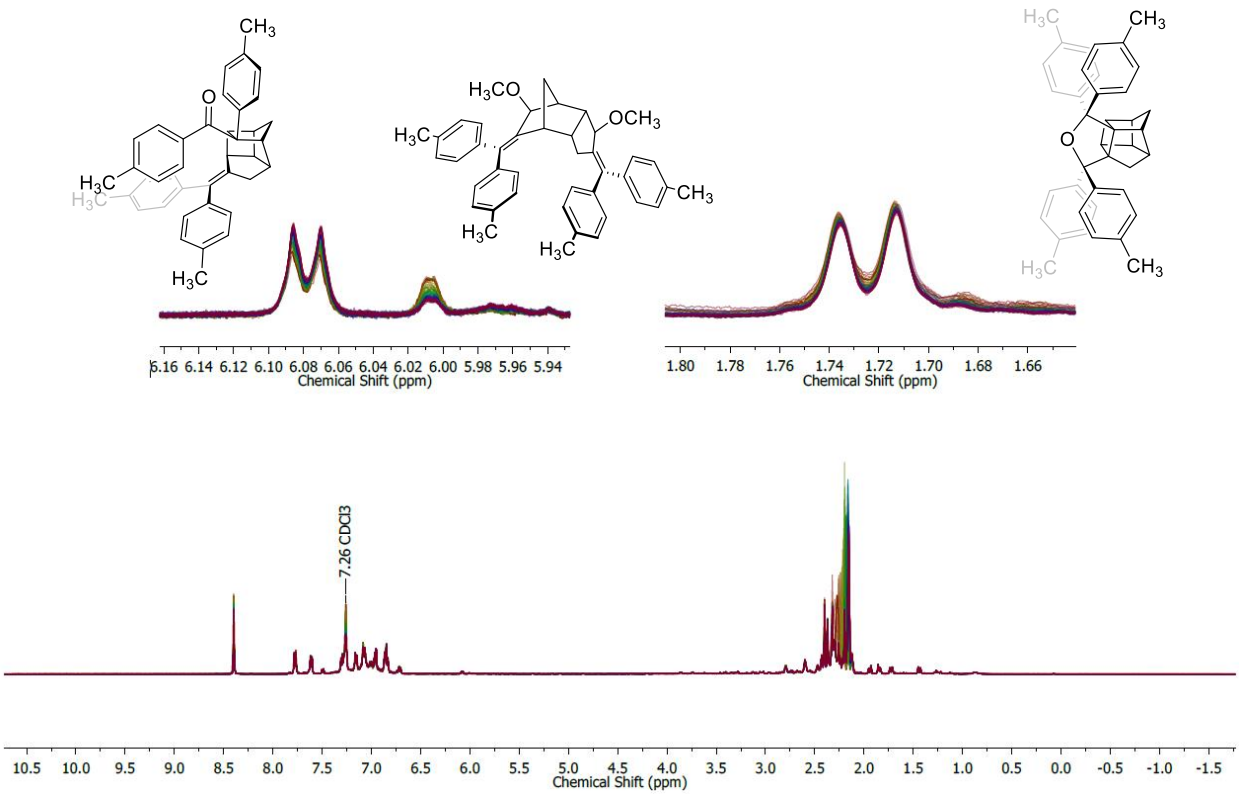

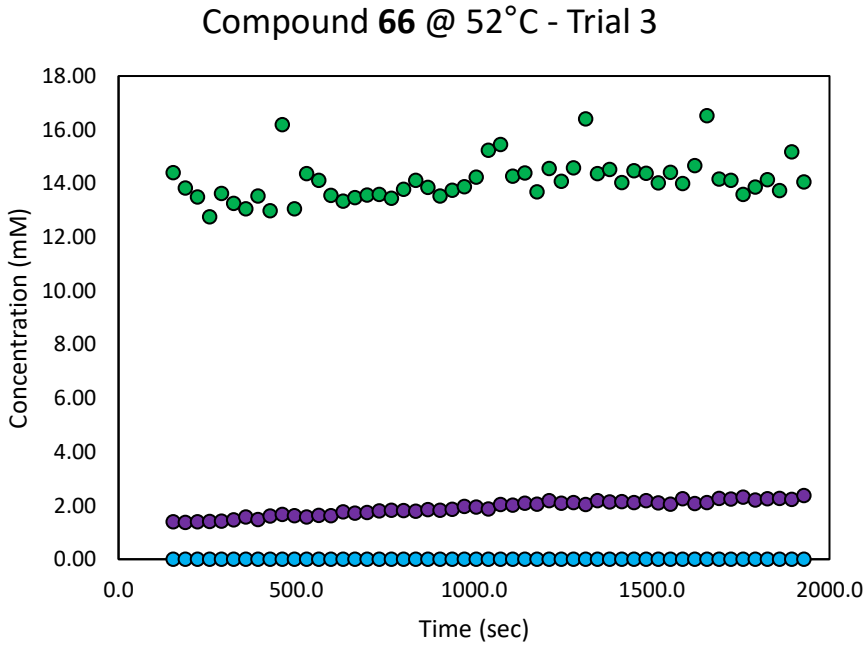

Compound 71 Kinetics Spectra

25°C – Trial 1

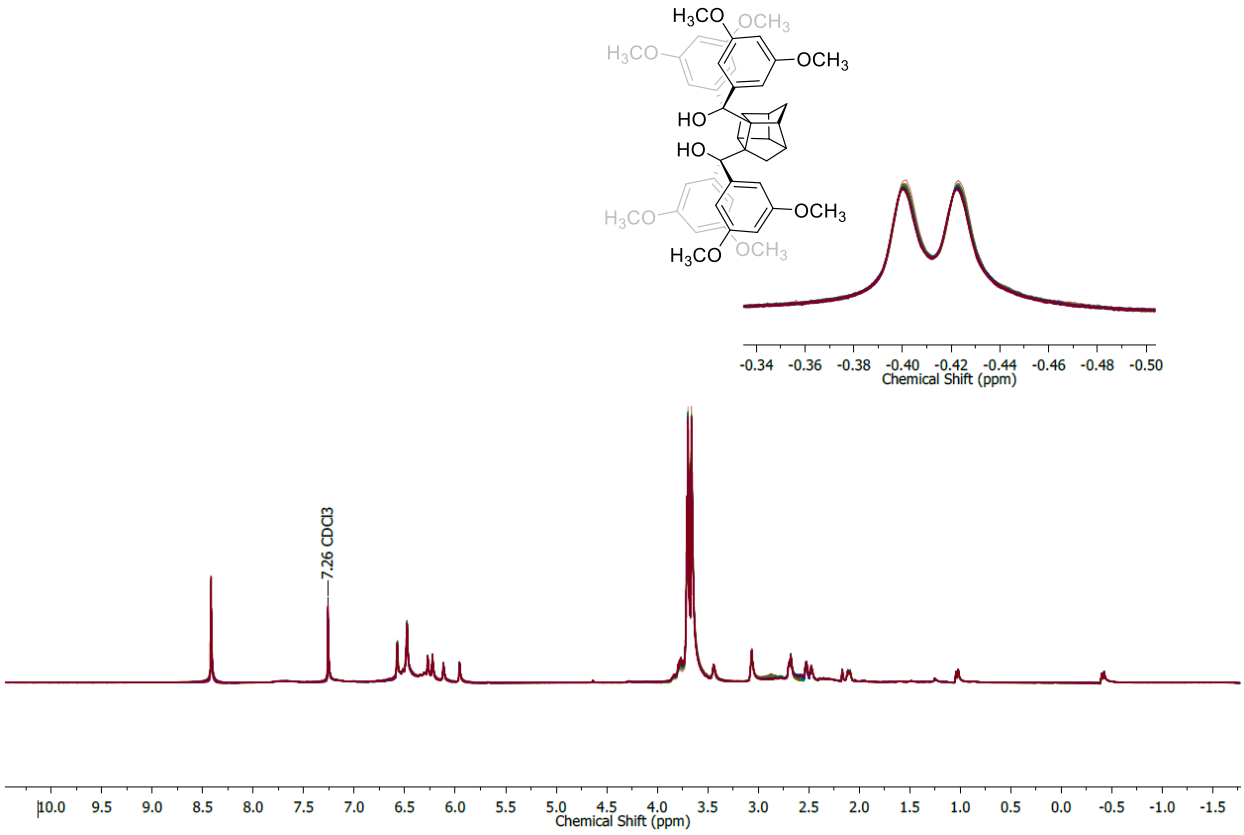

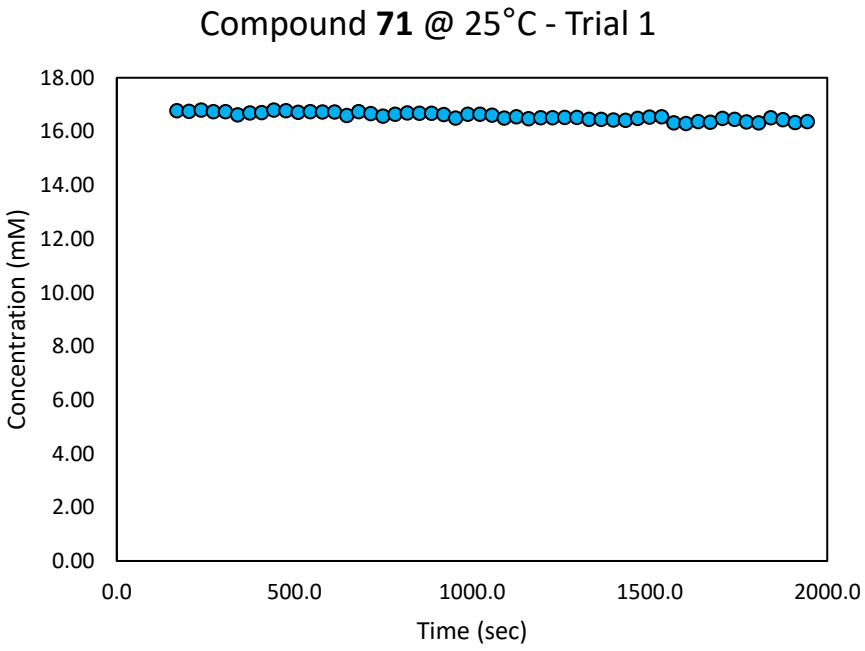

Compound 71 Kinetics Spectra

25°C – Trial 2

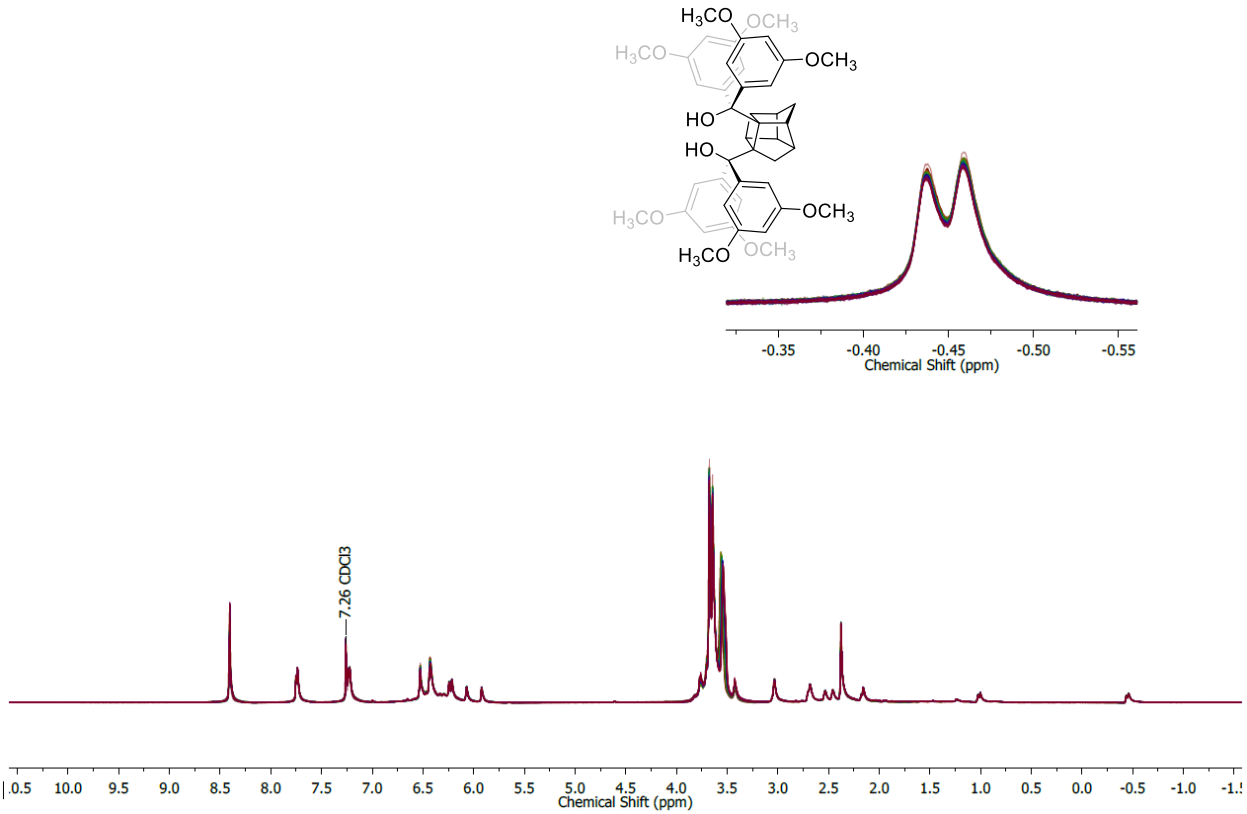

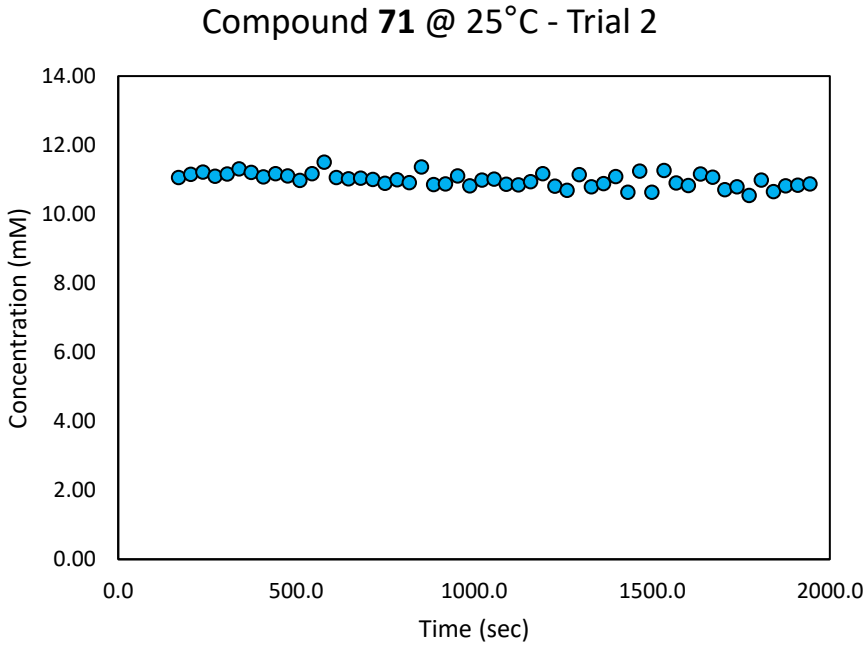

Compound 71 Kinetics Spectra

25°C – Trial 3

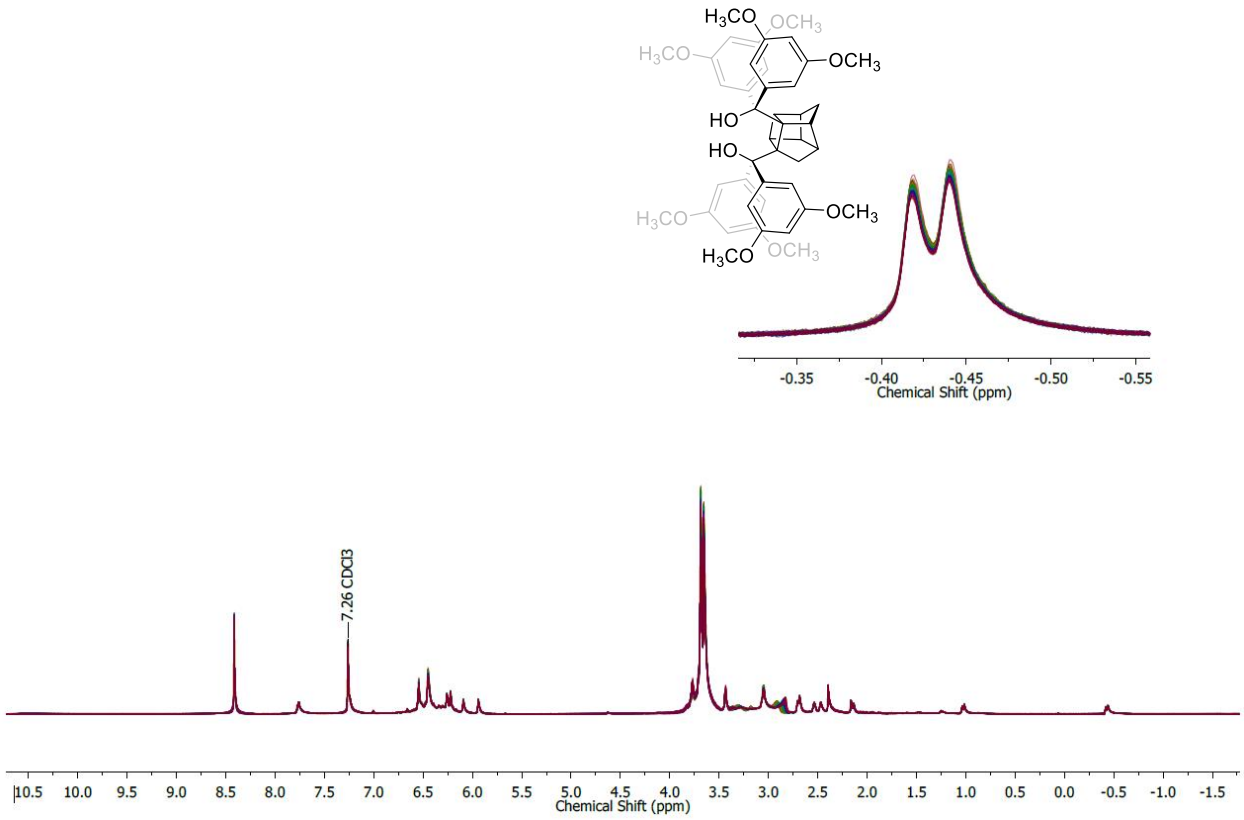

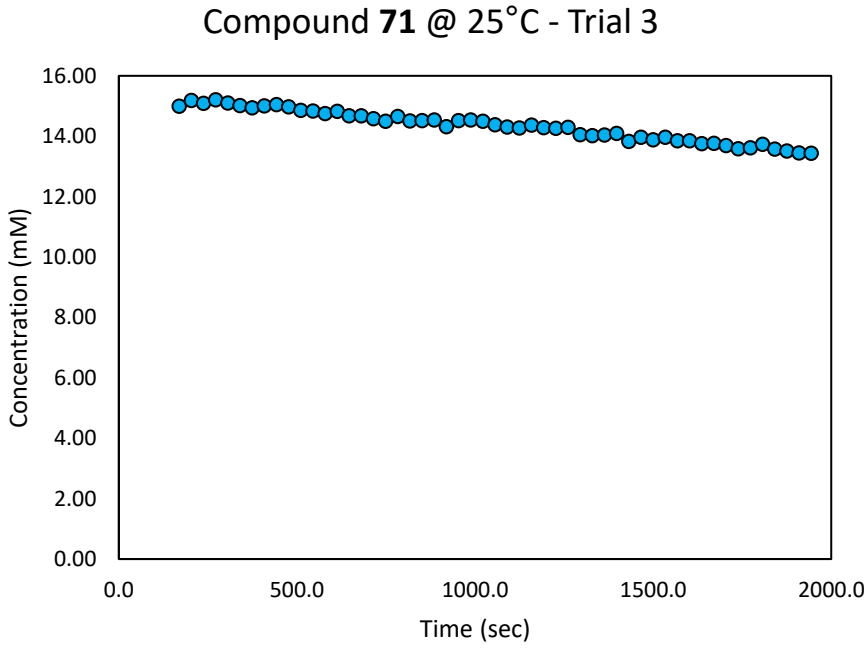

Compound 71 Kinetics Spectra

35°C – Trial 1

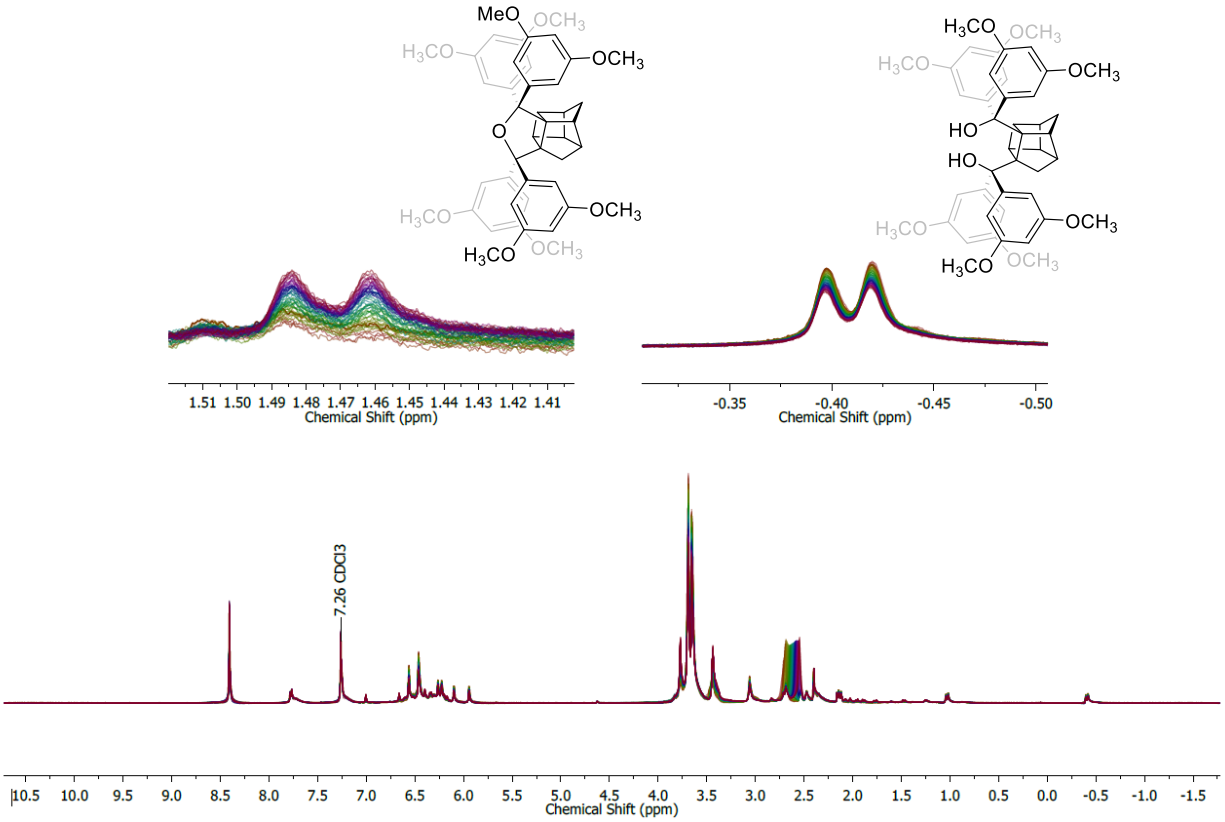

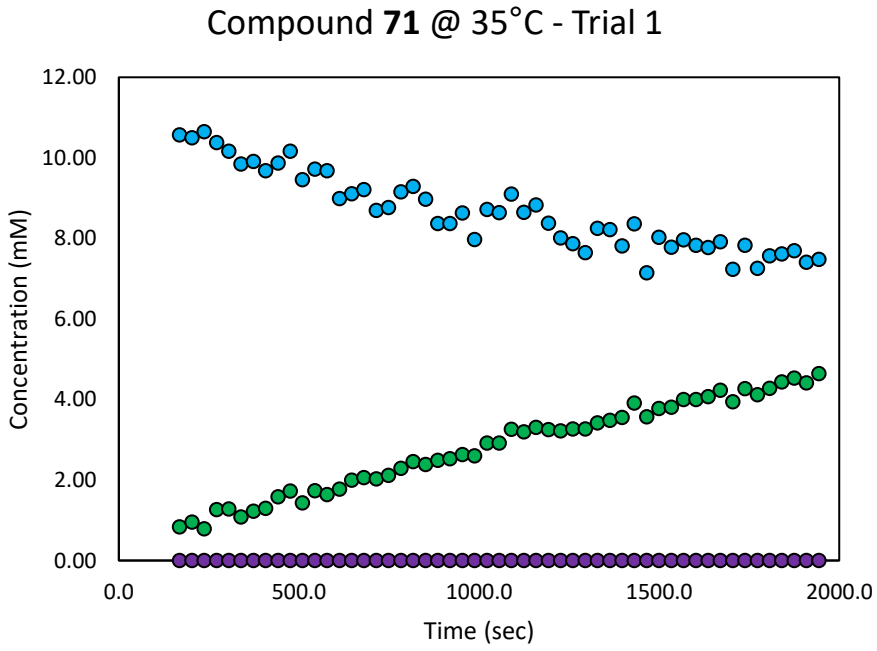

Compound 71 Kinetics Spectra

35°C – Trial 2

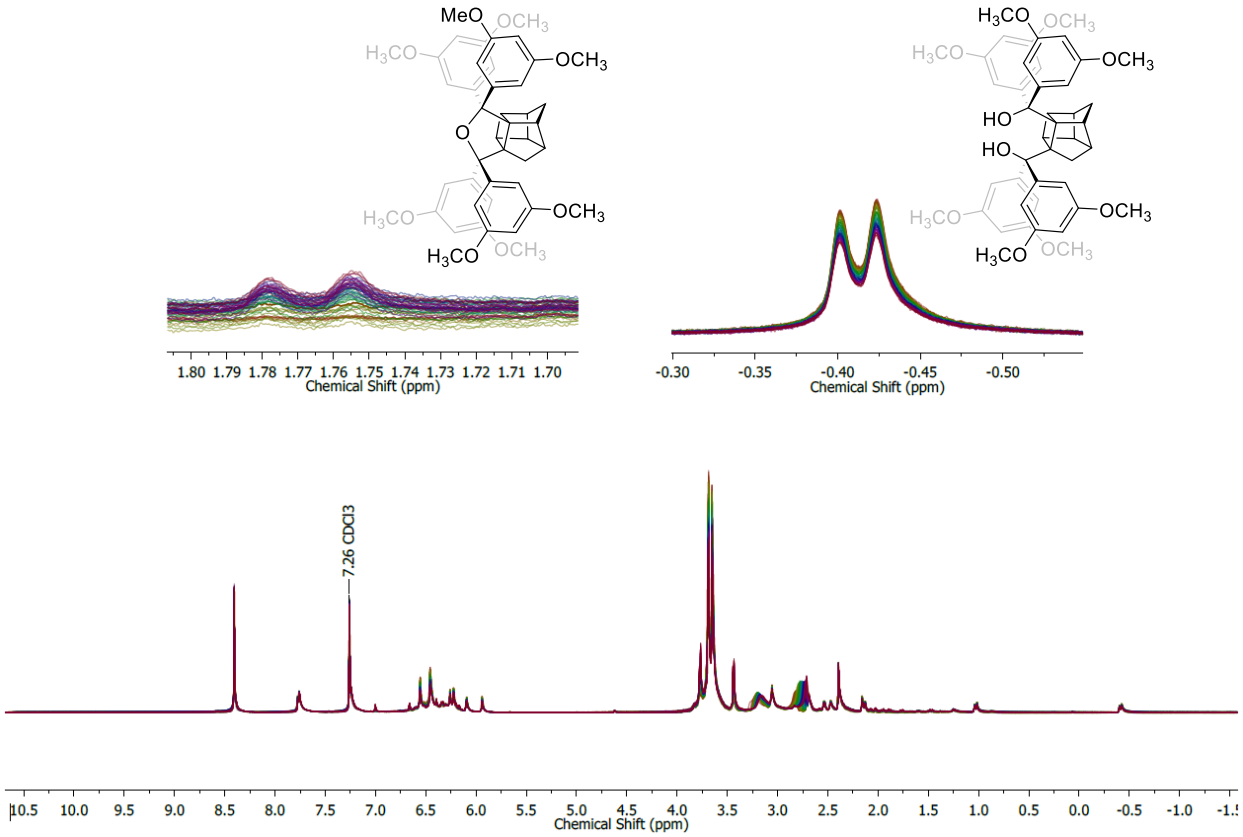

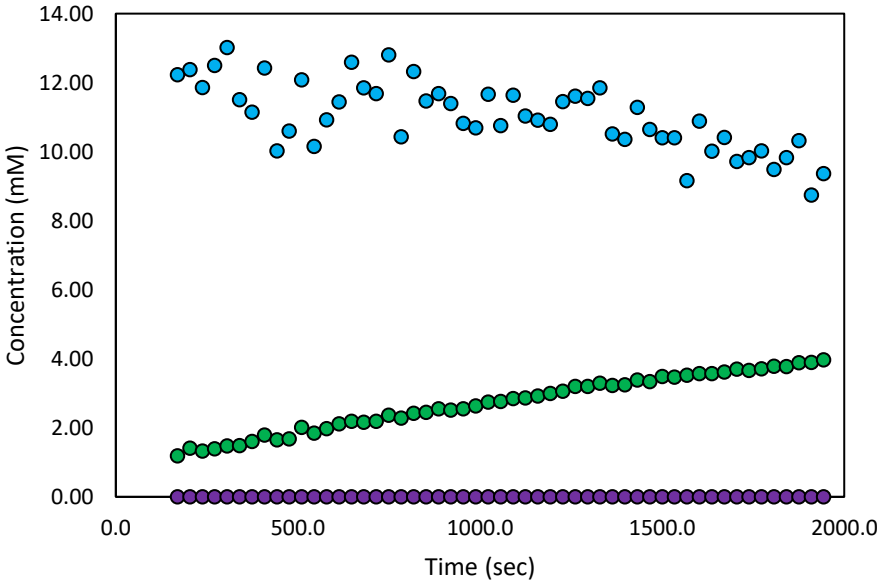

Compound 71 Kinetics Spectra

35°C – Trial 3

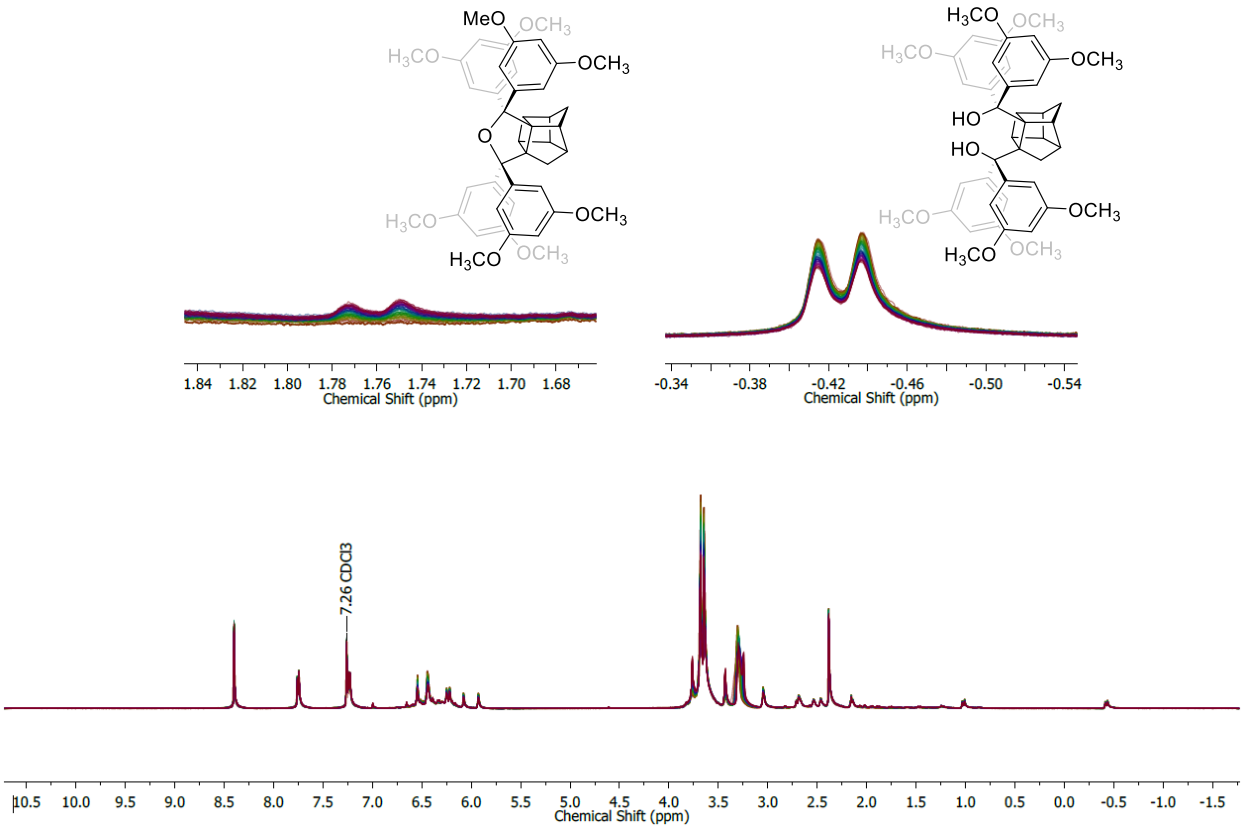

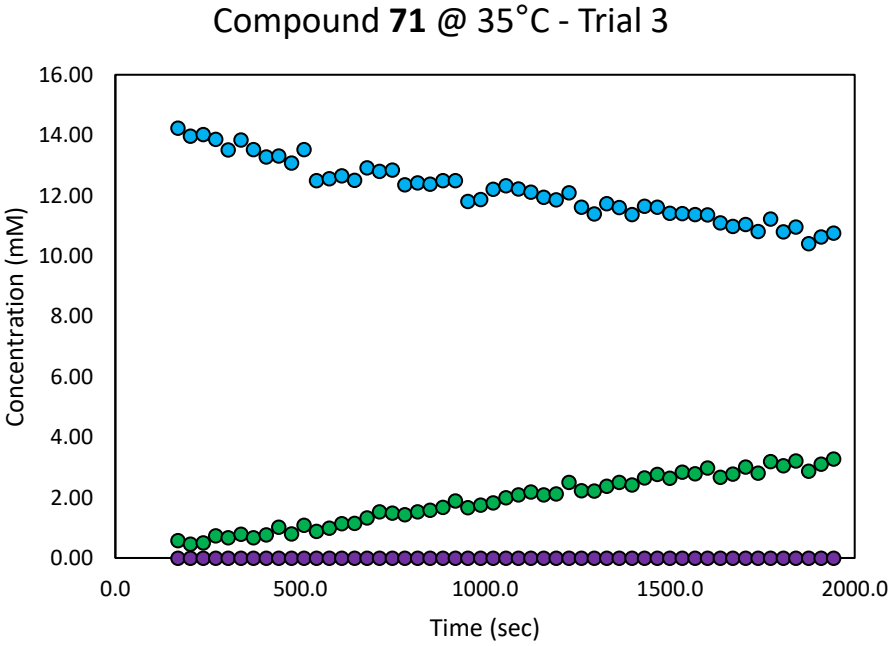

Compound 71 Kinetics Spectra

45°C – Trial 1

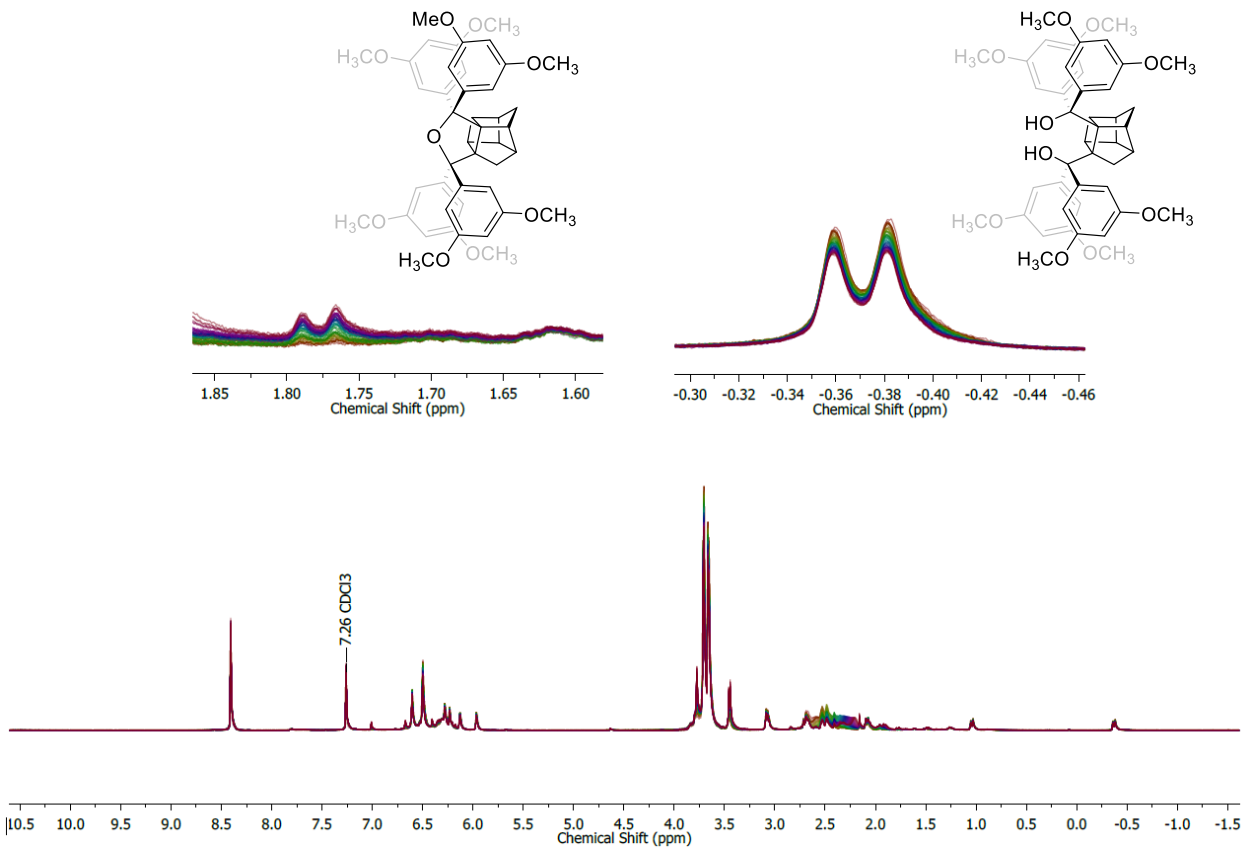

Compound **71** @ 45°C - Trial 1

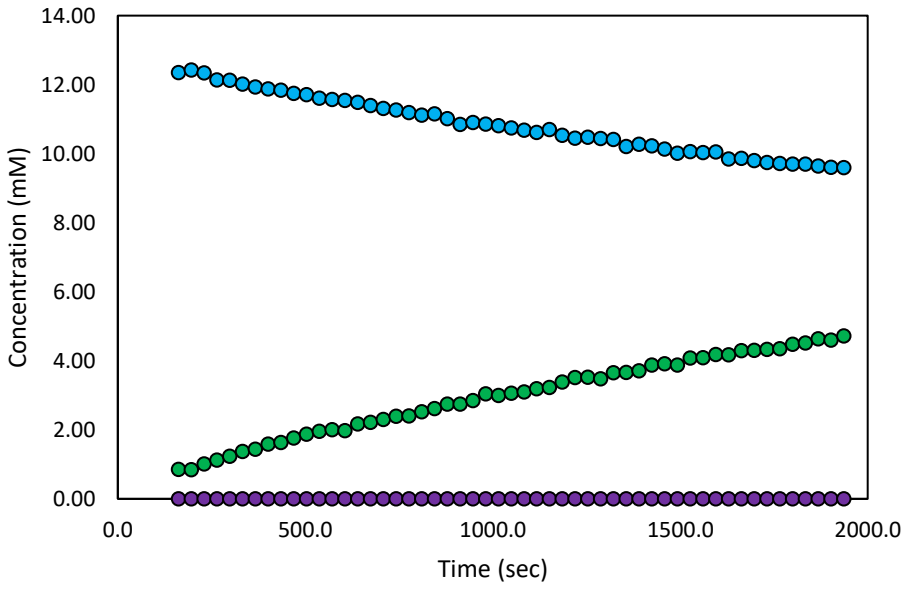

Compound 71 Kinetics Spectra

45°C – Trial 2

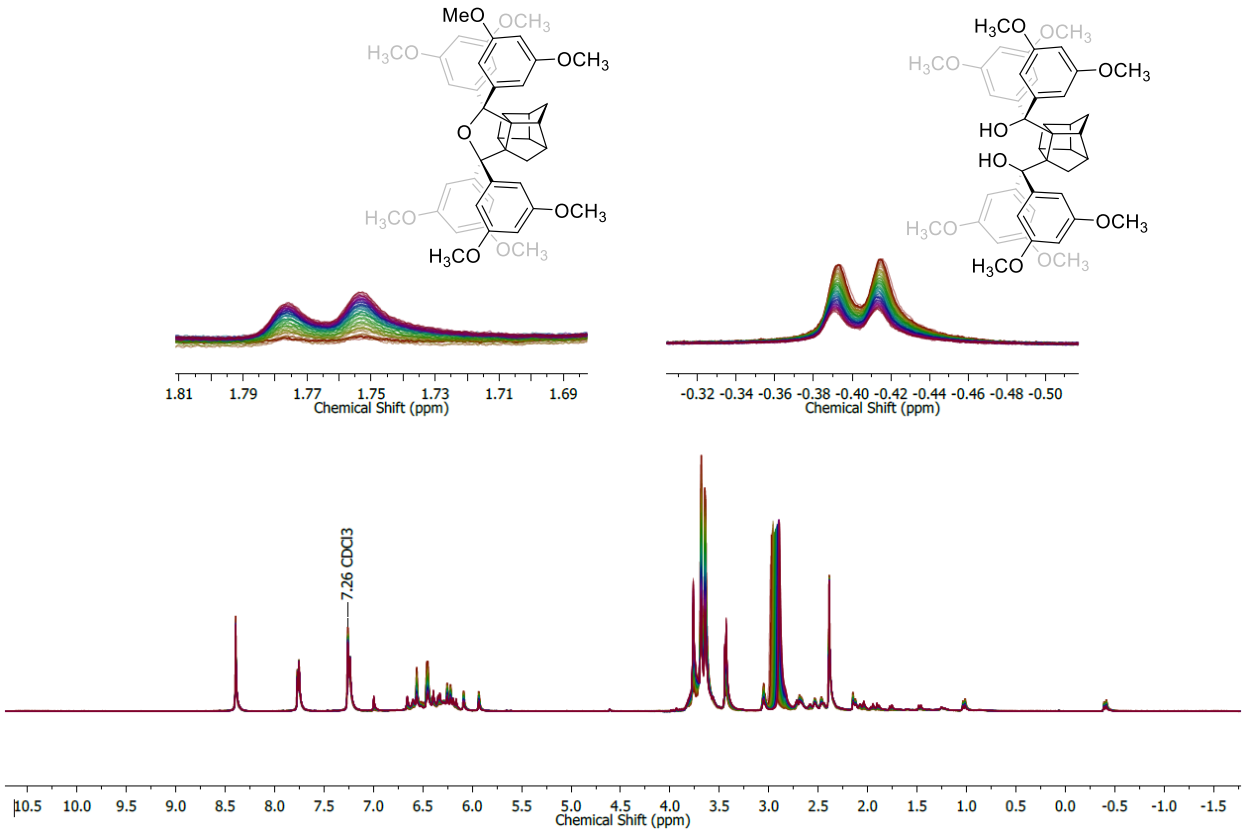

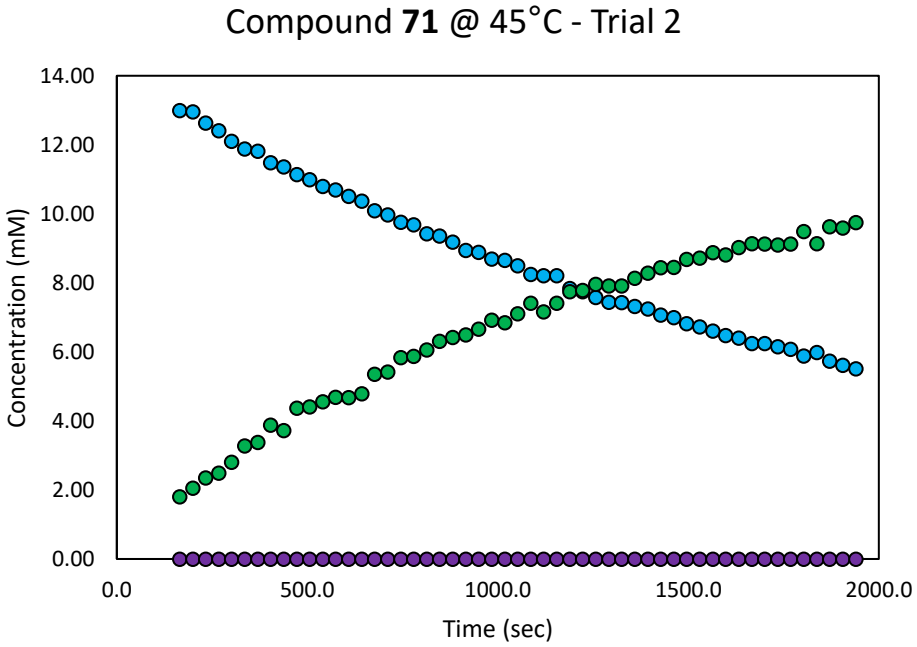

Compound 71 Kinetics Spectra

45°C – Trial 3

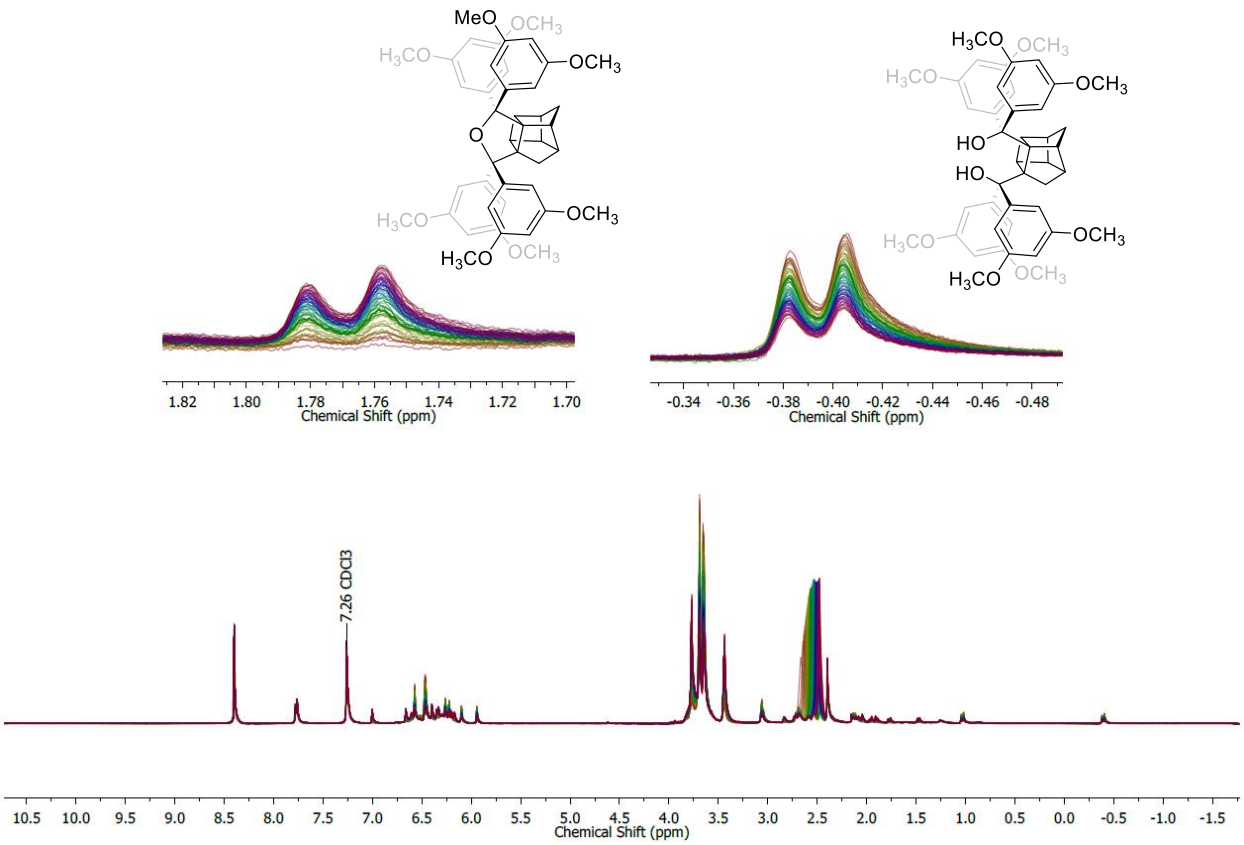

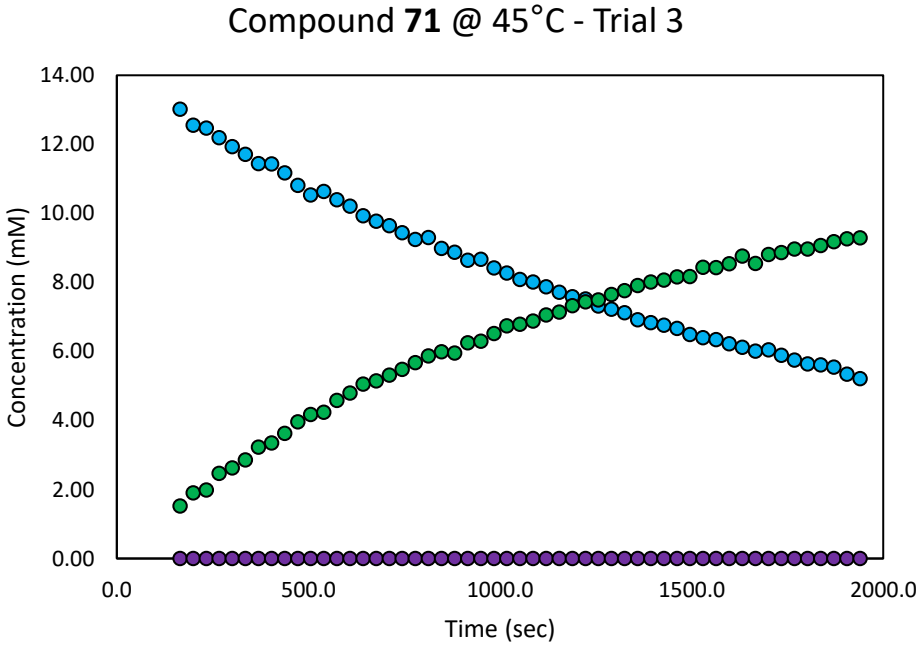

Compound 71 Kinetics Spectra

52°C – Trial 1

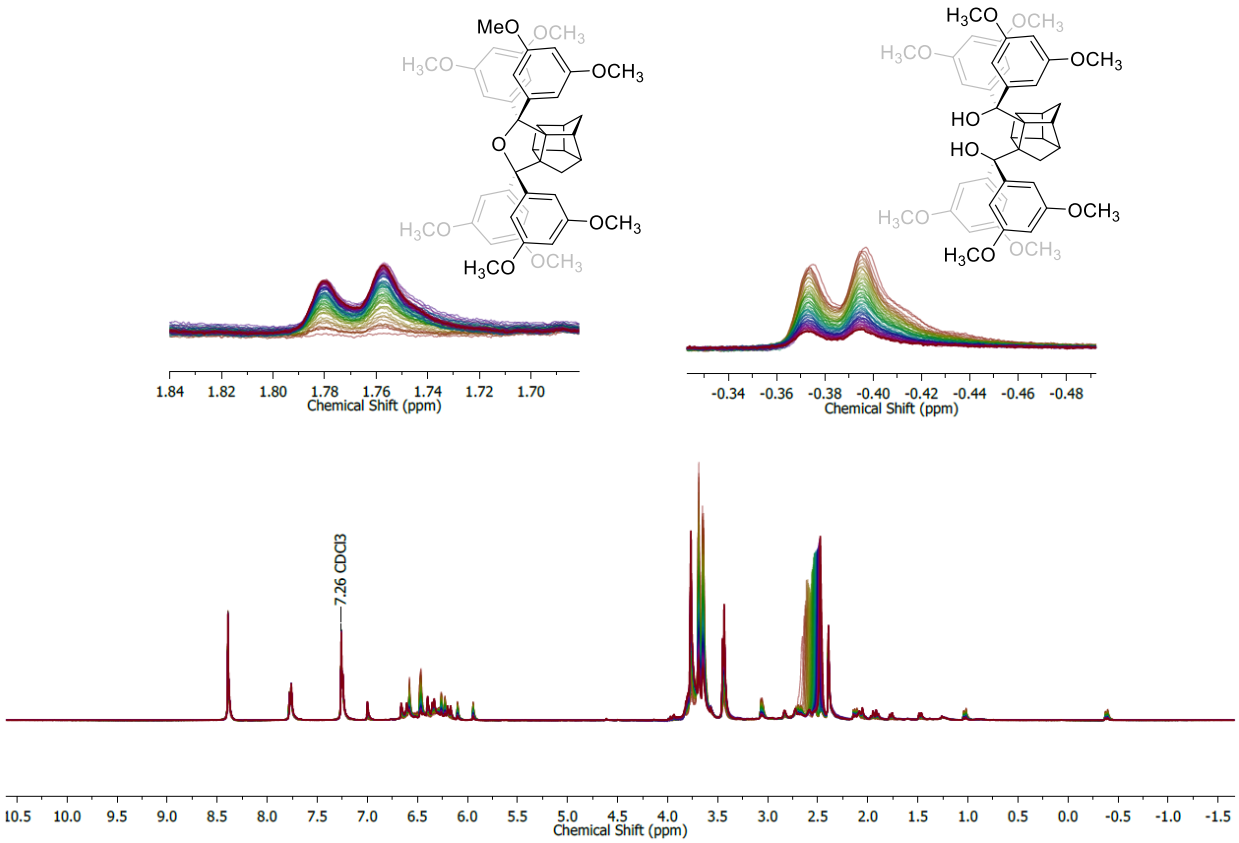

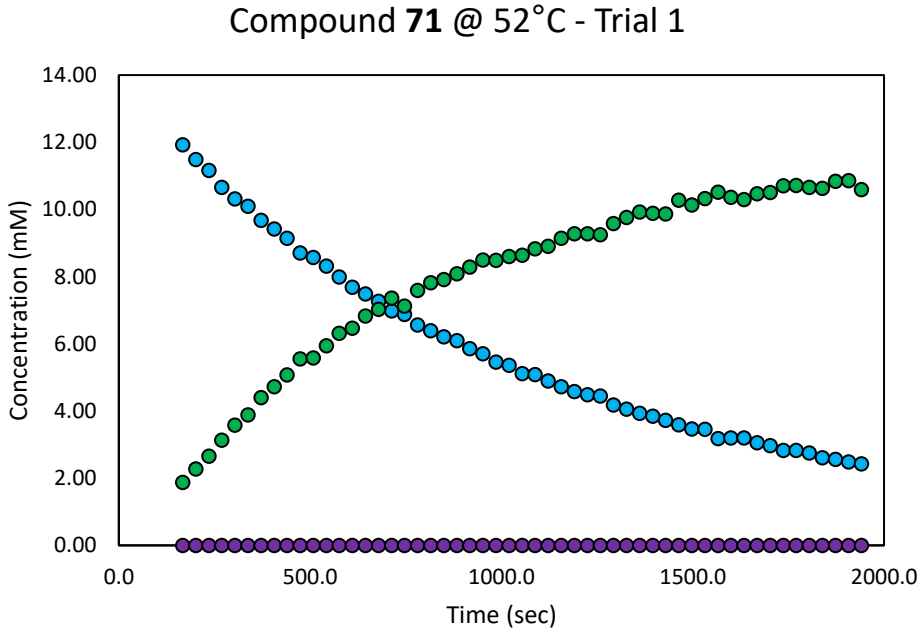

Compound 71 Kinetics Spectra

52°C – Trial 2

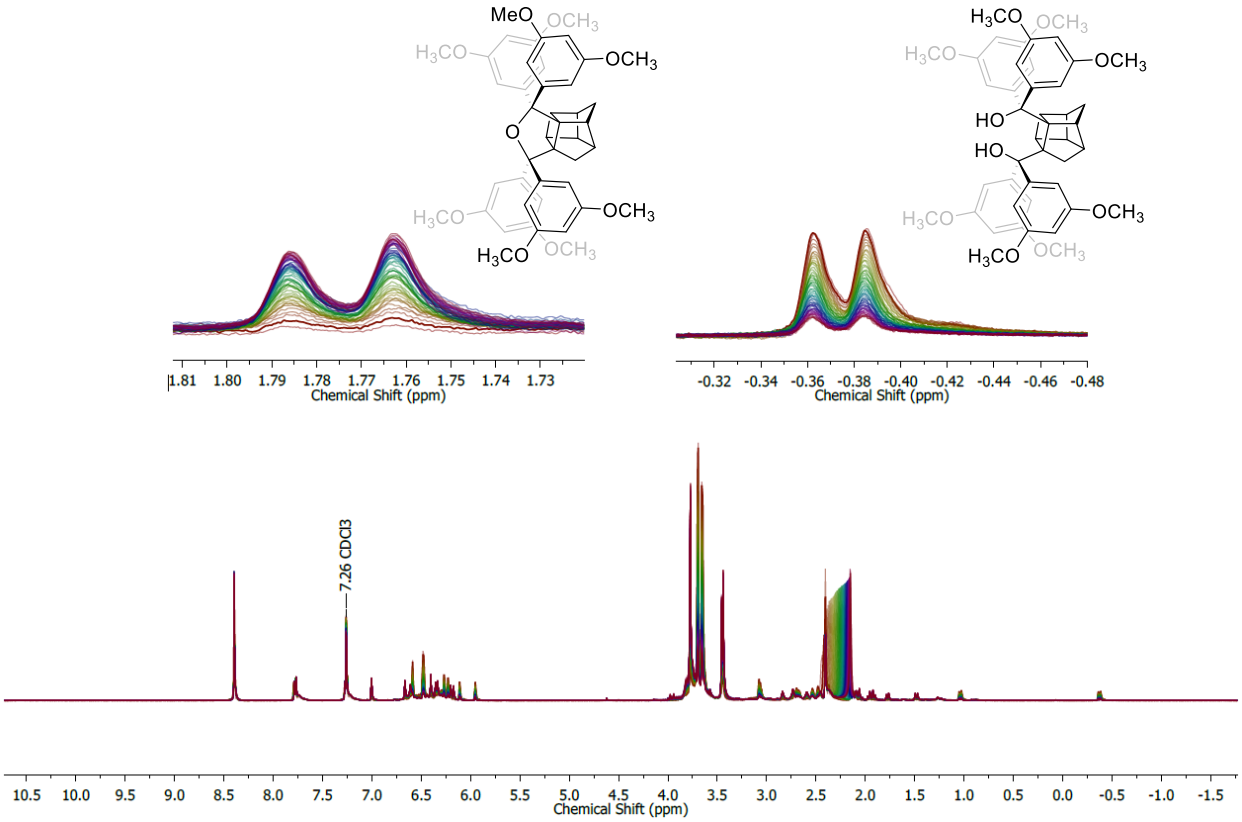

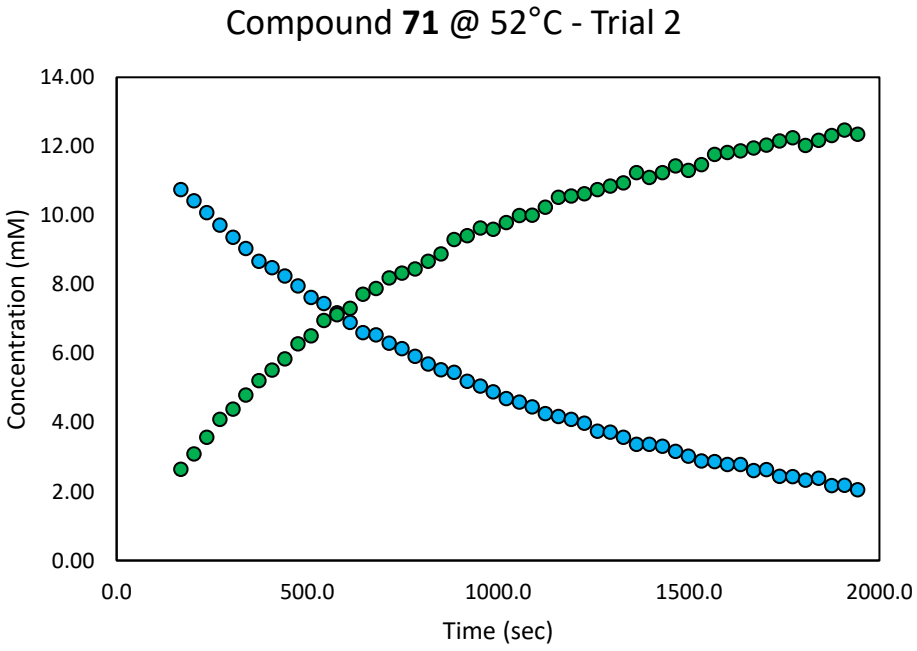

Compound 71 Kinetics Spectra

52°C – Trial 3

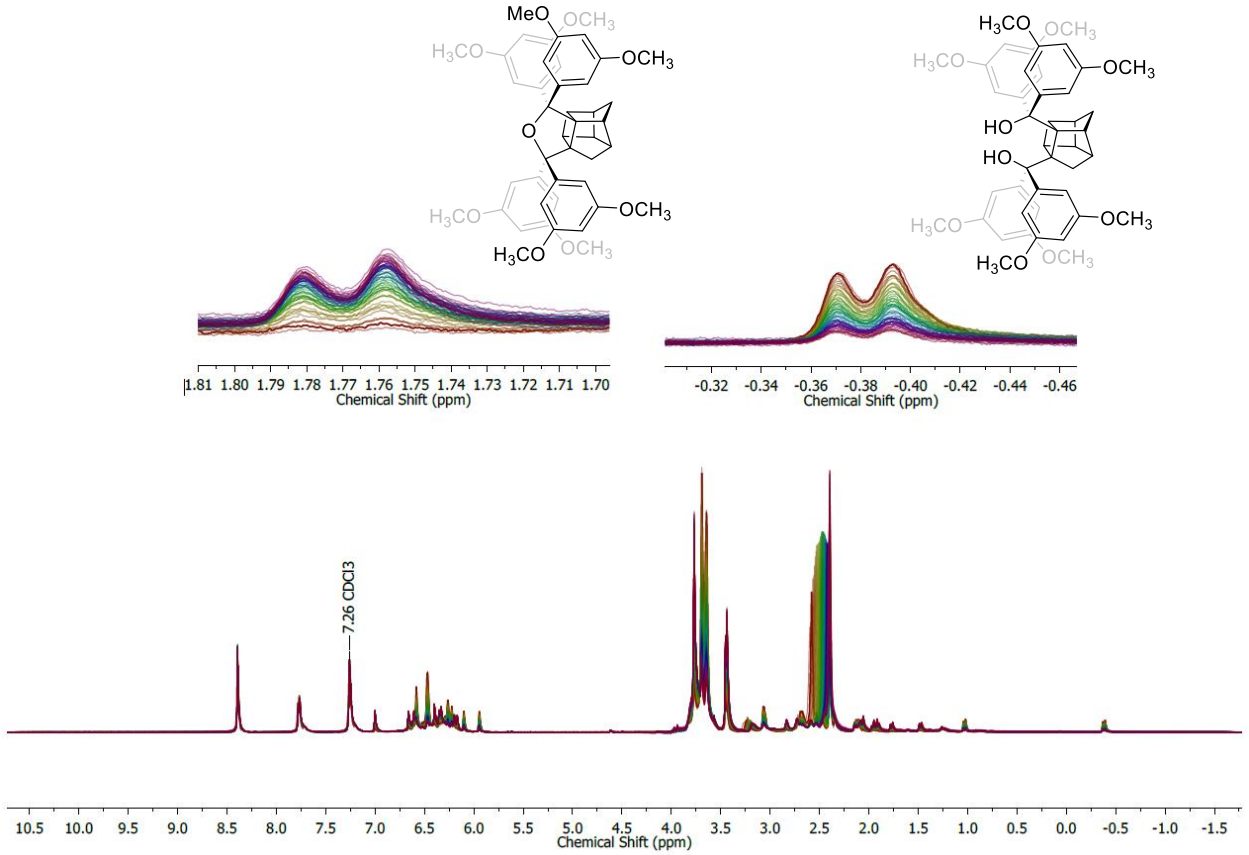

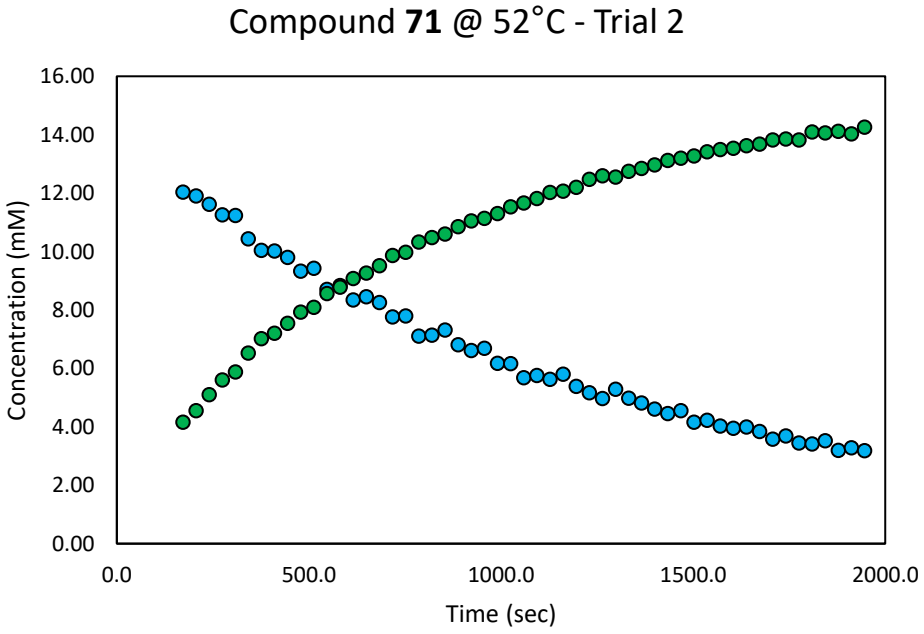

Compound 72 Kinetics Spectra

25°C – Trial 1

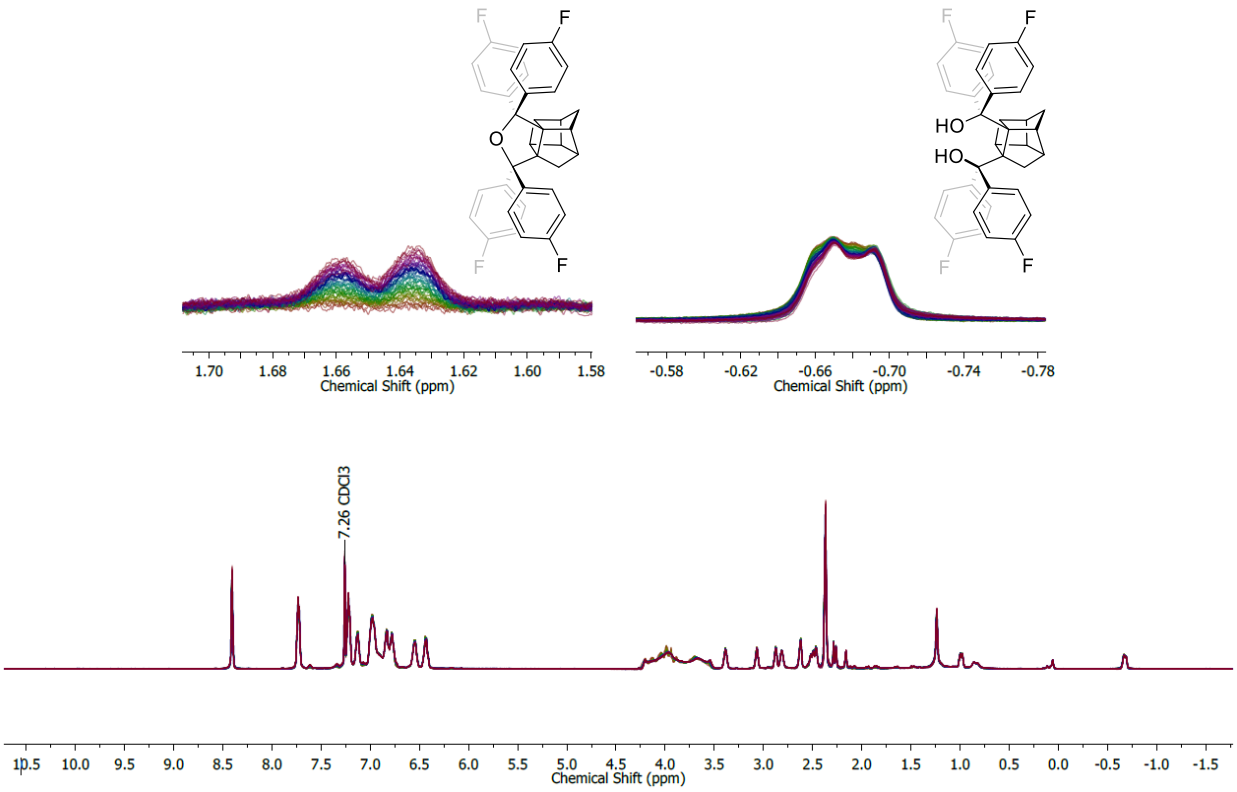

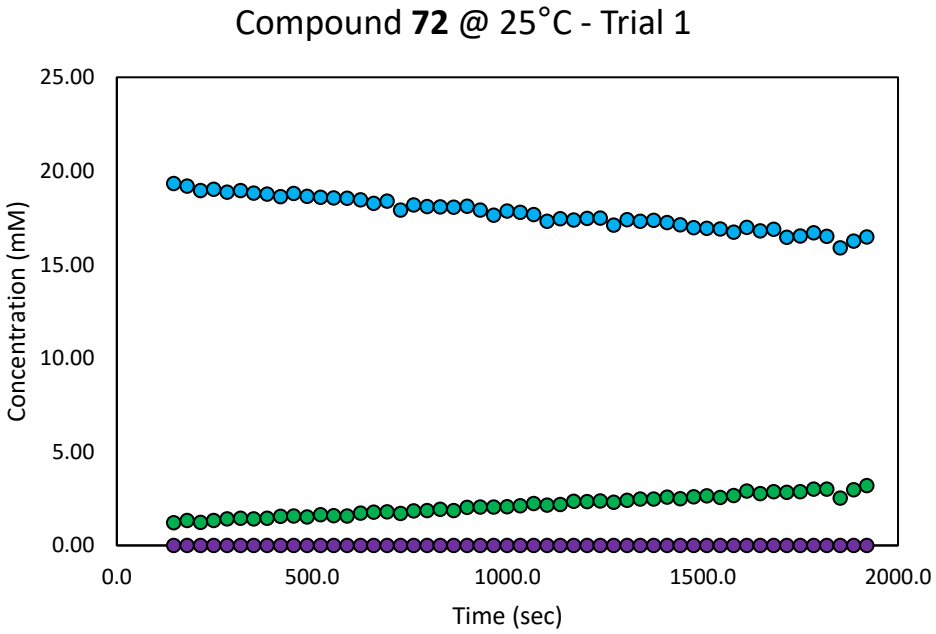

Compound 72 Kinetics Spectra

25°C – Trial 2

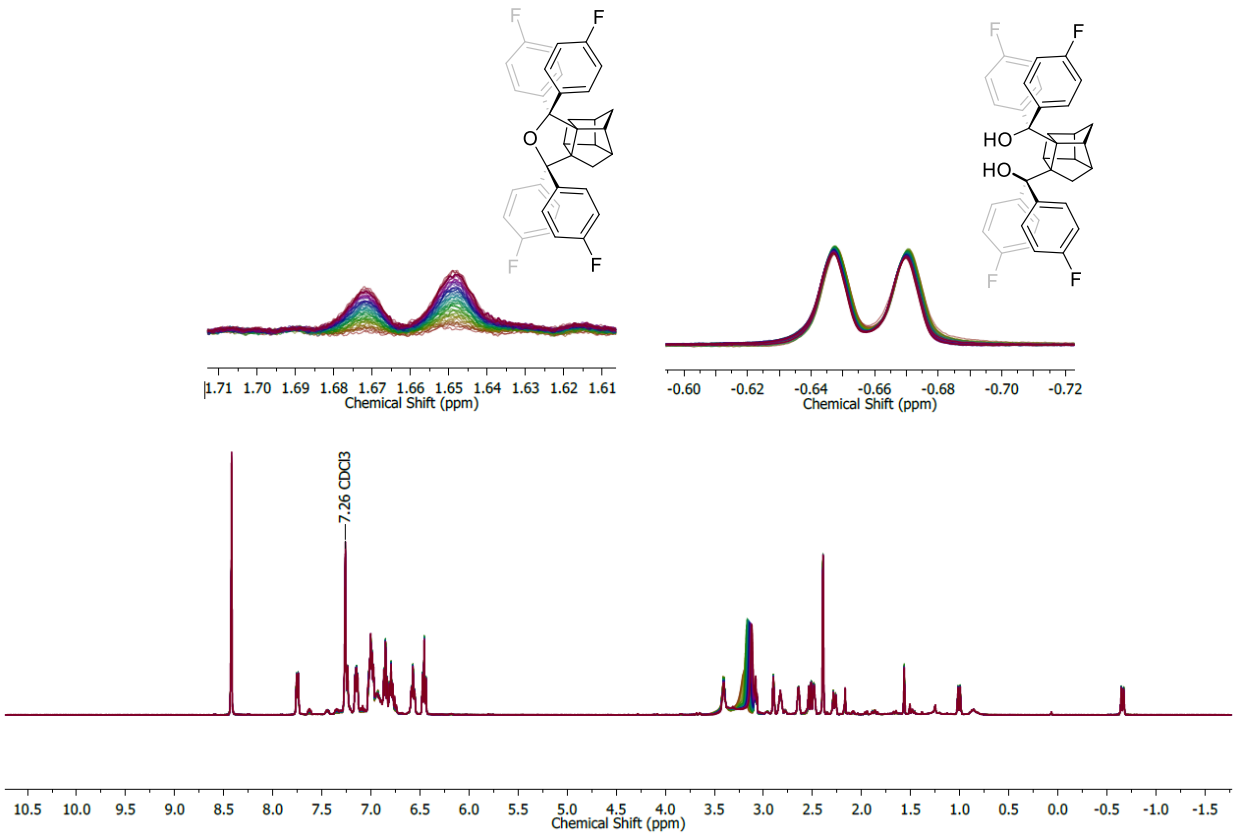

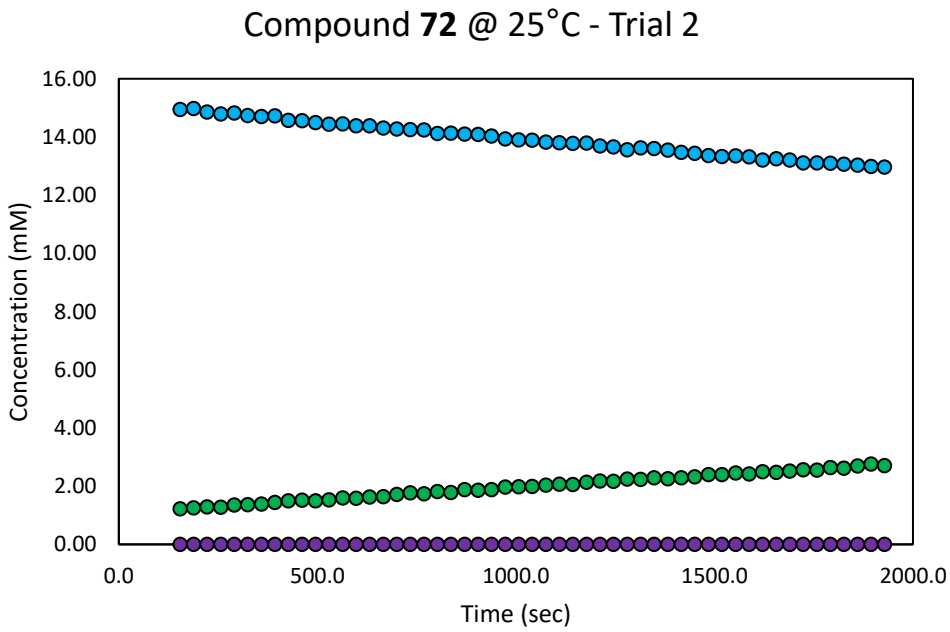

Compound 72 Kinetics Spectra

25°C – Trial 3

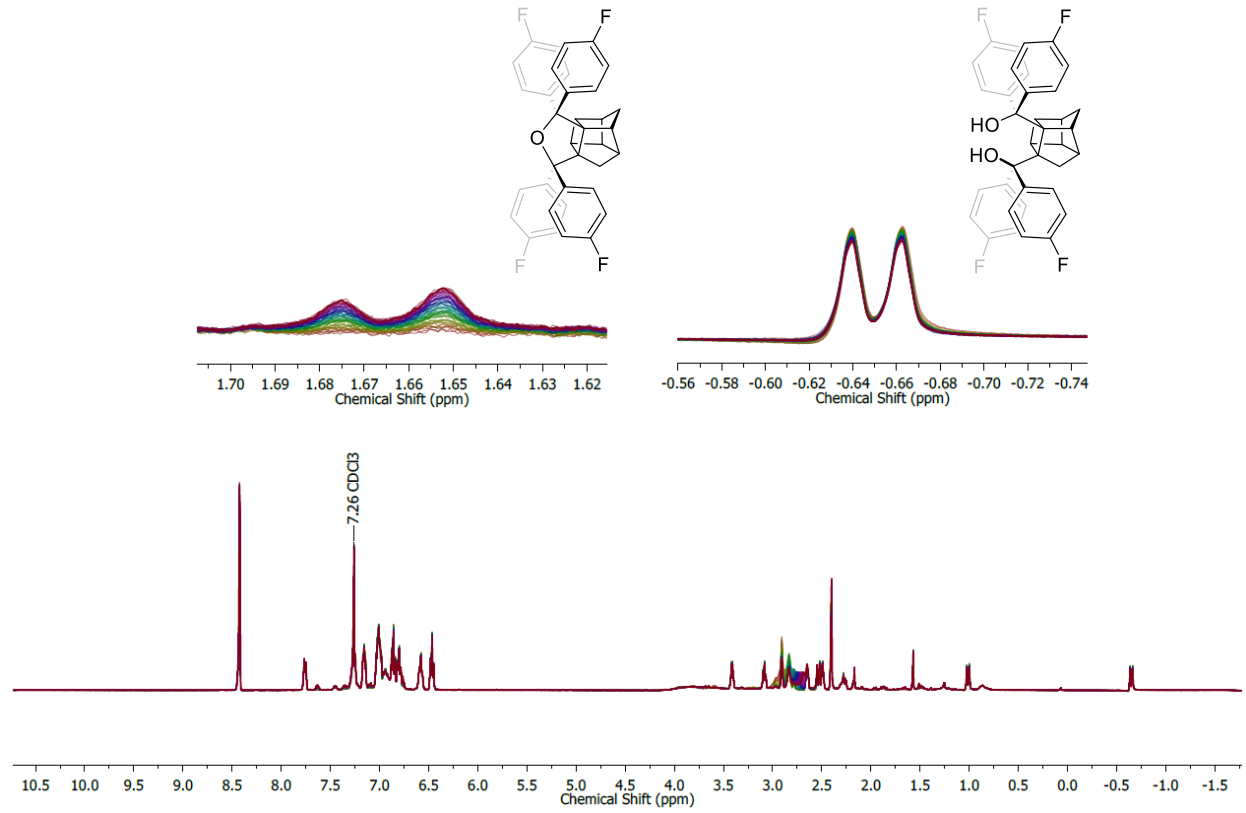

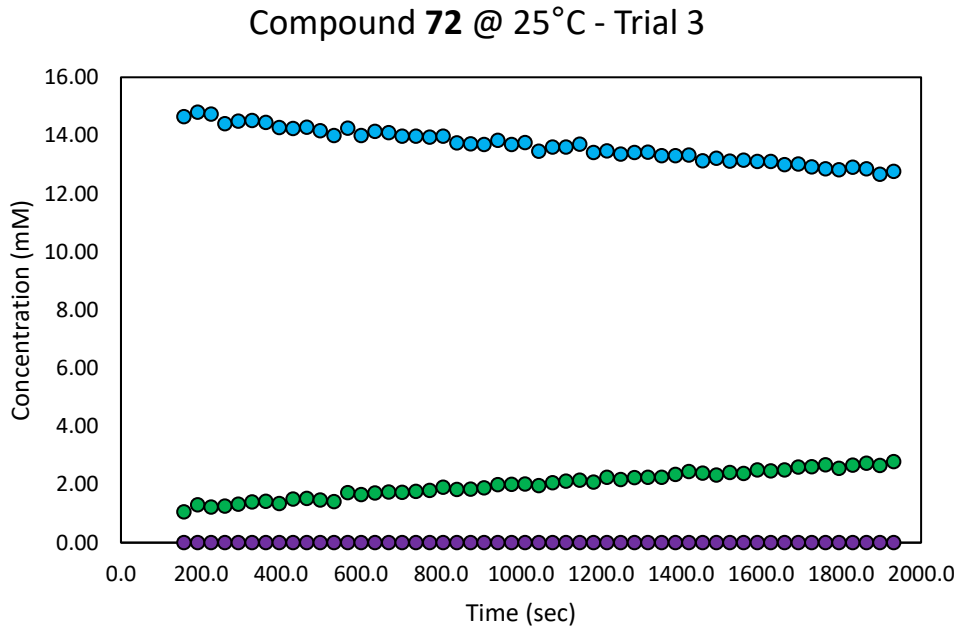

Compound 72 Kinetics Spectra

35°C – Trial 1

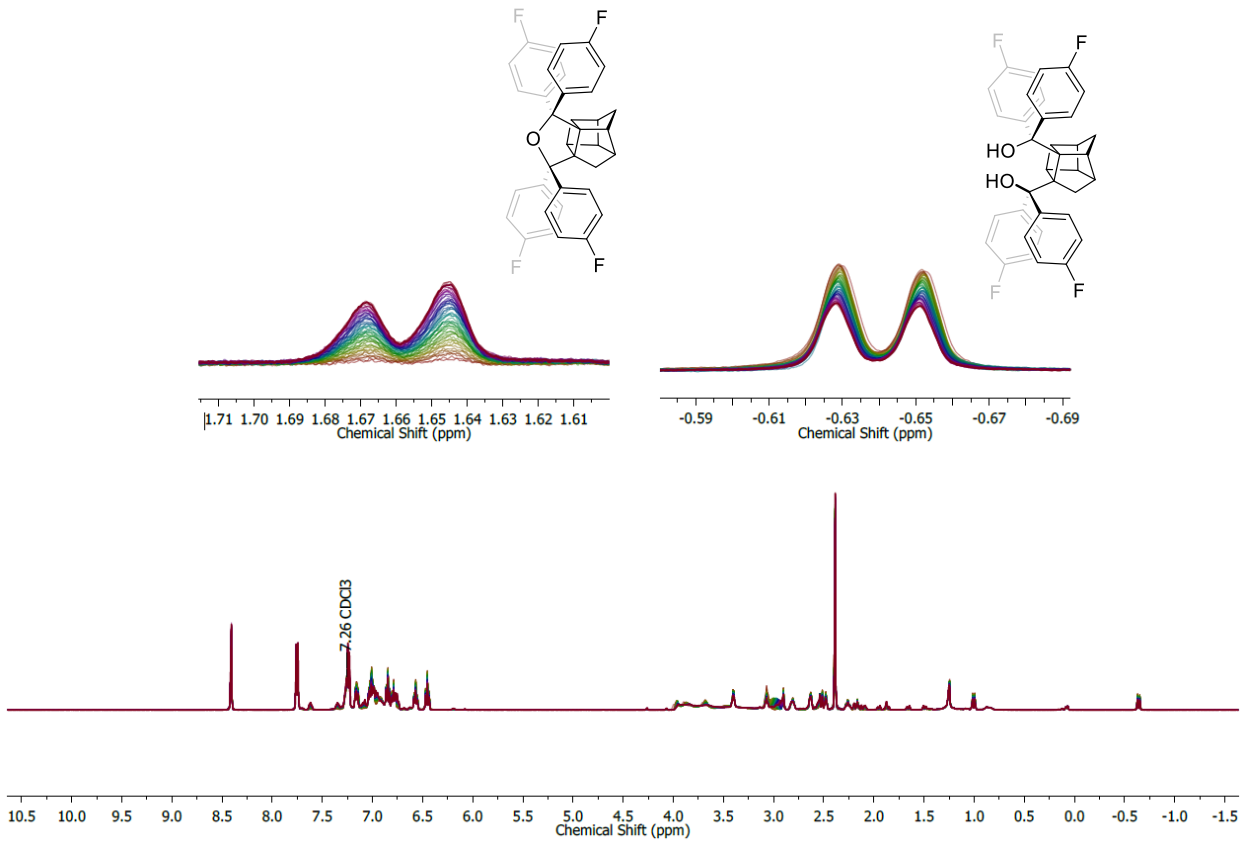

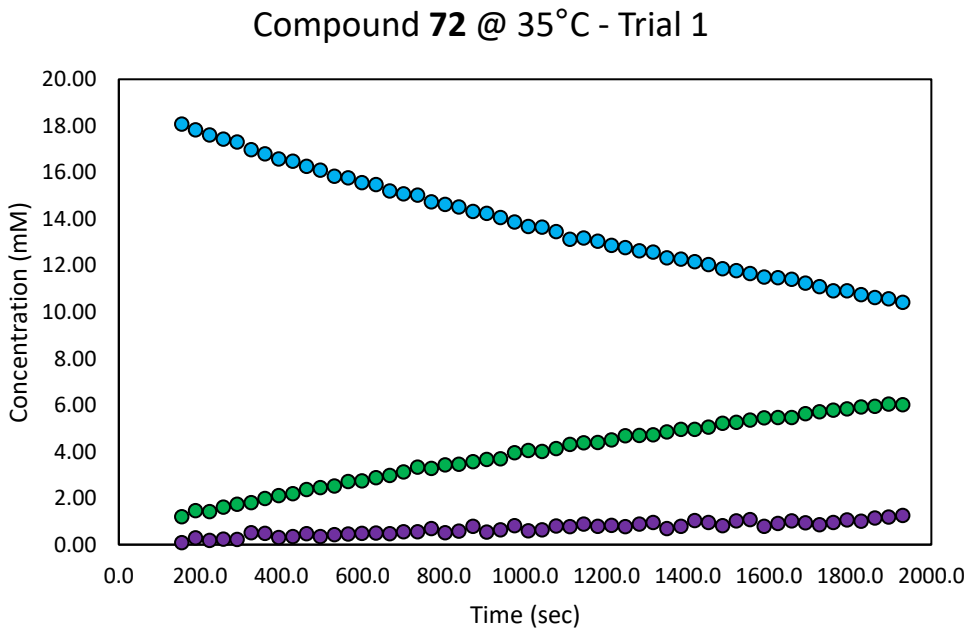

Compound 72 Kinetics Spectra

35°C – Trial 2

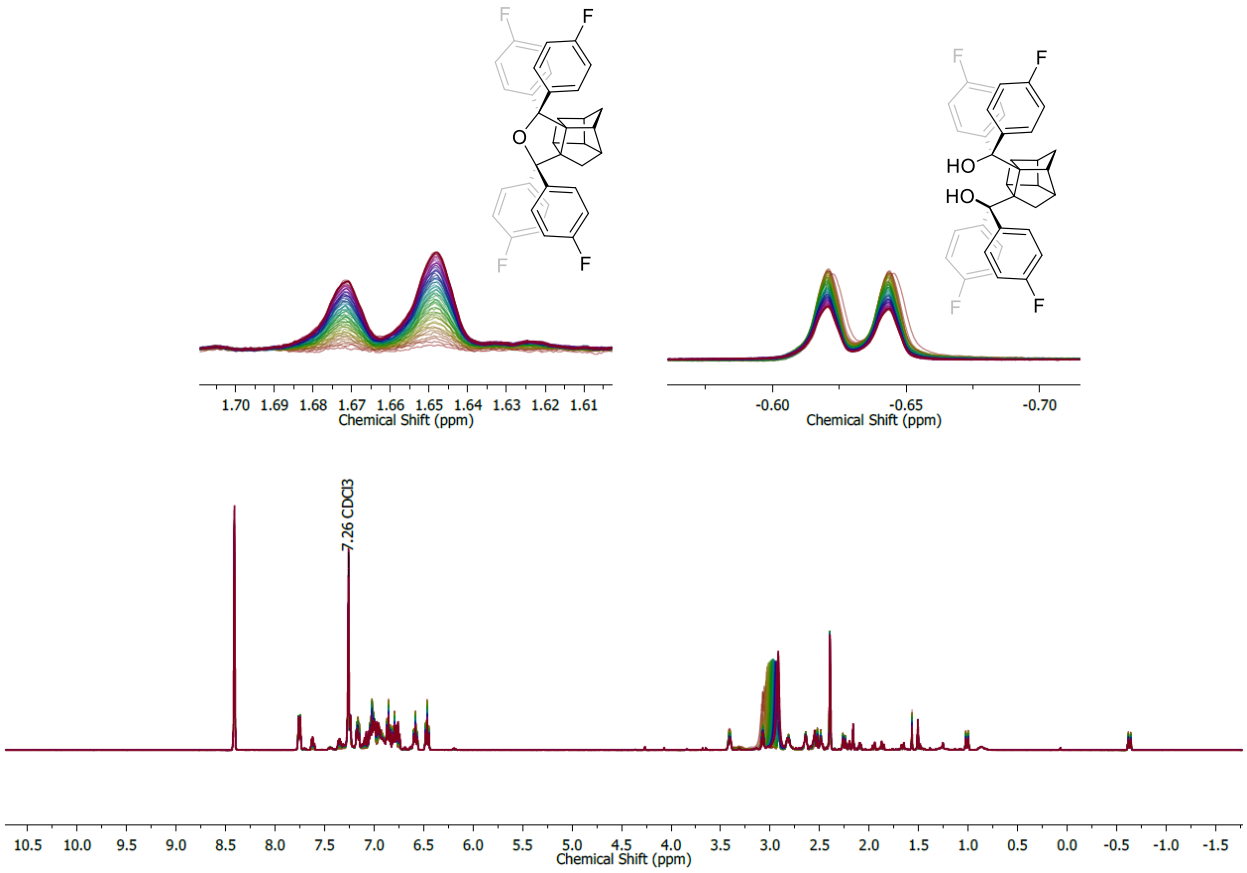

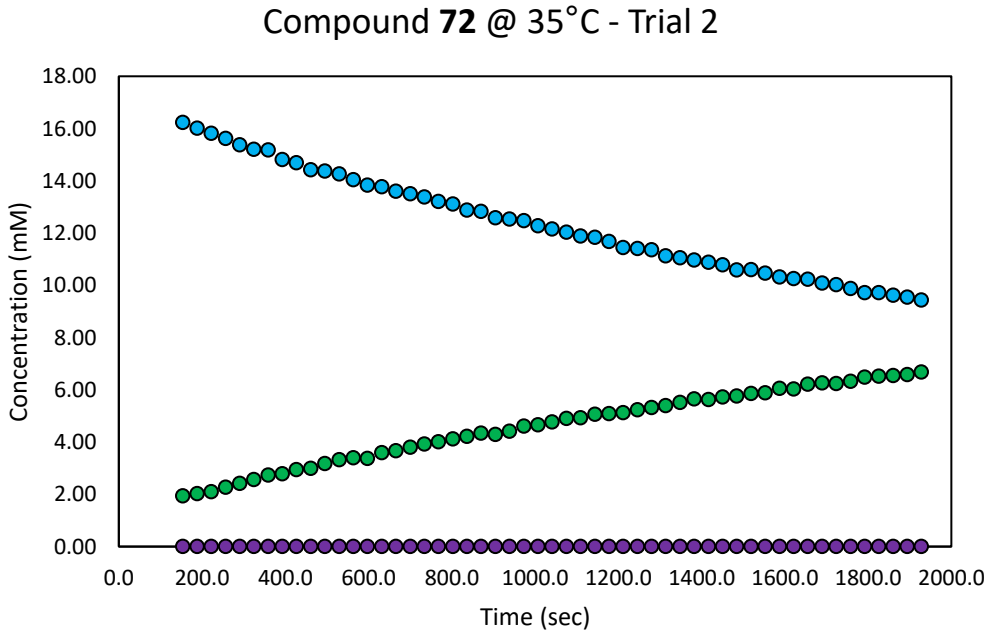

Compound 72 Kinetics Spectra

35°C – Trial 3

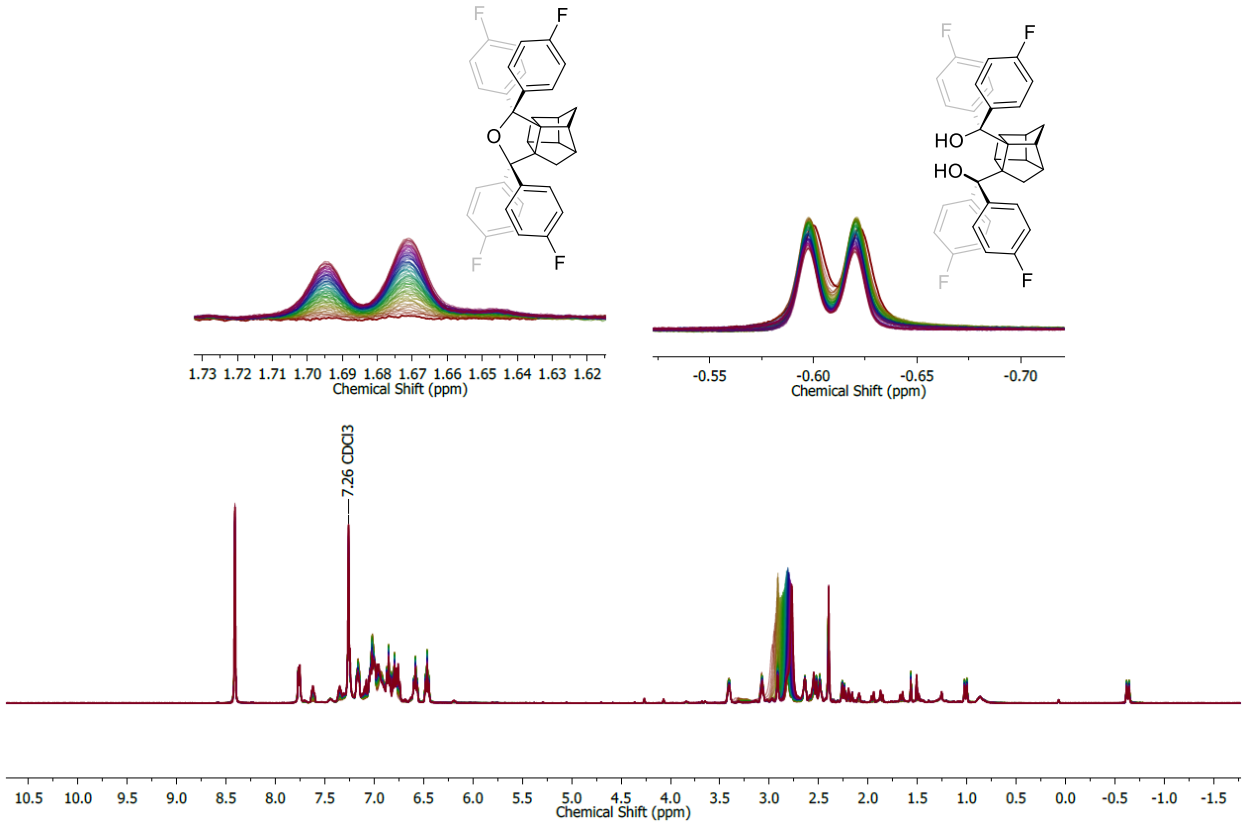

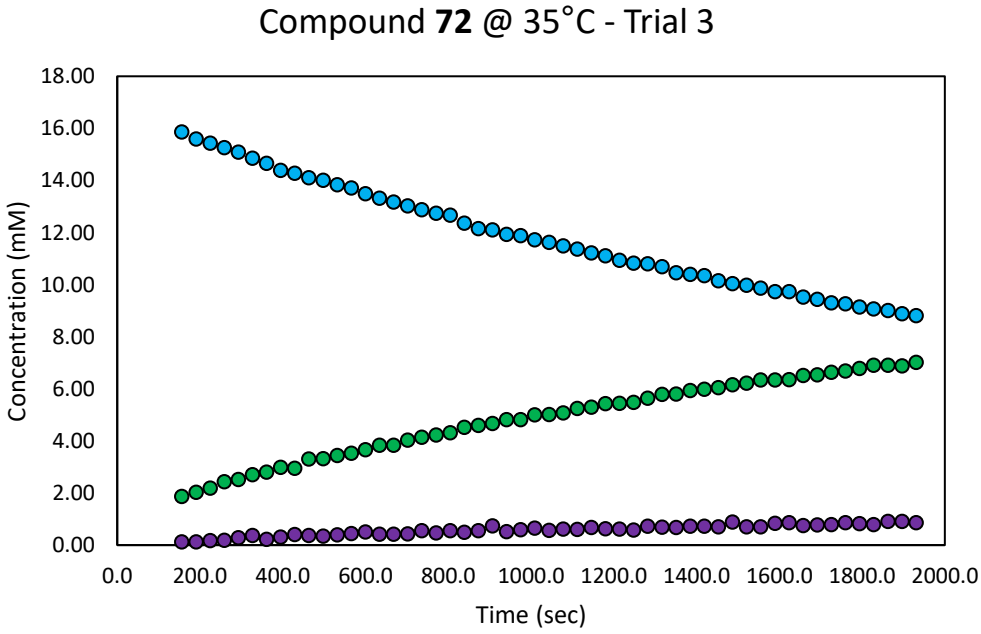

Compound 72 Kinetics Spectra

45°C – Trial 1

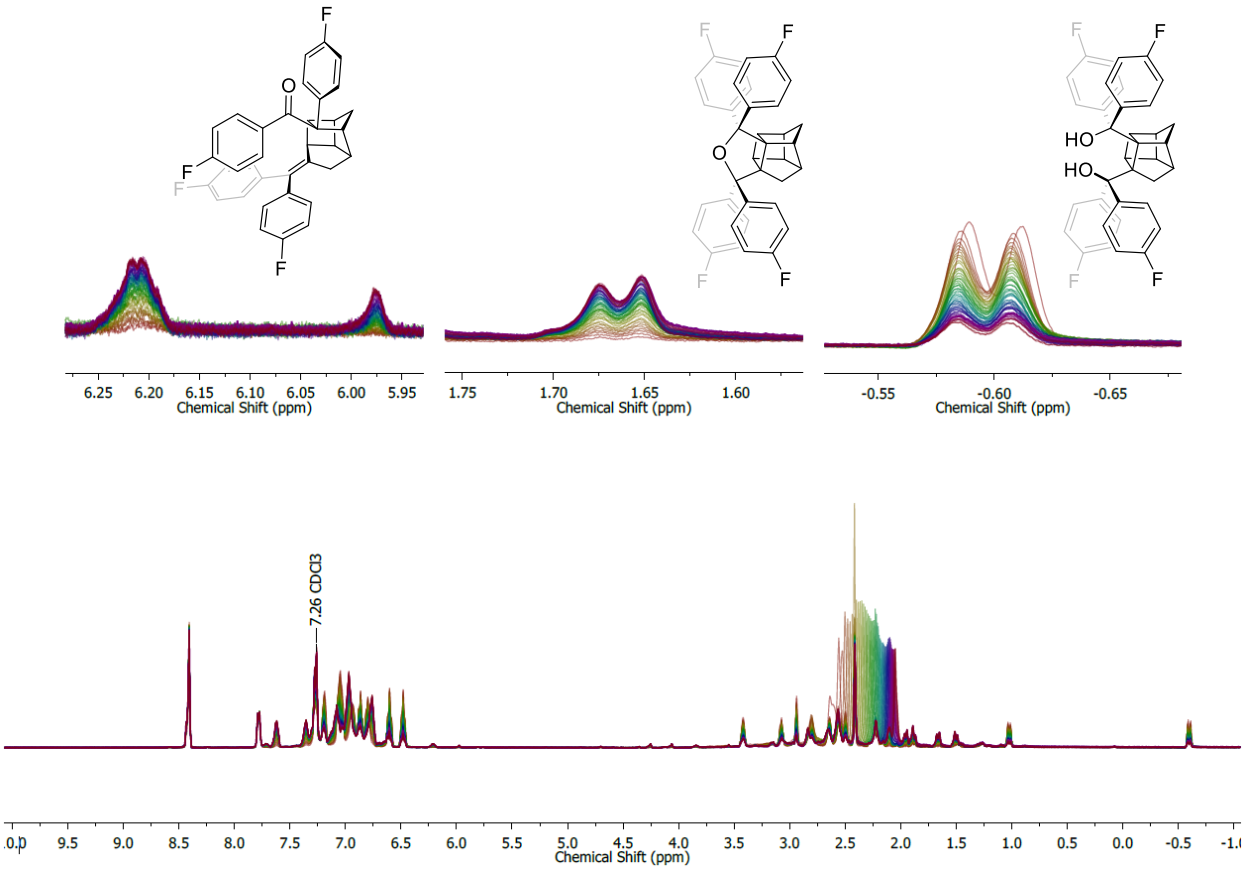

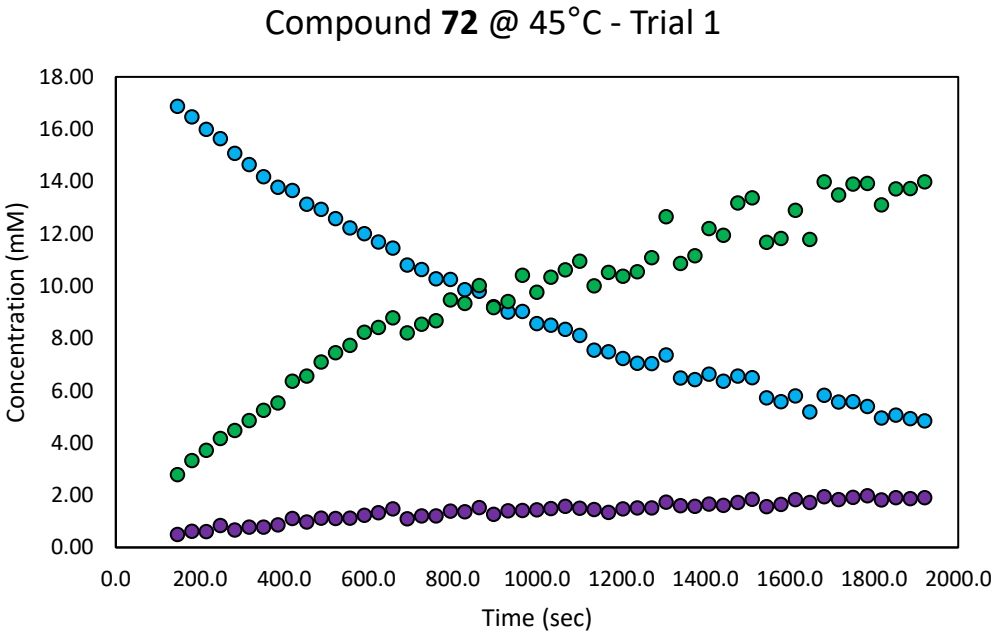

Compound 72 Kinetics Spectra

45°C – Trial 2

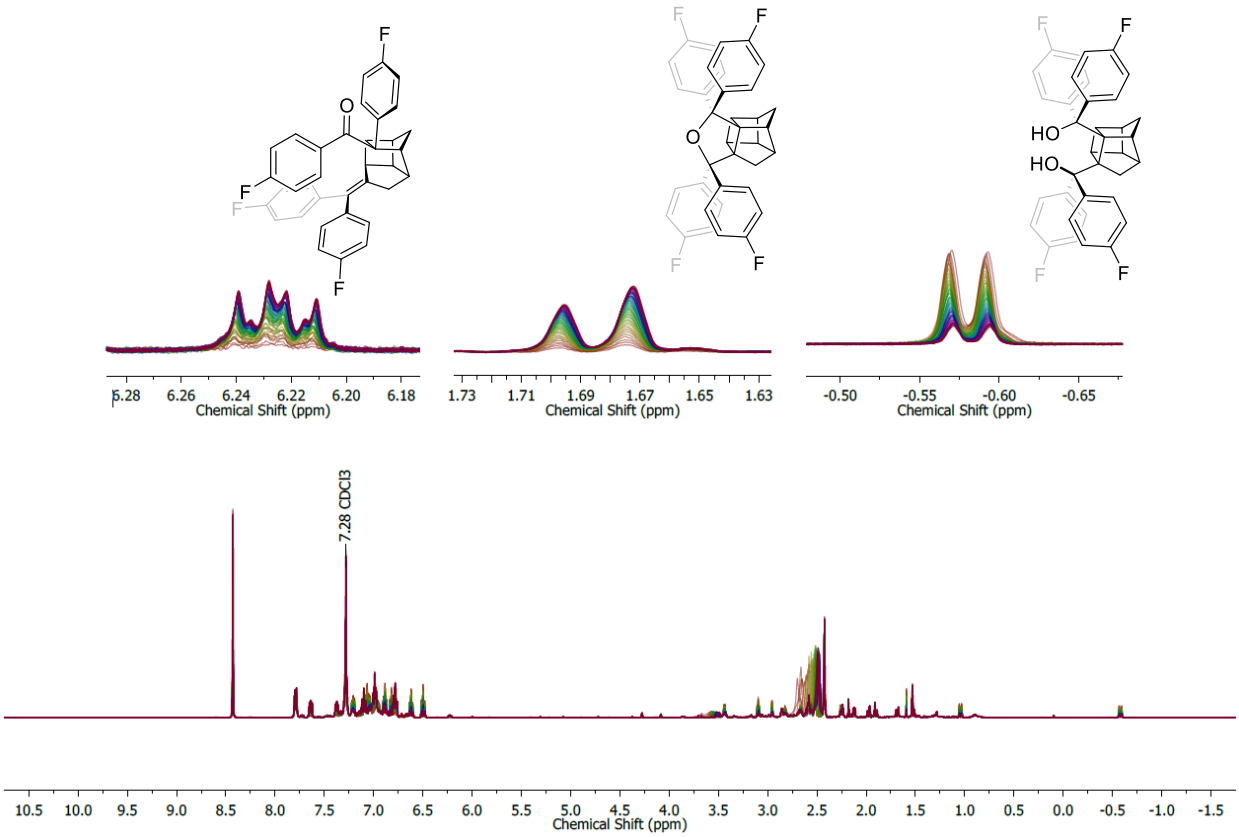

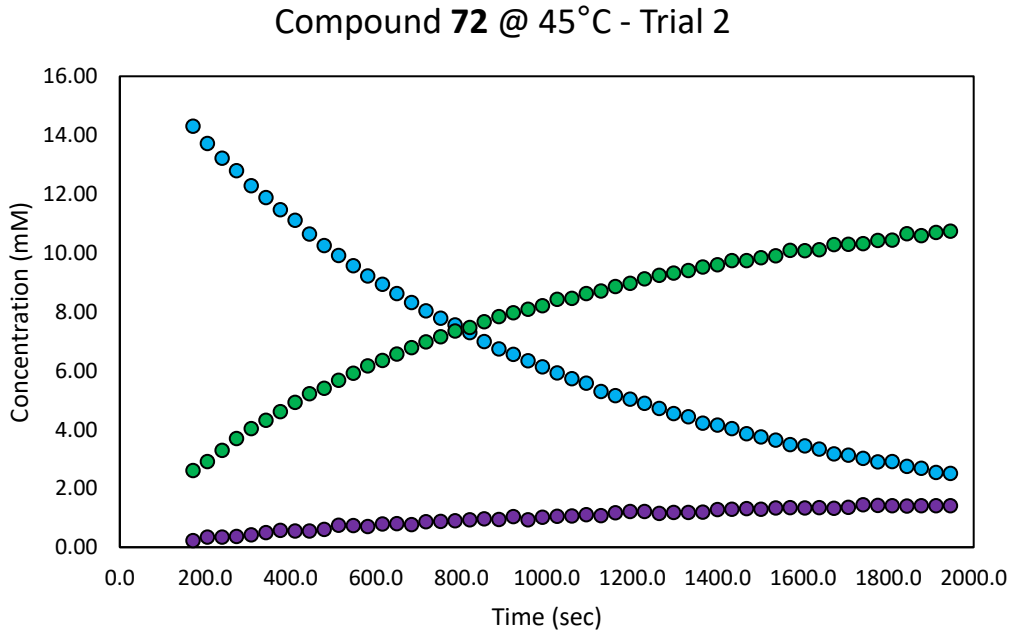

Compound 72 Kinetics Spectra

45°C – Trial 3

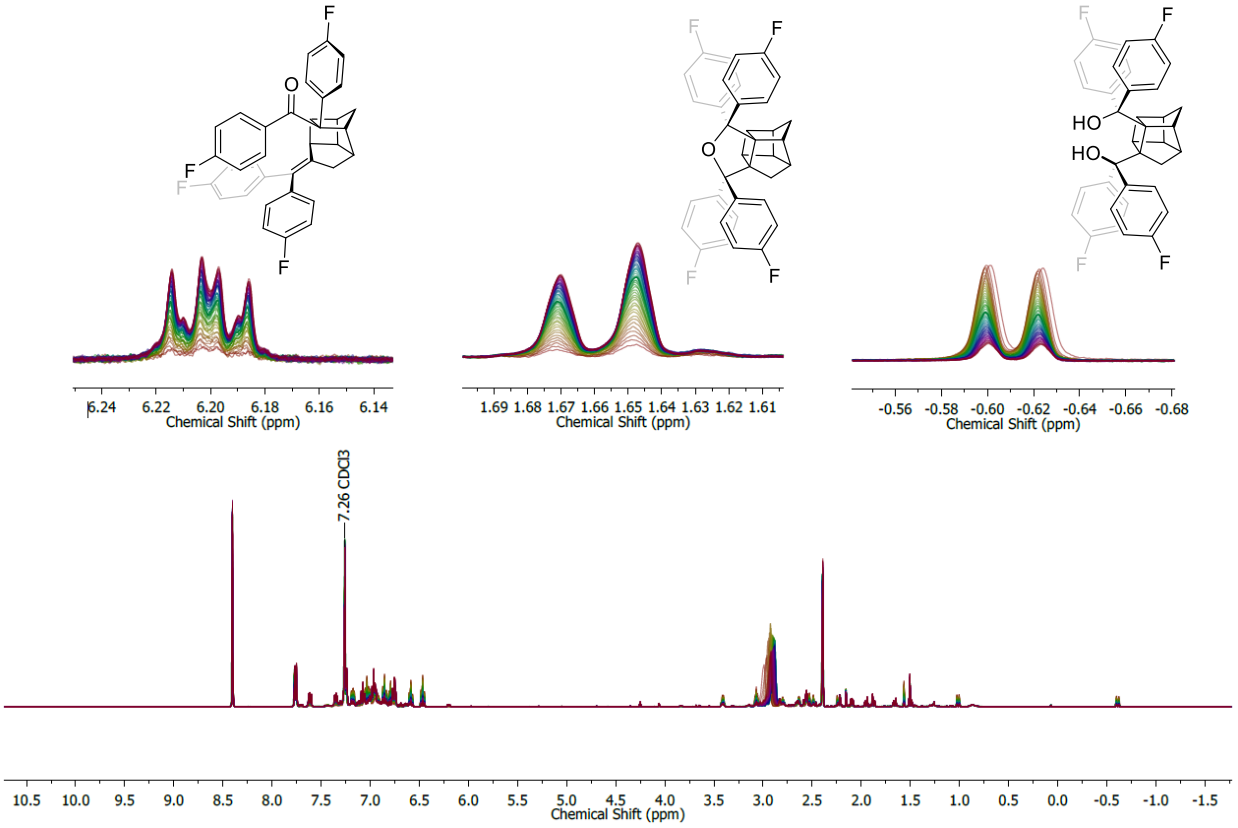

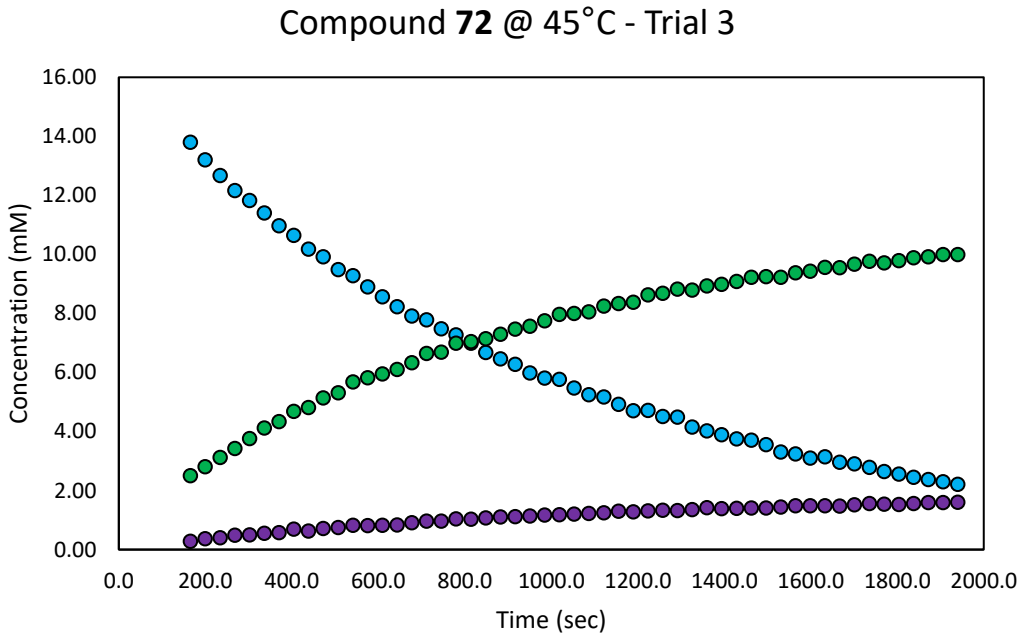

Compound 72 Kinetics Spectra

52°C – Trial 1

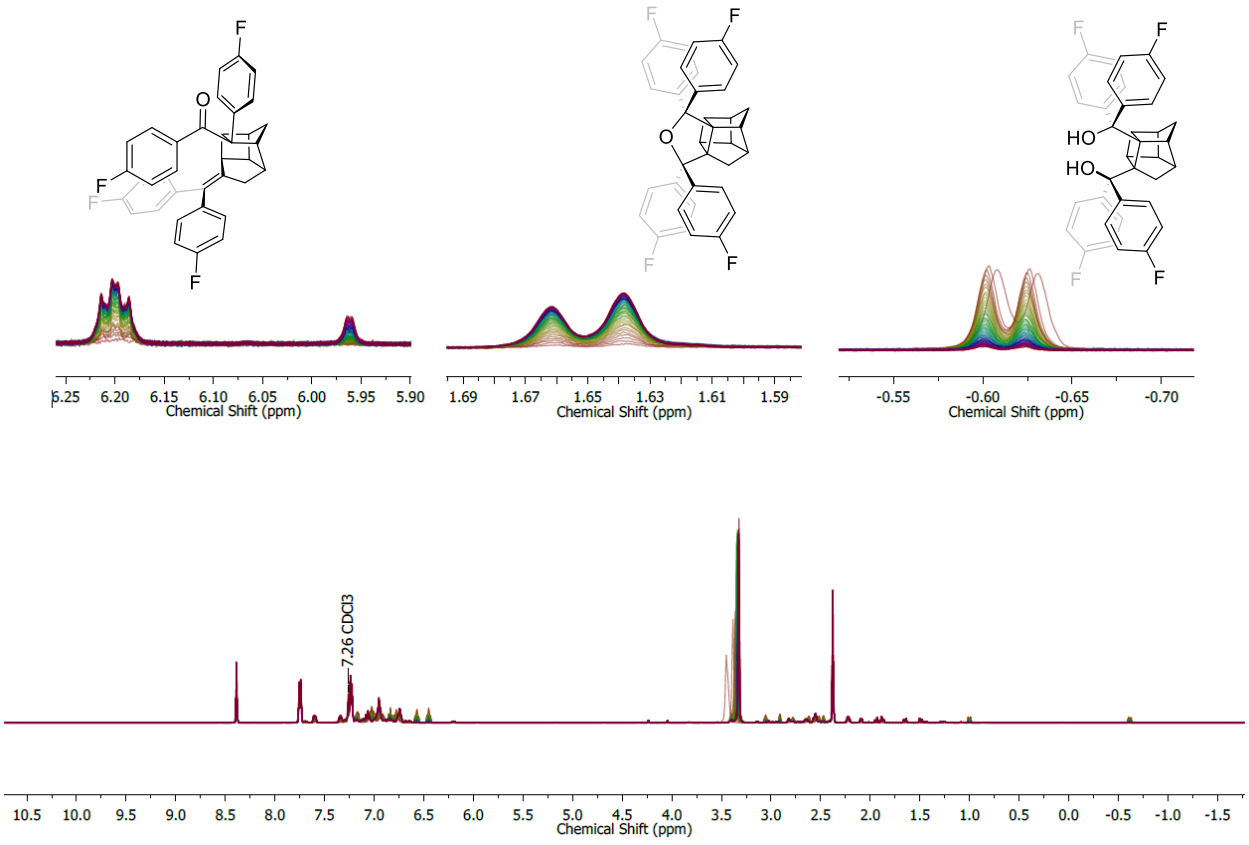

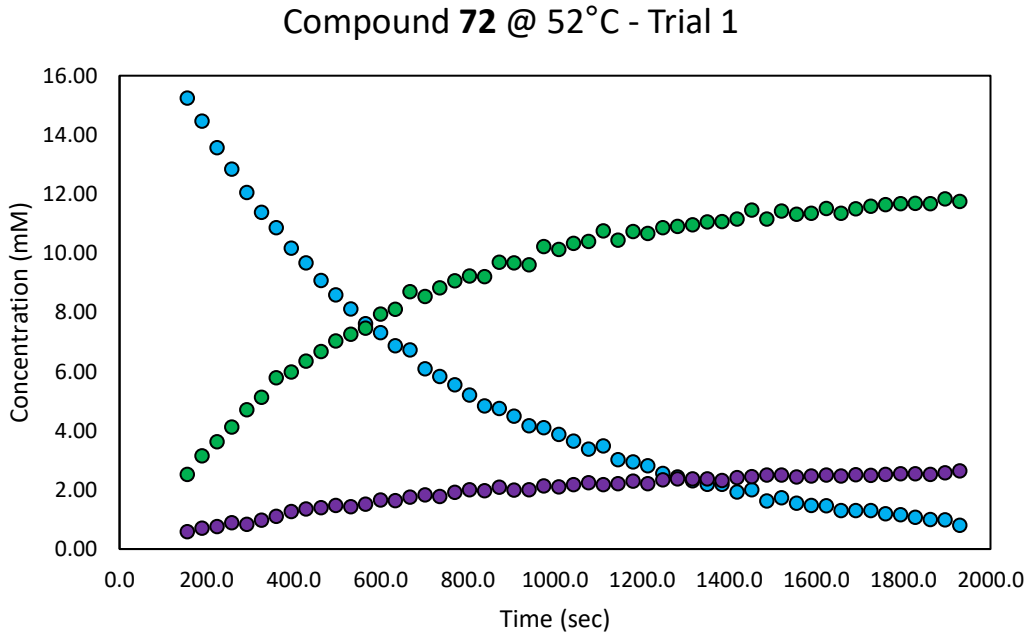

Compound 72 Kinetics Spectra

52°C – Trial 2

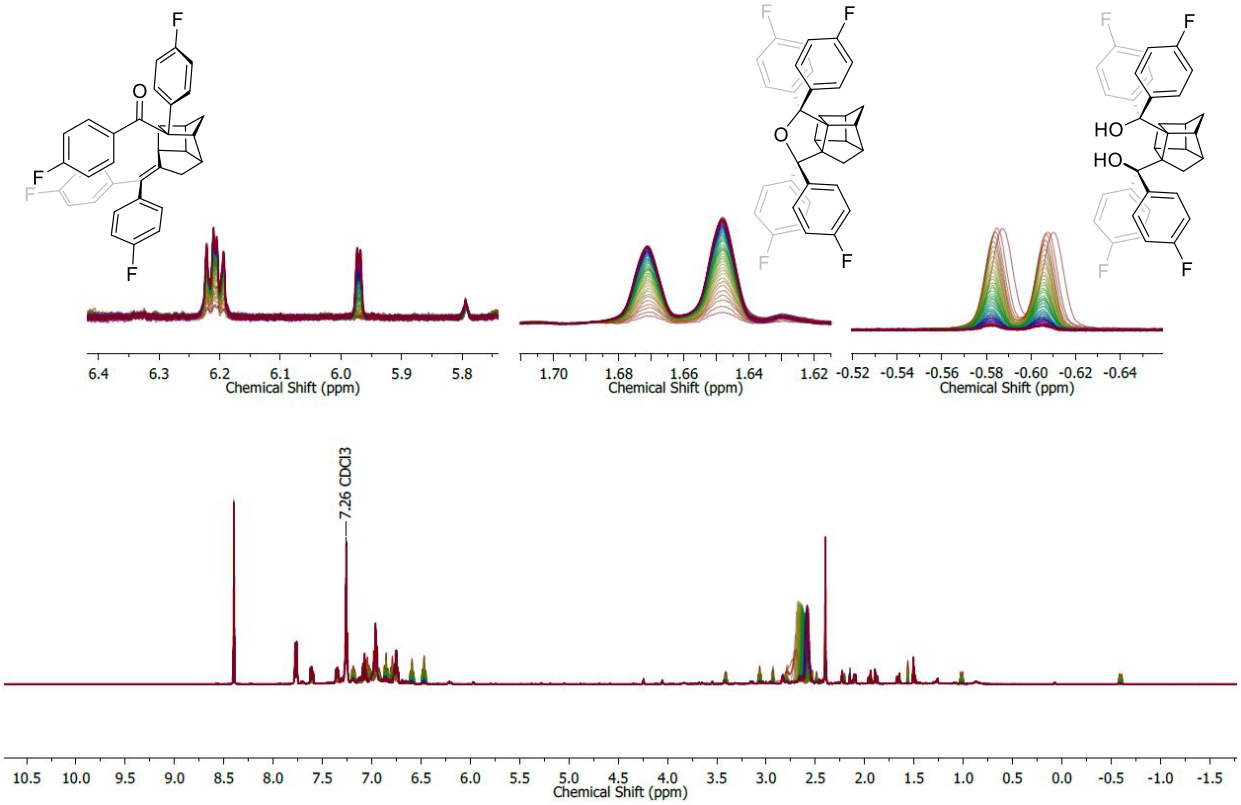

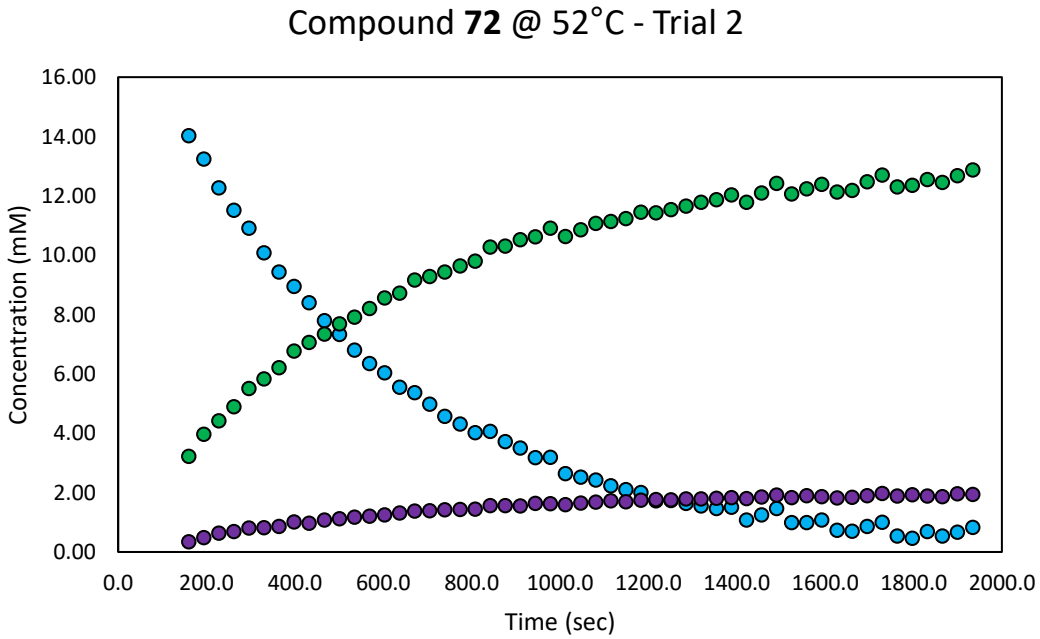

Compound 72 Kinetics Spectra

52°C – Trial 3

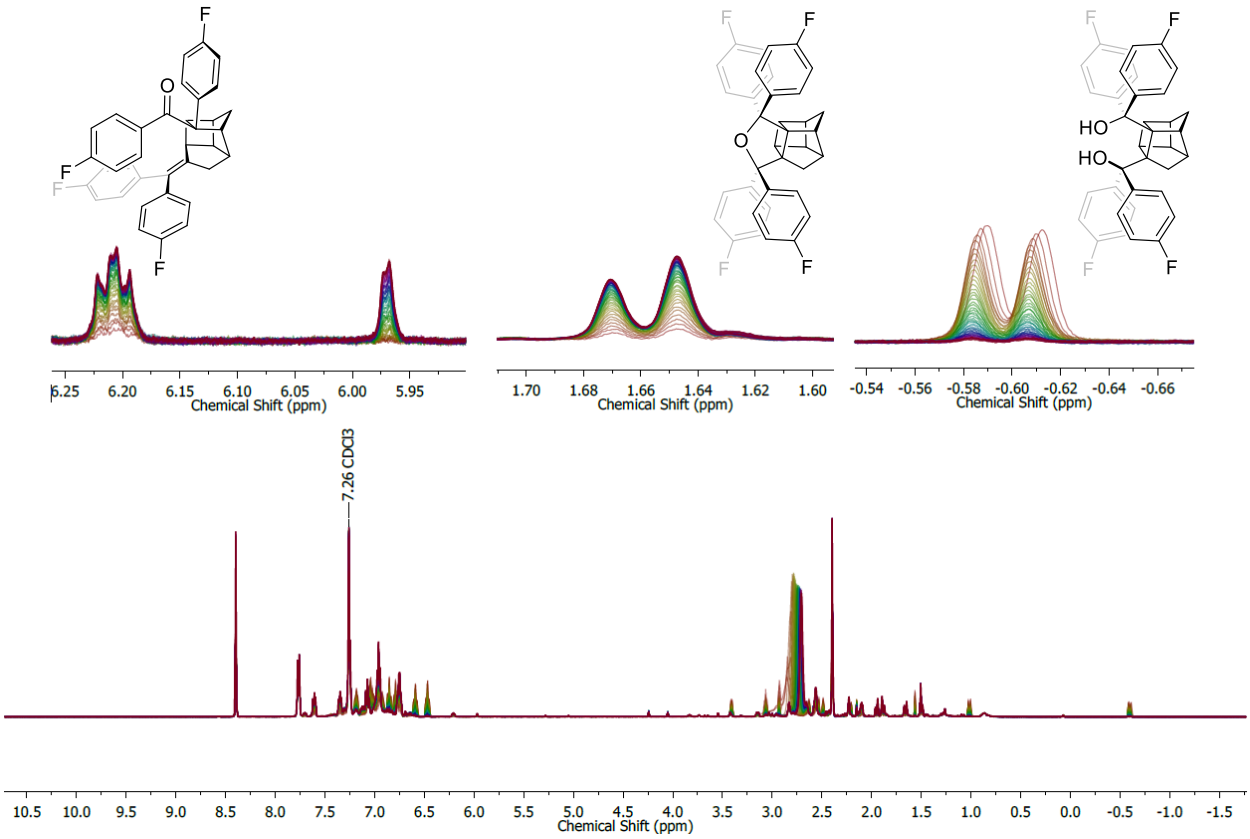

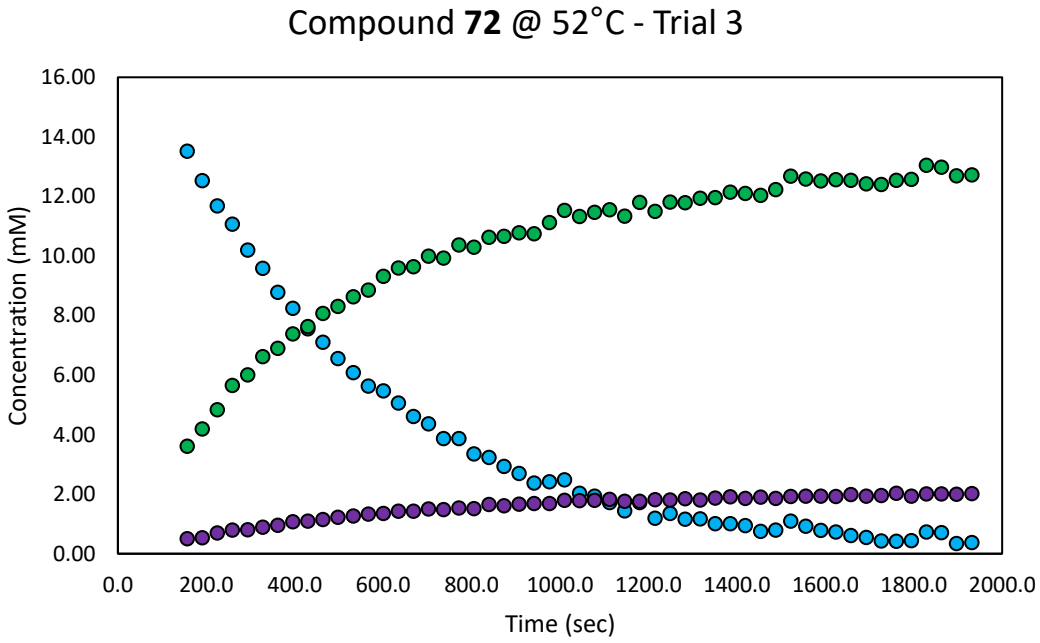

Compound 73 Kinetics Spectra

25°C – Trial 1

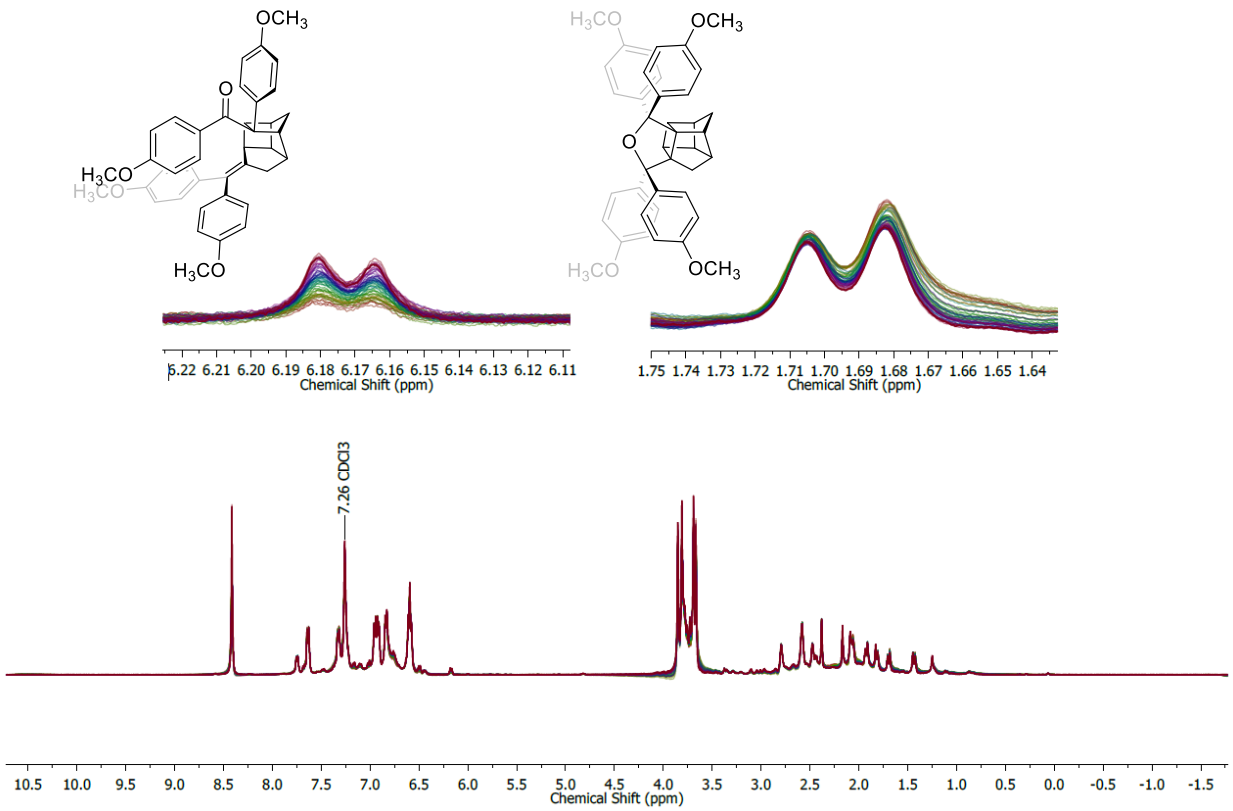

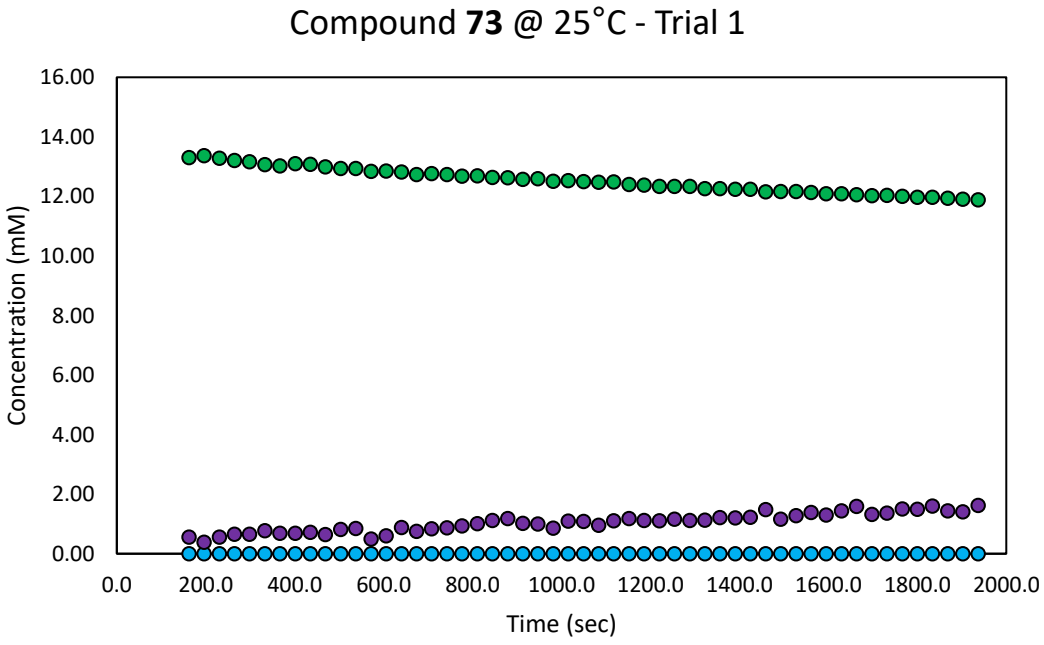

Compound 73 Kinetics Spectra

25°C – Trial 2

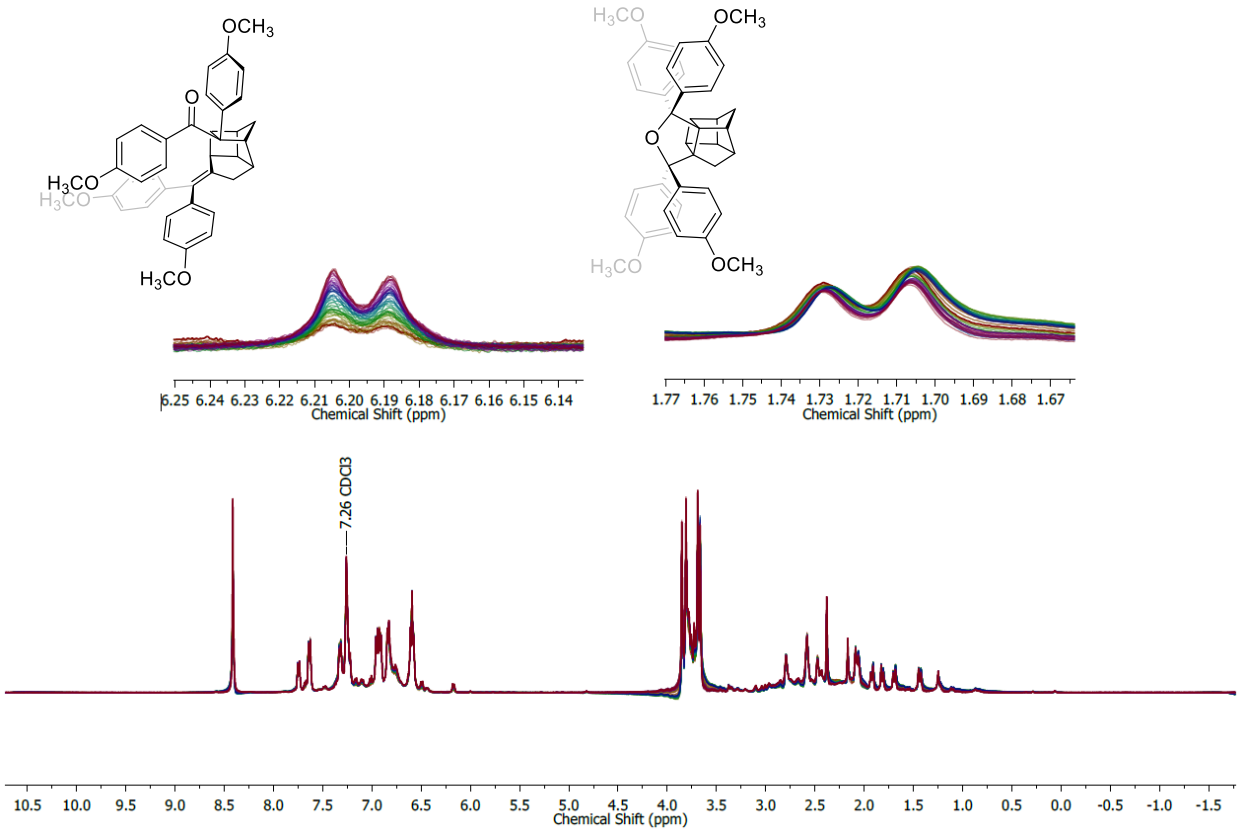

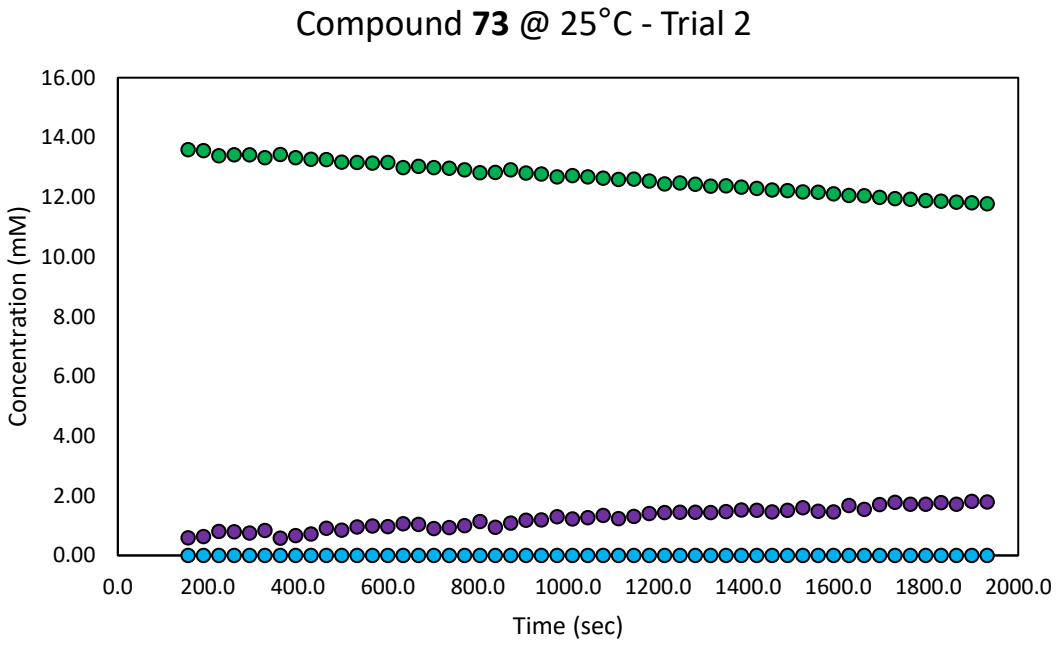

Compound 73 Kinetics Spectra

25°C – Trial 3

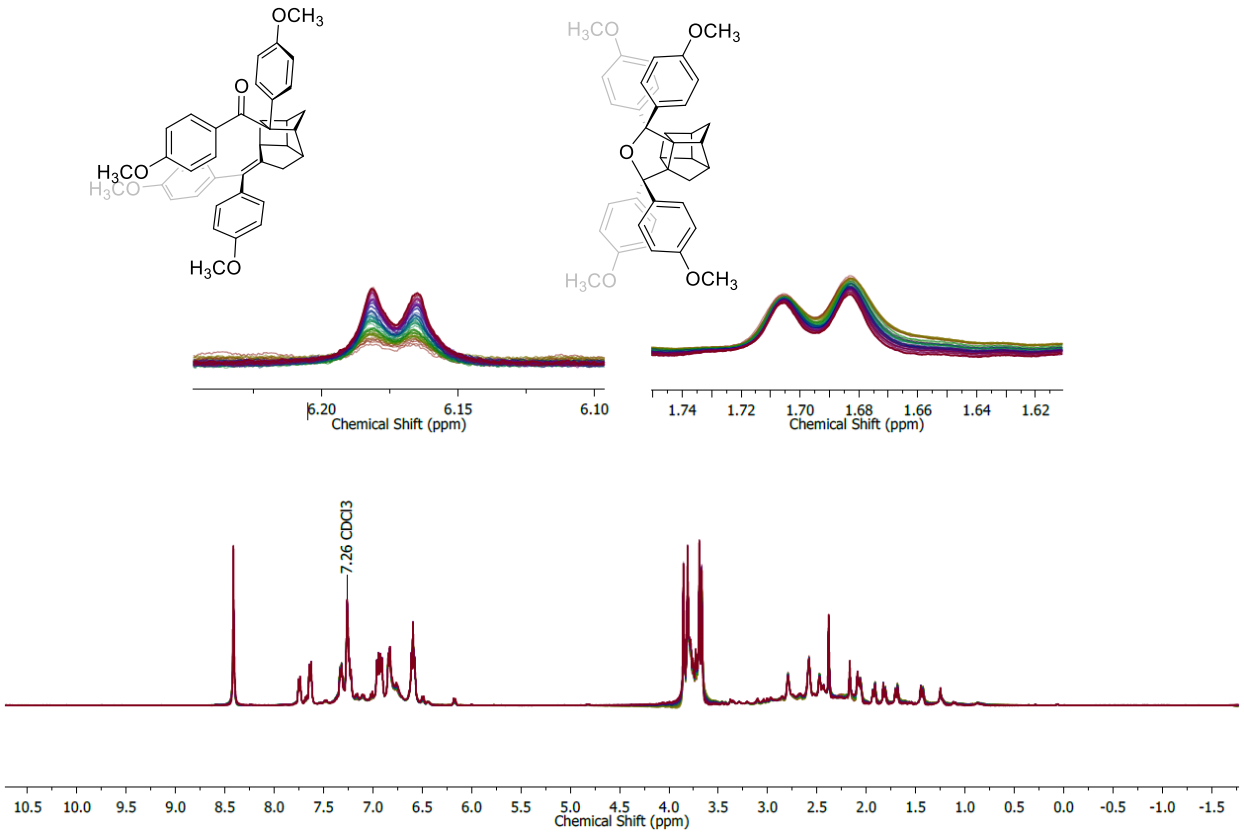

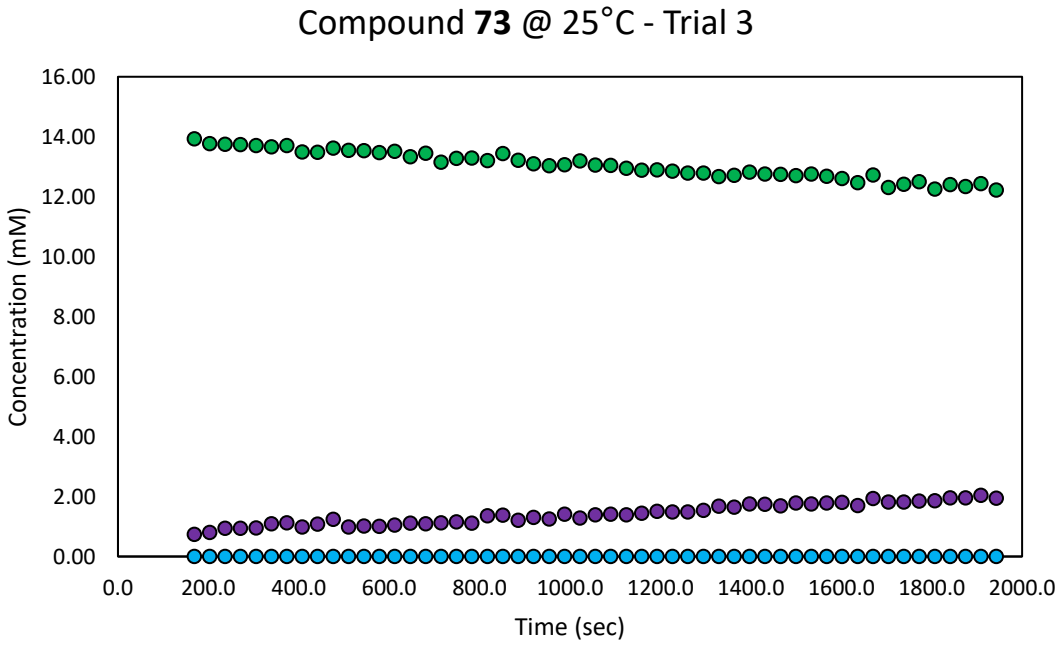

Compound 73 Kinetics Spectra

35°C – Trial 1

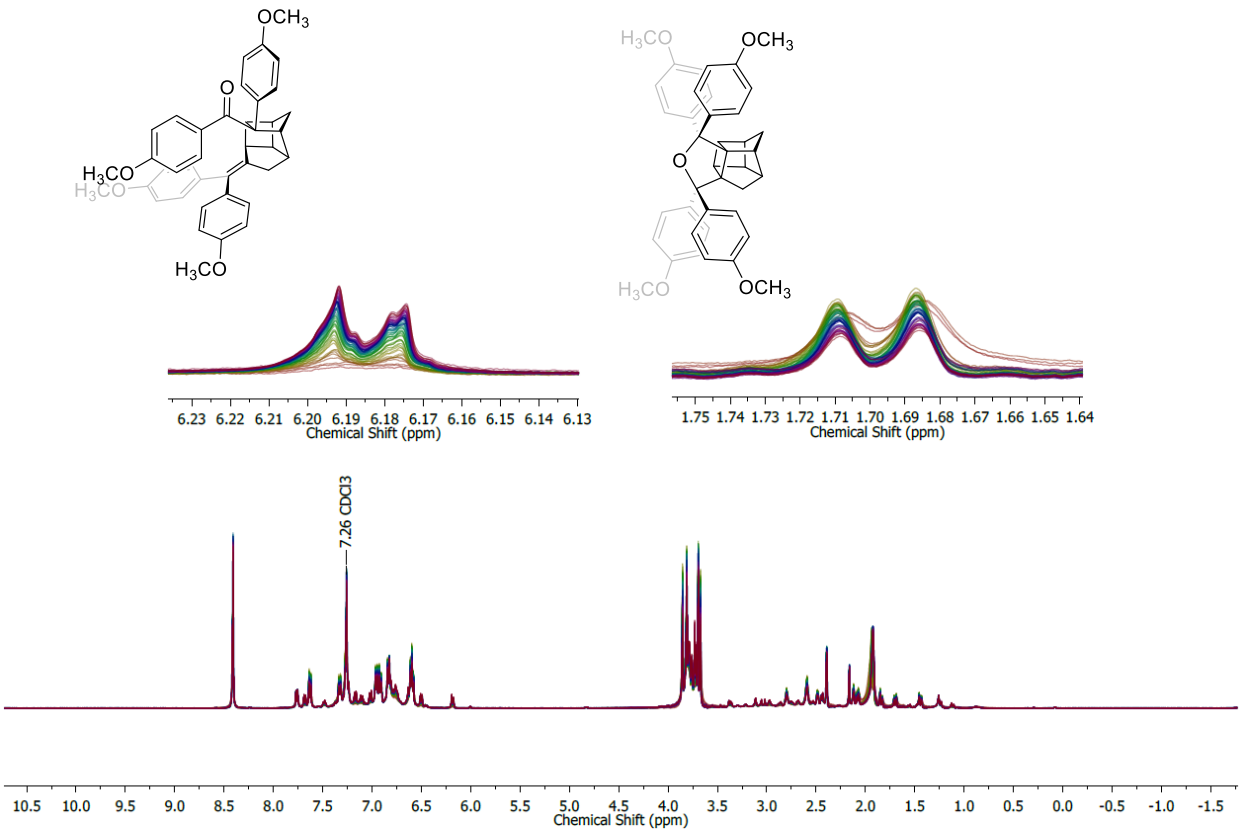

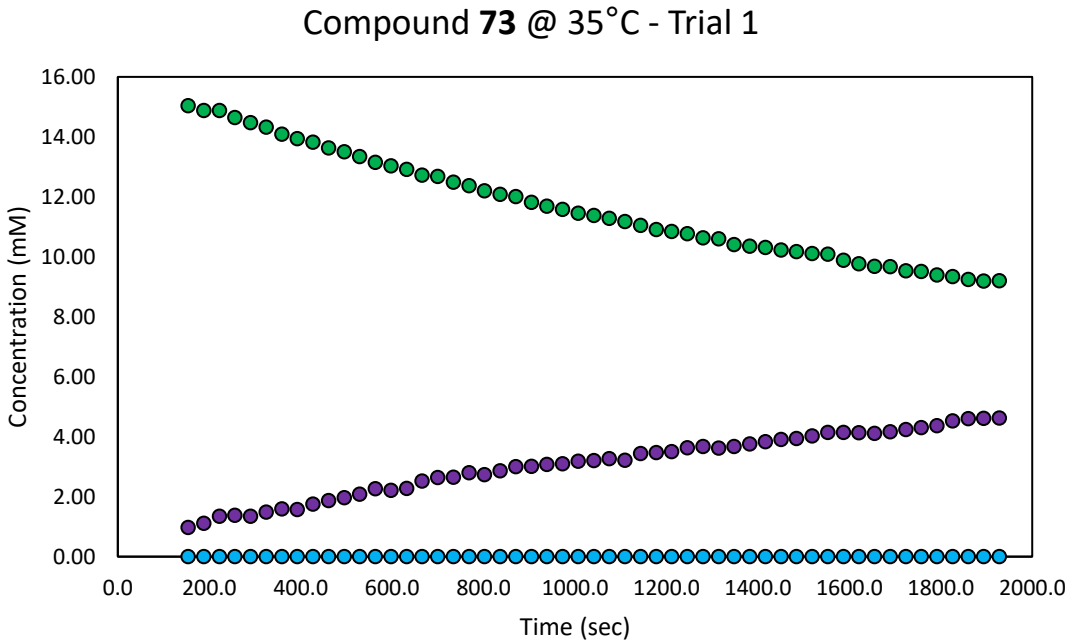

Compound 73 Kinetics Spectra

35°C – Trial 2

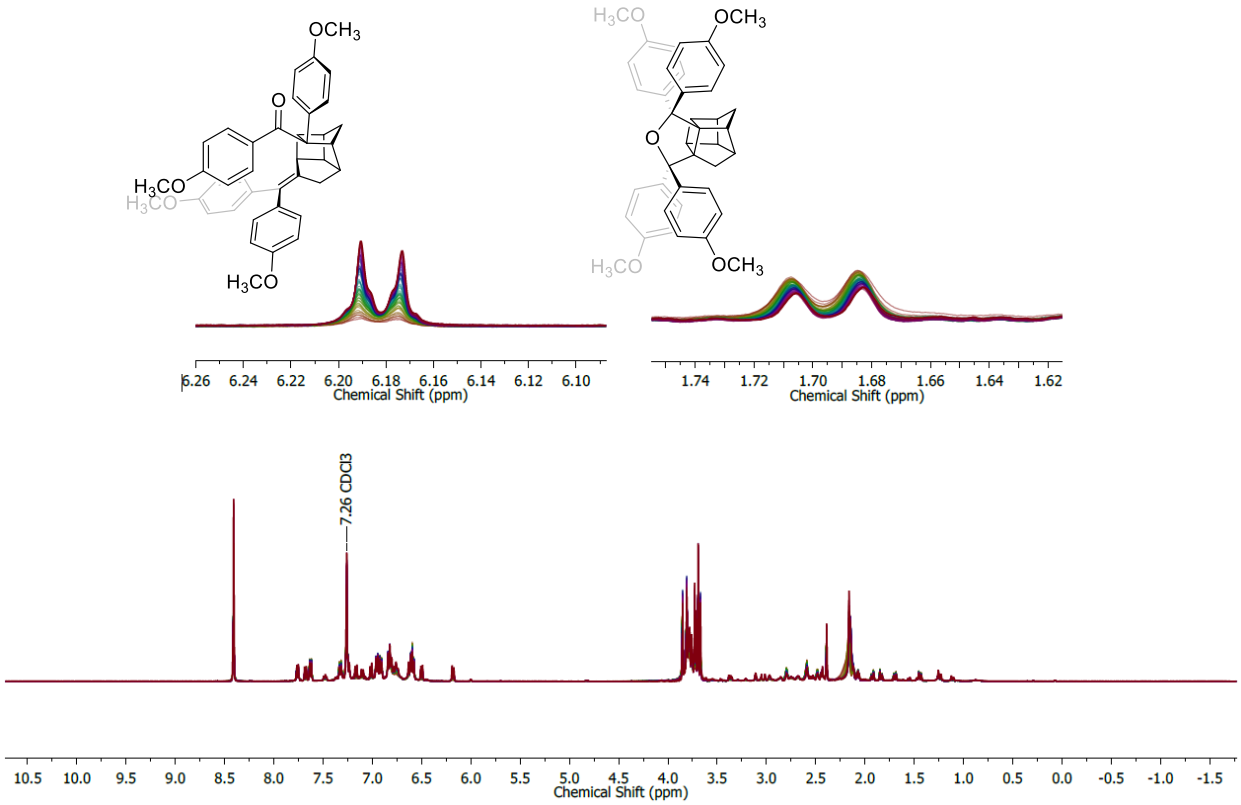

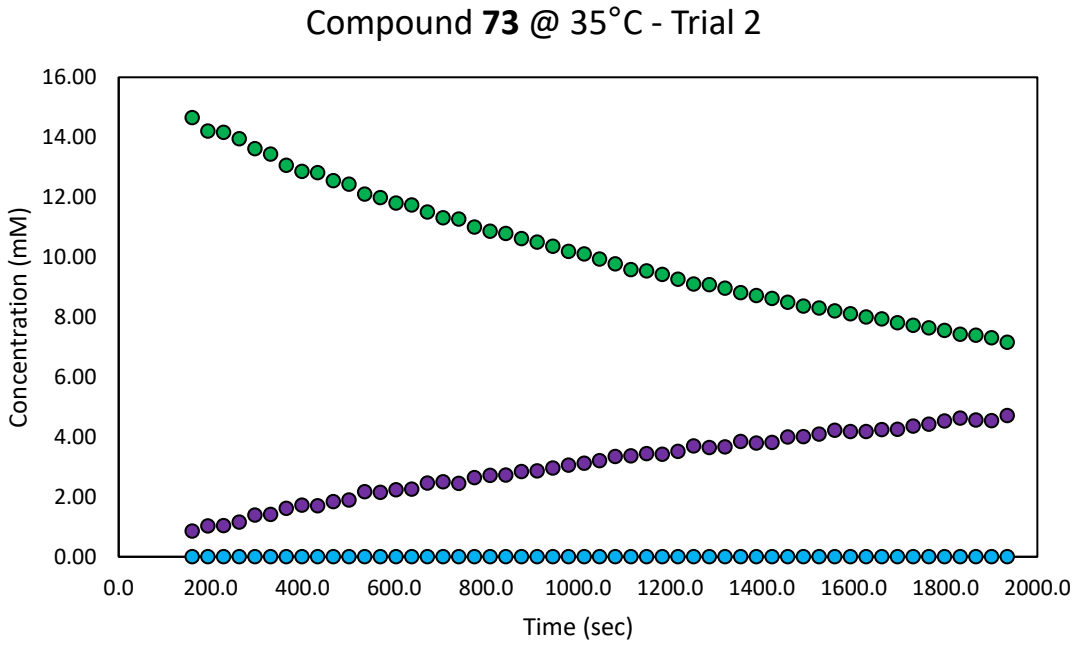

Compound 73 Kinetics Spectra

35°C – Trial 3

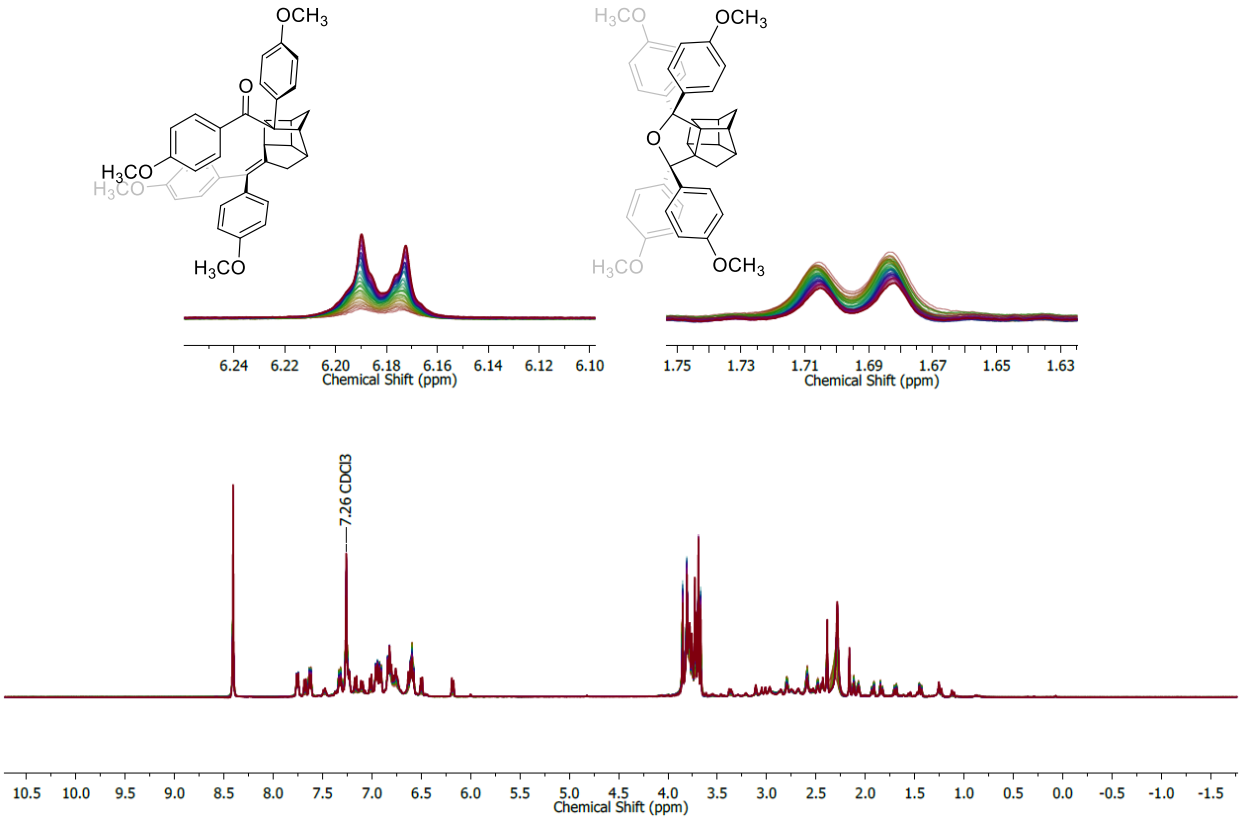

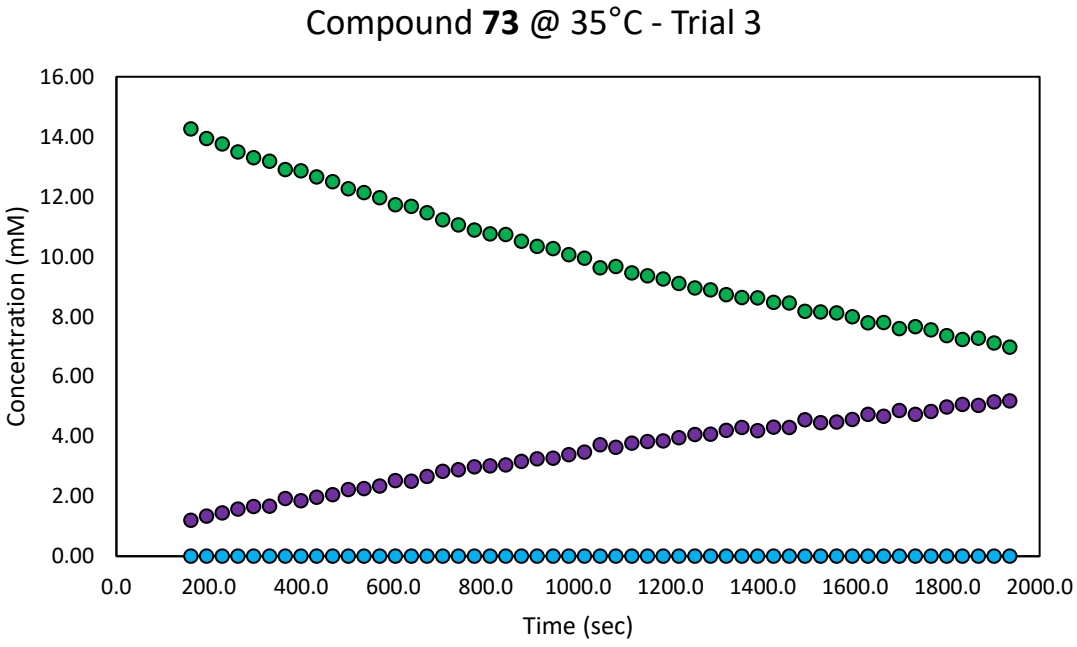

Compound 73 Kinetics Spectra

45°C – Trial 1

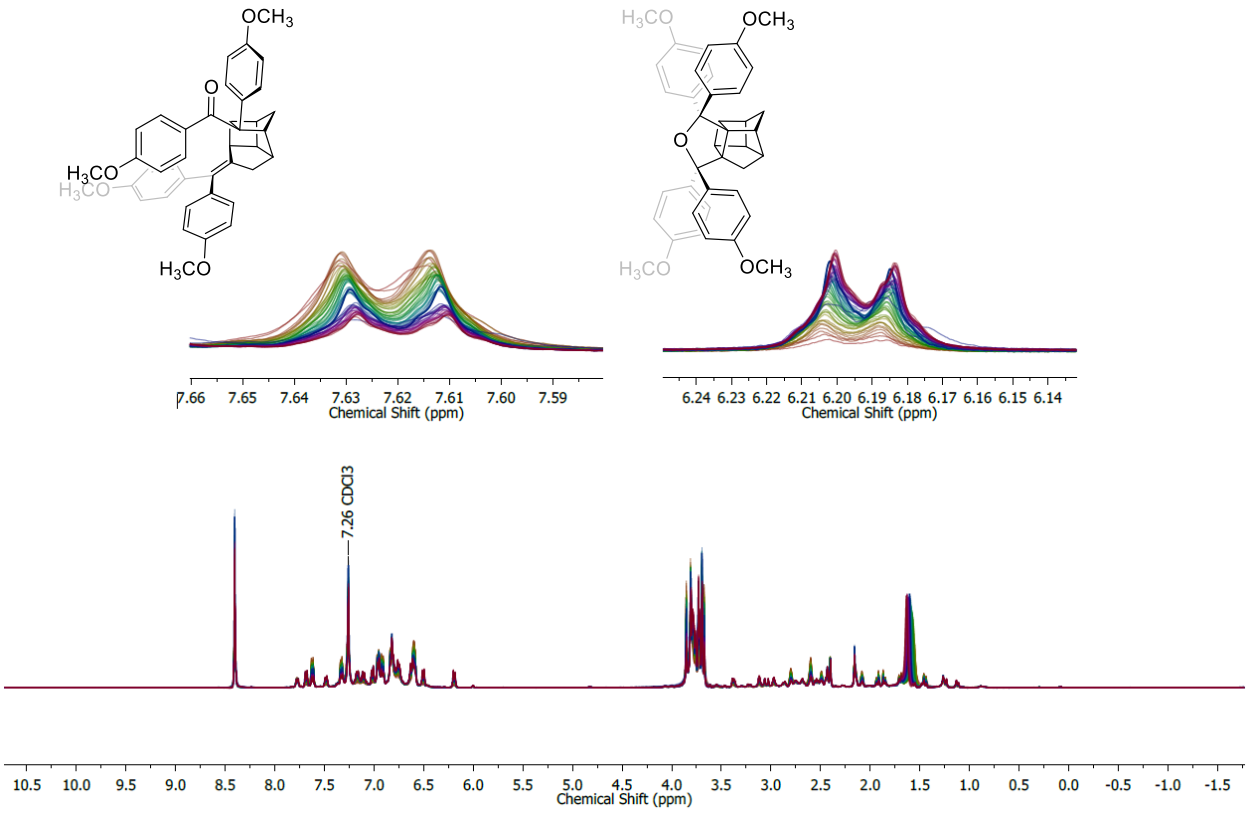

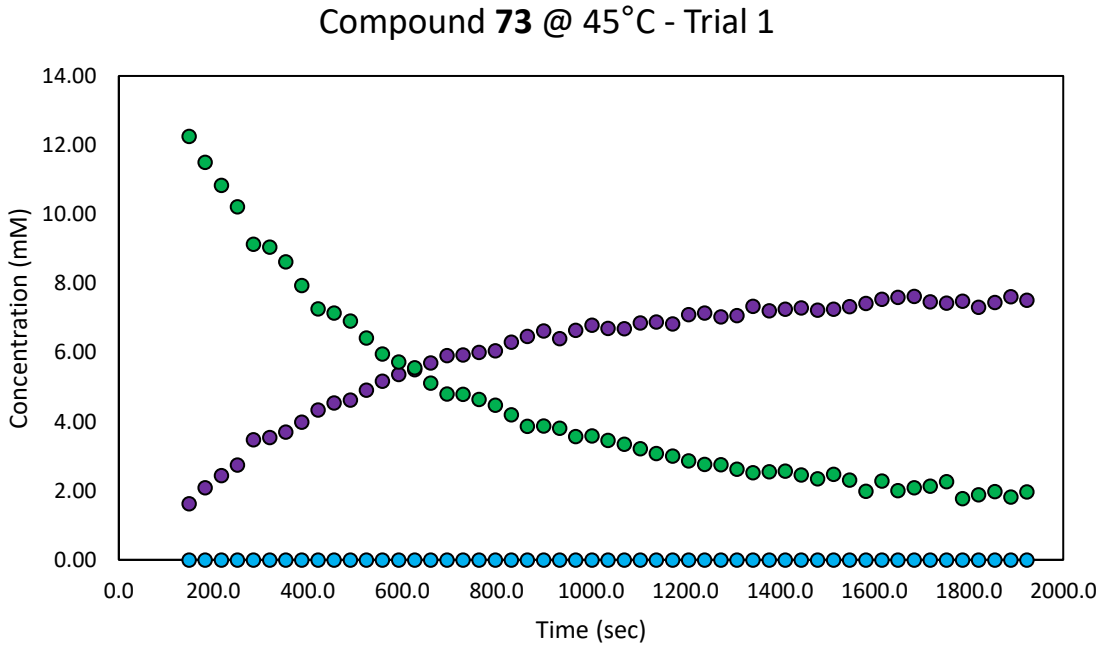

Compound 73 Kinetics Spectra

45°C – Trial 2

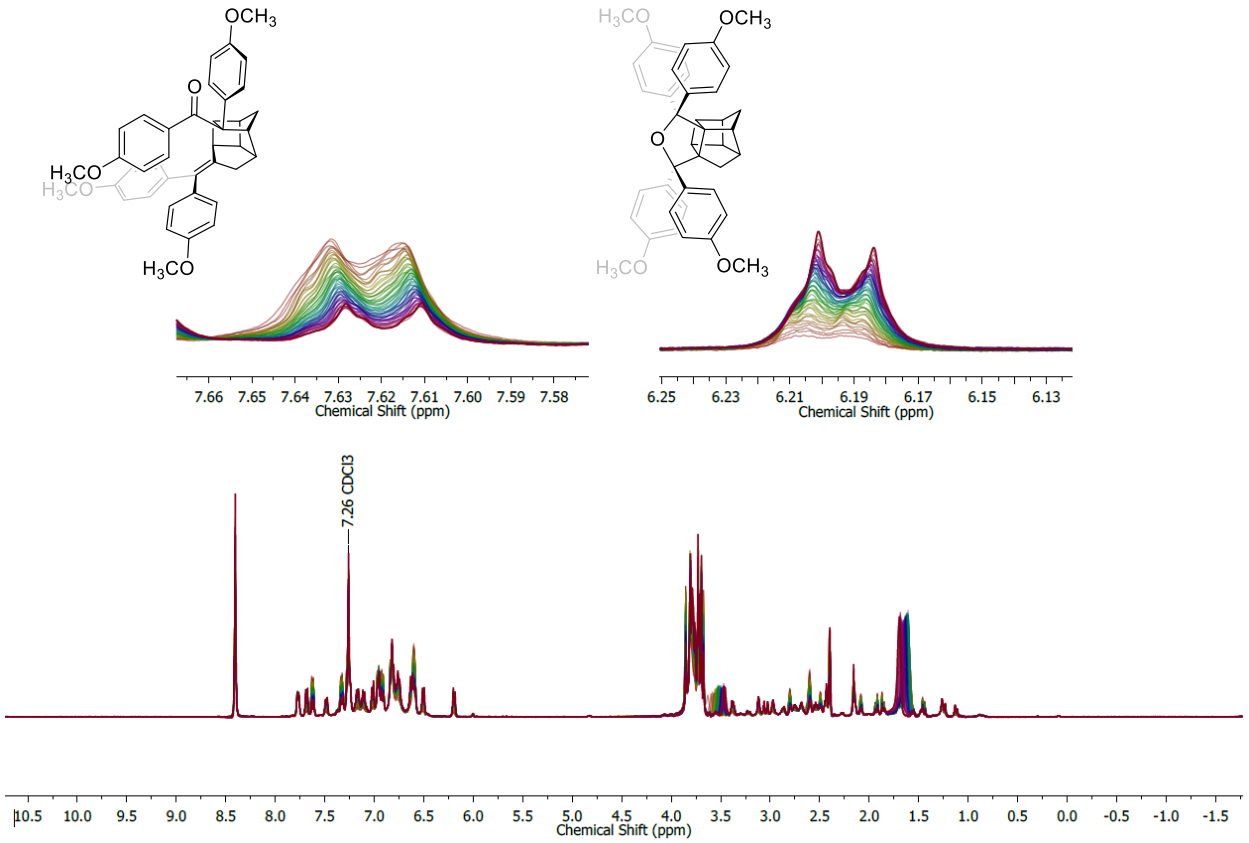

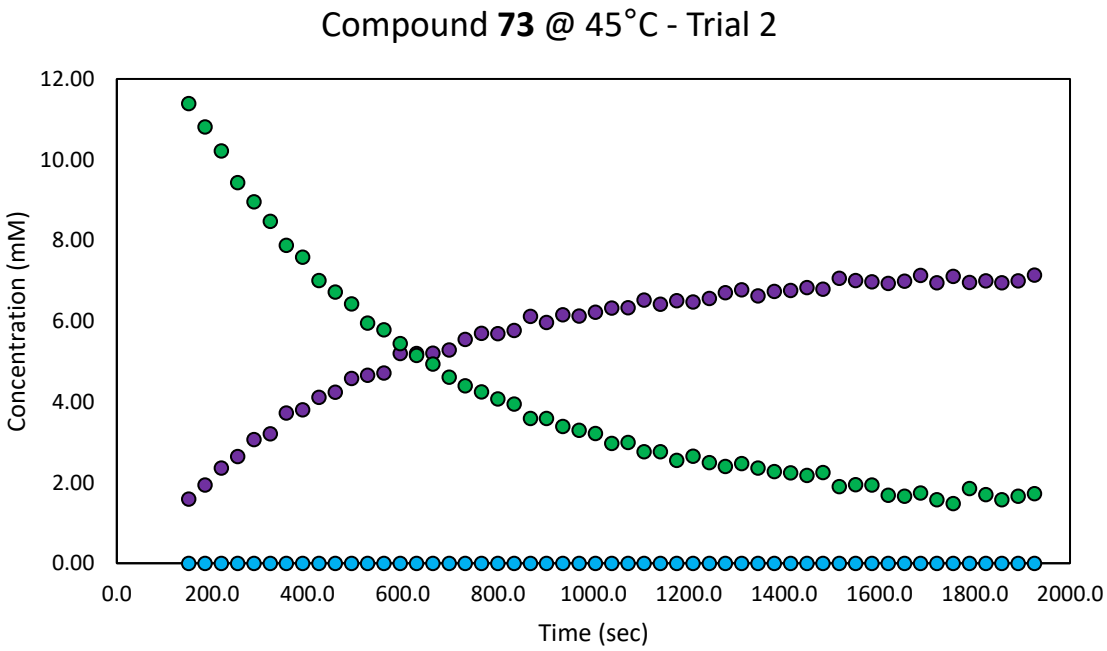

Compound 73 Kinetics Spectra

45°C – Trial 3

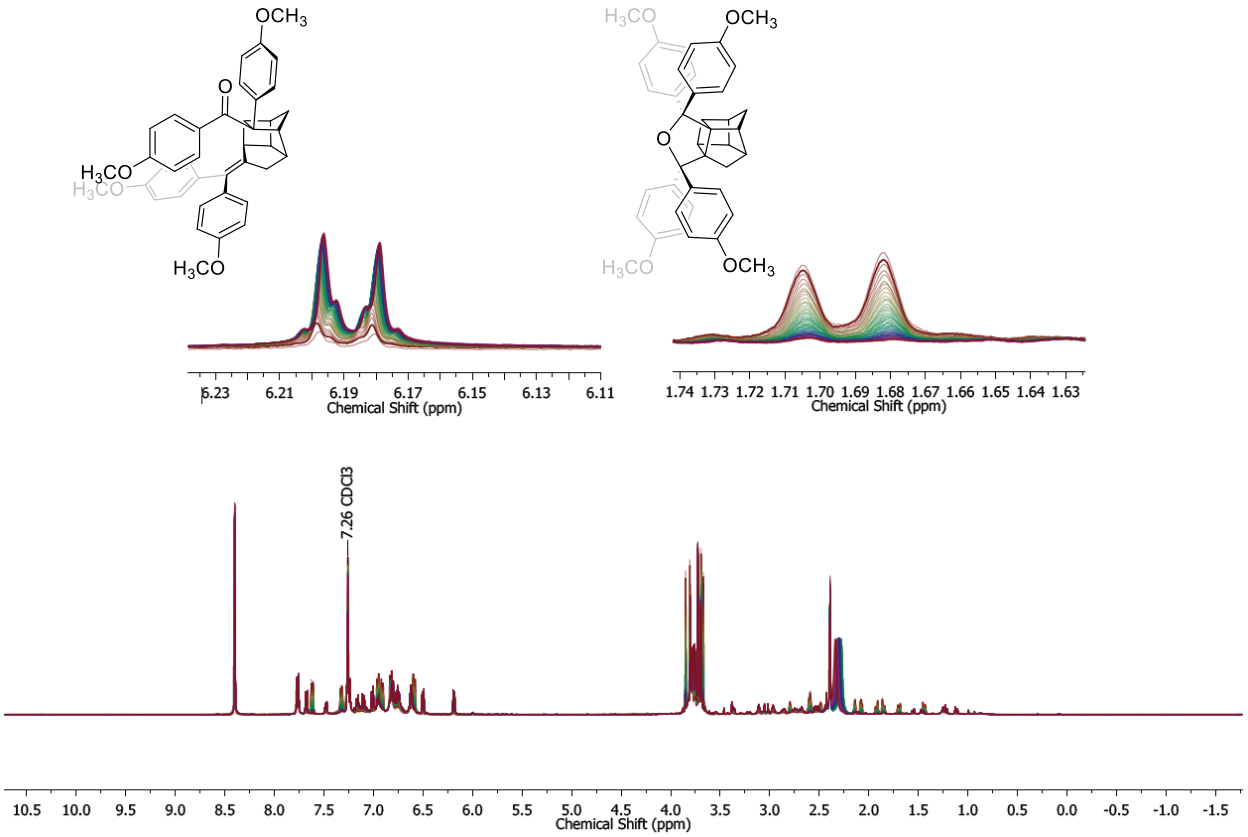

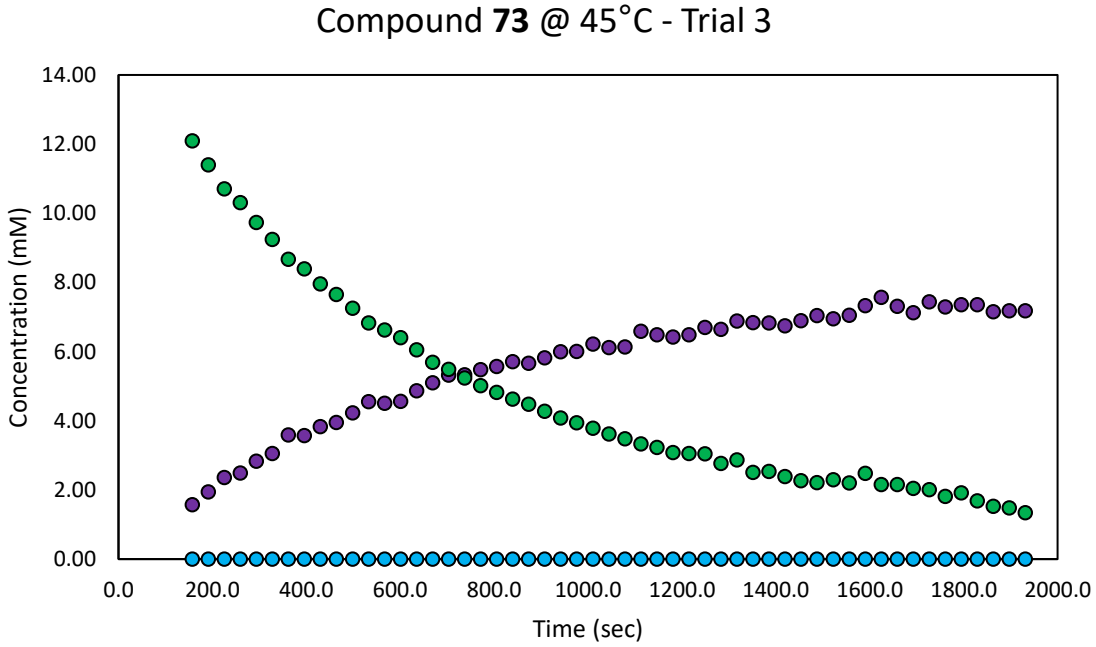

Compound 73 Kinetics Spectra

52°C – Trial 1

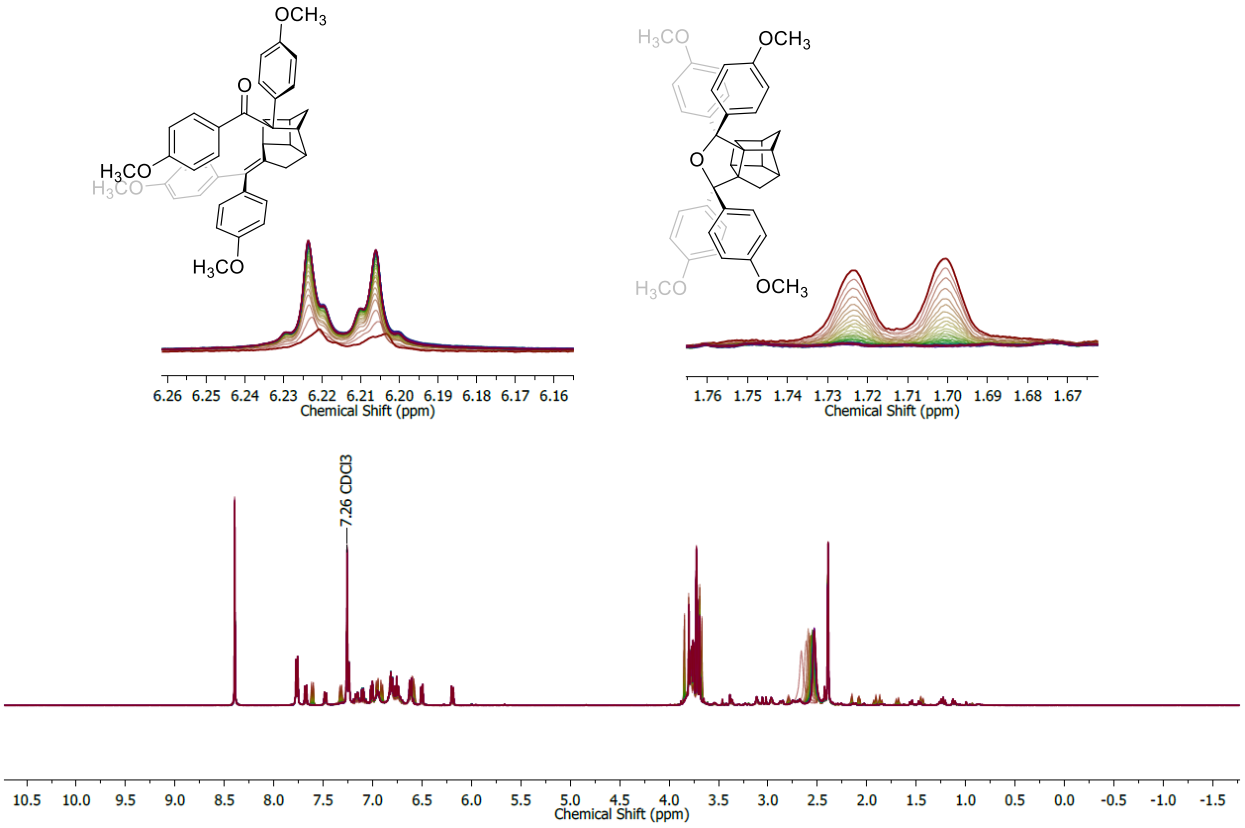

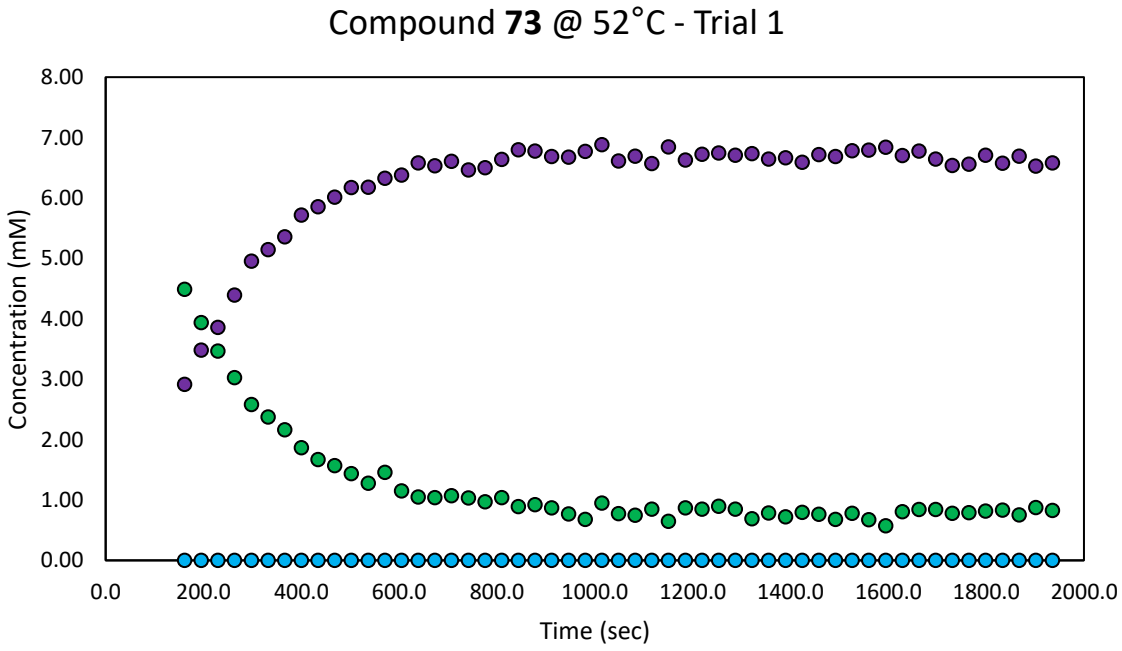

Compound 73 Kinetics Spectra

52°C – Trial 2

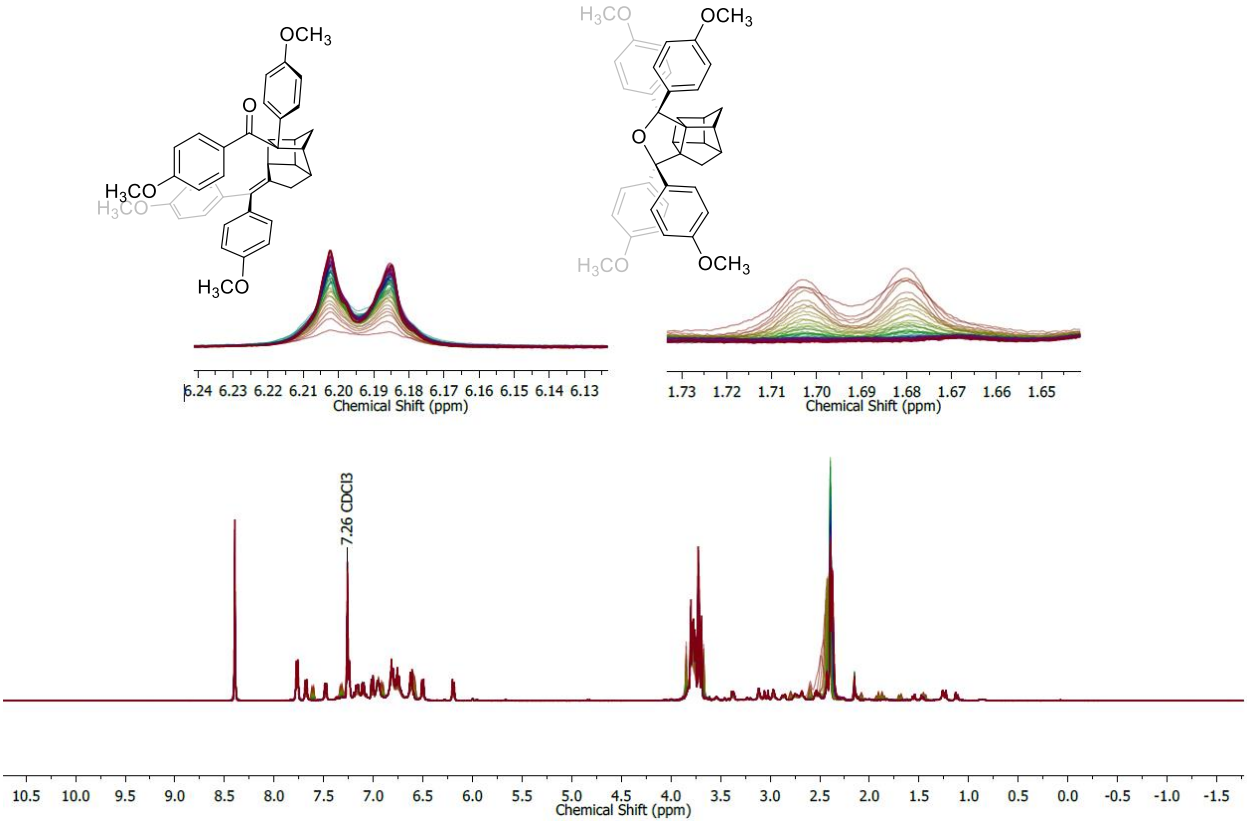

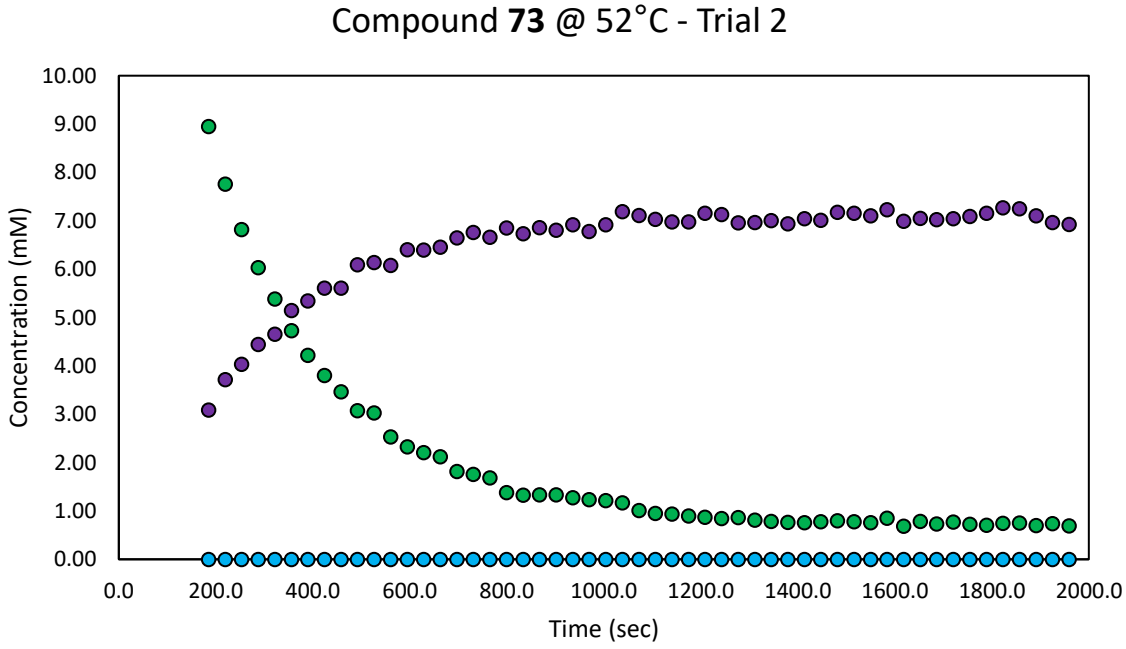

Compound 73 Kinetics Spectra

52°C – Trial 3